USING POLLEN RECORDS FROM NEW ZEALAND AND SOUTHERN CHILE TO RECONSTRUCT NEW ZEALAND CLIMATE VARIABILITY

OVER THE LAST 14,000 YEARS

BY

IGNACIO ALONSO JARA PARRA

A thesis submitted to the Victoria University of Wellington

in fulfilment of the requirements for the degree of

Doctor of Philosophy in Physical Geography

Victoria University of Wellington

Abstract

Climate variability in New Zealand (34-47°S), a long, narrow continental strip straddling the mid-latitudes of the Southern Hemisphere, results largely from the interplay between sub-tropical and sub-Antarctic atmospheric and oceanic circulation systems. Despite their importance to present-day New Zealand climate, these hemispheric-wide systems have only recently come under the spotlight of paleo-climate investigations with most attention having traditionally been centred on reconstructing climate trends. This PhD adopts a broader approach to climate reconstruction, by developing and comparing two new pollen-climate reconstructions from New Zealand (38-42°S) and one from Patagonia, Southern Chile (43°S). At each site, paleo-climate interpretations are based on the changes in climate-sensitive plant indicators. The influence of hemispheric atmospheric circulation on New Zealand climate history is assessed by: (1) comparing New Zealand climate/vegetation trends with published proxies from low- and high-latitudes, and (2) comparing New Zealand reconstructions with the Patagonian record. Finally, a multi-millennial pattern of Southern Hemisphere circulation over the last 14,000 cal yr BP (calendar years before AD 1950) is outlined.

The first record presented is a 16,000-year temperature reconstruction from a small alpine lake in South Island, New Zealand (41°S), based on pollen and plant macrofossils. Climate variations are interpreted from the relative abundance of lowland and highland vegetation. The results include a lifting of the altitudinal forest limits attributed to warming pulses between 13,000-10,000 cal yr BP and between 7000-6000 cal yr BP, and a decline of lowland relative to upland forest taxa interpreted as cooling trends between 10,000-7000 cal yr BP and over the last 3000 years.

The second record gives 15,000-year temperature and precipitation reconstructions from a peatbog in northern New Zealand (38°S), based on pollen and charcoal analysis. Temperature changes are assessed based on two quantitate reconstructions, whereas precipitation trends are inferred from variations in arboreal taxa with different drought tolerances. A long-term warming is inferred between 14,600-10,000 cal yr BP. Persistent dry conditions are recorded between 12,000-10,000 cal yr BP, followed by a long-term wet period between 10,000-6000 cal yr BP. The last 7000 years feature a

long-term drying trend that culminates with persistent drier conditions over the last 3000 years.

The third record provides a 16,000-year reconstruction from a small lake in Northwestern Patagonia (43°S), based on pollen and charcoal analysis. Climate conditions are inferred from the relative variations of pollen types with distinctive climate tolerances and complemented with changes in fire activity. These variations are in turn interpreted as resulting from changes in the position and/or strength of the Southern Westerly Winds (SWW). Cold and moist conditions attributable to stronger/northward-shifted SWW winds are observed between 16,000-13,600 cal yr BP. In contrast, warm and dry conditions suggestive of weaker/southward-shifted SWW are detected between 12,000-10,000 cal yr BP. The last 6000 years shows a trend towards colder conditions and increasing precipitation variability, suggesting a highly variable westerly flow over Patagonia.

A comparison between the New Zealand and the Patagonia records suggest: (1) weakened/southward-shifted westerly flow over the southern mid-latitudes between 13,000-10,000 cal yr BP caused rapid warming and peak temperatures in New Zealand, as well as dry conditions in Northern New Zealand, (2) Enhanced/northward-shifted SWW over the southern mid-latitudes between 9000-4000 cal yr BP caused decreasing temperatures in the South Island and increasing precipitation in Northern New Zealand and (3) Overall weakened/southward-shifted SWW after 4000 cal yr BP caused a decrease in temperature in the southern New Zealand site. Drier conditions in Northern New Zealand and the overall increase in climate instability at all sites may have resulted from more frequent El Niño events along with an increase in sub-tropical climate variability.

Acknowledgment

This thesis has been supported by a great number of generous collaborators from different institutions and countries.

First, I would like to thanks to my Primary Supervisor Prof. Rewi M Newnham for his outstanding academic support during all these years of work and study. He has always encouraged me to keep improving this thesis, contacted me with some of his collaborators, and assisting with the field work and academic activities. Thanks to Rewi’s support, I have had the opportunity to present the results of this thesis in several New Zealand and overseas congresses and conferences. Rewi has read, commented and edited every single chapters of this thesis, without his invaluable assistance, generosity and broad vision; this thesis would not have been possible.

I would like to give my most sincere thanks to Dr. Brent Alloway, my secondary supervisor, who has been a fundamental part of this project all the way through. As I said multiple times, Brent was the first person who suggested me to come to Victoria when I was finishing my studies in Chile, and therefore I would not have been at this stage without his initial encouragement. I must mention that Brent has been a pivotal element connecting Chilean and New Zealand research groups, and this thesis is just the first stone of this trans-Pacific collaboration. Additionally, Brent has allowed me participate as an academic assistant in several fieldwork and university fieldtrips, all of them wonderful experiences that I will always kept in my memory. Perhaps more importantly, I cannot leave the opportunity to acknowledge Brent’s personal support during my staying in In New Zealand. Working with him has been a fantastic, fun and a great honor.

I also want to thanks to Dr. Patricio Moreno from Universidad the Chile for his collaboration and assistance in this thesis. Patricio has kindly invited me to work along with him in Patagonia, giving me access to field equipment, fieldwork, sample material, and laboratory facilities. He also has founded the Patagonian part of this thesis, as well as financing my research work in Chile. It has been a great honor to have started my research career with Patricio many years ago, without his support I would have never had the chance of pursuit my latest academic progress. I want to extend my gratitude to all my colleagues from Laboratorio de Paleoecologia Quaternaria de la Universidad de Chile for their fantastic support for so many years. Especial thanks to Loreto Hernández, Rodrigo Villa-Martínez, Lucia Gonzalorena, Javiera Videla, Marcela Valenzuela, Oscar Pesce and William Henríquez.

I cannot leave the opportunity of acknowledging all the staff at the School of Geography and the School of Biological Sciences for their support and assistance during all these 4.5 years. Coming to New Zealand has been one of the best experiences in my life, and a great part of this has been related to with my involvement at Vic. The School of Geography has a fantastic working atmosphere build up from the professionalism, kindness and generosity of its staff members. Special thanks to my colleagues and friend Matt T. Ryan, Kosta Tashkoff, Sandra Fogliani, Amanda Taylor, Bill McLea, Chris Conway, Tui Arona, Jane, Chewings, Andrew Rae and Dez Tessler, Miranda Voke, Cheryl Johansen, and many others for their help, company and for making my life here so special.

Several other people have provided with crucial help for the development of my doctoral research. I want to thanks to Janet Wilmshurst, David Lowe, Courtney Foster, Aline Holmes, Andrew Rees, Aline Homes, Daniel Fernández and Margaret Harper, Fiona Mackenzie, Holly O'Connor, Maureen Gray and many many others.

Finally, I want to dedicate all this work to my family in Chile. Since my early childhood, my family provided me with an intellectual background which has proved to be vital for developing a vocation for academia. But more importantly, I will always be grateful to have had the incredible lucky to grow up in such a protective and affectionate environment. Jaime, Gloria, Natalia, Olivia, Luis Fernando, tio Ray, Anamaria y toda la familia: esto está dedicado para todos ustedes, los amo!

Contents

Index of Figures

Chapter One
Introduction

1.1 Research Problem and Presentation of the study

As a long and narrow continental strip straddling the mid-latitudes of the southwest Pacific (34-47°S), New Zealand experiences the effects of both sub-tropical and sub-Antarctic climate systems. Its insular character and relatively small size mean New Zealand atmospheric circulation is not significantly disrupted by the continental feedbacks observed in bigger landmasses. Hence it is not surprising that much of the modern climate variability from daily to decadal timescales is dictated by the combined effect of low- and high-latitude modes of climate variation such as El Niño Southern Oscillation (ENSO), Southern Annular Mode (SAM) and the Inter-annual Pacific Oscillation (IPO) on the prevailing westerly circulation (Jiang et al., 2013; Kidson et al., 2000).

Although the pattern of New Zealand climate change during the Late Quaternary is now reasonably well established, investigations of the evolving influence of these low- and high-latitude circulation systems are still at a nascent stage (Fletcher & Moreno, 2011; Gomez et al., 2013; Lorrey et al., 2014). Recent work has postulated the emergence of climate variability analogous to the modern SAM (McGlone et al., 2010) and to ENSO (Gomez et al., 2013; Moreno et al., 2014; Lorrey et al., 2014) during the Holocene period. Interestingly, most of these studies have highlighted the likelihood of a combined effect of more than one climate mode, as well as pointed out the necessity of comparing proxy data from regions where these large-scale modes are manifested in distinctive local patterns.

To better understand the influence of the Southern Hemisphere circulation in the recent New Zealand climate history, it is beneficial to compare equivalent proxy data from different locations in the southern mid-latitudes which depict the large-scale spatial heterogeneities that define present-day climate modes. This is the first of two main motivational challenges for this study. The second challenge is to generate proxy data with sufficient resolution and chronological control to study climate oscillations at millennial timescales. This PhD thesis addresses these challenges by developing and contrasting three new high-resolution pollen-climate reconstructions from sites at similar latitudes at both New Zealand (38-42°S) and Northwestern Patagonia (43°S).

1.2 Rationale and advantages of the proposed research

The particular approach adopted in this thesis is to exploit the similarities and differences between the atmospheric circulation of New Zealand and Northwestern Patagonia to elucidate millennial-scale hemispheric patterns of climate change by using palynology. The central and south parts of New Zealand and Northwestern Patagonia lie both at the northern edge of the Southern Westerly Wind belt, and therefore their climate regimes are dominated by changes in the strength and position of the overall zonally-symmetric circum-Antarctic vortex. Thus, paleo-climate variations (cooler, warmer, wetter or drier) of the same direction and timing are expected to be observed as a result of changes in the strength and/or position of the Southern Westerly Winds. This inference can primary be tested by comparing the New Zealand and Patagonian reconstructions generated in this thesis, and subsequently by comparing them with other published records from the Southern Ocean and Antarctica. On the other hand, divergent paleo-climate signals between New Zealand and Northwestern Patagonia are expected to result from a more intense sub-tropical circulation over the New Zealand territory. This is because climate regimes in northern New Zealand (34-38°S) are significantly influenced by circulation in the Tropical Pacific Ocean; whereas Northwestern Patagonia lacks a strong imprint of this low-latitude climate system. This inference can also be tested by comparing the records generated in this thesis with reconstructions from the Southern Ocean, Antarctica and the Tropical Pacific. Hence, by assessing the similarities and differences between pollen-based climate reconstructions from New Zealand and Northwestern Patagonia, this thesis is able to infer the evolution of the climate connections between these mid-latitude regions and the low- and high-latitudes of the Southern Hemisphere.

As a result of their similar position at the Southern Hemisphere mid-latitudes and their continental relief, New Zealand and Northwestern Patagonia share numerous advantages for developing pollen-based environmental reconstructions, including abundant postglacial sediment deposits and distinct climatically-driven spatial distribution of plant communities. These advantages have long been used to decipher climate trends from pollen profiles. For instance, in New Zealand the general spatial distribution of the mixed conifer broad-leaved forest and the beech forest communities follows distinguishable north-south and altitudinal temperature gradients; whereas in Northwestern Patagonia altitudinal distribution of evergreen and deciduous forest communities follows marked precipitation and temperature gradients resulting from the interception of the westerly flow by the continental mountainous relief. Thus, long-term variations in the pollen abundances in both regions can confidently be attributed to climate-driven changes in vegetation.

The development of high-resolution pollen analysis with detailed AMS radiocarbon chronologies and the improvement of several analytical techniques have allowed the fine characterization of a series of postglacial (the last 17,000 years) vegetation changes in pollen profiles in New Zealand and Western Patagonia. For instance, the introduction and application of a pollen-climate calibration using a pre-deforestation dataset allowed the extraction of quantitative temperature signals from several pollen records located in the northern and southern parts of New Zealand (e.g. Wilmshurst et al., 2007). In Western Patagonia, the lack of a modern pollen dataset has prevented the development of quantitative reconstructions; however, the calculation of ecologically-based pollen ratios of climate-sensitive taxa and their combination with highly-resolved charcoal analysis have allowed the timing and direction of several temperature and precipitation anomalies to be constrained at timescales ranging from multi-millennial to sub-centennial (e.g. Moreno, 2004). As a result of these and other analytical developments, some detailed paleo-climate records from these two regions have recently been published in the scientific literature (e.g. Augustinus et al., 2012; Pesce and Moreno, 2014) and these provide the impetus for the particular approach adopted in this thesis.

1.3 Aim of the thesis

The general aim of this thesis is to reconstruct the millennial-scale temperature and precipitation changes of New Zealand and Northwestern Patagonia in the last 15,000 years based on the vegetation history inferred from pollen profiles. Additionally, this thesis aims is to compare and contrast the inferred climate trends at the study sites to investigate the general atmospheric circulation patterns for the southern mid-latitudes and their relationship with low- and high-latitude climates.

The specific objectives to achieve these aims are to:

- Complete three high-resolution pollen sequences, two from New Zealand and one from Northwestern Patagonia.
- Complete a high-resolution charcoal record from Northwestern Patagonia.
- Describe the timing, direction and magnitude of vegetation changes observed in the three pollen records.
- Develop quantitative and/or qualitative climate reconstructions from each of the pollen records
- Propose a climate sequence based on the modern vegetation-climate relationship for each of the pollen sequences.
- Propose a climate sequence derived from the charcoal reconstruction in Northwestern Patagonia to complement pollen-based climate inferences.
- Assess the presence of convergent or divergent climate trends across the three study sites.
- Infer large-scale trends in Southern Hemisphere circulation over the last 15,000 years and their link with low- and high-latitude climate systems based on the similarities and differences between the three pollen records.
- Test for validity of the suggested trends by comparing them with other published climate proxies from New Zealand and Patagonia and from other Southern Hemisphere climate proxies.

1.4 Contributions of the thesis

- A new 15,000-year quantitative temperature reconstruction from the treeline in northwest Nelson area, central New Zealand.
- A new 15,000-year old quantitative temperature reconstruction from the lowland of the Waikato basin, northern New Zealand.
- A new qualitative precipitation reconstruction from the lowland of the Waikato basin, northern New Zealand.
- A new qualitative precipitation and temperature reconstruction from Northwestern Patagonia.
- A new quantitative fire history reconstruction from Northwestern Patagonia.
- A working hypothesis about the temporal evolution of the Southern Hemisphere mid-latitudes atmospheric circulation and its teleconnection with tropical and extra-tropical climate

1.5 Structure of the thesis

This thesis is composed of seven chapters grouped in three main sections. The first three chapters make up the introductory section. Chapter One briefly summarizes the general aims and structure of this thesis. In Chapter Two, relevant scientific literature covering the geology, physiography, climate and vegetation of New Zealand and Patagonia will be reviewed, and a brief synthesis regarding pollen-based climate reconstructions from these regions will be sketched. This chapter will also highlight the knowledge gaps and uncertainties that inform the research strategy. Chapter Three will review the methods for the stratigraphic, pollen and charcoal analyses used in this thesis, including their justification as valid methods to reconstruct vegetation and climate histories from sedimentary sequences. Chapters Four to Six comprise the results section of this thesis. Each of these three chapters will include the results and discussion of a single study site and will be structured as a full research article for publication. Finally, a synthesis chapter will summarize and integrate the main results of the previous three chapters, with reference to relevant published climate reconstructions from the Southern Hemisphere mid-latitudes and the Tropical Pacific regions, in order to evaluate the existence and extent of large-scale climate signals and their drivers. The last part of this final chapter will be dedicated to highlight and discuss some research gaps that paleo-climate investigation may address in the future.

1.6 Contributions and authorships of the thesis

I am the main author of every chapter of this thesis. I am the sole author of the three general introductory chapters (Chapter One to Three) and the final conclusion chapter (Chapter Seven). Similarly, I am the first author of the three result chapters aimed for journal publications. My contributions to this thesis include: (1) thesis research design, (2) fieldwork sediment collection, (3) analysis of all pollen and charcoal data, (4) writing and editing all chapters. My primary supervisor is Professor Rewi M. Newnham. He has contributed to this thesis in the form of: (1) reviewing and editing all chapters, (2) general guidance for data interpretation and suggested reference literature, (3) fieldwork assistance, and (4) financial support for field work, laboratory research including radiocarbon dating, and international conference attendances. My secondary supervisor is Dr. Brent Alloway. His contribution to this thesis include: (1) reviewing of Chapters Five, Six and Seven, (2) generation of geochemical data for Chapter Five and Six, and (3) general guidance concerning research planning.

Additionally, this thesis is a collaborative work between Victoria University of Wellington and Universidad de Chile. Specifically, this thesis has benefitted from the cooperation of Dr. Patricio Moreno from Universidad de Chile. His contribution has been in the form of (1) reviewing of Chapters Four and Six, (2) fieldwork assistance, (3) financial support for laboratory research and provision of laboratory facilities. Of the three result chapters aimed for journal publication, my primary supervisor will be the second author of Chapters Four and Five and third author of Chapter Six. My secondary supervisor will be third author of Chapters Five and Six. Dr. Patricio Moreno will be co-author of Chapter Four and second author of Chapter Six. Several other academics, students and university staff have provided assistance for the generation of this thesis. In the following paragraph I summarize the full authorship of each of the three result chapters aimed for publication.

Chapter Four: *Pollen-climate reconstruction from northern South Island, New Zealand (41°S) reveals varying high- and low-latitude teleconnections over the last 16,000 years.*

Ignacio A. Jara, Rewi M. Newnham, Marcus Vandergoes, Courtney Foster, David J. Lowe, Janet M. Wilmshurst, Patricio I. Moreno, James A. Renwick, Aline Homes

The collection of the pollen profile was conducted by Dr. Marcus Vandergoes and associated research team. Dr. Vandergoes has also provided the radiocarbon chronology for the site which was conducted at GNS Science, New Zealand. The stratigraphy and the plant macrofossil record presented in this chapter was the basis of the MSc thesis of Courtney Foster at University of Waikato, supervised by Professor David Lowe and Professor Newnham. The quantitative temperature reconstruction presented in this chapter was performed by Dr. Janet M. Wilmshurst from Landcare Research, New Zealand, while the plant cuticle identification and analysis was performed by Dr Aline Homes from Victoria University of Wellington.

Chapter Five: *Continuous pollen-based temperature and precipitation records of the past 14,000 years in northern New Zealand (37°S) and their linkages with low- and high-latitude atmospheric circulation*

Ignacio A. Jara, Rewi M. Newnham, Brent V. Alloway, Janet M. Wilmshurst, Andrew B. H. Rees.

The collection of this pollen profile was conducted by myself with the assistance of Professor Rewi Newnham, Professor David Lowe, Courtney Foster and Matt T. Ryan. The temperature reconstruction presented in this chapter was performed by Dr. Janet M. Wilmshurst. The radiocarbon dating was performed at the AMS facility at GNS Science. Dr. Brent Alloway conducted geochemical characterization of volcanic ash deposits.

Chapter Six: *Vegetation, fire and climate links in the Andean Nothofagus-forest of Northwestern Patagonia over the last 16,000 cal yr BP (43°S)*

Ignacio A. Jara, Patricio I. Moreno, Rewi M. Newnham, Brent A. Alloway.

The collection of the sediment section was conducted by myself with the assistance of Dr. Patricio Moreno, Dr. Brent Alloway and the field research team of Universidad de Chile. The radiocarbon dating was performed at AMS facility at University of California. Dr. Brent Alloway conducted geochemical characterization of the tephra deposits.

1.7 Publication arising from this thesis

The following publications have been produced including results from this PhD thesis:

(1) Ignacio A. Jara, Rewi M. Newnham, Marcus Vandergoes, Courtney Foster, David J. Lowe, Janet M. Wilmshurst, Patricio I. Moreno, James A. Renwick, Aline Homes. Pollen-climate reconstruction from northern South Island, New Zealand (41°S) reveals varying high- and low-latitude teleconnections over the last 16,000 years. 2015. Journal of Quaternary Science 30, 817-829

(2) Carolin Haenfling, Rewi Newnham, Andrew Rees, Ignacio Jara, Aline Homes and Beverley Clarkson. 2016. Holocene history of a raised bog, northern New Zealand, based on plant cuticles. The Holocene, 2016.

(3) Ignacio A. Jara, Rewi M. Newnham, Brent V. Alloway, Janet M. Wilmshurst, Andrew B. H. Rees. 2016. Continuous pollen-based temperature and precipitation records of the past 14,000 years in northern New Zealand (37°S) and their linkages with Southern Hemisphere atmospheric circulation. In Preparation for *The Holocene*.

(4) Ignacio A. Jara, Patricio I. Moreno, Brent V. Alloway and Rewi M. Newnham. Vegetation, fire and climate links in the Andean Nothofagus-forest of Northwestern Patagonia over the last 16,000 years. 2017. In preparation for *Quaternary Science Reviews*.

Chapter Two
Background

2.1 Overview, structure and terminology of the chapter

This thesis is a palynological investigation (i.e. the study of fossils of pollen and spores) based on two sediment sequences from New Zealand and one from Patagonia. The analysis and interpretation of these sequences involve a broad range of geological, geographic, climatological and ecological topics from these two widely separated lands in the Southern Hemisphere. Consequently, the background information presented in this chapter includes several different topics.

Beyond these introductory paragraphs, the chapter is divided into another 6 general sections that provide background information about the spatial and temporal domains in which this thesis is embedded, as well as a brief revision of the publications relevant to the research questions presented in Chapter One. Section two provides a general overview of the physiographic elements of the general study areas: the Southern Hemisphere, New Zealand and Patagonia. The third section gives an introduction to the key time frames for the thesis –the Last Glacial Maximum, the Last Termination and the Holocene period. Section four presents a brief synthesis of the general relationships between vegetation and environment with a particular emphasis on both study regions, and is followed by a brief section about the use of pollen records as a tool to reconstruct past environments. The sixth section provides a summary of the key previous palynological investigations relevant to the thesis. In the final section, the topics and considerations addressed in the previous sections are used to develop the research hypotheses that underpin this thesis.

The terminology used in this chapter is mostly intuitive and straightforward, although it is worth defining some concepts a priori. The terms low-, mid- and high-latitudes refer to the latitudinal regions around 0-30°S, 30-60°S and 60-90°S, respectively (Briggs and Smithson, 1986). “Summer” and “winter” refer to three months of austral summer (December, January and February) and austral winter (June, July and August) respectively. Similarly, the terms "tropical" and "extra tropical" refer to the regions where the latitudinal atmospheric circulation is predominantly of easterly and westerly origin respectively (Barry et al., 1992). The term "beech" is used to refer broadly to the tree genera of the Nothofagaceae family present in Chile, Argentina and New Zealand, i.e., *Fuscospora*, *Lophozonia* and *Nothofagus*, following the revision made by Heenan and Smissen (2013). The time scales using in this and all other chapters for the Quaternary period is "cal yr BP", which correspond to calendar years before AD 1950.

2.2 The physical setting

Until around 180 million years before the present, New Zealand and Patagonia were physically connected, forming the supercontinent Gondwanaland. Today, these two regions are widely separated by the Southern Pacific Ocean, yet both landmasses straddle north-south trending plate boundaries extending accross overlapping latitudinal ranges, representing two of the few continental landmasses extending southwards well into the mid-latitudes of the Southern Hemisphere. As a result of common geological histories and geographic positions, these regions feature a notable range of similar physiographic features including axial cordilleras, volcanic margins, glacial activity, westerly-dominated atmospheric circulation, and related floras. This section will briefly summarize some of these features.

2.2.1 The Southern Hemisphere

In contrast to the Northern Hemisphere, the Southern Hemisphere is predominantly oceanic with more than 90% of its total surface covered by sea water (Figure 2.1). It can be described as a series of ocean basins separated by scattered, relatively small continental landmasses which are all crossed at their southern margins by the clockwise circumpolar flow of the Southern Ocean. South from the Southern Ocean and across the South Pole sits the Antarctic continent covered by ice sheets several kilometers thick (Figure 2.1). The relative uniformity of the Southern Hemisphere geography and the pronounced thermal and pressure contrast between the low- and high-latitudes contributes to what it is perhaps the main characteristic of its atmospheric circulation: a vigorous mid-latitude westerly jetstream flowing with great zonal (latitudinal) symmetry at the surface level, known in the literature as the Southern Westerly Winds (Figure 2.1; SWW) (Hall and Visbeck, 2002). Although the core of the SWW is centered in a relative narrow band between 49-53°S, variations in the position and strength in its northern periphery influence climate patterns across the entire mid-latitude band from seasonal to decadal timescales. For instance, the SWW intensify at their core and contract southward during the summer months, whereas they weaken at their core and expand northward during the austral winter (Trenberth, 1991). This zonal variation at seasonal scales controls, to a significant extent, the latitudinal distribution of precipitation in the continental landmasses across the mid-latitudes (Garreaud 2007). At decadal timescales, a strengthening and southward migration of the SWW observed since the mid-1970s (Marshall, 2003) has been linked to warming and decreasing precipitation across the terrestrial mid-latitudes (Thompson and Solomon 2002; Gillet et al., 2006; Thompson et al., 2011).

The variability of the Southern Hemisphere atmospheric circulation results from the combined effects of different climate systems (Fogt et al., 2011). To better understand climate variability at sufficiently large spatial scales and to better predict its impacts, scientists have characterized quantifiable “modes” or “patterns” of climate variation. These modes are usually characterized by the alternation of two opposite states or polarities, and are expressed as quantifiable indexes. The Southern Annular Mode (SAM; also known as the Antarctic Oscillation) is the main mode of climate variation in the mid- and high-latitudes and explains most of the year-by-year variability in this part of the hemisphere (Thompson et al., 2000). It is defined as the difference in the sea level pressure between the mid- and the high-latitude bands, and therefore defines the relative position of the SWW belt. During the positive phase of SAM, there is a strengthening in the pressure gradient between the mid- and high-latitudes, and a concomitant poleward shift of the SWW. During the negative phase of SAM this pattern is inverted, bringing an equatorward movement of the SWW. Thus, the positive (negative) phase of SAM is associated with reduced (increased) SWW flow and overall warmer (colder) and drier (wetter) conditions over the terrestrial regions across the mid-latitudes, including most of New Zealand and western Patagonia. These variations in the position and strength of the SWW are well captured by the seasonal to decadal trends of the SAM (Thompson et al., 2000).

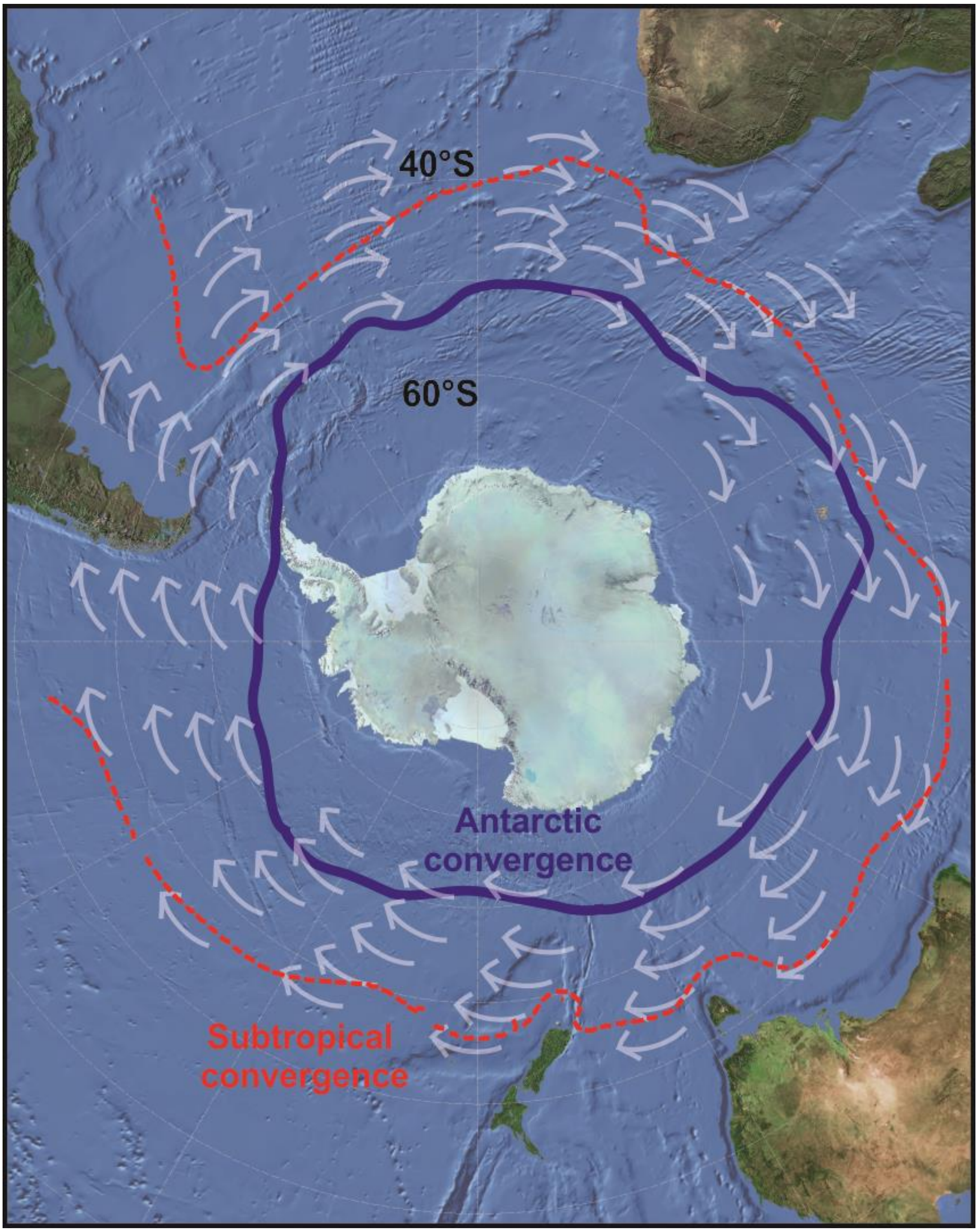

Figure 2.1 Southern Hemisphere physiographic map showing the general oceanic and atmospheric circumpolar circulation. The white arrows represent the position and direction of the Southern Westerly Winds.

Whilst the SAM represents a Southern Hemisphere phenomenon; El Niño Southern Oscillation (ENSO), probably the most important coupled ocean-atmosphere phenomenon in the world, is originated in the Tropical Pacific. Thus, it directly impacts the atmospheric circulation of the Southern Hemisphere low latitudes, but also the circulation of the mid- and high-latitudes via atmospheric teleconnections (Garreaud and Battisti, 1999). ENSO involves the weakening and strengthening of the easterly trade winds across the Tropical Pacific driven by sea surface temperature (SST) anomalies between its western and eastern margins. El Niño (La Niña) years are characterized by positive (negative) SST anomalies in the eastern and central Pacific Ocean, resulting in weaker (stronger) easterly trade winds. The natural frequency between El Niño and La Niña years is rather variable and depends on the intensity at which an ENSO event is defined. In general, anomalous El Niño events have occurred every 2-8 years during historical times (Quinn et al., 1987). ENSO has conventionally been associated with overall climate impacts of opposite signs at both margins of the Tropical Pacific Ocean (i.e. Northern Australia, Indonesia versus equatorial South America), where cooler and drier anomalies are observed in the west and wetter and warmer anomalies in the east during El Niño years. However, the influence of ENSO in the South Pacific is in most cases linked to the SAM variability, and therefore its effects might be more symmetric across the mid- and high-latitudes. For instance, El Niño years occur more commonly in association with the negative phase of the SAM, and La Niña with the positive phase (Fogt et al., 2011). Thus, climate anomalies at inter-annual scales associated with ENSO tend to be, similar to SAM-related variability, zonally symmetric and so of the same sign in the mid-latitudes. More recently, a variation of ENSO termed "Modoki" has been recognized as a SST anomaly occurring primarily in the central Pacific and producing distinctive temperature and precipitation anomalies of opposite sign compared to the conventional ENSO response in the tropics (Ashok et al 2007); yet, the relationship between ENSO-Modoki and the SAM seem not to be significantly different to the conventional ENSO (Wang and Cai, 2013), and therefore its effects on the mid- and high-latitudes might be indistinguishable from the canonical ENSO.

Superimposed on the ENSO and the SAM modes, and modulating the interaction between them, the Tropical Pacific experiences SST variations at decadal timescales characterized by temperature anomalies between the Eastern and Western Pacific ocean termed Pacific Decadal Oscillation (Mantua and Hare, 2002). These variations are not just restricted to the equatorial band as for ENSO but, rather, they are longitudinally extended into the Northern and Southern Pacific Ocean.

2.2.2 The New Zealand physical setting

2.2.2.1 Physiography

The three main islands that comprise the New Zealand archipelago (i.e. the North, South and Stewart Islands; hereafter referred simply as New Zealand) extend for about 1500 km between latitude 34-47°S and occupy an area of about 260,000 km^2 in the southwest Pacific Ocean (Figure 2.2). The New Zealand mainland archipelago is only a minor portion of a vast, mostly sunken continental platform termed *Zealandia* in which outlying island groups such as the Kermadec, Chatham and Auckland islands -located as far as 1000 km from the mainland- correspond to marginal emerged territories. The oldest rocks of New Zealand date back to Paleozoic times 500 million years ago, yet Mesozoic metamorphic sandstones form the principal continental basement. The ultimate source of these sandstones can be traced to present-day Australia and the Antarctic continent. This connection, together with the fossil evidence indicates that New Zealand was kept attached to these two continents after the initial fracture of the Gondwanaland continent. The estimated date for the final separation from Australia and Antarctica, the formation of the Zealandia continent, is about 90-80 million years ago (Kula et al., 2007).

The northeast to southwest extension of the New Zealand territory, the rugged topography with dominant north-south oriented axial cordilleras, and the active volcanism in the central North Island are all products of the tectonic setting straddling the Pacific and Australian continental plates. The activity of this tectonic margin dates back to 20 million years ago with the beginning of the Kaikoura Orogeny (Cotton, 1916), when the uplift of modern mainland New Zealand began. The general orography of New Zealand, including the mountain ranges, volcanic zones and main fault systems are all the result of this orogenic process which continues today (Suggate et al., 1978).

The glaciations of the Quaternary period (roughly occurring in last million years) represent no more than a minuscule part of New Zealand geological history, yet this most recent chapter in the country's natural history has left notable footprints in the landscape. For instance, the cyclical extension and contractions of glaciers associated with successive glaciations sculpted u-shaped valleys, produced ice-carved rocks, and large-scale moraine complexes and outwash plains in the South Island and certain parts of the North Island; whereas changes in the sea level associated with continental ice sheet fluctuations in polar regions have left prominent ocean terraces in the coastal areas of the North and the South Islands (Suggate et al., 1978). The cold and windy conditions during glacial intervals were associated with periglacial solifluction and extensive deforestation, all of which promoted erosion and aggradation processes at large scales. The result of these processes can be seen in the extensive loess formations in many parts of New Zealand, as well as in submarine aggradation terraces (Suggate et al., 1978). Finally, as subsequent sections will discuss, Pleistocene glaciations have influenced important aspects of the broad pattern of plant distribution of New Zealand (Wardle, 1983).

2.2.2.2 New Zealand climate

Lying within the domain of the Southern Westerly Winds (SWW), the climate of New Zealand is temperate with an overall continuous eastward airflow of troughs and anticlyclones (Figure 2.2; Kidson, 2000). Mean annual temperatures range from 15°C in the warmest areas of the North Island to less than 10°C at Stewart Island. The relatively small size of the territory and its insular characteristic implies low thermal contrasts from daily to inter-annual timescales compared to other bigger continental landmasses. In addition to the westerly activity, northern New Zealand extends into the subtropical circulation domain and easterly and north-easterly cyclones originated in the low-latitudes of the southwestern Pacific (associated with the position of the South Pacific

Convergence Zone) reach the territory with relative frequency, bringing warmer temperatures and convective rains to the north and east of the country (Figure 2.2; Khatep et al., 1984). However, most of mainland New Zealand territory extends into the northern boundary of the year-round influence of the SWW, and therefore temperature and precipitation regimes at seasonal timescales are largely dominated by the annual changes of their position and strength, with cold/wet winters and relatively warm/dry summers.

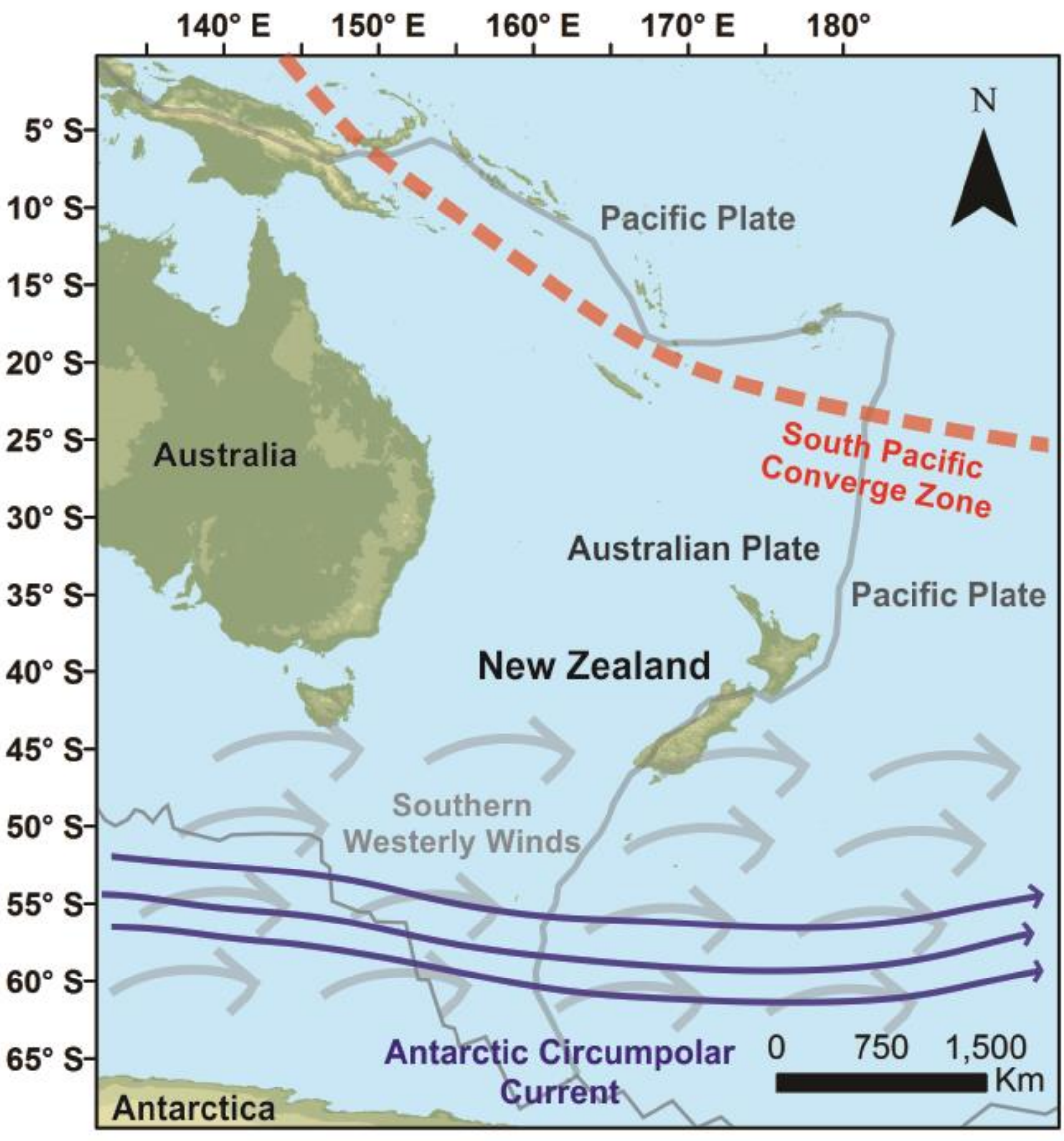

Figure 2.2 Physiographic map of mainland New Zealand with the tectonic setting and general atmospheric circulation.

The interaction of the atmospheric circulation with a rugged axial topography is responsible for a strong east-west gradient in rainfall (Salinger and Mullan, 1999). This is more pronounced in the South Island where the intersection of the SWW with the Southern Alps determines a dramatic precipitation decline from ultra-wet conditions (more than 10,000 mm/year) recorded at the west facing slopes of the Southern Alps, to the semi-dry conditions (750 mm/yr) observed at the eastern plains of Canterbury and Otago. This pattern is less pronounced in the North Island due to both a weaker SWW influence and more subdued topography, although western districts such as Taranaki, or western Waikato tend to have higher annual rainfall than eastern districts such as the Wairarapa and Hawkes Bay.

As described above, New Zealand transitional position between the Southern Hemisphere low- and high-latitudes means that climate variability is, to a large degree, explained by the atmospheric pattern outlined the Section 2.2.1. Departures from climate means, on a seasonal to an inter-annual basis, are explained by the combined effects of ENSO, SAM and the PDO (Kidson and Renwick 2002; Ummenhofer and England, 2006; Kidston et al., 2009). For instance, during El Niño years there is a relative weakening of the sub-tropical circulation over New Zealand and a more intense westerly circulation (Salinger et al., 1995). This brings overall colder temperatures to most of the country and abundant precipitation in the west-facing districts (Ummenhofer and England, 2006). The same general pattern is observed during the negative phase of the SAM. Climate anomalies in the northern and eastern parts of New Zealand are, however, less strongly influenced by the westerly flow and more affected by the circulation of the sub-tropical Pacific. Thus, the relationship between these modes of climate variation and the climate anomalies tends to be opposite to the rest of the country (Ummenhofer and England, 2006).

2.2.2.3 New Zealand native vegetation

The information about New Zealand vegetation presented here is general and limited to those aspects relevant to this thesis. A comprehensive revision of the evolution, biogeography and ecology of the New Zealand flora can be found in Cockayne (1928;

republished in 2011) and Wardle et al. (1983, 1991), whereas a concise outline of the key taxonomic groups of the main plant communities is provided in Newnham (1990). Additionally, an overview of the geological history and biogeography of the New Zealand flora is presented by Mildenhall (1980), whilst different aspects of the New Zealand and Patagonian vegetation have been compared by Schmithusen (1966) and Wardle et al. (2001). More specific and relevant regionally-oriented information about New Zealand plant communities is provided in Chapters Four and Five.

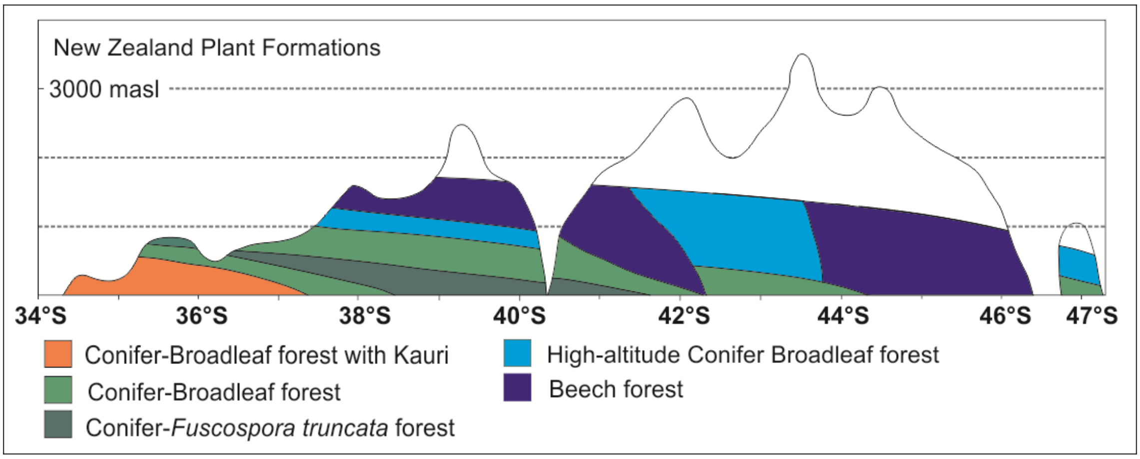

Figure 2.3 Altitudinal and latitudinal distribution of main native plant formation of New Zealand. Modified from Schmitussen (1966).

Before human colonization dated at ~750 cal yr BP (McGlone and Wilmshurst, 1999; Wilmshurst et al., 2008), New Zealand was almost completely vegetated with a highly endemic vegetation (McGlone, 1983; Figure 2.3). New Zealand flora is composed of approximately 2300 vascular species of which around 85% are endemic. The great majority of the 30 to 40 recognized endemic genera have less than 5 species, which is suggestive of a relatively recent process of expansion and diversification (Wardle et al., 1991). The core of New Zealand indigenous vegetation can be related to the floras of former Godwanaland landmasses such as New Caledonia (e.g. *Prumnopitys*), Australia (*Ackama*), Tasmania (*Cheesemania*), and Southern South America (*Gunnera, Griselinia*). Additionally, several other important floristic elements bear relationship with more recent connections with Malayo-Pacific floras such as *Parsonia* (tropical

Australia and Pacific islands), *Nestegis* (Hawai'i) or *Ascarina* (Malaysia and Polynesia*)* (Mildenhall, 1980). A lack of strong seasonal variability in temperature and precipitation dictated by an oceanic climate, relates to the fact that all forest communities of New Zealand are evergreen in nature. Two groups of native forest communities have long been discerned based on their floristic composition and spatial distribution: mixed conifer-broadleaf forest and southern beech (*Fuscospora*/*Lophozonia*) forest (Figure 2.3). The broad distribution of these forest types throughout New Zealand has been shaped primarily by spatial variability in temperature and precipitation, glaciations, and latter by human activities.

Conifer-Broadleaf forest community prevails in low- and mid-elevations of both islands, although it may extend up to mountainous terrain in the absence of beech species in some parts of the North Island and western South Island. A relatively high diversity of emergent trees, mostly conifers of the genera *Podocarpus*, *Prumnopitys*, *Dacrycarpus*, *Dacrydium* and *Phyllocladus* form the higher floristic stratum. In old-growth forest stands, these conifers are usually present in association with angiosperm trees such as *Beilschmiedia*, *Metrosideros*, *Knightia*, *Nestegis*, *Laurelia*, *Schefflera*, *Pseudopanax*, *Melicope*, and many others. Below the canopy, dense, dark interiors hold a rich ensemble of shrubs and small trees including, but not restricted to, the genera *Carpodetus*, *Myrsine*, *Pittosporum*, *Griselinia*, and several species of *Coprosma*. This forest community is also characterized by the presence of a diverse range of ferns growing either from the ground such as *Blechnum*, *Hypolepis*, *Lastreopsis*, *Polystichum* and *Pneumatopteris*, or having an epiphytic habit, such as *Asplenium*, *Pyrrosia*, *Arthropteris* and *Lygodium.* Broadleaved-conifer understory is also rich in lianas such as *Clematis*, *Freycinetia*, *Metrosideros*, *Muehlenbeckia*, *Parsonsia*, *Ripogonum*, *Rubus*, and *Passiflora*. North of 38°S, *Agathis australis* –an emergent conifer tree of the Araucariaceae family- was a primary element in lowland and montane forests (Figure 2.3), although its occurrence is now limited to smaller patches due to two centuries of human logging activities.

In the South Island the mixed broadleaved-conifer forest is restricted to the lower elevations, reduced in their floristic diversity and progressively replaced by beech forest and grassland plains in areas with colder temperatures or lower precipitation. At higher elevations and latitudes with colder temperatures, drier conditions and typically thin, impoverished soils; the floristic diversity of the sub-canopy declines progressively and beech trees become the most common elements of the canopy (Figure 2.3). In the areas where beech trees are absent, this forest community develops into alpine low forest and shrubland where cold-tolerant conifers of the genera *Phyllocladus*, *Libocedrus* and *Podocarpus* form the canopy layer and several angiosperms such as *Coprosma*, *Dracophyllum*, *Hebe*, and *Myrsine*, are present at the understory. Several of the broadleaved-conifer genera listed above are also present in the beech forest community, although the diversity of the latter community is notably lower. *Fuscospora*/*Lophozonia* species define the beech forest community as the main components of the canopy level. The five extant southern beech species (formerly ascribed as *Nothofagus* species, but after Heenan and Smissen (2013), recognized as the genera mentioned here) are all evergreen. Of the five species (i.e. *Fuscospora truncata*, *Fuscospora solandri*, *Fuscospora cliffortioides*, *Fuscospora fusca* and *Lophozonia menziesii*), *F. truncata* is the only one consistently found north of 38°S due to its demand for warm temperature and fertile soils (Figure 2.3). *F. Solandri* is commonly found in lowland to montane areas of both islands, while *L. menziesii* and *F. fusca* are more common in montane to subalpine environments. *F. cliffortioides* represents the main alpine species extending up to the arboreal limit in mountainous areas. While beech species tend to suppress other emergent trees and develop in largely even-aged stands, *Dacrydium cupressinum* is perhaps the only emergent tree that grows in association with beech species. The main genera of the understory of the Beech forest community are *Coprosma*, *Pseudopanax, Metrosideros, Elaeocarpus, Libocedrus* and *Hebe*. Hybridization among beech species is a common feature with hybrid stands of the all *Fuscospora* species being noted by early botanists (Cockayne and Allan, 1934). Interesting to note is that beech forest is absent from certain areas in the North and South Island that are well into its range of environmental tolerance (Figure 2.3). These beech gaps are located in southern North Island and in central west South Island, and may be due to the effect of glaciations and/or longer term tectonic movements (Wardle, 1988).

2.2.3 The Patagonian physical setting

2.2.3.1 Physiography

The Patagonian region (37-56°S) comprises the southernmost region of South America, including the southern territories of Argentina and Chile (Figure 2.4). Patagonia represents the only continental landmass in the Southern Hemisphere that extends beyond 50°S, with its southern-most tip lying less than 1000 km from the northern-most point of the Antarctic Peninsula. Two main physiographic regions define the Patagonian continent: (1) the tectonically-active western margin including the highly-dissected fiords on the Pacific margin and the southern portion of the Southern Andes (maximal elevation of 3700 masl); and (2) the vast, flat eastern Patagonian plains extending from the Andes to the Atlantic Ocean. A complete review of the physiographic setting of Patagonia is found in Coronato et al. (2008).

The Patagonian batholith is the dominant bedrock extending across the whole extension of Patagonia. Due to a strong denudation and erosional environment, this intrusive body is continuously being exposed and weathered across the Patagonian region. Its origin dates back to Late Paleozoic and Mesozoic times and relates to the subduction of oceanic lithosphere when the Patagonian region was part of the western margin of the Gondwanaland continent (Herve et al., 2007). This same subduction, now associated with the Nazca and Antarctic plates has been responsible for the uplift of the Andes Cordillera over the past 20 million years (Figure 2.4; Jordan et al., 2001; Ramos and Ghiglione, 2008), and for the active volcanism and seismicity observed today.

The profound impact of Quaternary glaciation on the Patagonian landscape has long been recognized and investigated by the scientific community (Caldenious, 1932; Mercer, 1976; Clapperton, 1990). During the glacial-interglacial cycles of the Quaternary, the Patagonian landscape underwent dramatic changes in extent and relief due to sea level change and glacial activity. The geomorphic footprints of the repeating ice advance and retreat from the Andes are evident today across this entire region in the form of extensive u-shaped valleys, glacial lakes, multiple moraine emplacements, erratic boulders, ice wedges, and several different types of other glacial deposits (Rabassa et al., 2005). The Northern and Southern Patagonian ice fields are the only continental ice sheets in the Southern Hemisphere outside Antarctica at present-day, yet they are only isolated remnants of what was once a continuous 1800 km-long ice sheet extending along Patagonia during the last glacial period (Hulton et al., 2002).

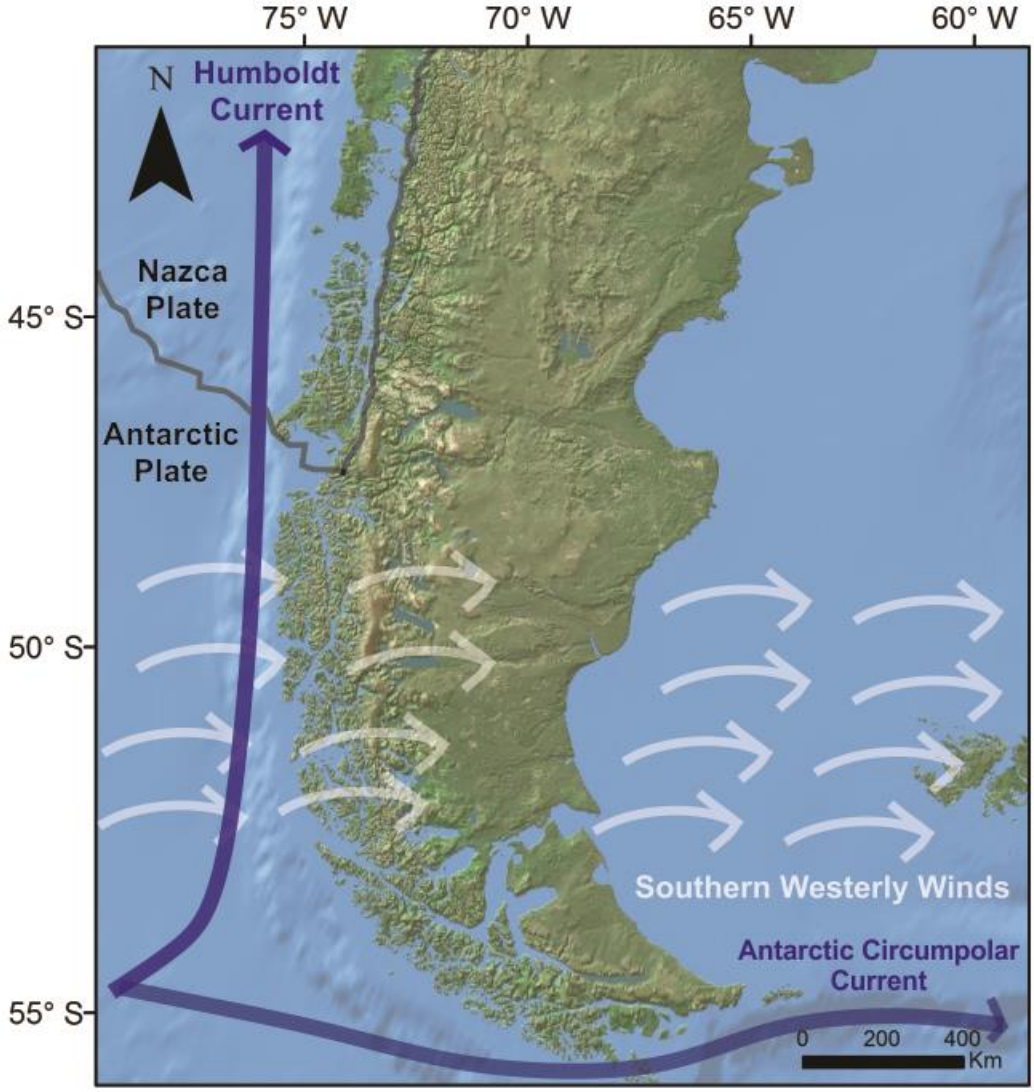

Figure 2.4 Physiographic map of the Patagonian region with tectonic setting, relief and general circulation setting.

2.2.3.2 Climate of Patagonia

The climate of Patagonia is dictated by the SWW and its intersection with the Andean relief, in a comparable fashion to the South Island of New Zealand (Garreaud et al., 2009). The influence exerted by the SWW increases towards its core, which is reflected in a rapid increase in precipitation from about 1000 mm/yr at 38°S to more than 7000 mm/yr at 50°S on the western flanks of the Andes. Although precipitation originated in the Atlantic Ocean might be significant in some parts of eastern Patagonia, there is a drastic contrast between the hyper humid conditions in the western margins and the arid conditions (200 mm*yr^{-1}) of the eastern plains. This contrast occurs in less than 100 km and it is explained by the opposite relationship between annual precipitation and the SWW intensity between western Patagonia (strongly positive) and the eastern plains (strongly negative) (Garreaud, 2007; Garreaud et al., 2013). Westward of the Andes, north of 45°S, pronounced summer precipitation minima occur as part of the seasonal cycle of the SWW (Kitzberger and Veblen, 2003). South of that latitude, precipitation is more evenly distributed thought the year. The steep relief also results in marked altitudinal gradients. The westerly fronts release abundant orographic precipitation as they traverse the mountains, thus producing an altitudinal increase in moisture; whereas temperature declines with rising altitude, resulting in the snowed peaks that characterize the Southern Andes. This strong association with the SWW and its variability is expressed by the fact that a great amount of the inter-annual variability is explained by the SAM (Aravena and Luckman, 2008). During positive phases of SAM, southward shifts of the SWW and the sub-tropical Pacific anticyclone bring a decrease in the annual precipitation through most of the western margin, whereas the opposite is observed in the eastern plains. Thus it is not surprising that the notable decrease in precipitation observed over the last few decades is a result of the persistent positive trend of the SAM (Garreaud et al 2009).

2.2.3.3 The native plant formations of Patagonia

The succinct description of Patagonian plant communities presented below is based on the formal definitions made by German geographer Josef Schmithüsen (1956) and biologist Erich Oberdorfer (1960). More in-depth descriptions may be found in Villagran (1980; 1993) and Heusser (2003).

The spatial climate trends described in the previous section define, in broad terms, the distribution, structure and composition of vegetation formations of Patagonia. The relatively moister western districts and some limited areas in the eastern flanks where the passage of precipitation fronts delivers rainfall, sustain dense, lush evergreen forest; deciduous *Nothofagus* communities dominate in drier and colder areas in the northern and southern border of Patagonia and at higher elevations. Thus, relative to New Zealand, Patagonian forest communities express adaptations that are common to the more marked seasonal fluctuation of continental climates (Wardle et al., 2001).

The eastern plains (not shown in Figure 2.5) show a rapid decrease in arboreal coverage as precipitation plummets eastwards from the Andes, resulting in the establishment of a sharp transition from *Nothofagus*/*Austrocedrus* forest to grassland communities (Iglesias, 2013).

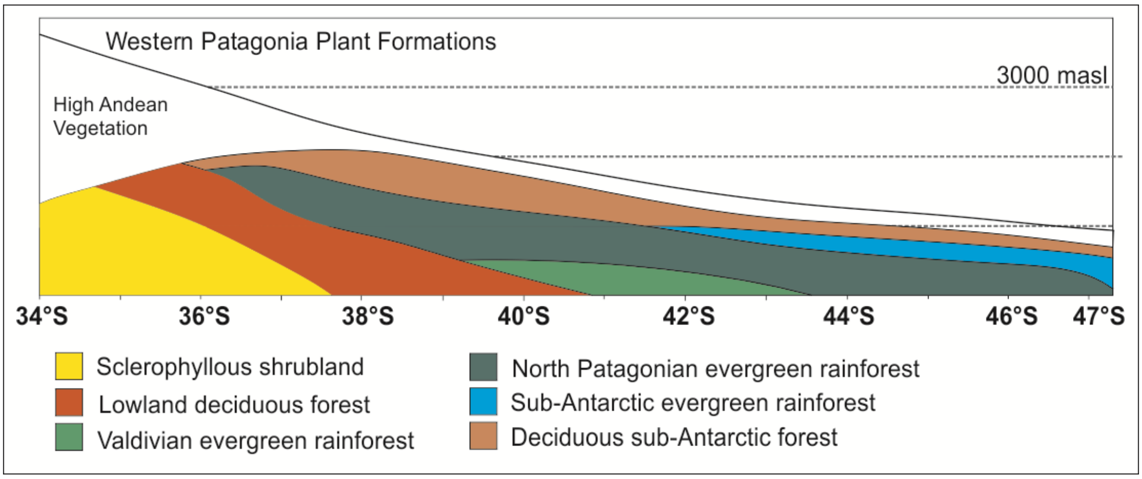

Figure 2.5 General altitudinal and latitudinal distribution of native plant formations of western Patagonia. Modified from Schmitussen (1956).

Increasing orographic rainfall and the thermal lapse rate set the stage for the transition from lowland and mid-elevation evergreen forests to high-Andean deciduous forest. The same climate gradients determine a decrease in the treeline from around 1800 masl at 38°S, to less than 600 masl at 53°S (Veblen, 1996). The general spatial distribution of the plant formations of Patagonia can, therefore, be understood as a series of vertically-stacked vegetation bands with altitudinal limits decreasing southwards (Figure 2.5; Schmithüsen, 1956). The brief sketch of the general emplacement of such plant formations presented here follows Heusser (2003). Additionally, a floristic description of the main forest communities of Northwestern Patagonia will be provided in Chapter Six.

Valdivian evergreen rainforest is the dominant forest ensemble of lowland Northern Patagonia between 40-43°S, where frosts are not common and rainfall is abundant albeit seasonally variable. This formation is characterized by the dominance of the deciduous *Nothofagus obliqua*, the broadleaf tree *Eucryphia cordifolia* and, to a lesser degree, by the evergreen *N. dombeyi*. The fact that the first two of these species are drought-tolerant relative to the latter; and the presence of sclerophyllous elements such as species from the Proteaceae family *Gevuina avellana* and *Embothrium coccineum*; indicates that this forest community is well adapted to the marked summer precipitation deficit found in northern Patagonia (Steubing et al., 1983; Veblen 1996). The highest floristic diversity of all the Patagonian forest community occurs in the Valdivian canopy and understory, which is rich in broadleaf trees, shrubs, lianas, epiphytes and ferns. Although no tree fern species are found in the understory of this or any other forest community of Patagonia, the multi-branched bamboo species *Chusquea quila* (Poaceae) is commonly found forming dense copses in forest gaps or recently disturbed areas.

The Northpatagonian evergreen rainforest replaces Valdivian rainforest at 800-1000 masl at 40°S, but this transition occurs near sea level at 43-44°S. Northpatagonian rainforest is marked by the continuous dominance of *N. dombeyi,* although in many cases in association with other emergent trees such as *N. betuloides, N. nitida, Drimys winteri, Weinmannia trichosperma* and several species of the Myrtaceae family, many of them also present in Valdivian ensembles. In general terms, these forest communities represent an impoverished version of the Valdivian rainforest, lacking the same degree of floristic diversity at the canopy and sub-canopy level. Relevant to this thesis is the presence of cold-tolerant conifers *Podocarpus nubigena* (Podocarpaceae), *Saxegothaea conspicua* (Podocarpaceae) and *Fitzroya cupressinum* (Cupressaceae).

Subantarctic evergreen rainforest replaces Northpatagonian communities in the windy and poorly drained western fiords south of 48°S. It is dominated by *Nothofagus betuloides*, *Drimys winteri* and *Tepualia stipularis* and shows a rather discontinuous distribution intermixed with Magellanean moorland communities, which dominate in water-logged soils. This latter moorland community is characterized by the presence of species adapted to extremely high precipitation and waterlogged environments and/or saturated soils, such as *Donatia fascicularis*, *Astelia pumila* and *Sphagnum magellanicum*.

A *Sub-Antarctic forest* community dominated by deciduous *Nothofagus pumilio* and *N. Antarctica* extends across most of the length of Patagonia, replacing Northpatagonian assemblages at about 1000 masl at 40°S and replacing Subantarctic evergreen communities near sea level at 52°S. This forest community generally represents the altitudinal arboreal limit in Patagonia, and therefore its distribution is more or less continuous in the Southern Andes. On the eastern slopes of the Andes, deciduous Subantarctic forest is progressively replaced by Patagonian shrub and grassland communities. This latter plant formation reaches the Atlantic coast from 44 to 54°S dominating in the predominant cold/dry climate of the eastern plains.

2.3 The temporal frame

2.3.1 The Last Glacial Maximum (26,000-18,000 cal yr BP)

The Last Glacial Maximum (LGM; equivalent to Marine Isotope Stage 2) represents a global interval of maximal ice sheet and sea ice extension, minima global sea level (~120 m below present-day) and atmospheric CO_2 concentration (100 parts per million lower than 1850 AD), and overall reduced global fire activity (Shackleton and Opdyke, 1973; Barnola et al., 1987; Denton et al., 1989; Broecker and Denton 1990; Lambeck et al., 2002; Peltier and Fairbanks, 2006; Daniau et al., 2010). This interval corresponded to the peak and culmination of the last glacial period, a phase of long-term decline in temperatures which started 120,000 years ago. The last glacial is, in turn, only the latest of a series of global fluctuations in temperature, ice extent, sea level and CO_2 that occurred over the last several hundred thousand years with a recurrence of approximately 100,000 years (Broecker and Denton 1990a).

As concluded by Huybers and Denton (2008), the LGM occurs simultaneously in both polar regions because the Northern Hemisphere summer insolation and the Southern Hemisphere summer duration are both at their minima (Figure 2.6). The extreme environmental conditions and the conspicuous evidence observed worldwide have prompted widespread interest in the LGM amongst the scientific community. In the Southern Hemisphere, the LGM was characterized by several degrees of cooling, although more pronounced in the high latitudes than in the tropics. This difference strengthened the low-to-high latitude thermal gradient, which was associated with a more intense and northward-shifted westerly circulation, extended Antarctic ice sheets and continental ice in New Zealand, Tasmania and Patagonia (Denton and Hughes, 1981; Toggweiler and Russell, 2008).

In the Southern Hemisphere low-latitudes, this period was characterized by a compression of the tropical convergence zones which caused overall colder and drier conditions, with sea surface temperature dropping between 2-3°C in tropical ocean basins (Ballantyne et al., 2005) and terrestrial temperatures dropping by 2-6°C (Farrera et al., 1999). Similarly to the Northern Hemisphere, the LGM cooling seems to be more pronounced in the high-latitudes, where annual temperatures were at least 6°C colder than present (Hulton et al., 2002). In the continental mid-latitudes of the Southern Hemisphere the LGM has been characterized as cold, dry and windy (Heusser et al., 1999; Hesse and McTainsh, 1999; Lorrey et al., 2012), although western-facing areas might have experienced an increase in precipitation as the SWW shifted northward (Kohfeld et al., 2013).

2.3.2 The Last Termination (18,000-11,000 cal yr BP)

Whereas the LGM denotes a period of extreme global conditions, the Last Termination represents a period of transition from maximum continental and oceanic ice extent, to the present-day remnants found in Antarctica, Greenland and the few continental ice caps. This transformation, occurred between 18,000-11,000 cal yr BP, has been proposed to result from a complex succession of events originated in the high-latitudes of both hemispheres and propagated across the world via ocean and atmospheric teleconnections (Denton et al., 2010). Even though the orbital changes observed during this transition were relatively gradual (Figure 2.6), the succession of events involved abrupt rearrangements of the earth systems, including the cryosphere, atmosphere, hydrosphere and biosphere. A complete and illustrative review of the paleo-climate aspects of the Last Termination has recently been presented by Denton et al. (2010). The global transition out of the LGM was marked by a series of warming pulses that were "anti-phased" between hemispheres, superimposed on a longer-term atmospheric CO_2 rise (Shakun et al., 2012). The conditions required to trigger the end of the LGM seemed to be associated with a rapid increase of the Northern Hemisphere summer insolation and Southern Hemisphere summer duration, together with expansion of the Northern Hemisphere ice sheets to an unstable extent (Raymo, 1997).

Although the precise sequence of events that occurred during the last termination is still in debate, the current understanding involve an increase in the Northern Hemisphere summer insolation as the initial driver for the last glacial-interglacial transition (Alley et al., 2002). Increased temperatures in the Northern Hemisphere high latitudes have been argued as the driver for the collapse of the Northern Hemisphere continental ice sheets and the resulting discharge of a large amount of icebergs and melt water to the Atlantic Ocean (Bond et al., 1992). During the Last Termination, at least two distinctive pulses of iceberg discharge occurred between 18,000-15,000 and 12,900-11,700 cal yr BP, known as Heinrich 1 and Younger Dryas events, respectively (Denton et al., 2010).
Bursts of icebergs into the North Atlantic sector were in turn linked to a rapid slowdown of the North Atlantic Overturning Circulation, the onset of prominent cooling phases in the Northern Hemisphere, and to rapid warming of the Southern Ocean and Antarctic region (Bard et al., 2000; Shakum et al., 2012). This sequence of anti-phased events is supported by Antarctic ice core records, which feature the onset of the Last Termination around 18,000 cal yr BP, and two rapid warming pulses that match the cooling phases recorded in the Northern Hemisphere (Figure 2.6). Critically for this thesis, Antarctic warming pulses are thought to be associated with persistent southward displacements of the SWW, and with the resulting out-gassing of CO_2 from the Southern Ocean.

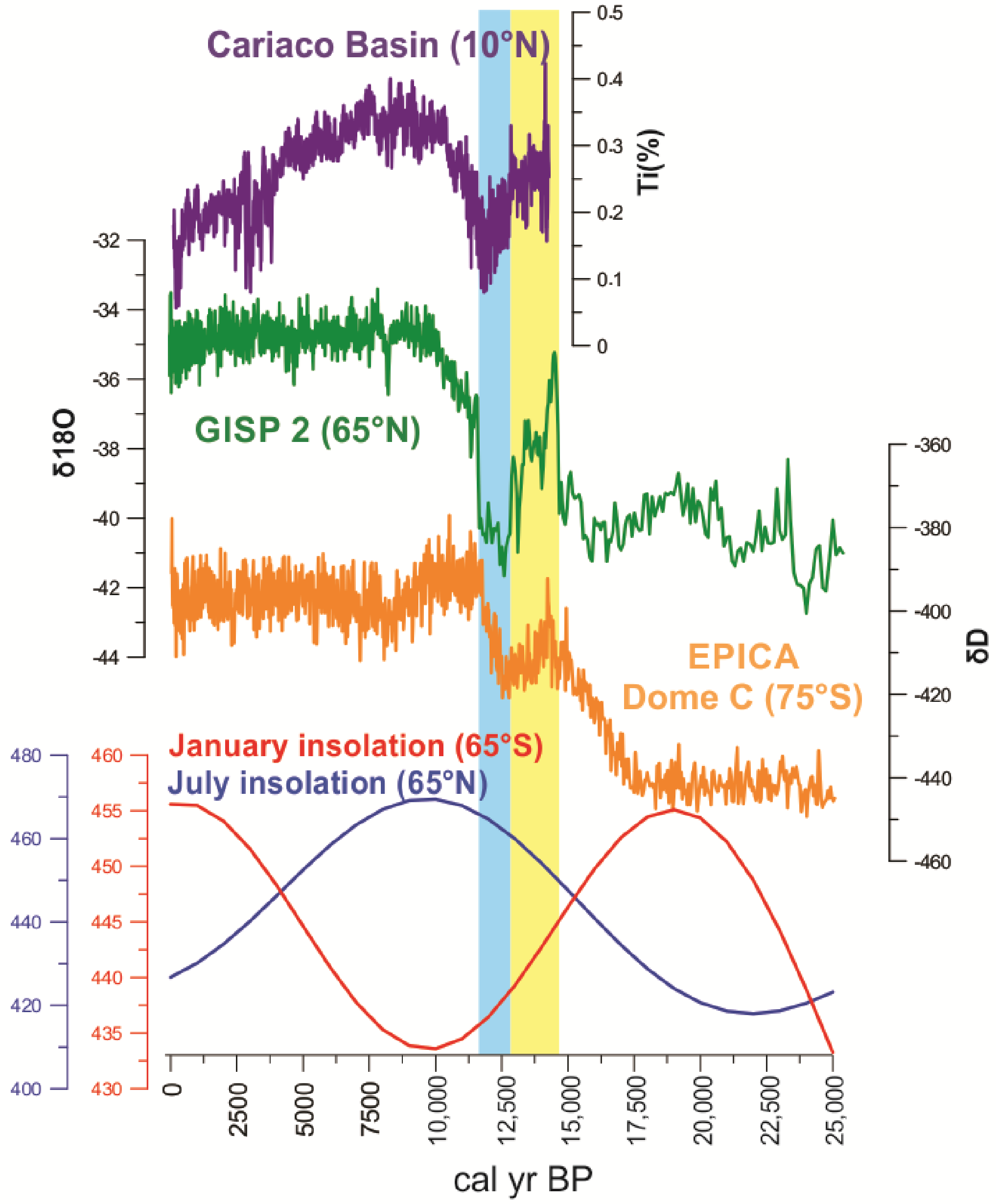

Figure 2.6 The LGM, Last Termination and the Holocene based on selected records mentioned in the text along with summer insolation variation at 65°N and 65°S. The yellow and light blue bands correspond to the Antarctic Cold Reversal and Younger Dryas climate intervals (data obtained from Haugh et al., 2001; Grootes et al., 1997 and Jouzel et al., 2007).

This mechanism has been proposed to explain the increase in global CO_2 during the Termination (Toggweiler et al., 2006; Anderson et al., 2009). A CO_2 rise of sufficient magnitude and temporal extension has been argued as the final requirement for a transition into permanent postglacial conditions (Denton et al., 2010).

In the Southern Hemisphere, the Last Termination is marked by a temperature reversion recorded in Antarctic ice cores between 14,500-12,900 cal yr BP known as the Antarctic Cold Reversal (ACR; Figure 2.6; EPICA community members, 2004). This reversal was marked by a pause in the previously rapid CO_2 rise, and by cooling in Antarctica and the Southern Hemisphere mid- and high-latitudes (Newnham et al., 2012). The Southern Hemisphere low latitudes, on the other hand, showed climate trends more in phase with the Northern Hemisphere (Pedro et al., 2015). Specifically for the ACR, a northward displacement of the ITCZ and the SWW was associated with drier conditions in the Southern Hemisphere low-latitudes and increasing precipitation in the west-facing mid-latitudes. Conversely, the two warming intervals that preceded and followed the ACR (equivalent to Heinrich 1 and Younger Dryas events in the Northern Hemisphere respectively) seem to be associated with persistent southward shifts of the ITCZ and the SWW (Muller et al., 2008; Toggweiler et al., 2006). Unlike the ACR pattern, these changes appear to correlate well with increasing precipitation in the tropical and sub-tropical regions of the Southern Hemisphere, and overall warmer and drier conditions in the west-facing mid-latitudes as shown by Denton et al (2010).

2.3.3 The Holocene period (last ~12,000 years)

Compared to large-scale reorganization of the earth system during the Last Termination, the Holocene period appears as an interval of more stable conditions worldwide. Northern (Southern) Hemisphere summer insolation shows steady decreases (increases); whereas summer duration in the Southern Hemisphere decreases (Figure 2.6; Huybers and Denton, 2008). However, significant changes in sea-level, hydrology, vegetation and fauna during this period are attested by multiple lines of proxy evidence. Interestingly, the climate system has been operating under warmer post-glacial temperatures and higher atmospheric CO_2 concentrations, background conditions that approach present-day values and that are linked to the emergence of climate variations of different magnitude and timescales, resembling more the present-day patterns of climate variations. Thus, Holocene environmental variability is undoubtedly relevant for placing the current climate change trends into more comparable paleo-climate context.

To some extent, the first part of the Holocene can be seen as a continuation of the sequence of changes that brought the earth out of the last ice age (Mackay, 2005). After the overall cold and drying conditions experienced during the Younger Dryas, the Northern Hemisphere reached a period of peak warmer conditions between 12,000-8000 cal yr BP (referred as the "Holocene Climate Optimum") early in the Holocene period. This "optimum" was characterized by an increase in precipitation in tropical areas and stronger summer monsoons in the Northern Hemisphere, probably in response to an ITCZ in a persistent northerly position (Figure 2.6; Kutzbach 1981; Haug et al., 2001). However, a short-lived cooling event is widely recorded at 8200 cal yr BP by several records in the Northern Hemisphere, and by a limited number in the Southern Hemisphere (Walker et al., 2012). This cooling is perhaps the only arguable world-wide climate event during the Holocene, which seems to have produced climate alterations that were similar, albeit at a much lower scale, than the Younger Dryas (Alley et al., 1997). The fact that this event is well constrained in ice cores and has been detected in several marine and terrestrial records worldwide, has prompted the idea of using it as a marker for the early-middle Holocene transition (Walker et al., 2012).

A northward position of the ITCZ probably caused drier conditions in the Southern Hemisphere low-latitudes at the beginning of the Holocene, as has been suggested from a weaker monsoonal activity in the Amazon Basin (Cruz et al., 2005). In the mid-latitudes, on the other hand, a summer-like structure of the SWW winds, characterized by a strengthening at its core and a weakening in its northern margin has been proposed for the early Holocene (Lamy et al., 2010). This configuration resulted in overall warmer and drier conditions in the west-facing regions of the Southern Hemisphere mid-latitudes (Fletcher and Moreno, 2011). During the latter part of the Holocene, a reversion of this pattern seemed to have progressively taken place, with a more southern position of the ITCZ and a more winter-like configuration with increasing westerly intensity over the mid-latitudes (Lamy et al., 2010). The second part of the Holocene is also known for the emergence of ENSO and SAM modes of climate variability, and the progressive establishment of their present-day frequency (Moy et al., 2002; Conroy et al., 2008; Moreno et al., 2014). Based on proxy evidence and partial historical information, well-defined temperature anomalies at centennial timescales have arguably taken place during the later part of the Holocene, the best known occurring in the last millennium and termed the Medieval Optimum and the Little Ice Age (Osborne and Briffa, 2006).

2.4 Vegetation environment relationships

Paleoecology is the field in which fossils of biological organisms are investigated to reconstruct past ecosystems. The general aim is to gain a better understanding of the long-term (longer than classic ecological timescales) environmental evolution based on documented changes in taxa in order to constrain natural responses to future scenarios of environmental change (Imbrie and Newell, 1964).

Quaternary paleoecological records have shown the profound impact of glaciations upon the environment which resulted in fundamentally changed ecosystems. These records rely on an array of fossil material; ranging from amoeboid protists (e.g. Foraminifera), to animal fossils such as beetles (Coleoptera), Chironomids (Diptera); and plant remains such as cuticles and pollen. Discounting bio-molecular markers, there are two main types of plant fossil classically used for paleoecological studies: plant macrofossils (plant remains visible to the eye) and pollen (male microgametophytes of seed plants). With sufficient botanical and ecological knowledge, plant fossils preserved in lakes and bogs represent a powerful tool to reconstruct past vegetation. Used together, pollen and macrofossils can provide a great amount of information about the past local and regional vegetation and its temporal evolution, thus providing insights into underlying environmental mechanisms and drivers.

What type of environmental variables can be investigated based on plant fossil studies?

In the following paragraphs, two critical environmental gradients that affect plant distribution in New Zealand and Patagonia are revised: climate variability and disturbance regimes. Other environmental factors, notably edaphic conditions (Clark et al., 1999), rock type (Jaffre, 1992), relief and exposition (Fontaine et al., 2007), and anthropogenic activities (Ramirez-Marcial et al., 2001) all influence the establishment and maintenance of vegetation communities. Nonetheless, their effects are spatially more limited. At a regional level, variability in temperature, effective moisture and disturbance regimes are the main driving forces behind the altitudinal and latitudinal distribution of vegetation.

2.4.1 Climate

The role of climate in controlling the pattern of distribution of living plants at global scales has been recognized since the world's vegetation classification was formalized in the 19th century. For instance, it is generally recognized that the greatest diversity in plants, from the species to the family level, occurs in the warm tropical areas (Woodward, 1987). Another general example is the poleward and upslope expansion of forest communities as a response to the sustained planetary warming observed in the last few decades (Harsch et al., 2009). Although broad, these examples are useful to have an idea of what type of changes in plant distribution could past climate variations have produced; and to conclude that paleoecologists can study vegetation changes to infer climate alterations during past ages.

One of the most relevant characteristics of New Zealand and Patagonian vegetation communities is that their composition, structure and distribution are determined in great extent by the marked climate gradients established across the rugged landscape of these two regions (see sections 2.2.2 and 2.2.3). Strong relationships between vegetation and climate occur at different taxonomic levels, from plant community to individual sensitive species; and at different spatial scales, from hemispheric to local. At the community level for instance, the transition from evergreen forest to eastern Patagonia steppe is governed by the strong west-east gradients in precipitation. At the same time, the altitudinal zonation of the Valdivian, Northpatagonian and sub Antarctic deciduous forest communities in Patagonia are a palpable example of the effects of altitudinal gradients of temperature and precipitation resulting from the intersection of the SWW with the Andes (Villagran, 1990). Similarly, the transition from broad-leaved to beech forest across New Zealand is broadly associated with an increase in the amplitude of climate variability including more frequent frosts (Wardle, 1985).

Figure 2.7. The *Fuscospora cliffortioides* treeline at 1250 masl in Nelson Lake National Park, New Zealand is an illustrative example of climate control over vegetation distribution. Photo Ignacio A. Jara.

Another illustrative example of how regional climate gradients condition vegetation distribution is the dominance of deciduous *Nothofagus* forest communities in high elevations and at the northern and southern limits of Patagonia, all areas where temperature fluctuations and summer droughts are more pronounced (Veblen, 1996). New Zealand, on the other hand, lacks the extreme seasonal variability of more extensive continents, and consequently deciduous forest communities are absent.

At the species level, distribution patterns can also be related to changes in climate conditions. For instance, within the New Zealand lowland conifer forest, *Dacrydium cupressinum* is more commonly found in moist areas with fertile soils, whereas *Prumnopitys taxifolia* and *Podocarpus* species are more common in drier areas (McGlone and Topping, 1977). Another illustrative example is the species *Ascarina lucida* with a distribution that is strongly controlled by its inability to cope with severe droughts and frosts (Martin and Ogden, 2005). In Patagonia, comparable cases are the tree species *Eucryphia cordifolia* and *Nothofagus obliqua*, which become the dominant emergent trees on the lowland forest on Northwestern Patagonia due to their relative tolerance to summer droughts (Ovington, 1983).

If the broad vegetation-climate relationships exemplified above have resulted from a long history of biogeographic processes, the vegetation of New Zealand and Patagonia is also affected by ongoing climate trends, which are clearly exemplified by the plant responses to the present-day modes of climate variation presented in section 2.2.1. Based on tree-ring chronologies, Villalba et al. (2012) have shown that the trend towards the positive phase of SAM observed during the last decades has produced a negative growth response of several tree species in Patagonia due to a significant SAM-related decline in water availability. Also in Patagonia, this same trend has been linked with widespread fires in the *Austrocedrus* forests on both western and eastern sides of the Andes (Hotz and Veblen, 2012). Interestingly, Villalba et al. (2012) show the opposite SAM relationship for two subalpine trees in New Zealand; that is, positive growth response to the current SAM trend. The authors have suggested that this latter response may due to an increase of warm and moist sub-tropical fronts. Also in New Zealand, it has been shown how the growth of *Agathis australis* in northern New Zealand is correlated with ENSO variability based on tree ring chronologies (Fowler et al., 2012), arguably associated with the growth of this species being favored by drier and sunnier summers associated with El Niño conditions in this part of the country (Ogden et al., 1992).

2.4.2 Volcanism, fires and disturbance regimes

Beyond broad climate controls, a range of disturbance agents operating at different spatial scales can influence local and regional vegetation composition and dynamics.
At shorter timescales, disturbances such as treefall gaps or stand-replacing fires affect the regeneration dynamics of forests transiently, yet plant communities exposed to frequent disturbance events may ultimately exhibit long-term changes in their composition. For instance, it has been proposed that the extensive even-aged stands of *Nothofagus* in the slopes of the Andes represent an early stage of ecological succession which is maintained by the high frequency of volcanic and seismic disturbances

(Veblen and Ashton, 1978). The lack of such disturbances at similar latitudes in the Coastal Cordillera has similarly been proposed as one of the causes for the dominance of broadleaf communities and the general absence of beech. Similarly, extensive stands of *Dacrycarpus dacrydioides* and *Dacrydium cupressinum* forest in southwestern New Zealand dominate over flat areas that are frequently disturbed by landslides and fluvial flooding (Duncan 1993). Vegetation surveys and pollen analysis have shown that forest that once surrounded eruptive centers in the North Island has been devastated by historical and prehistorical eruptions in New Zealand (McGlone et al., 1989; Wilmshurst and McGlone 1996). However, unlike the *Nothofagus* communities in Patagonia, New Zealand lacks a regional vegetation type associated with catastrophic disturbances (McGlone, 1989). In the mixed conifer-angiosperm forest of New Zealand, ecological succession after forest disturbance starts by the early colonization of herbs, ferns and mosses in case of complete forest obliteration, and by pioneering broadleaf taxa in case of partial forest destruction (Wilmshurst et al., 1997). This initial stage is usually followed by the development of angiosperm forest seedlings a few decades after the disturbance, and by mature angiosperm forest development at about 100 years after the event (Wardle, 1980). Eventually, podocarps usually replace the angiosperms trees as the main canopy emergent elements. If soils become poorer in nutrients, the forest might be replaced by wetland vegetation. In the beech forests the ecological succession is simpler since beech seedlings are usually early colonizer in disturbed forests, presenting uniform even aged stands (Newnham, 1989).

Charcoal records indicate that wildfires were a recurrent disturbance during pre-human times in New Zealand (McGlone, 1989). Unlike Australia where humans have been managing fire for al least 40,000 years, New Zealand evergreen forest communities are poorly adapted to fire (e.g. general absence of re-sprouting species), and therefore fire disturbance seems to exert a significant and more permanent impact upon forest structure and composition (Wardle et al., 1983). Forest damage or even deforestation after fire disturbances have been reported in both North and South Island, where the usual response is the replacement of forest patches by scrubland with the colonization of fast-growing woody species (e.g. *Leptospermum scoparium*, *Aristotelia serrata*) and ferns (*Pteridium* spp.) (Wardle et al., 1983; Wilmshurst et al., 1997).

Figure 2.8. Devastated even-aged stands of *Nothofagus* trees in the proximities of Volcan Chaiten (43°S) in the western slope of Patagonia are an example of the regular impact of disturbances on forest communities in Patagonia. Photo: Ignacio A. Jara

The higher abundance of fire-adapted species in the *Nothofagus* forest communities of the Patagonian Andes indicates that they are better adapted to regular wildfire disturbance (Veblen, 1996). Severe wildfires in *Nothofagus* forest in mesic and xeric areas result from the accumulation of dry fuel after periods of sustained drought. In such environments, regular anthropogenic burns have allowed the fire-adapted conifer *Austrocedrus chilensis* to expand and form a shrubland community eastwards from the Andes (Veblen and Markgraf, 1988). Other species such as *Nothofagus antarctica* are known for their ability to re-sprout after fires; whereas the bamboo *Chusquea quila*, one of the most abundant understory species in beech forests, proliferates rapidly in gaps generated by wild burns (Gonzalez et al., 2002).

2.5 Pollen records and past vegetation-climate change

Pollen bears several critical advantages for reconstructing vegetation and climate histories relative to other vegetation fossils. Pollen grains are widely produced by wind-pollinated plants and they are resistant enough (protected by an extremely strong external layer rich in the polymer *sporopollenin*) to be well preserved in the fossil record. Therefore, quantification is usually statistically robust. Also, pollen shape and size (ranging from 10-150 μm) vary greatly among the different taxonomic groups, thus providing the opportunity to recognize a great number of different taxa. Due to their microscopic size, a relatively small quantity of raw material is required to work with (Chapter Three offers a detailed description of pollen processing and analysis). Furthermore, there are a relatively high number of suitable deposition environments in New Zealand and western Patagonia because of the abundant precipitation experienced by these two regions. Critically, pollen assemblages may represent plant communities which can be, in turn, associated with particular climate or disturbance regimes. Thus, continuous sedimentary sequences such as lakes or peatbogs can provide not only a 'snapshot' of vegetation-climate relationships (some of which are highlighted in the previous sections), but also a temporal progression of those relationships. In other words, pollen records provide an opportunity to reconstruct vegetation histories and investigate putative environmental drivers and time-evolving interplays. Nonetheless, it is necessary to mention that the palynological technique also has some complications in comparison with other climate proxies. For example, differences in pollen production may lead to an inaccurate picture of the vegetation represented by a certain pollen ensemble. A notable example is the *Fuscospora* pollen in New Zealand pollen sequences, a widely dispersed pollen type that is commonly overrepresented so that in many cases masks the variability of other less abundant pollen types (Bussell, 1988).

Because of these and other advantages, palynological studies have a long history and they form an important component of Quaternary sciences. There is an extensive body of literature focusing on pollen-based paleo-environmental reconstructions, and pollen inventories support the application of this technique in many regions of the world. New Zealand and Chile are not exceptions, as palynological studies in these two regions have progressed in the last decades. The ultimate result of this is a vast literature now available. The following section discusses some of the pollen-based vegetation-climate trends from New Zealand and Patagonia that are of particular relevance to this thesis.

2.6 Palynological investigations in New Zealand and Patagonia

2.6.1 New Zealand

Palynological studies comprise the main source of information concerning Quaternary vegetation history in New Zealand (Newnham et al., 1999; Barrell et al., 2013). Pollen sequences have been used to qualitatively and quantitatively reconstruct temperature changes throughout the country (Newnham et al., 1999; Wilmshurst et al., 2007). Recent studies have focused on vegetation-climate patterns during and after the LGM, known locally as the *Late Otiran Period*. Grassland (e.g. Poaceae Asteraceae, Apiaceae) and podocarp shrubland (*Halocarpus*, *Phyllocladus*) dominated the landscape south of 38^{o}S during the *Late Otiran Period*, in analogous fashion to that observed today above the treeline (McGlone, 1995). This pattern has been interpreted as indicating the prevalence of regional cold and windy conditions (Newnham et al., 2013). The few remnant forest patches were mostly of beech forest (Newnham et al., 1989), with mixed broadleaved-conifer forest being probably confined to the northern-most areas. Reaforestation accompanied the Last Glacial Termination started by about 18,000 cal yr BP in northern New Zealand (Newnham et al., 1989; Sandiford et al., 2003) with the rise of *Dacrydium* and *Prumnopitys* forest, and by about 16,500-14,000 cal yr BP in central and southern regions with the expansion of *Fuscospora*, *Podocarpus* and *Prumnopitys* (McGlone et al., 2004). There is pollen evidence, in the form of an increase in shrub and herb pollen, of a cold episode during the Last Termination, inferred from a rapid increase in grasses and decrease in montane forest taxa recorded in northern New Zealand between 13,700-12,500 cal yr BP (Newnham and Lowe, 2000; reviewed in Barrell et al., 2013). This cooling is also recorded in sites from the South Island, which tend to show an earlier onset and closer resemblance with the timing and direction of the Antarctic Cold Reversal (McGlone et al., 2004; Vandergoes et al., 2005, 2008; Newnham et al., 2012). A second warming pulse is inferred by 12,500 cal yr BP, based on the rapid expansion of lowland and montane conifers in the northern sites (Newnham and Lowe, 2000; Hajdas et al., 2006; see also Chapter Four) and by the expansion of conifer shrubland in the southern sites.

The Holocene is regionally known as the *Aranuian* period, in which tall podocarp forest covered most of the lowlands and beech forest established in the montane to sub-alpine zones. Additionally, several records show an increase in pollen diversity and the appearance of drought and frost intolerant species, suggesting the establishment of a mild cold/wet climate with reduced seasonality between approximately 10,000-5000 cal yr BP (McGlone and Moar, 1977). There seems to be a consensus that the climate in New Zealand became increasingly variable throughout the Holocene, with cold, droughts and wildfire disturbances becoming increasingly frequent (McGlone and Moar., 1977). This is thought to be related to the impact of the climate variability associated with the present-day modes of atmospheric variation and, later, by human arrival (McGlone, 1989). Under these conditions, relatively drought tolerant taxa such as *Podocarpus*, *Prumnopitys*, *Phyllocladus* or *Agathis* showed continuous expansions in northern New Zealand (Newnham et al., 1989).

2.6.2 Patagonia

Pioneering palynological research in Patagonia started almost a century ago with work conducted by Von Post (1929), Auer (1934) and by Swedish geologist Carl Cadenius. Several analyses on radiocarbon-dated sequences revealed more details on the large-scale changes in the composition and structure of the Patagonian vegetation since the LGM (Heusser, 1984; Villagran, 1990). The integration of these pollen reconstructions and the development of highly-resolved pollen profiles have led to the recognition of a broad, coherent pattern of millennial-scale changes in vegetation and climate. Glacial chronologies and pollen-based reconstructions from northern and southern Patagonia indicate maximum continental ice extension and a temperature decline of about 6°C during the LGM (Kaplan et al., 2008; Heusser et al., 1999; Moreno et al., 1999). In the lowlands of Northern Patagonia (38-43°S), the LGM was characterized by dominance of a parkland composed of *Nothofagus* and grasses from the Poaceae and Asteraceae families; whereas Magellanic Moorland with *Astelia*, *Donatia* and *Pilgerodendron* thrived in areas with poorly-drained soils (Heusser et al., 1999). In southern Patagonia, there are no pollen sequences for this period since this area was extensively covered by ice. A reduction of at least 8°C has been inferred from sea surface temperature reconstructions from marine sediment cores off the Pacific coast (Caniupan et al., 2011), whereas precipitation was also reduced due to a northward position of the SWW (Zolitschka et al., 2013). Under this scenario, in the marginal unglaciated areas a treeless landscape with scarce vegetation is the most logical scenario.

Increases in *Nothofagus* and other thermophilous trees indicate fast reforestation in response to a warming pulse started at around 18,000-17,000 cal yr BP, which marked the regional culmination of the LGM and the onset of the Last Glacial Termination in Northern Patagonia (Denton et al., 1999; Moreno et al., 1999). The *Nothofagus* expansion in Southern Patagonia seemed to have been spatially asynchronous, with northern sites showing gradual increments between 16,000-11,000 cal yr BP, and southern sites showing a later and faster forestation between 14,000-9000 cal yr BP (Heusser 1995; Kilian and Lamy, 2012). Several sites in Northern Patagonia show a reversion of this warming/reforestation trend, recording an expansion of the cold-resistant tree *Podocarpus nubigena* between 15,000-12,500 cal yr BP (Moreno and Leon; 2003; Jara and Moreno, 2014; Pesce and Moreno, 2014). This reversion is followed by a second warming pulse by about 11,700 cal yr BP, which has been argued to represent the regional onset of the Holocene in Northern Patagonia. In this region, the early Holocene is marked by the expansion of thermophilous taxa *Eucryphia cordifolia* and *Cadcluvia paniculata* between 10,000-7500 cal yr BP. A period of sustained warm/dry conditions resulting from a southward position of the SWW is inferred from the relative summer-drought tolerance of the former species, and by peak fire activity in many records on the western side of Northern Patagonia (Abarzua and Moreno, 2008; Jara and Moreno, 2014). This period was followed by the expansion of cold-tolerant and hygrophilous taxa between 7000-5000 cal yr BP, suggesting a middle Holocene cooling trend and increase in precipitation (Abarzua and Moreno 2008; Moreno 2004). High heterogeneities characterized northern Patagonian pollen profiles after 5000 cal yr BP, showing oscillations at sub-millennial timescales (Jara and Moreno, 2012; Moreno et al., 2014).

In Patagonia, pioneering charcoal analysis showed a fire-free environment during the LGM and progressive incremental activity during the Last Termination and the Early Holocene (a review of those works is available in Heusser, 2003). Early studies on charcoal accumulation in sediments have emphasized the role of both climate and humans in modulating long-term fire trends (Heusser, 1987; Huber et al., 2004). Climate can directly influence fire activities by drying vegetation fuel or by lightning; and also indirectly through changes in vegetation type with different fire regimes (Huber and Markgraf, 2003). More recent studies on macroscopic charcoal (see Chapter Three for more detail) from western Patagonia have suggested that wildfire intensity and frequency have been modulated by millennial-scale changes in the SWW (Abarzua and Moreno, 2008). In particular, high fire activity between 11,000-9000 cal yr BP has been explained in the context of a southward/weakening of the SWW.

Despite the fact that regional fires increments coincide roughly with the reported onset of human colonization of Nonwestern Patagonia (Dillehay et al., 2008), the association of a long-term periods of frequent wildfires with the expansion of thermophilous and drought-tolerant pollen types suggest that fire activity was ultimately modulated by drought and/or warm conditions (Whitlock et al., 2007; Jara and Moreno, 2014). This interpretation is further supported by the close link between climate and historical fires in Patagonia (Kitzberger et al., 1997; Holz and Veblen, 2011). The integration of this and other studies have summarized what seems to be a coherent multi-millenial pattern of fire activity for southern South America (30°S), documented as anomalies with respect to pre-industrial values (1850 AD; Power et al., 2008). This pattern is characterized by: (1) negative anomalies between 21,000-12,000 cal yr BP; (2) positive anomalies between 12,000-7000 cal yr BP; (3) negative anomalies between 6000-3000 cal yr BP and (4) heterogeneity in regional fire activity after 3000 cal yr BP.

2.7 Synthesis, working model and research hypothesis

Despite the 8000 kilometers that separates New Zealand and Patagonia, these two regions share remarkable environmental similarities, including not only physiographic traits such as axial cordilleras, glacial and volcanic activity, and west-east climate divides, but floristic affinities at taxonomic and ecological levels. These resemblances stem from their overlapping positions in the mid-latitudes but also from shared geological and biogeographical histories. Critical for this thesis is the presence of vegetation communities with climate-driven distributions, which enable pollen-climate inferences to be made and compared. This thesis is also nourished by one notable difference between these two regions; i.e., the isolation of Patagonia from tropical and sub-tropical atmospheric circulation imposed by its continental characteristic and the presence of the Southern Andes. In New Zealand, on the other hand, there is a significant sub-tropical contribution to precipitation (Kidson & Gordon, 1986). The strong imprint of the extra-tropical westerly circulation on the climate of Patagonia is manifested, for example, in the strong correlation between rainfall and westerly intensity across the continent (Moy et al., 2009; Garreaud et al., 2013); and also in the fact that the seasonal cycle of the SWW controls the distribution of summer-drought forest formations in the northern region. In contrast, rainfall is not usually a limiting resource for New Zealand vegetation.

Since present-day spatial and temporal distribution of rainfall in New Zealand results from the interaction between sub-tropical and extra-tropical atmospheric systems, it is often difficult to identify a single atmospheric mechanism explaining the moisture trends documented in proxy records. This general disparity may explain the fact that vegetation-based reconstructions in western Patagonia have been interpreted as proxies for precipitation; whilst rainfall reconstructions in New Zealand have proved more elusive (Lorrey et al., 2012). By comparing records from New Zealand and Patagonia, the relative influence of extra-tropical (westerly) and sub-tropical (easterly) circulation systems over New Zealand can be reconstructed in time. Then the present-day climate trend might be analyzed in a longer-term perspective.

This working model will be applied in the hypotheses adopted in this thesis. In order to distinguish between the relative strength of sub-tropical and extra-tropical circulation in New Zealand, the null hypothesis is proposed as:

H_0 = *There is no difference in the timing and direction of the major pollen-based climate trends between New Zealand and Patagonia in the last 14,000 years.*

If H_0 cannot be rejected, then changes in the position and strength of the extra-tropical SWW have been the main drivers of vegetation change in New Zealand during the period stated in the hypothesis.

If, on the other hand, there is sufficient evidence to rejected H_0, then the alternative hypothesis H_1 is proposed as:

H_1 = *There are significant differences at millennial timescales between the pollen-based climate trends of New Zealand and Patagonia.*

Thus, in the cases of rejection H_0 and proving H_1, then changes in the sub-tropical (easterly) circulation have been the main drivers of vegetation change in New Zealand.

Chapter Three

Pollen and Charcoal methodology

3.1 Structure of the chapter

This chapter is divided into two general sections broadly aligned with the methodological procedure used to prepare, analyse and report pollen data (Figure 3.1). The first section focuses on taphonomic processes; that is, mechanisms behind pollen production, dispersal, deposition and preservation. In other words, this first section deals with the processes occurring from the time pollen grains are released by the source plant, to the time of sampling for palynological investigations. The second section describes the specific field and laboratory methodology applied for the sampling, preparation and analysis of the sediment samples. This section includes the various analytical procedures used to generate salient information from pollen data, but also discusses the stratigraphic and chronological analysis performed on the sediment sections from which the pollen profiles are developed. The discussion of each methodology includes background and theoretical information, along with the specific applications used throughout this thesis. For the sake of brevity, fern spores are also included in the terms "pollen" and "pollen grains". Although the term "palynology" is generally used to refer to the study of pollen and spores; for this thesis it will also include the analysis of charcoal particles.

3.2 Pollen and charcoal particles in sediment sections

Although morphological descriptions of pollen grains and investigation regarding their role in plant reproduction have been carried out for centuries; the Swedish Professor Lennart von Post (1884-1951), widely acknowledged as the founder of modern palynology, was pioneering in the use of pollen analysis both to correlate different geological strata and to reconstruct past vegetation. Further remarkable contributions to palynology were made by Wodehouse (1935), Faegri and Iversen (1950) and Ducker and Knox (1985). Altogether, these seminal investigations recognized the critical role that pollen taphonomy, site selection, and sampling strategies have all for developing investigations on fossil pollen, establishing the basis for modern palynological analysis.

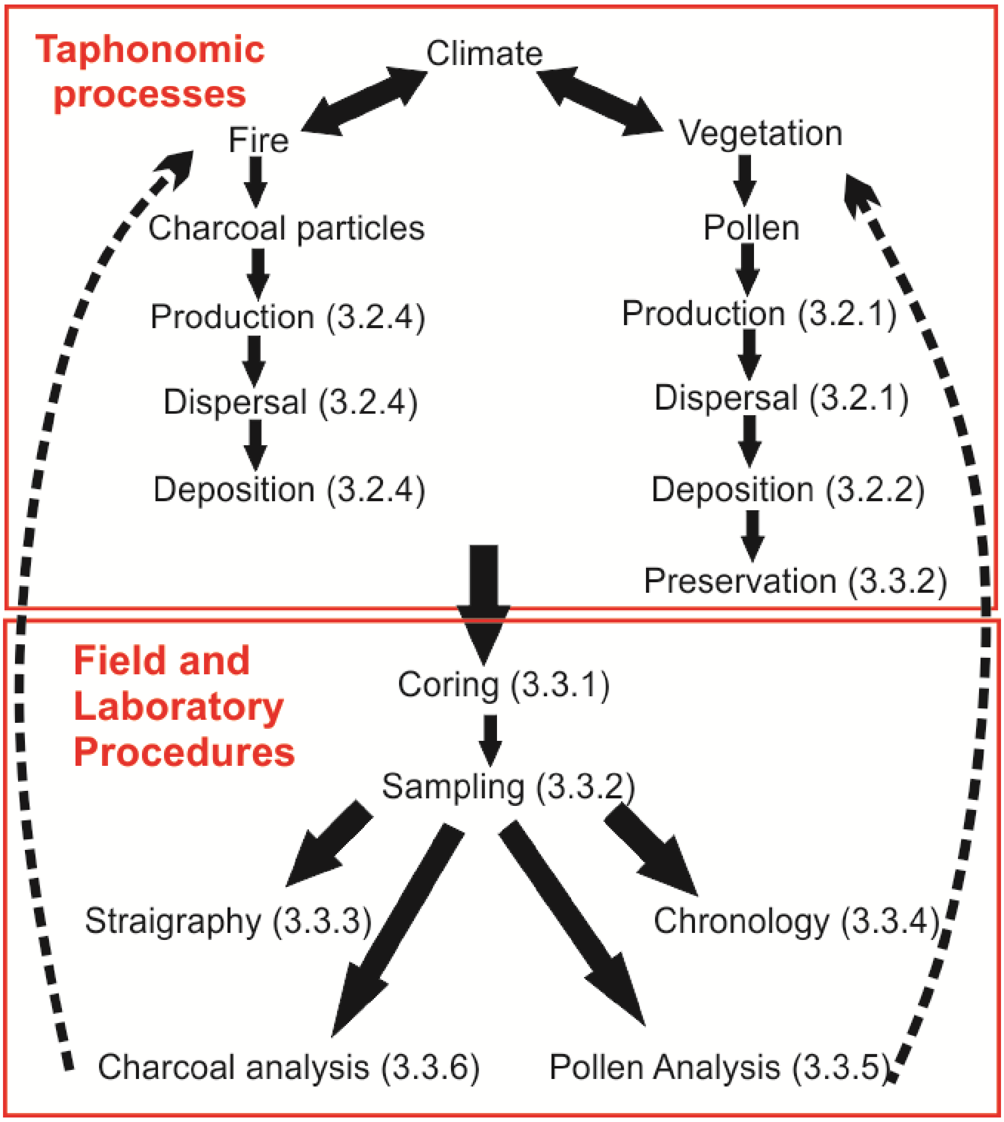

Figure 3.1 Diagram outlining the general structure of the chapter including the main sections.

3.2.1 Pollen production and dispersal

Pollen is produced by all seed-bearing plants (*spermatophytes*) as part of their reproduction cycle. Its main biological function is to transport and transfer the male genome to the female counterpart contained in the ovum. The word *palynology* (Hyde and Williams, 1940) derives from the Greek verb *palynein* which means *to spread* or *to disseminate* (Erdtman, 1969). The origin of this term makes reference to one of the most noticeable features of pollen: it is produced and released to the atmosphere in large quantities and may travel considerable distances. Pollen release by wind-pollinated (anemophilous) species is usually preferred on dry or windy days when enormous amounts of pollen can be liberated. For example, at the beginning of every boreal spring, a dense cloud of pollen dust is spread extensively over the temperate zones of Europe (Jansonius and McGregor, 1996).

A comparatively small number of pollen-producing plants are anemophilous, the great majority having adapted their reproductive systems to be pollinated by specific groups of insects (entomophily), birds (ornithophily), bats (chiropterophily). Yet, wind-pollination is an important process in pollen analysis since wind-transported pollen usually dominates both modern and fossil ensembles (Jansonius and McGregor, 1996). Additionally, pollen may be transported by water which, as discussed latter, can be a significant transport mechanism in several sedimentary sections.

Although pollen grains are initially produced in clusters of 4 (tetrads), they usually travel as individual units (monads) once released from the stamen. The distance to which wind-transported pollen grains can travel depends on a series of different variables, beginning with meteorological factors, which include wind direction, intensity and the incidence of rain; and followed by ecological factors such as the height of the plant and the density of the vegetation cover. For instance, in forest situation most of the pollen spectra belong to canopy species growing no more than 10 metres away (Kershaw and Strickland, 1990), whereas distance size from pollen source tends to increase in more open settings. In any situation, small abundances of exotic pollen grains might be observed in samples from sites located thousands of kilometres away from their original source (an example in Figure 3.2).

While anemophily is the preferred pollination mechanism amongst gymnosperms (plant producing naked seeds), the majority of angiosperms (seed enclosed by carpels) employ more specific mechanisms. Notable exceptions in the latter are families such as Poaceae, Chenopodiaceae or Cyperaceae which have adapted to be almost exclusively wind-pollinated. The transport mechanism is in many cases related to pollen morphology. For example, it has been noted that anemophilous angiosperms species tend to produce comparatively small (20-40 μm), smooth, oblate grains (Jansonius and McGregor, 1996). Pollen grains from conifers (division Pinophyta from Gymnosperms) adopt three distinctive forms: small (20 μm), spherical, unornamented grains (e.g. Cupressaseae); large (>50 μm), unornamented grains (Araucariaceae); and large grains with characteristic aerodynamic sacs (Podocarpaceae) (Kershaw and McGlone, 1995).

For the Southern Hemisphere conifers, sac-bearing (saccate) pollen grains are diagnostic of the Podocarpaceae family, where usually two, and rarely three, sacs are presented. Pollen sacs represent a conserved and distinctive trait amongst the gymnosperm family, and amongst the Pinaceae family in the Northern Hemisphere. Their development is thought to be related to the wind transport of large and heavy pollen grains, although the prevention of desiccation has also being proposed as a function (Wodehouse, 1935). In both New Zealand and Patagonia, the three canonical gymnosperm pollen shapes are present, whereas angiosperm pollen is dominated by tricolporate grains (grains with a total of 6 apertures, 3 long-narrow incisions and 3 pores).

Figure 3.2. A *Eucryphia spp*. grain observed in the sediments of Adelaide Tarn (Chapter Four) as an example of exotic pollen which source (possible Tasmania or Patagonia) is thousands of kilometres away from the study site

3.2.2 Pollen deposition and preservation

Pollen grains are usually deposited in low energy environments associated with fine silt/clay fractions. Their density is approximately 1.5 times that of the water and therefore they usually sink through the water column rapidly once they get incorporated into the water bodies of lakes or wetland (Flenley 1971). In peat-forming wetlands (mires; McGlone, 2009) pollen grains get trapped in the surface layers and then incorporated into the lower sediments as the surface vegetation continues to grow and accumulate. Once forming part of the sediment matrix, pollen grains might be removed, reworked or damaged if the lake or wetland catchment dries out or in the case of an abrupt input of lithic material. Vertical pollen movement or downward penetration of pollen-bearing sediments in lakes is usually thought to be minimal in comparison to the rate at which the sediment accumulates (Clymo and Mackay, 1987).

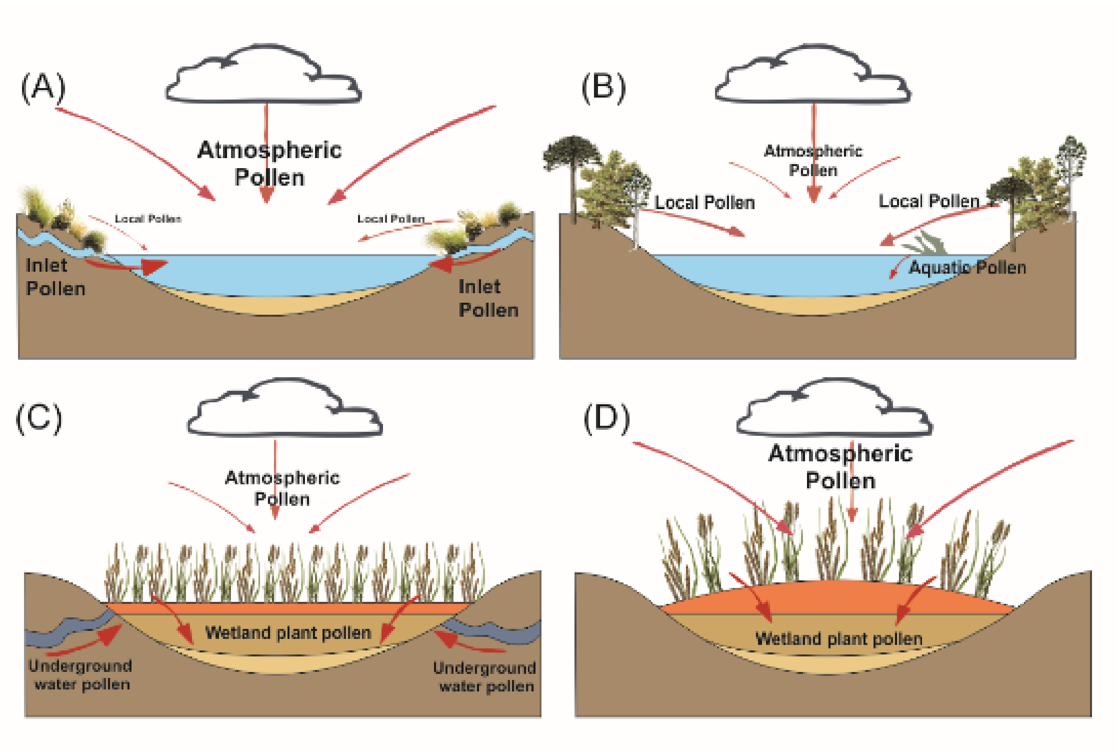

Figure 3.3. Pollen deposition in different lake and wetland environments. See text for details, modified from Tauber (1965).

In open lake basins with one or more water inlets, a significant amount of pollen arrives from soils or other washed areas of the catchment suspended in the water flow (Figure 3.3A); whilst pollen delivered from the atmosphere is maximized in enclosed basins (Figure 3.3B). Additionally, local aquatic plants might represent an important part of the fossil pollen assemblage in small shallow lakes (Zhao et al., 2006). Similarly; in mires where the water is flowing in from land drainage (minerotrophic fens), extra-local pollen transported by underground water flow might be significant (Figure 3.3C); whereas in rain-fed mires (ombrogenous bogs), most of the pollen arrives from the atmosphere (Figure 3.3D; Bunting, 2008). Pollen from local plants growing over the surface of fens and bogs represents in most cases a considerable proportion of the total pollen deposited (McGlone, 2009).

The preservation of fossil pollen in soils and sediments depends principally on the amount of sporopollenin (biological polymer resistant to degradation) contained in the exine (outer pollen wall) and the degree of anoxia that limits microbial decomposition (Jansonius and McGregor, 1996). Pollen preservation in lakes depends on the absence of major water level fluctuations that expose lacustrine sediments to the atmosphere. If lake level regression occurs, the shallowest areas of the lake will be the first to get exposed, and therefore pollen grains in these areas are more prone to degradation. In wetland areas, aerobial decomposition of pollen might be significant in the surface but highly reduced once the sediments encounter the water table, where anaerobic conditions prevail. Nonetheless, oscillations of the water table levels may cause changes in the degree of preservation (Clymo, 1965). Periods of high water table result in lower aeration and better pollen preservation; whereas decomposition and pollen deterioration is higher during periods of low water table.

The size and location of the study site will influence the provenance of the pollen which is deposited on it (Tauber 1965; Jacobson and Bradshaw, 1981; Prentice, 1985; Bunting et al., 2004). In general, small basins located amidst dense forest will not be able to capture considerable amounts of pollen carried on air currents above the canopy. In those sites, the pollen assemblage will mainly be composed of grains from local plants transported through the trunk spaces under the canopy, and from pollen of species growing at the site itself (Figure 3.3B; Moore et al., 1991). The pollen assemblage of larger basins, on the other hand, will have an important component of extra-local pollen transported in the air (Jacobson and Bradshaw, 1981). Additionally, larger lakes usually have one or more input streams, increasing the changes to incorporate water-transported pollen from different parts of the watershed (Figure 3.3A).

This thesis is based on sedimentary sequences obtained from two small (<1 km^2) lakes and a single relatively large (75 km^2) peat bog. At both lakes, sediment cores were taken at the deepest part of the basins where less sediment disturbance is expected. One of the lakes is a closed-basin (Chapter Six) and therefore the representation of local pollen is expected to be maximal. The other lake has a single inlet (Chapter Four) and therefore it should incorporate extra-local pollen. Additionally, this latter site is located at high elevation (1250 masl) and therefore it is expected to receive pollen from lowland areas (Markgraf, 1980). In the case of the bog (Chapter Five), it is an ombrogenous peatbog and therefore we expected to find a good representation of both the regional and the local vegetation growing at the site. Two of the pollen records presented in this thesis are complemented by macrofossil analyses from the same sedimentary sequence, undertaken by separate researchers (Chapters Four and Five).

3.2.3 Charcoal as an indicator of fire

Charcoal analysis in Quaternary sequences has become one of the central tools for reconstructing long-term fire histories. Charcoal particles, defined as charred pieces from the incomplete combustion of vegetal matter, are well preserved in soils, lakes and peat sediments and can be counted or measured to infer past fire regimes (Patterson et al., 1987). After Iversen (1941) pioneered the use of charcoal analysis to infer environmental changes, Wright (1974) introduced the concept of charcoal accumulation rate (CHAR; particles*cm^{-2}*yr^{-1}) to reconstruct fire frequencies. A direct link between fire scars in tree rings and peaks in CHAR in lake sediments was demonstrated by Clark (1990), and since then, CHAR has been generally accepted as a proxy for fire occurrence and biomass burnt. Nonetheless, this relationship is not always straightforward and documented fires without increments in CHAR and, conversely, CHAR peaks during fire-free intervals have both been reported (Clark, 1988). One of the underlying causes of this mismatch is that charcoal particles are not exclusively deposited as a direct result of fire events, but also from several other causes such as run-off or sediment mixing (see next section). Detecting discrete individual fires within stratigraphic sections means that processes operating at ecological timescales need to be identified from the geological archive, and therefore high sampling resolution (usually finer than typically employed for pollen analysis) is required.

3.2.4 Charcoal production, dispersal and deposition

Vegetal charcoal is generated at temperatures between 300-500 °C (Glaser et al., 2002). Although few investigations have been conducted, the amount of charcoal fragments produced during a wildfire is intuitively assumed to be proportional to the extent and intensity of the event. Additionally, the vegetation type may influence the amount and size of charcoal particles produced. For instance, particles from monocotyledon grasses can be differentiated from wooden charcoal based on the presence of parallel leaf veins and void stomatal complexes (Mustaphi and Pisaric, 2014).

Charcoal particles are primarily transported in the air and by water currents. As with pollen, the input of charcoal from water sources may be significant in catchments with one or more inlets, with evidence that charcoal particles are more abundant in sediments proximal to inlet streams than in the centre parts of the lake basin (Patterson, 1978). Water-transported charcoal might be also enhanced in specific disturbance events, for example under an extreme event of post-fire runoff (Clark, 1988).

For air-transported charcoal particles, the distance travelled is a function of the height reached by the convective air plume during fire. This plume is in turn related to the temperature reached by the fire at the ground level. In simple terms therefore, the traveling distance is proportional to the fire temperature (Patterson, 1987). Additionally, wind speed and direction at the time of, or soon after, a wildfire is probably the most relevant factor influencing the transport of charcoal particles. Charcoal deposition occurs over just a few metres from the fire perimeter (Lynch et al., 2004), yet outside of this range the final distance that a particle can be transported is inversely proportional to its size (Patterson et al., 1987). Charcoal particles >1000μm are rarely deposited outside the fire perimeter; whereas fragments between 100-1000 μm are usually deposited within the first kilometres from the combustion zone. Small charcoal fragments (5-20μm), on the other hand, can be considered as dust particles and, as such, they might be wind-transported for thousands of kilometres (Figure 3.4; Clark, 1988). Thus, when studying charcoal in sediment samples, small *microscopic* particles (<100μm) identified in pollen slides are assumed to represent both fires occurring locally and outside of the catchment area; whereas larger *macroscopic* particles (>125μm) are assumed to represent fires occurring in no more than 7 km of the site (Whitlock and Millspaugh, 1996).

Charcoal particles have high buoyancy compared to mineral clasts or pollen grains. However, this does not precludes that a particle reaching the surface of a lake or wetland becomes wet and sinks relatively fast. Big charcoal particles are more buoyant than small ones (Nichols et al., 2000). It is interesting to note that sediment reworking and re-deposition pose a special threat to charcoal analysis since this technique is based on the identification of discrete short-lived fire peaks (Figure 3.4; Patterson, 1987). While the charcoal particles deposited during or soon after a fire event are referred to as *primary* charcoal, the charcoal deposited from surface runoff or sediment mixing is termed *secondary* charcoal (Figure 3.4; Witlock and Larsen 2001). The deposition of *secondary* charcoal can take place several years after a fire event. Thus, the detection of individual fire events depends on ability to separate the primary from the secondary charcoal in a CHAR time series (Withlock and Larsen, 2001; see section 3.4.3).

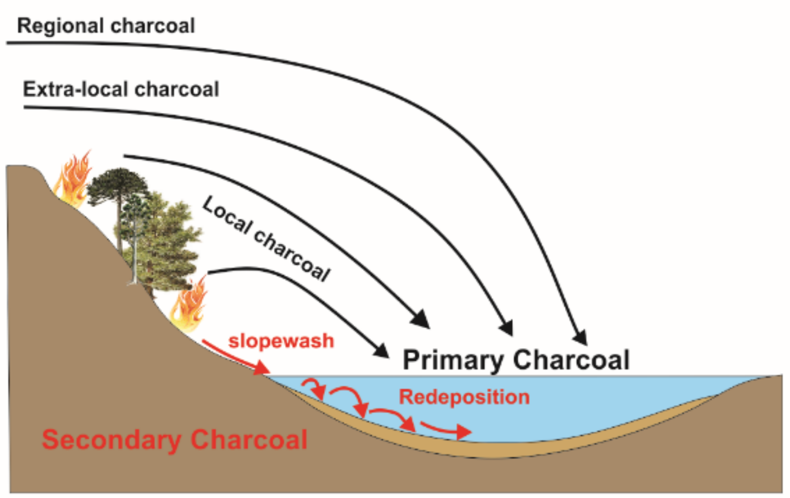

Figure 3.4. Sources of *primary* and *secondary* charcoal. Modified from Withlock and Larsen (2001).

3.3. Sediment analysis

3.3.1 Coring

A great number of field devices have been designed to penetrate sediments and obtain vertical sediment sections without disturbing the original stratigraphic integrity. The sample sections retrieved usually have a cylindrical shape and are termed “cores”.

While bogs have solid surfaces from which to obtain the cores, coring in lakes should be performed from an anchored solid platform (either a vessel or a raft), an exception being lakes located in frost environments where coring might be conducted from the frozen surface during the winter season.

A wide range of coring devices have been developed for different types of depositional environments. In general, the system must be more complex, heavier and bigger, as the depth of penetration increases. In this thesis research, two different coring systems were used.

The coring system used to extract the peat cores is the so-called *Russian Sampler* (Figure 3.5; Jowsey, 1966). This device is built around a twistable D-shape steel chamber of 50 cm length with one sharp edge and an anchor blade. The bottom extreme of the device has a conical head which facilitates the penetration of the sediments. The chamber moves downward with the anchor blade parallel to the sediment to be sampled, which are captured by rotating the chamber 180° around the blade to longitudinally cut a semi-cylinder or "D-section" of sediments. If properly operated, the sediments will be captured inside the chamber and thus withdrawn intact. Once on the surface, the chamber is twisted in the opposite direction to expose the sediment for sampling and storing. The process is repeated with extension rods applied to enable subsequent, deeper 50 cm-long core sections to be extracted (Figure 3.5). This coring system is suited for penetrating coarse, dense fibrous peat sediments. For this thesis, a Russian Sampler that takes 50 cm-long sediment D-sections was used for core retrieving at Moanatuatua peatbog (Chapter Five).

Lake sediments are usually softer than peat sediments, and in those cases the Russian corer does not always preserve the stratigraphy of the sediments in optimal form. For lacustrine sections, a Livingstone Piston Corer (Figure 3.6; Livingstone, 1955) is better suited since the sediments are not trapped by mechanical cutting but by the generation of a negative pressure inside the coring chamber. This system includes a steel tubular chamber and a running piston attached to the surface by an independent cable. A rod that runs inside the chamber ensures the piston is kept at the base during insertion so that no sediments are incorporated into the chamber. Once the chamber with the piston at its base is positioned at the initial coring depth, the internal rod is lifted and the chamber is moved down vertically to penetrate the sediments while the piston remains fixed. This action generates a negative pressure that minimises disturbance and compression of sediments during the coring process.

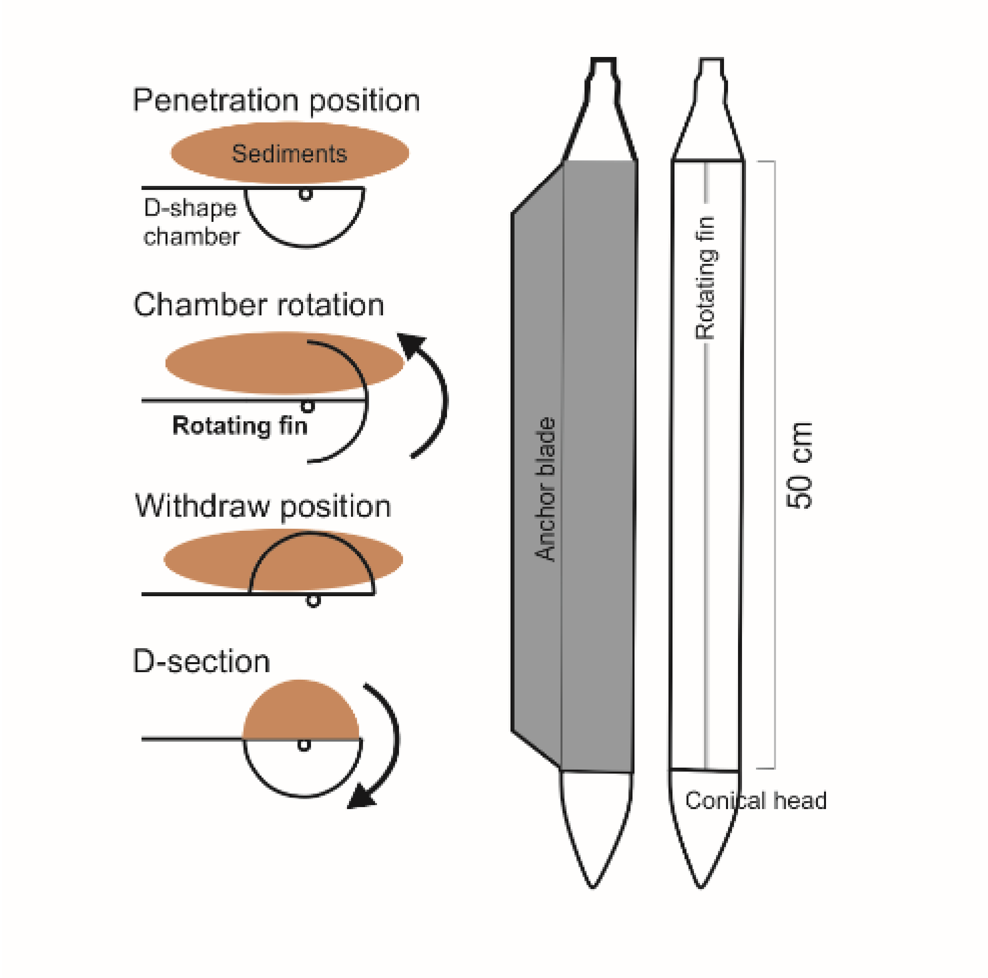

Figure 3.5. The Russian Sampler coring device. Modified from Jowsey (1966).

The penetration of sediments with a Livingston piston core ceases when the piston reaches the roof of the chamber, otherwise the corer will keep descending without capturing any more material but compressing or destroying the underlying sediments. The sediment cores are captured and maintained inside of the tubular barrel thus allowing the recovery of usually long, undisturbed tubular sections (Figure 3.6). Once at the surface, the piston is removed from the top of the chamber and the cores are extruded out of the chamber by slicing the barrel back towards the top of the internal rod. The process is repeated with extension rods applied to enable subsequent, deeper 1 m-long core sections to be extracted. With a 5-cm diameter chamber there is enough material not only for pollen analysis but also for independent samples for stratigraphic, charcoal or radiocarbon analyses. For this thesis, a square-rod Livingstone corer (Wright, 1967) of 100 cm long and 5 cm diameter was used from an anchored platform at Adelaide Tarn (Chapter Four) and Lago Espejo (Chapter Six). At both sites, a modified plastic chamber corer (100-cm long, 7.5-cm wide) with a rubber piston was used to capture the sediment-water interface and first centimetres of sediments (Schneider, 1969). These near-surface cores were sub-sampled in the field. A piston corer was also used at Moanatuatua peatbog with partial success since only half of the complete section was able to be recovered due to the dense nature of the peat sediments.

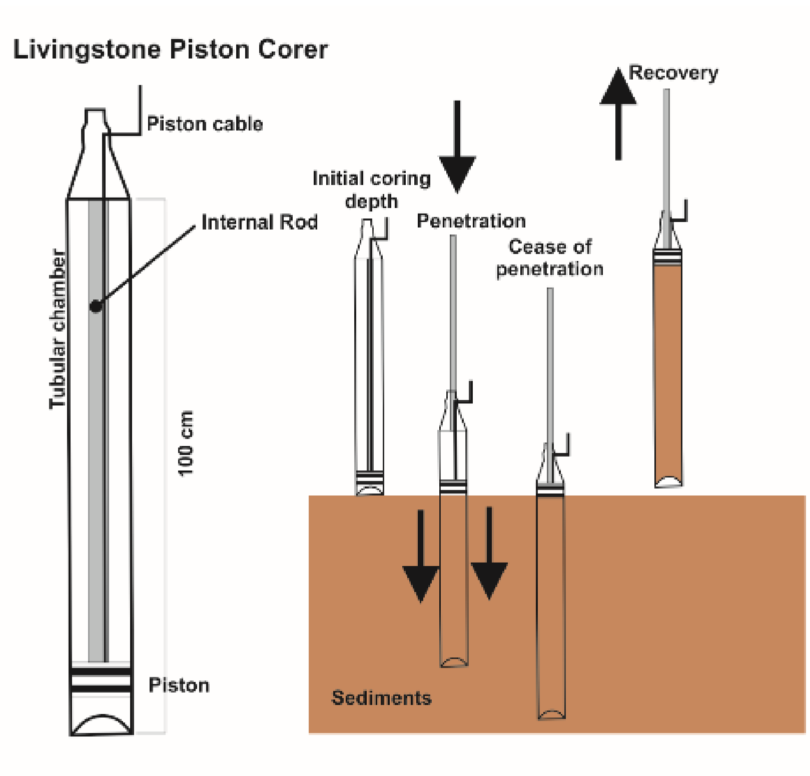

Figure 3.6. The Livingstone Piston Corer. Modified from Wright et al. (1984)

Once removed from the coring chamber, the cores from all sites were wrapped in cellophane. The cores from Moanatuatua peatbog and Adelaide Tarn were transferred to PVC pipes, whereas the cores from Lago Espejo were transferred to wooden cases. All cores were stored in refrigerated cold rooms at 4°C.

3.3.2 Sampling resolution

Choosing an appropriate sampling interval requires consideration of a number of factors including the research question and timescale, sediment accumulation rate, and the time available for research relative to the degree of detail required. To facilitate the calculation of pollen concentration and accumulation rates, an equal volume of sediment should be sampled, ideally at regular time intervals if these can be estimated. The general aim of this thesis is to detect and compare pollen changes at millennial-scale between different sites (see Chapter One), and therefore a sampling resolution between 50-100 years for pollen analysis (see section 3.3.5) was chosen to ensure detailed comparisons. This calculation was based on an estimation of the age of each section based on preliminary radiocarbon chronologies (Chapter Four and Six; see section 3.3.4) or by the use of previously reported ages (Chapter Five). The fixed sample interval that approaches the closest to the desired sample resolution for pollen analysis was preferred in order to simplify the sampling process and considering the preliminary nature of the chronologies at that time. Taking into account the original experimental design of developing two pollen records in New Zealand and compared them with a "master reference sequence" from Patagonia, and considering the 4-year duration of the research project; the priority was to perform the highest resolution for the Patagonia site. As a result, the sample resolution of the New Zealand sites was half that of the Patagonia site. The final mean sampling resolution was of 150-110 years for Adelaide Tarn (Chapter Four) and Moanatuatua (Chapter Five) in New Zealand, and 50 years in Lago Espejo (Chapter Six) in Patagonia.

Although pollen analysis was the technique chosen to achieve the main objectives of this thesis; macroscopic charcoal analysis was also used. This latter analysis was, however, limited to Lago Espejo because the development of a high-resolution charcoal stratigraphy in addition to pollen analysis for every single site was beyond the scope of a 4 years-long thesis. Lago Espejo was chosen over the two sites in New Zealand since the relationship between the climate variable aimed to be reconstructed in Patagonia (the Southern Westerly Winds) and changes in charcoal accumulation in sediment sequences is well established (Whitlock et al., 2007; Abarzua and Moreno, 2008). For macroscopic charcoal analysis of Lago Espejo, contiguous samples were taken at every centimetre throughout the sediment cores. All the samples for stratigraphic, pollen and charcoal analyses were taken at the same time in order to minimize the stratigraphic damage associated with re-opening the cores. One cubic centimetre (1cc) was taken for pollen, charcoal and stratigraphic analyses for all sites.

3.3.3 Stratigraphic documentation

3.3.3.1 Visual inspection

The basic lithological characteristics of the cores such as their length, colour, compaction, banding, and the presence of tephra or charcoal layers were noted *in-situ* in the field immediately after core retrieval, when the sediments are least disturbed. These field notes were consulted when drawing up the final stratigraphic descriptions in the laboratory. Stratigraphic columns for Adelaide Tarn (Chapter Four), Moanatuatua (Chapter Five) and Lago Espejo (Chapter Six) were developed based on the compilation and assemblage of all visual observations, and corroborated with information obtained by additional lithological analysis (see following sections). The information was then digitized and edited using the CorelDraw graphic editor.

3.3.3.2 Lost on Ignition analysis

This is a common, relatively simple, and inexpensive procedure that allows the estimation of the weight percent of organic, carbonaceous and siliciclastic content of fixed-volume sediment samples without requiring the use of chemicals (Galle and Runnels 1960; Waugh and Hill Jr, 1960). The method is based on the sequential weighting of dry samples during a series of heating pulses at different temperatures in a muffle furnace. Loss on Ignition is based on the *Differential Thermal Analysis* principle (Pask and Warmer, 1954), which states that the differences arising from weighing the samples before and after furnace heating will be a precise estimation of the amount of the fraction lost during the ignition (Heiri et al., 2001). Thus, the organic fraction will be removed from the sediments at 500-600°C, and the carbonaceous fraction at 900-1000°C. The standard procedure for estimating weight lost relative to dry samples has been described by Dean Jr. (1974). Initially, fresh samples are weighed and then dehydrated in an oven at 105°C. A second weighing after drying will provide an estimation of the water content. This is followed by heating at 550°C which oxidizes (burns) the organic content. The resulting ashes are weighed to obtain the organic content. A final ignition at 950°C will in turn oxidize the carbonate fraction. The resulting ashes contain the siliciclastic fraction unable to be burnt at such temperatures. Loss on Ignition analysis was conducted exclusively in the sediment section from Lago Espejo (Chapter Six) because: (1) the lithological analysis for Adelaide Tarn (Chapter Four) was conducted at University of Waikato as part of a parallel investigation in which grain size analysis was preferred (Foster, 2013) (see next section); and (2) the performance of Loss on Ignition has proven not to be useful to characterize the lithological variations at Moanatuatua peatbog (Chapter Five) (Gehrels, 2009).

3.3.3.3 Grain Size analysis

Grain size analysis is one of the oldest and most common sedimentological analyses for lake sediments, less so for peat sequences where minerogenic content is much smaller. The analysis is performed in order to estimate the relative abundance of different sized particles such as clays (<3.9µm), silts (3.9–60 µm) and sands (60–2000 µm) with respect to a total volume unit. The traditional measuring method includes sequential sieving for sands and gravels and hydrometry for silts and clay quantification, although laser diffraction analysis is now a widely-used method for estimation of particle size distributions in lake sediments (Beuselinck et al., 1998). This method is based on the fact that different size particles diffract light in different angles when exposed to a monochromatic beam of light (λ=750 nm). As mentioned above, this method was preferred to describe the lithology of Adelaide Tarn (Chapter Four) at University of Waikato. At Waikato, the laser diffraction method was performer by Courtney Foster using a Mavern Masterizer 2000 grain sizer after a pre-treatment with H_2O_2 to remove the organic matter (Foster, 2013). The lithology of the Moanatuatua and Lago Espejo core sections was analysed at Victoria University of Wellington and Universidad de Chile, where the facilities for grain size analysis were absent and therefore the methods described in the previous sections where preferred.

3.3.4 Chronology

3.3.4.1 The radiocarbon method

Among the various dating techniques for late Quaternary organic samples, the radiocarbon method was one of the first to be developed and it is now by far the most widely used. Radiocarbon is preferred over other dating techniques for several reasons, including its accuracy, comparatively low cost and well established methodology. A simplified description of the principles and techniques of radiocarbon dating follows, based on the information provided by Bradley (1999). A more complete review of the technique can be found in Taylor (1997) and Walker (2005).

Principles

Radiocarbon atoms (^{14}C), the least abundant of the three Carbon isotopes that occur naturally, are formed in the upper atmosphere as a result of the collision of highly-energy cosmic neutrons with atoms of Nitrogen 14 (^{14}N). Radiocarbon nuclei are rapidly oxidized to $^{14}CO_2$. The free diffusion of CO_2 throughout the atmosphere ensures a homogenous distribution around the world and therefore spatial variations of atmospheric radiocarbon are not significant. As part of the carbon cycle, $^{14}CO_2$ is incorporated into the metabolism of photosynthetic organisms. Radiocarbon atoms in organic vegetal molecules are then transferred to animals via the trophic chain. The continuous cellular replacement during the lifetime of living organisms ensure, in principle, that the amount of radiocarbon inside of their bodies remains constant and in relative balance with the atmosphere. Critically, this balance is broken from the moment a living organism dies, as new radiocarbon is no longer incorporated. The amount of radiocarbon in dead organisms will decrease at a rate which is proportional to the rate at which radiocarbon decays to ^{14}N. Since the decay rate of radiocarbon is well known, it is possible to determine, with great precision, the time of death of an organic sample based on the amount of remaining radiocarbon atoms.

Measurement of radiocarbon

The development of traditional radiocarbon principles and analysis was initiated by Libby (1946) and Anderson et al. (1947). Traditional radiocarbon measurement involved the indirect estimation of ^{14}C content by detecting and measuring the particles emitted during radiocarbon decay, in this case beta particles (high-energy electrons). A major limitation of this *decay counting* method is that, with a decay rate of about 15 particles$*min^{-1}*gr^{-1}$, it will take several days for a sample containing 1-10 gr of Carbon to achieve an analytical precision of about 80 years (Linick et al., 1989). Thus, relatively large samples and long times are required. This and other limitations were mostly overcome by the use of mass spectrometry techniques since the late 1970s (Muller, 1977). In this method, the concentration of all carbon isotopes, including ^{14}C, from an organic sample is estimated by separating them according to their different atomic masses (a complete review of the technique is found Linick et al., 1989). Thus, this technique is not based on the *indirect* estimation of radiocarbon content via beta particle counting, but on the *direct* measurement of the total amount of radiocarbon. Apart from requiring significantly smaller samples (1 mg of Carbon after sample cleaning is sufficient to obtain a precision of about 50 years), results using this method are produced more rapidly (the age determination take about one hour on a mass spectrometer). Both techniques are, however, limited by the contamination with background radiocarbon content, which limits precise measurements of samples to those older than approximately 50,000 years in age. For this thesis, all radiocarbon samples were conducted with the Accelerator Mass Spectrometer method.

Radiocarbon samples from all sites were taken individually from the sediment cores with a metallic spatula and tweezers, and subsequently dehydrated overnight in an oven at 80°C. For Adelaide Tarn, leaf, twig and root fragments were sampled and submitted for dating. Samples from Moanatuatua peatbog included all of the above plus wood material. The sediment section of Lago Espejo lacked plant macrofossil remains and therefore 1 cubic centimetre of bulk sediment was sampled and dated. The total number of radiocarbon dates submitted was 16 for Adelaide Tarn, 13 for Moanatuatua peatbog, and 13 for Lago Espejo. The criteria for the resolution of radiocarbon analysis was that ages of the main pollen transitions were constrained by at least one radiocarbon date; however funding availability was another factor. Approximately one radiocarbon date every 1000 years was the average radiocarbon resolution for Adelaide Tarn and Moanatuatua peatbog. In Lago Espejo the radiocarbon resolution was of about 1200 years, since the record presented a lower number of pollen transitions to constrain. For the Adelaide Tarn and Moanatuatua peatbog samples, AMS radiocarbon analysis was conducted in the Rafter Radiocarbon Laboratory at GNS, Lower Hutt, New Zealand. For Lago Espejo samples, AMS radiocarbon analysis was conducted in the Keck Carbon Cycle Accelerator Mass Spectrometry Laboratory at University of California, Irvine, United States.

Radiocarbon calibration

If the ^{14}C content in the atmosphere has remained constant through time, and if no nuclear bomb tests had occurred; then all radiocarbon dates could be directly translated into the calendar timescale. Unfortunately, high-resolution radiocarbon chronologies of annual tree-rings demonstrated the discrepancies between these two timescales, and therefore radiocarbon ages have to be converted or “calibrated” rather than simply translated into the calendar time frame (Reimer, 2009). Changes in the atmospheric concentration of radiocarbon over time arises from a variety of processes, including variations in radiocarbon production in the upper atmosphere due to variable cosmic ray flux, changes in the exchange rate of carbon between different geological reservoirs, and variation in the rates of carbon exchange between the biosphere, the hydrosphere and the atmosphere. In combination, these factors produce different radiocarbon concentrations in marine and terrestrial environments, as well as inter-hemispheric differences (Hogg et al., 2002). As a result, different calibration curves have been developed to deal with these variations. The relationship between the radiocarbon and the calendar timescales is rather complex, and therefore radiocarbon calibration - unlike the symmetric error of radiocarbon content estimations - may deliver asymmetric, multi-peak calendar ranges. For this thesis all radiocarbon ages were calibrated. Calendar ages are reported either as 95% confident ranges or two standard deviation ranges, with calendar year before the present (AD 1950) as temporal unit (cal yr BP) (see section 3.3.4.3). The weighted mean of those ranges is used as the ages scale for plotting purposes. For this thesis, the Southern Hemisphere “Cal13” curve, a calibration curve designed for terrestrial samples from the Southern Hemisphere, was used for the calibration of all ages at Adelaide Tarn and Moanatuatua (Hogg et al., 2013); whereas the IntCal13 was preferred for samples older than ^{14}C 11,000 years at Lago Espejo following the recommendation of Dr. Patricio Moreno.

3.3.4.2 Tephrochronology

Tephra deposits are generated as a result of the injection of pyroclastic material to the atmosphere during explosive volcanic eruptions (Alloway et al., 2013). Tephra layers offer several advantages through their use as chrono-stratigraphic markers. First, they are usually easily recognized in soil, lake or peat sediment sections (although some of them might be invisible to the naked eye in which case they are termed “cryptotephras”). Second, tephras are deposited instantaneously in relationship to geologic timescales, and therefore they can be seen as markers for an instant event (isochronous). Third, volcanic ashes are usually deposited over a wide area, thus facilitating inter-site correlations (Westgate and Gorton, 1981; Alloway et al., 2013). The two regions studied for this thesis, Chile and New Zealand, are both active volcanic areas (see Chapter Two); hence, they are prime locations for tephra studies. No tephra layers were detected in the Adelaide Tarn sediment section, but tephrochronological analysis was performed at Moanatuatua peatbog (Chapter Five) and Lago Espejo (Chapter Six). At both sites, the analysis was based on a geochemical characterization of the tephra layers and comparison with reference samples of known provenance and age. This analysis was conducted by Dr. Brent Alloway at Victoria University of Wellington, New Zealand. The methodology for geochemical fingerprinting included the sampling of tephra material and the isolation of individual glass shards. Major elements, including Silica (SiO_2), Aluminum oxide (Al_2O_3), Titanium oxide (TiO_2) and several others were determined using a JEOL Superprobe (JXA-8230) with the ZAF correction method (for more detailed see Boekestein et al., 1983). More Details regarding these analyses can be found in the Appendices Two and Three.

3.3.4.3. Age-depth modelling

Due to costs and other constraints, only a limited number of levels in a sedimentary sequence can be dated in any given project. Thus, the relationship between the sediment depth and age needs to be assessed through the construction of an age-depth model “anchored” with the dated horizons. Age-depth models provide maximal and minimal ages for the section, as well as an estimation for the age of every depth. This latter variable allows the calculation of an estimated sedimentation rate ($cm*year^{-1}$), a requirement for pollen accumulation rate calculations (see section 3.3.5.3). There are several different approaches to construct an age model based on radiocarbon chronologies, ranging from simple linear interpolations to complex Bayesian modelling. In each case, the researcher will rely on at least one, and usually more than one, assumption. For example, linear interpolation models rely on the assumption that the accumulation rate changes at the exact position of the dated levels; whereas smoothed spline models assume the absence of abrupt sediment disturbances, a reasonable statement in relatively stable depositional systems such as lakes or mires.

Bayesian age modelling was chosen for all the three study sites presented in this thesis. The reasons behind the selection of this method is that it arguable has advantages over other more “classical” approaches, including a more secure statistical framework where assumptions are explicitly stated and uncertainties reduced. As a result, these types of models are now widely applied in Quaternary studies (Blaauw et al., 2007; Ramsey, 2009). Specifically, we used the Bayesian approach developed by Blaauw and Christen (2011) which includes the software Bacon operated via the R platform. Thus, the discussion in this section will be limited to this type of age modelling. It is important to note that such discussion is limited to the general concepts behind the method. A formal mathematical explanation regarding the application of Bayesian statistics to radiocarbon age modelling is provided in Ramsey (2009).

As discussed in section 3.3.4.1, radiocarbon calibration is a complex procedure that generates asymmetric (as opposed to normally distributed) calendar probability ranges. Bayesian age modelling is based on the assertion that models constructed from mathematical regressions that depend on symmetric error distribution are unsatisfactory (Ramsey 2009; Blaauw, 2010). Bayesian age modelling deals with this problem by using the entire calendar probability ranges of all dated levels simultaneously (Blaauw and Christen, 2005). In simple terms, the procedure consists in selecting a single year from each of calendar ranges of the dated level, to then draw an age-depth model (e.g. smooth splines) that intersect all dated levels. By randomly selecting new sets of single years from the dated calendar ranges over multiple times, Bayesian modelling generates a “cloud” of many and sometimes overlapped age models (Blaauw 2010). The underlying assumption of this type of modelling is that, even though the precise year within the calendar range of each dated level will never be known, a trustworthy approximation can be drawn from the generation of a great number of models. Thus, by using the calendar ranges of the dated levels the Bayesian approach provides a (modelled) calendar probability range for all depths of the section. Understandably, the probability of each individual model as a whole will be related to the sum of the probability of the individual calendar years from the dated levels that such model intersects. Additionally, prior assumptions about the depths and the order of deposition can be made (Bronk and Ramsey, 2007). Since a single “best” age for each depth needs to be used for plotting pollen and charcoal data, Bayesian modelling software is able to calculate both the median and weighted mean of modelled calendar age ranges.

3.4. Pollen analysis

3.4.1 Pollen processing

The physical and chemical preparation of the pollen samples is referred to palynologists as *processing* and has the final goal of concentrating pollen grains from each sediment sample. To achieve this, pollen processing consists of treatments which aim to remove all the rest of the components of a sediment sample. In simple terms, a series of different treatments are conducted in order to remove specific fractions. After every step centrifugation separates the pollen-enriched fraction deposited in the bottom from the liquid pollen-deprived fraction which is removed by decantation. Key textbooks describing in detail the standard procedure for pollen processing are Faegri and Iversen (1989) and Moore et al. (1991). Although modifications in the order of processing steps might take place depending on the different sediment characteristic or based on the preference of the researcher or laboratory technician, the following basic steps are described in the order used in this thesis:

- Potassium Hydroxide (KOH) digestion. Soaking the samples with a solution of KOH breaks the organic matrix of the sediments apart and dissolves the humic acids, a process usually referred as *deflocculation*. For this thesis, Potassium Hydroxide (KOH) at a concentration of 10% was added, followed by placing the samples in a boiling bath at 80°C for 15-20 min.
- Sieving. Samples are poured through a sieve mesh of around 100-125 µm, allowing pollen grains that pass through to be separated from larger particles. Samples might be submerged in an ultrasound tank to break apart small agglomerations frequently present in samples rich in fine-grained material (Owen, 1990). This was the case of the samples from the basal portion of the Lago Espejo sediment section (Chapter Six).
- Hydrochloric acid (HCl) treatment. This treatment is used to dissolve the carbonate fraction. It is especially useful in carbonaceous sediments such as tufa or lake marls. The standard procedure consists of adding 5-10 ml of 10% HCl to

the samples which are then placed in a boiling bath for 5 minutes. The presence of carbonates is indicated by fizzing due to the production of carbon dioxide. This treatment is also used to dissolve the *Lycopodium* tracer tablets (contained in sodium bicarbonate medium) used to calculate pollen concentration.

- Hydrofluoric acid (HF) treatment. A concentrated solution (30-40%) of this extremely corrosive chemical is applied to the samples to dissolve the silica fraction. The samples are placed in an 80°C boiling bath to accelerate the dilution. Boiling times vary depending upon silica content. For this thesis, all samples were boiled for one hour. Direct HF exposure to the skin or fume inhalation are extremely toxic and therefore alternative treatments such as density separation are sometimes preferred. After the treatment with HF, the samples should be washed with a less concentrated acid such as HCl 10% or acetic acid to remove the silicofluorides generated in the HF reaction. For this thesis, HF was used in lake sediments (Chapter Four and Six) but not for the peat samples, which had limited silica content (Chapter Five).
- Acetolysis reaction. This treatment consists of an acid hydrolysis reaction that removes the cellulose matrix of the organic fraction. For this, sulphuric acid (95-97%) and acetic anhydride are used in a proportion of 1:9. These components react explosively to the exposure of water thus pollen samples need to be previously dehydrated with, for example, glacial acetic acid. Acetolysis reaction usually leaves pollen grains with a yellowish stained colour which aids in their identification.
- Silicon oil mounting. Unlike other widely used mounting media such as glycerine jelly, silicon oils behaves as a dense liquid and thus mounted pollen grains can be moved and rotated under the microscope. For this reason silicon oil was the preferred mounting medium for this thesis. A minor disadvantage is that pollen slides tend to last less time in comparison with other mounting media because the oil media tend to drains out of the sample. Dehydration of the samples is required in order to prevent irreversible clumping because silicon oil is highly hydrophilic. For dehydration, the use of an alcohol such as tert-Butyl alcohol is the standard procedure and the procedure used in this thesis.

3.4.2 Pollen identification and counting

The pollen counted in a pollen slide is assumed to represent an unbiased subgroup of the total pollen content of the sediment sample as long as a significant number of pollen grains are counted (ideally over 300 grains) (Birks and Gordon, 1985). The analysis of fossil pollen is performed under an optical microscope with a magnification that ranges from 400 to 1000 times. Pollen identification in fossil samples is based on comparison with reference samples or published pollen catalogues. The process consists of assigning a pollen grain to a previously-documented pollen category or taxon. Both quantitative (e.g. size, number of apertures) and qualitative (e.g. smooth or rugged surface, oval or rounded shape) characteristics are used for identification. Nevertheless, there are always a certain number of pollen grains that cannot be classified into any pre-existing category. In those cases, a distinction is made between *unknown* grains, referred to grains whose identification was prevented because no known category matches their features; and *unidentified* grains, whose identification was prevented because of their damage or deterioration.

Regarding this thesis, pollen identification was assisted by pollen catalogues of Moar (1993) and Newnham (unpublished reference material) for the New Zealand sites, and by the catalogue published by Heusser (1971) for the Patagonian site. The taxonomic resolution ranged from family (e.g. Poaceae; Chapter Six) to species (e.g. *Podocarpus nubigena*; Chapter Six) level. Pollen identification in the New Zealand sites (Chapter Four and Chapter Five) was facilitated by the fact that New Zealand flora shows a relatively high number of monospecific genera. The identification of conifers posed a special challenge in both study regions since there is little morphological variation among different species belonging to the families Podocarpaceae (Chapter Five) and Cuppressaceae (Chapter Six). The relatively large size of podocarp pollen made them prone to deterioration at Moanatuatua (Chapter Five). In this case, broader morphological groups were made. For example, "*Prumnopitys*/*Podocarpus*" grouped all the species of these genera into a single category (see Chapter Five for a more detailed discussion).

3.4.3 Pollen percentages

Pollen percentages are a means of conveying the relative variation of one pollen taxon with respect to all the others, thus reducing the distortion arising for counting different totals of pollen grains at each sample. The percentage is established as a proportion of some pollen sum (e.g. total terrestrial pollen). In this case, the palynologist has to decide which pollen types are going to be included in the pollen sum. There are different criteria in the palynology literature, yet the most accepted one is that pollen types belonging to the same ecological group should be included in an independent sum. For example, wetland pollen types reflecting local vegetation should be included in a different sum than terrestrial pollen in a peatbog record (Birks and Gordon, 1985).

3.4.4 Pollen concentration and influx

A limitation of percentage values is that they are not absolute frequency data, and therefore the change of one pollen taxon will, in most cases, alter the abundances of all the others so that the total percentage sum is maintained equal (Birks and Gordon, 1985). Interdependence of percentage data also limits statistical analysis. To overcome this problem, absolute data can be calculated in palynological studies in the form of the total number of pollen per volume unit of sediment (concentration) or the total number of pollen deposited per unit area per unit time (accumulation rate). The calculation of these variables requires the addition of a known number of exotic microscopic markers during pollen processing (section 3.3.5.1). Pollen accumulation rate further requires the sediment depositional times provided by the age-depth model (section 3.4.3), which gives this variable independence with respect to changes in the sediment accumulation rate (Birks and Gordon, 1985).

3.4.5 Pollen diagrams

After the calculation of the percentage, concentration and accumulation rate, pollen data should be expressed in a simple and unambiguous graphical way. The first pollen diagram might have been presented in the original publication of Von Post (1929), although subsequent changes have been made in order to simplify data presentation. The standard modern pollen diagram depicts the desired number of pollen taxa in non-overlapping columns with independent X axes. All taxa are plotted in relationship to the section depth or age as the Y axis (Faegri and Iversen, 1975). Hence, values of taxa located at the same stratigraphic level will form a horizontal line. The abundance values can be drawn either as single points (which form a polygon when joint) or as bar histograms (Birks and Gordon, 1985). The order of taxa in the diagram follows ecological criteria, according to the vegetation community to which they belong. The pollen records of the three sites analysed in this thesis were plotted as *resolved* diagrams according the distinction made by Birks and Gordon (1985).

3.4.6 Pollen zonation

Pollen diagrams with a great number of samples are usually subdivided into a series of formal units or zones which help not only to summarize the record, but also to perform a more structured description of the pollen sequence and to compare a specific section with others from different sites (Faegri and Iversen, 1975). The major zones of the record can be demarked by a visual identification of the depths at which the main pollen changes took place, although most of the time quantitative methods are used. For this thesis, all pollen sequences were initially zonated by a visual inspection of the diagrams, and subsequently complemented by statistical ordinations.

For pollen data from sediment sections, a statistical ordination that takes account of the stratigraphic order of the record (termed stratigraphically-constrained) is required; otherwise samples that have similar composition but are far apart in the stratigraphy might be grouped together, thus generating zones that lack any stratigraphic integrity. The stratigraphically-constrained ordination implemented in all the sequences of this thesis is based on a cluster analysis termed Constrained Incremental Sum of Squares (CONISS, Grimm 1987). CONISS is an agglomerative method that operates based on the identification of the most similar adjacent samples and merges them together to create a first cluster of samples. This process is then successively repeated so that all samples are eventually amalgamated to form a single cluster. At each step, the merging that gives the least increase of the dispersion (variance) within-clusters is preferred followed the Incremental Sum of Squares principle (Ward Jr, 1963). For optimal merging following this principle, CONISS generates a dissimilarity matrix of Square Euclidian Distances between all samples (Grimm, 1987). At the end, a cluster tree termed “dendrogram” shows the hierarchical association of the samples that minimizes the total variance within-clusters (Grimm, 1987; Bennett, 1996). CONISS ordination was applied to the percentage data of all pollen records presented in this thesis. At each site, percentage pollen was previously square-root transformed. Pollen data included only taxa with abundances equal or over 5% in at least one samples (Grimm, 1987).

3.4.7 Pollen corrosion analysis

As discussed in Section 3.2.3, fluctuations in the position of water table in mires might be related to variations in pollen preservation. Thus, by quantifying the amount of degraded pollen, it is possible to derive an indirect estimation of water table variability (Lowe, 1982). However, some pollen types have different predisposition to corrosion than others, and therefore changes in the abundance of some of those grains might drive changes in the total amount of deteriorated pollen that are unrelated to water table variations. To avoid any bias that might arise from differential pollen abundances, it is necessary to calculate the percentage of corrosion for single selected taxon as a reference, and then compare the sample corroded estimation with that particular taxon. An example of such an analysis is presented fully in Chapter Five.

3.4.8 Principal Component Analysis

Multivariate analysis has been applied to pollen data for ~50 years and it has since become a standard procedure in palynological studies (Birks, 2013). In general, multivariate techniques reduce the number of variables used to interpret a dataset. Principal Components Analysis (PCA) is one of the most widely used multivariate techniques in palynology. In simple terms, PCA consists in the generation of a limited set of new variables (termed *principal components*) defined as linear combinations of several of the original variables. The statistical power of the PCA will depends on a strong correlation between the principal components and the original pollen data. The new variables are aimed at capturing most of the variability of the original pollen dataset with the only limitation being that they have to be uncorrelated (orthogonal) to each other (Birks, 2013). Since principal components are independent of each other, they can be assumed to represent independent drivers of pollen variability. PCA is therefore a statistical analysis that detects and summarizes the main trends in the pollen data, allowing a simplified description of most of the variability of the fossil assemblage and facilitating the evaluation of the environmental drivers behind pollen variability.

Standardization is necessary to prevent the principal components being dominated by the taxa with the larger values. If the original pollen variables have been normalized, then the principal axis will also be normally distributed and thus able to be used for hypothesis testing using parametric methods. An illustrative explanation of this technique and its application to ecological data can be found in Ellison and Gotelli (2004). Principal components analysis of the pollen data was performed for two of the three sites presented in this thesis (Chapter Five and Six). The PCA analyses in these two sited were performed on pollen percentage data and included microscopic and/or macroscopic charcoal data. Only the three main principal components were used because the aim was to summarize the major trends in pollen data. For the Adelaide Tarn pollen record (Chapter Four), the main pollen trends and their association with climate variables were assessed with the aid of a pollen ordination (section 3.4.6) and with the development of qualitative (3.4.9) and quantitative (3.4.10) climate reconstructions.

3.4.9 Qualitative vegetation-climate inferences

The interpretation of the results obtained from the analyses discussed above provides insights into the nature of the environmental drivers behind the observed pollen variability. An essential step for paleo-climate inferences from palynology is to translate pollen abundance into vegetation variability and then relate the latter to climate changes. These inductive processes require knowledge of both the regional plant ecology and the climatic controls on species and communities (Faegri and Iversen, 1975). General qualitative climate inferences made from the pollen-vegetation relationship of the three sites presented in this thesis are based on the *indicator species approach* which uses the presence, absence and variations of taxa with well-documented climate tolerances (Iversen, 1944). The underlying assumption is that the amount of wind-transported pollen in a sediment sequences is proportional to the environmental abundance of the species represented by those pollen types. Similarly, the great amount of pollen produced by wind-pollinated plants is used as a basis to infer the absence of a particular species if its pollen type does not occur in the sediment section (Faegri and Iverson, 1975). A limitation of the method arises in cases when several species that grow in different climate districts present indistinguishable pollen types. In these cases, association with other taxa with more limited distribution may be used as a point of distinction. For this thesis, the climate interpretations are underpinned by the established climate-sensitive character of the New Zealand and Patagonian vegetation communities (see Chapter Two); and the fact that most of the southern temperate trees of these two regions are wind-pollinated.

3.4.10 Quantitative climate reconstructions

Mathematical analysis of modern pollen datasets have long been used to obtain quantitative climate estimates from fossil pollen samples (Webb and Bryson, 1972). Qualitative descriptions of the temporal variation of a pollen stratigraphy are a univariate analysis because descriptions are made using one taxon at a time. Yet, most taxa respond to multiple climate variables in unison and therefore developing climate estimations from pollen ensembles is, intrinsically, a multivariate problem. The goal of using multivariate analyses is thus to integrate the responses of several pollen types to more than one climate variable. For doing so, quantitative climate reconstructions apply fossil pollen responses to modern pollen-climate estimates (Faegri and Iversen, 1975). In general, any multivariate statistical approach that aims to link modern climate-pollen relationship with fossil data is based on several assumptions including that: (1) the modern climate is the main driver of vegetation distribution and composition, (2) the abundance of the different pollen taxa respond to the climate parameter to be estimated, (3) this response has not changed in time and (4) the effect of other environmental parameters is negligible (Birks, 1985). Multivariate analysis can be used with several different methods that are broadly classified according to the way in which the climate-pollen relationship is established. In this section we will describe the two methods used in the result chapters of this thesis: the modern analogue technique and the partial least squares regression.

The modern analogue technique was initially developed by Guiot (1990) and is based on the selection of a set of modern pollen samples, termed *analogues*, which most resemble the fossil samples. Thus, this method is based on *similarities*. Since its development, this method has been used for pollen-based climate reconstructions in many different regions including North America (e.g. Williams and Shuman, 2008), Europe (Davis et al., 2003), and New Zealand (McGlone et al., 2010). The similarities between the modern analogues and the fossil samples are assessed based on spectra composition and pollen abundance. Then, a climate estimate can be made by averaging the climate conditions of the closest analogues. A weighted average is preferred in order to ensure that the closest analogues exert a greater influence on the climate estimate. The modern analogue technique suffers, however, from several complications, notably relating to the estimation of error from extrapolated modern climate values, as well as in cases where past pollen samples lack a close modern analogue.

Unlike techniques based on similarities, partial least squares (PLS) is a method based on *calibration* (Wold et al., 1984). In this type of methods, a single mathematical function (termed *transfer function*) that relates modern pollen abundances with climate is used to *calibrate* the fossil samples (Webb and Bryson, 1972). In the partial least squares method the *transfer function* corresponds to a linear combination that captures the most variability of all pollen taxa. In other words, the partial least squares methods is a modified Principal Components Analysis (Brewer et al., 2007; see section 3.3.2.6). Ecologically, this method assumes a linear response of plant species to climate variables, yet in many cases this is unrealistic as plant-climate relationship tend to be unimodal (Brewer et al. 2007). Optionally, the partial least squares can be used with weighted average values. In this case, the transfer function is calculated as an average of the climate conditions in all the samples where a certain taxon is present, but weighted by abundance of the taxon in each of the samples (ter Braak and Juggins, 1993).

For this thesis, quantitative temperature reconstructions were performed on both New Zealand sites (Chapter Four and Chapter Five). This technique could not be applied in the Patagonian pollen record since modern pollen datasets for western Patagonia are absent. In New Zealand, early studies about the representation of modern vegetation in pollen spectra were conducted by McGlone (1982). The first attempts of applying multivariate analysis to link modern pollen-climate relationships to fossil ensembles were made by Norton et al. (1986). For this thesis, Chapters Four and Five used both the modern analogue technique and the partial least squares method, with the pre-deforestation pollen dataset published by Wilmshurst et al. (2007). This dataset overcomes the difficulties imposed by the drastic anthropogenic destruction of the majority of the native forest in the past 800 years, and it is the one who has allowed the development of temperature reconstructions having the strongest statistical relationship with mean annual temperature to date. At the two New Zealand sites, the modern analogue technique was applied with Chi-square dissimilarities distances using the 10 closest analogues; whereas the partial least squares method was applied with a linear transfer function. These two methods were used to estimate mean annual temperatures. All temperature reconstructions were cross-validated using 1000 bootstrapping cycles, and then compared against instrumental climate information and against qualitative climate reconstructions based on pollen taxa with well understood climate responses.

3.4.11 Superposed Epoch Analysis

Superposed Epoch Analyses (SEA) (Prager and Hoenig, 1992) is a statistical analysis that allows the detection of time-consistent responses to individual events that occur recurrently in a time series. This method consists of averaging all the individual responses to those events to obtain a single representative response. The underlying rationale of applying SEA in time-series data is that consistent response of a particular variable (based on its intrinsic characteristics) to recurrent disturbance events should be discernible from individual responses (driven by external time-changing variables) by integrating (averaging) a large number of individual responses to those events (Adams et al., 2003).

The sediment section of Lago Espejo presented a great number of tephra deposits, and therefore SEA analysis was used in Chapter Six to evaluate the impact of recurrent volcanic ash fallout on vegetation and charcoal accumulation. This specific application of SEA has been recently applied in other pollen and charcoal reconstructions from Patagonia (Jara and Moreno, 2014; Henríquez et al., 2015). In this approach, each tephra horizon is considered as an independent event (represented as time “0”) and the responses of the pollen and charcoal variables before (negative time) and after (positive time) each event are isolated from the record and then averaged. For Chapter Six, the pollen accumulation of *Nothofagus* and Poaceae, as well as the macroscopic charcoal accumulation rate (see section 3.5.3) were analysed at a time-window of 150 years for pollen data and 90 years for charcoal accumulation data centred at each volcanic event. These specific pollen taxa were selected for the analysis because of their abundance and ubiquity throughout the pollen record and because they have been previously documented as pioneer, fast-growing species that usually colonize disturbed areas (Donoso et al., 2006). The different size of the time-window between the pollen and charcoal data stem from the lower resolution of the pollen respective to the macroscopic charcoal record. In order to average responses occurring in different portions of the record that have different accumulation rates, all pollen and charcoal data were interpolated to fixed time intervals equal to the median sample resolution of the records. To minimize the statistical weight of outliers, the data were normalized by subtracting the mean value from every individual value at each window (Genries et al., 2009). Since pollen percentages were calculated in reference to a shared total, any change in one taxon might lead to changes in rest of them. To avoid this bias, SEA was performed on pollen accumulation rate data. Consistent positive or negative changes of the averaged pollen and charcoal data were testing using 95% confidence intervals calculated from a Monte Carlo randomization using 3000 replications. Additionally, the averaged value of the intervals immediately after and before the tephra was compared using nonparametric Wilcoxon test with a null hypothesis of equal pre and post tephra averages.

3.5 Charcoal Analysis

3.5.1 Charcoal processing

The method for charcoal processing used in this thesis follows the procedure of macroscopic charcoal analysis in sieved sediment samples discussed in Whitlock and Larsen (2001). The sieving of sediments samples at contiguous levels is the preferred method for sediment sequences that lack annual lamination. The preparation of the charcoal samples is significantly simpler and faster than pollen processing. For this thesis, equal 1-cc samples were deflocculated in a solution of 10% Potassium hydroxide. The samples were then sieved to separate all the particles bigger than 125 µm in two different size fractions: 125µm-250µm and larger than 250µm. The two charcoal fractions were then suspended in water and then counted in gridded plastic plates under a stereoscope at magnification of 10 and 20 times.

3.5.2 Charcoal identification

In the majority of the cases, charcoal particles are recognized by: (1) black colour, (2) flake-like planar shape, and (3) angular border. In case of doubt, the particle was broken using a dissecting probe. Charcoal fragments break significantly easier than other organic particles and black minerals. When a charcoal fragment is broken, it does in multiple parts. Some charcoal particles distinctively pulverize when punctured by a probe. Charcoal fragments are also distinguished from black minerals by their buoyancy. Charcoal from monocotyledon grasses were identified by the presence of parallel leaf veins and void stomatal complexes (see section 3.2.5).

3.5.3 Charcoal concentration and influx

The total number of charcoal particles counted in a sample is usually converted into concentration and charcoal accumulation rate (CHAR; see section 3.2.4). CHAR is the standard variable used for reconstruction of fire history (Whitlock and Larsen, 2001). Fixed-volume samples facilitate the calculation of CHAR because the number of counted particles can be directly converted into charcoal concentration. As explained in section 3.3.2, the experimental design included a macroscopic charcoal analysis only for Lago Espejo (Chapter Six).

3.5.4 Charcoal peak detection

In an idealized sediment section with a sedimentation time of 10 year per centimetre (for example), a charcoal analysis of continuous 1-cm samples will be sufficient to distinguish individual fires that occurred at intervals equal or longer than 10 years. Yet wildfire might occur at frequencies higher than that, and therefore in many cases a single 1-cm sediment sample might contain charcoal generated in more than one fire. For this reason CHAR peaks in this thesis are interpreted not as individual wildfires but as a "fire events", a term that has been adopted in the literature to describe one or more wildfires occurring within a defined time (Agee, 1993).

CHAR records have are complex, highly variable signals; therefore, several, often complex, numerical techniques have been developed to analyse CHAR time series. A now-classical approach is to decompose the CHAR series by a de-trending analysis that separates the charcoal produced during fire events or *peak* charcoal, from the charcoal that is being deposited due to other processes than fire (Clark et al., 1996). This latter component, termed *background* charcoal, includes charcoal from previous fires that has been stored in the watershed and which is slowly and continuously released to the sediment basin. Thus background charcoal is not related to specific fire events (Whitlock and Larsen, 2001). Long-term changes in the amount of background charcoal might occur as a result of changes in the type of vegetation (e.g. from grassland to forest) or from extra-local fires (Millspaugh et al., 2000); whereas changes in peak charcoal occur at shorter scales and are assumed to result from the occurrence of fire events in proximity to the study site. In Chapter Six of this thesis, the CHAR record was analysed using a time series analysis provided by the software CharAnalysis (Figure 3.7; Higuera et al., 2009). CharAnalysis is a statistical tool designed to identify CHAR peaks and interpret fire events. The following explanation of the method is fairly simple and limited to general principles. For a more detailed analysis see Higuera et al. (2010). The first step of the analysis is to interpolate the CHAR record into fixed temporal intervals in order to reduce the bias in fire detection due to changes in the sediment accumulation rates. Then, the background charcoal is modelled applying a smoothing fitting to the interpolated signal. For Chapter Six, a 500-year Lowess (locally weighted scatterplot smoothing) function was applied. Peak charcoal can be calculated either by subtracting the background signal from the interpolated signal or by a ratio between those two variables. For Chapter Six, peak charcoal was calculated as the positive values resulting from the subtraction of the background charcoal from the interpolated charcoal series. Finally, individual fire events are modelled as positive values of peak charcoal that exceed certain threshold. For Chapter Six, the resulting peak values that exceed the upper end (90, 95 or 99% percentiles) of a Gaussian distribution of all the peak values are then interpreted as fire events by the software.

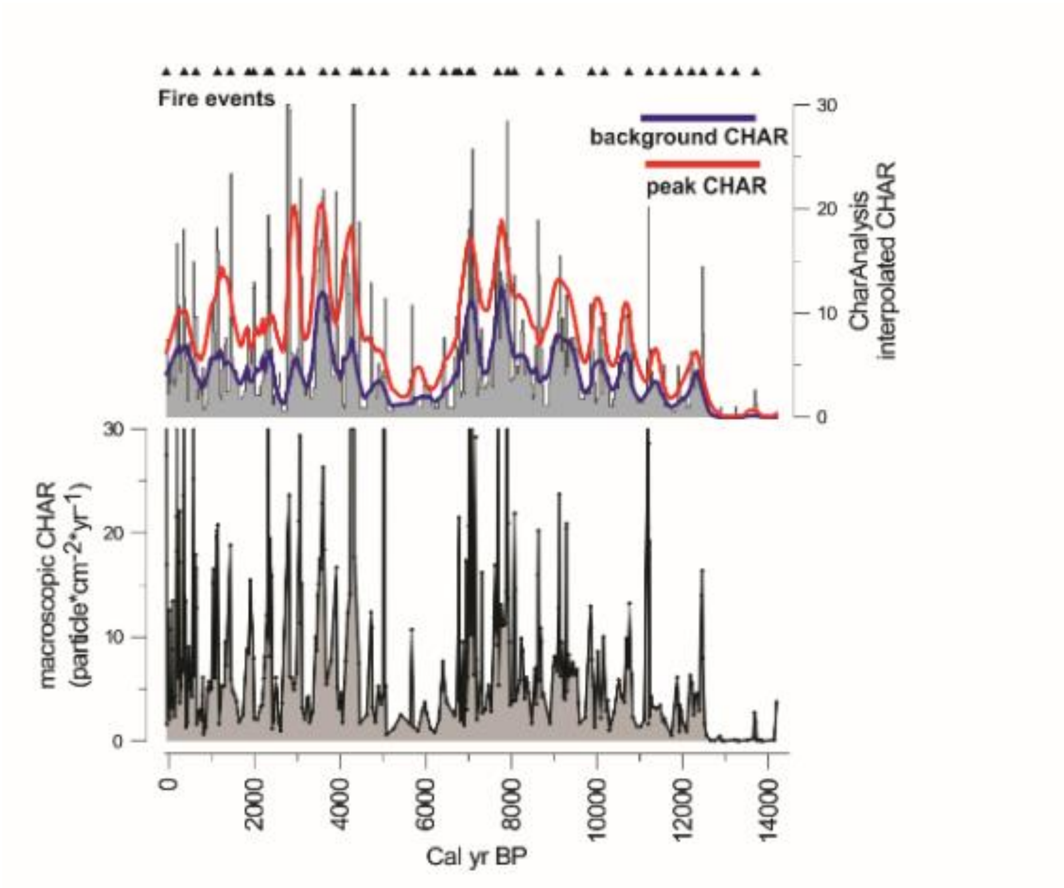

Figure 3.7. CharAnalysis. An examples of a time CHAR timeseries analysed with the CharAnalyis software. The modelling of the background CHAR, the peak CHAR and Fire events was conducted following the same procedures described in section 3.4.3. Modified from Jara and Moreno (2014).

Chapter Four

Pollen–climate reconstruction from northern South Island, New Zealand (41°S), reveals varying high- and low-latitude teleconnections over the last 16 000 years

4.1 Abstract

I present a 16,000-year vegetation and climate reconstruction from pollen and plant macrofossil records obtained at a small alpine lake in South Island, New Zealand (41°S). The expansion of lowland forest taxa suggests a lifting of the altitudinal forest limits because of a warming pulse between 13,000- 10,000 cal yr BP and between 7000-6000 cal yr BP, while their decline relative to upland forest taxa indicates cooling phases between 10,000-7000 cal yr BP and over the last 3000 years. The modern treeline was first established locally by 9700 cal yr BP. Forest persisted at the site until 3000 cal yr BP then disappeared from the record. Close correspondence between the temperature trends inferred from the pollen and macrofossil records and proxies from Antarctica and the Southern Ocean suggests a strong teleconnection between New Zealand and the Southern Hemisphere high-latitudes between 15,000-6000 cal yr BP. I note that the breakdown of this coupling, a cooling trend in Adelaide Tarn and the local disappearance of beech forest after 3000 cal yr BP occur during a period of increased frequency of El Niño events, suggesting an enhanced teleconnection with the low-latitudes during the late Holocene.

4.2 Introduction

New Zealand is particularly well suited to climate reconstructions using vegetation archives because of the climate sensitivity of its vegetation and a late settlement history that precludes anthropogenic disturbance for all but the last 750 years (Newnham et al., 1999; Wilmshurst et al., 2008; Barrell et al., 2013). Critically, its location straddling the southern mid-latitudes (34–47°S) makes it sensitive to atmospheric variability originating in both the Tropical Pacific to the north and the extra-tropical Southern Ocean to the south (Kidson et al., 2002; Ummenhofer and England, 2007). These teleconnections strongly influence the modern inter-annual climate variability observed in New Zealand, yet little is known about how they may have operated before the instrumental era. There is therefore a pressing need to develop well-dated sensitive climate proxies from New Zealand's natural archives that can reveal the influence of low- and high-latitude atmospheric circulation over New Zealand climate in a longer-term context.

Here I present a high-resolution pollen record spanning the last 16,000 years from a small lake, Adelaide Tarn, near the modern treeline in Northwest Nelson, a mountainous region in central New Zealand (41°S). Pollen data are complemented by plant macrofossil evidence to document the local and regional vegetation and climate history. A vegetation-based reconstruction from this sector is pertinent to large-scale climate teleconnections for two main reasons. First, Northwest Nelson is located on the current northern margin of year-round influence of the southern westerly wind belt, and therefore its vegetation history should reflect latitudinal shifts in this hemispheric-wide extra-tropical atmospheric circulation system. Second, Adelaide Tarn is situated at the present-day treeline in a region of strong relief, which permits the detection of climate-driven altitudinal shifts of this major ecological boundary and of other vegetation units downslope.

4.3 Study region

4.3.1 Physical setting

Northwest Nelson (40–41°S, 172–173°E), in the north-west corner of New Zealand's South Island, is a region of mostly high relief and rugged topography representing the northernmost part of the Southern Alps (Figure 4.1). The highest peaks, ranging from 1600 to 1800m in elevation, occur in the predominantly granitic Tasman Mountains. The region lacks modern glaciers, unlike higher elevations in the central and Southern Alps to the south, but there is unequivocal geomorphic evidence for alpine glaciation during the Pleistocene (Shulmeister et al., 2005; McCarthy et al., 2008).

Adelaide Tarn (40°56'0''S, 172°32'0'E; 1250 m) is a small lake (0.06 km^2) sitting in a glacial cirque (3.8 km^2) in the Douglas Range amid the Tasman Mountains. With a current maximum water depth of 7.6 m, Adelaide Tarn is fed by a single inlet on its south-eastern border and drained by a single outlet on its north-western edge (Figure 4.1).

4.3.2 Atmospheric circulation

The position of New Zealand in the mid-latitudes of the southern Pacific Ocean and its topography marked by the presence of axial cordilleras are the main factors determining its broad-scale climate regimes. A north–south gradient in mainland temperatures results from the interaction between warm sub-tropical Pacific and cold sub-Antarctic oceanic waters.

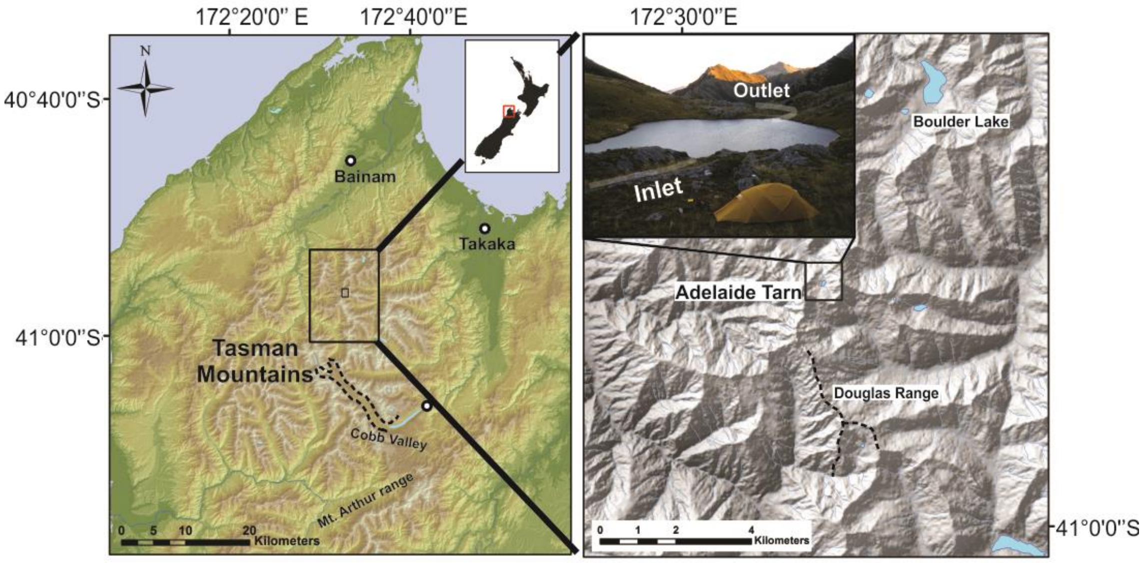

Figure 4.1. Digital Elevation Model of Northwest Nelson region and the geomorphic emplacement of Adelaide Tarn. The left image include the climate stations and other physiographic units mentioned in the text. The superposed photograph on the right panel shows Adelaide Tarn looking toward the north and highlights the lake's inlet and outlet.

The oceanic setting serves to moderate the pronounced seasonal fluctuations that characterize the climate of more continental landmasses at equivalent latitudes. The main pattern of precipitation regimes across the country follows the east–west gradient imposed by the intersection of the predominant westerly circulation with the topographical barrier of the axial cordilleras. This pattern results in relatively high precipitation totals in western regions (up to 10,000mm*yr^{-1}) and much lower precipitation in the east (500 mm*yr^{-1}).

A significant amount of the modern climate variability across New Zealand is explained by low- and high-latitude modes of climate variability such as El Niño Southern Oscillation and the Southern Annular Mode (SAM) (Kidson et al., 2002; Kidston et al., 2009). In general, La Niña years are associated with stronger sub-tropical easterly flow which results in overall warmer conditions across the country and higher annual precipitation in the north and east, whereas El Niño years are associated with stronger extra-tropical southwesterly flow resulting in overall higher annual rainfall and lower temperatures in the southern and western districts (Kidson and Renwick, 2002; Thompson et al., 2011; Figure 4.2). Positive phases of SAM are associated with a reduction of the westerly flow over New Zealand resulting in decreased precipitation over western districts and higher temperatures over most of the country, while the opposite scenario is observed during negative phases (Renwick and Thompson, 2006; Figure 4.2). Data from climate stations in Northwest Nelson derived from the National Climate Database (www.cliflo.niwa.co.nz) provide an adequate representation of the modern regional climate setting. High annual precipitation with minor seasonal differences prevails in the relatively flat and exposed northern areas of Northwest Nelson as the westerly fronts are complemented by a substantial presence of storms from the north during summer months. The eastern part of Northwest Nelson, on the lee side of the Tasman Mountains, has a more continental climate with significantly lower annual precipitation because of a strong rain shadow effect, and a marked precipitation minimum during summer resulting from a meridional shift of the zone of maximum westerly sourced precipitation. Mean annual temperatures in Northwest Nelson vary from 12.5 °C at 25 m to 8.5 °C at 823 m of elevation. These values give a regional lapse rate of 5.5 °C per 1000 m, which is close to the environmental lapse rate calculated for the central Southern Alps (6.0 °C per 1000 m; Hales and Roering, 2005). Based on its elevation (1250 m), the regional lapse rate and its position relative to the closest climate stations, I estimate Adelaide Tarn to have a mean annual temperature of ~6.2 °C with total annual precipitation ≥2500 mm, resulting predominantly from the westerly circulation. However, its relatively northern location is likely to result in summer precipitation minima, similar to those of the eastern areas of Northwest Nelson.

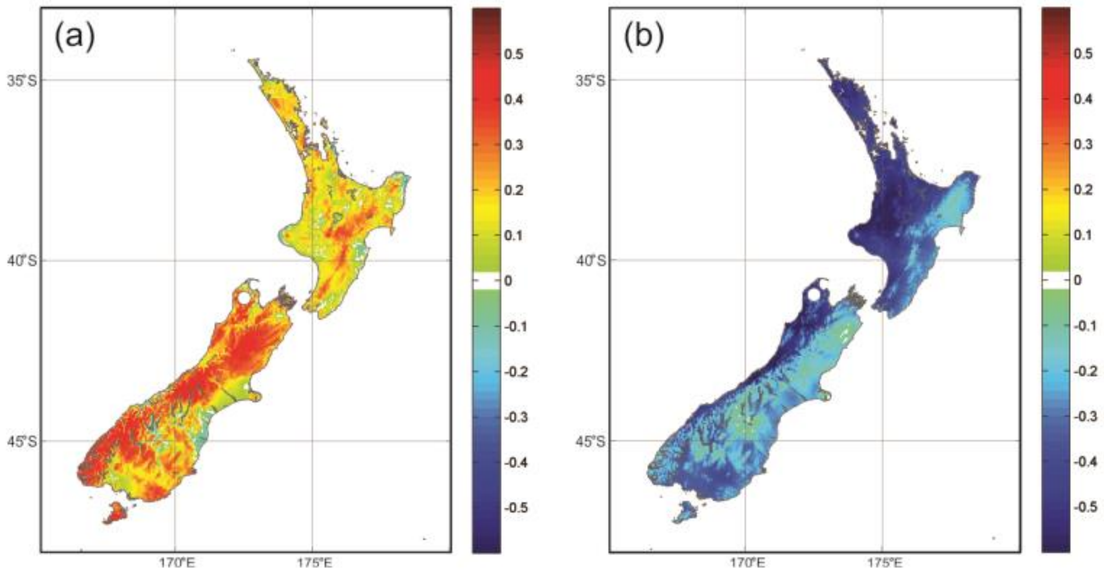

Figure 4.2. Correlation maps for mean annual (May-April) surface temperatures and (a) the SAM index, and (b) El Nino 3.4 SST. Both correlations are calculated based on a 1979-2008 regression. The white circle denotes the location of Adelaide Tarn.

4.3.3 Vegetation in Northwest Nelson

Native forest in Northwest Nelson can be broadly classified into two main forest communities: conifer–broadleaf forest at lower elevations and *Fuscospora/Lophozonia* (southern beech) forest at higher elevations up to the treeline (Wardle, 1991). The altitudinal distribution of these communities is primarily controlled by regional temperature, and thereafter by local environmental factors such as soil moisture and quality, aspect, and slope. Therefore, the altitudinal zonation of vegetation in Northwest Nelson can be used as a modern analogue for interpreting past changes in temperature from pollen profiles in the region.

Lowland to montane areas at elevations lower than 600 m, where soils are relatively fertile and temperatures moderate throughout the year, support a relatively diverse and structurally complex conifer–broadleaf forest community. The forest canopy is mainly dominated by the tall conifer *Dacrydium cupressinum* and may include others such as *Prumnopitys taxifolia*, *P. ferruginea*, *Podocarpus totara* and *Dacrycarpus dacrydiodies* in poorly drained sites. The sub-canopy typically comprises angiosperm trees including *Metrosideros robusta*, *M. umbellata*, *Weinmannia racemosa* and *Coprosma lucida*, while the understorey features the tree-ferns *Cyathea smithii* and *Dicksonia squarrosa*, epiphytes such as *Griselinia lucida* and the fern *Asplenium polyodon*, lianas such as *M. fulgens* and *M. diffusa*, and several shrub and herb species including *Raukaua simplex* and *Myrsine australis*. In the mountainous regions above 600 m, where soils are generally less fertile and temperatures lower, conifer–broadleaf forest is usually replaced by the floristically less diverse southern beech forest. Notably, in certain areas in the Cobb Valley subalpine–conifer forest featuring *Phyllocladus alpinus* and *Halocarpus biformis* develops largely in the absence of southern beech species. Otherwise, *Lophozonia menziesii* or *Fuscospora cliffortioides* typically dominate the southern beech forest canopy with an understorey represented by an impoverished version of the conifer–broadleaf forest sub-canopy described above. The most common species occurring beneath the canopy are *Coprosma macrocarpa*, *Leucopogon fasciculatus*, *Leptecophylla juniperina*, *Kunzea ericoides*, and *shrubs forms* of *P. alpinus* and *H. biformis*.

The average regional treeline elevation is about 1350 m, 30–100m above the elevation of Adelaide Tarn. However, because of the rugged regional topography the treeline may descend to 1200 m in steep bedrock gullies or steep slopes with thin soils (such as at Adelaide Tarn), or ascend to 1500 m in rocky well-drained slopes and ridges (Williams, 1993). In addition, goats, sheep and several other grazing animals introduced since 1850 have had significant browsing impacts in the alpine vegetation of Northwest Nelson. *Fuscospora cliffortioides* is the most conspicuous arboreal species of the treeline of Northwest Nelson and around Adelaide Tarn. Additionally, *Lophozonia menziesii* and *Dacrophyllum traversii* are the other trees most commonly found near the treeline, while several species of the genera *Coprosma*, *Raukaua* and *Griselinia* are abundant in the sub-canopy treeline forest stands. The herbaceous ground cover of these treeline communities includes a combination of monocotyledonous genera such as *Astelia* and *Uncina*, in association with multiple dicotyledonous groups such as *Anisotome* (Apiaceae), *Ourisia* (Plantaginaceae) and *Lagenophora* (Asteraceae).

A 0.5–3.0-m-tall shrubland community dominated by *Olearia colensoi* and *Dacrophyllum uniflorum* is usually found above the treeline of the Douglas mountain range (Figure 4.1). Other shrub species include *Halocarpus biformis*, *Brachyglottis* *bidwillii*, *Gaultheria crassa*, *Hebe albicans* and several species of the genus Coprosma. This shrubland community may extend up to 1500 m in sunny and well-drained bedrock ridges or hillslopes, where it is usually superseded by tussock grassland formed by several species of the genus *Chionochloa*. In the few mountainous areas above 1500 m, these tussocklands usually give way to open grassland areas with scattered patches of *Oreobolus pectinatus* cushionfields and patches of *Helichrysum intermedium* and *Hebe ciliolata*. These open cushionfield and grass patches represent the limit of the alpine vegetation before giving way to non-vegetated high-alpine colluvium landforms. Vegetation surrounding Adelaide Tarn consists primarily of *Chionochloa* tussock grassland. Additionally, *Hebe biformis* and *Dacrophyllum uniflorum* form dense thickets on scree areas to the east of the site. Approximately 100 m to the north, *Fuscospora cliffortioides* forms a dense treeline boundary on the steep mountain slopes. Restiads, primarily *Empodisma minus* and *Carex* spp., are prominent in the boggy margins of Adelaide Tarn, while aquatic plants *Potamogeton* (probably *P. cheesemanii*) and *Isoetes* spp. grow in the shallow muddy margins (Marcus J. Vandergoes, pers. obs.).

4.4 Methods

4.4.1 Sediment retrieval

Two overlapping sediment cores (AT 1115 and AT 1116) were collected from an anchored platform at the deepest part of Adelaide Tarn (water depth ~7m). Each core comprises multiple 1-m length sections retrieved with a 5-cm-diameter square-rod piston corer (Wright, 1967). The two series showed the same stratigraphic units, thus enabling a single site composite sequence to be constructed devoid of any break between individual core segments. Additionally, a gravity core was collected to retrieve the water–sediment interface. The replication of stratigraphic features in the gravity and overlapping cores allowed us to construct a single site sequence (hereafter referred to as a single core) that extends continuously up to the present.

4.4.2 Stratigraphy and chronology

The broad lithological properties of the cores were described through visual inspection, standard photography and X-ray images after carefully cleaning the core surfaces (see

Chapter Three for more details about these methodologies). The images are not presented here but were used to confirm field-based lithological correlations between the two overlapping core series. Magnetic susceptibility analysis was performed at Victoria University of Wellington using an MS2 Bartington magnetic meter with a loop sensor type M.S.1C. Grain size analysis was performed on the sub-2-mm-diameter fraction using a Malvern Master sizer 2000 at the University of Waikato, after pre-treatment with H_2O_2 and deflocculation. Data are expressed as percentage of clay (<3.9 mm), silt (3.9–60 mm) and sand (60–2000 mm) with respect to volume units. Grains >2 mm in diameter were not characterized except for gravel layers noted in the lithostratigraphy.

The chronology of the sediment sequence is constrained by 16 accelerator mass spectrometry radiocarbon dates obtained from plant macrofossils. Radiocarbon calibration was performed using the SHCal13 dataset (Hogg et al., 2013) included in the software CALIB 6.01 (Stuiver, 1993). I developed a Bayesian age–depth model with the aid of the Bacon package using R software (Blaauw and Christen, 2011; see Chapter Three for more details about age modelling). This method enabled the calculation of a weighted mean and a 95% confidence interval for the calendar age distribution of every level in the sedimentary sequence, including the individual pollen and plant macrofossil sample layers. The pollen and plant macrofossil data are plotted against their weighted mean calendar age indicated by the model.

4.4.3 Pollen record

I processed and analysed 110 samples extracted from constant volume ($1cm^3$), 1-cm-thick sections taken at 5-cm intervals throughout the core. The sample processing followed standard procedures (Faegri and Iversen, 1989, see Chapter Three). I counted 300 terrestrial pollen grains from each pollen slide and calculated percentages based on the terrestrial pollen sum along with pollen concentrations and pollen influx (influx: $grains*cm^{-2}*yr^{-1}$) for individual taxa. The percentages of aquatic pollen, fern spores and tree fern spores were calculated from the sum of all terrestrial pollen taxa plus the respective ecological group. Pollen percentage and influx diagrams were generated with the software Tilia version 2.0 (E. Grimm, Illinois State Museum, Springfield, IL, USA).

A pollen zonation was determined based on the visual identification of the main pollen percentage changes, assisted by a stratigraphically constrained ordination (CONISS) provided and executed by the same software.

4.4.4 Plant macrofossil record

The same 110 sample levels used for pollen analysis were used for plant macrofossil analysis, although not all samples yielded identifiable material. The sample processing involved separation by wet sieving at 90 µm, and was followed by counting individual specimens with the aid of a square gridded transparent slide under a stereomicroscope. The identification of fossil remains was based on photographic and herbarium references from the University of Waikato.

For the Nothofagaceae, leaf fragments that could not be confidently identified from leaf morphology, isolation of the cuticle layer and examination the cellular pattern by light microscopy was conducted. The cuticle analysis confirmed the morphology based identification of all *Lopohozonia menziesii* and *Fuscospora cliffortioides* specimens but showed that the few fragments ascribed to *F. fusca* were instead *L. menziesii*. The category 'Nothofagaceae undifferentiated' refers to leaf fragments that could not be identified beyond family level by these methods. I assume these specimens are either *L. menziesii or F. cliffortioides* because only these Nothofagaceae trees occur at treeline altitude today and only these two Nothofagaceae species have been positively identified in the macrofossil assemblages.

Fragments of grass, sedge and rush stems dominated the macrofossil assemblages but could not be taxonomically separated and so were recorded as 'graminoid'. To counter the problem of quantifying fragments, a transformation was applied in which eight fragments equated to one complete unit. Macrofossil data are expressed with the aid of a relative abundance scale as follows: (1) rare, (2) uncommon, (3) frequent, (4) common, (5) abundant. As the site elevation falls within the regional limits of the present-day treeline, a long-term absence of arboreal macroscopic plant remains will be interpreted as a lowering of the treeline, and the presence of these remains as the occurrence of treeline around and/or above the site.

4.4.5 Temperature reconstructions

I estimated the thermal changes around Adelaide Tarn by developing three different temperature reconstructions from the pollen data. Two of those reconstructions are quantitative, obtained using the transfer function approach and applying both the (i) partial least squares regression and (ii) modern analogue technique to the New Zealand pre-deforestation pollen dataset (Wilmshurst et al., 2007). Alternatively, a temperature reconstruction was calculated from a pollen– temperature proxy (PTP) using individual taxa with well-established thermal affinities that are prominent in the Adelaide Tarn record. The PTP is calculated as the normalized base-10 logarithm of the ratio of *D. cupressinum* + *Prumnopitys taxifolia*+ *P. ferruginea* pollen influx to the combined pollen influxes of *Lophozonia* + total grasses. All these taxa are prominent through most of the Adelaide Tarn pollen record, and are broadly representative of their respective vegetation communities with temperature-controlled altitudinal patterns observed in the region today. Despite that both *Prumnopitys* species are not significantly correlated with mean annual temperatures (Table 4.1), I decided to include these species in the PTP index because they have much the same position than *Dacrydium* as dominant emergent trees in the lowland conifer-broadleaf forest of Northwest Nelson. I excluded the taxon *Fuscospora* as it includes species found from low to subalpine elevations. Most of the taxa included in the PTP are strongly correlated with mean annual temperature (MAT) in the New Zealand pre-deforestation database (Table 4.1), and as expected the PTP index shows a strong positive correlation with MAT (correlation coefficient = 0.58; $p < 0.001$) in the same dataset (Figure A2.1 in Appendix 2). Thus, positive (negative) values of PTP indicate the relative dominance (subordination) of the more thermophilous *D. cupressinum* and/or *Prumnopitys* spp. over the other, cool indicator taxa under relatively warm (cold) conditions.

4.5. Results

4.5.1 Stratigraphy and chronology

The sediment core features sand and gravel units at the base of the cores. The sequence has a total length of 570 cm and is dominated by organic silts (relative average abundance 51%) and clays (45%), with a minor content of sands (4%). I recognize three main sedimentary units (Figure 4.3):

Taxon	Correlation with MAT	Rank out of all taxa (N=82)
Dacrydium cupressinum	**0.51**	5th most thermophilous
Fuscospora	**-0.38**	6th least thermophilous
Poaceae	**-0.49**	4th least thermophilous
Lophozonia menziesii	**-0.51**	3rd least thermophilous
Prumnopitys taxifola	0.06	50th most thermophilous
Prumnopitys ferruginea	-0.09	16th least thermophilous

Table 4.1. Spearman rank correlation r values for key Adelaide Tarn taxa in the New Zealand pre deforestation pollen database versus mean annual temperature (MAT). All correlations significant at p=0.05 are marked in bold. Data from Wilmshurst et al. (2007).

1. The lower unit (560–480 cm) comprises inorganic grey silts and clays. The basal portion of this unit features thin (<1 cm thick) inorganic laminae and three prominent (>2 cm thick) gravel layers. A yellowish silt layer is evident at 494–493 cm.

2. The middle unit (479–238 cm) comprises brownish black silt and clay units with abundant macrofossils in its upper portion. Organic laminae occur and yellowish silt layers are particularly abundant. A gravel layer is observed between 391-389 cm.

3. The upper unit (237–1 cm) comprises organic-rich dark brown silt and clay with abundant diatoms and macroscopic remains. Additionally, horizontal yellowish silt layers and a series of organic-rich laminae containing liverworts, mosses and undeterminable concentrations of macrofossils are observed at various levels.

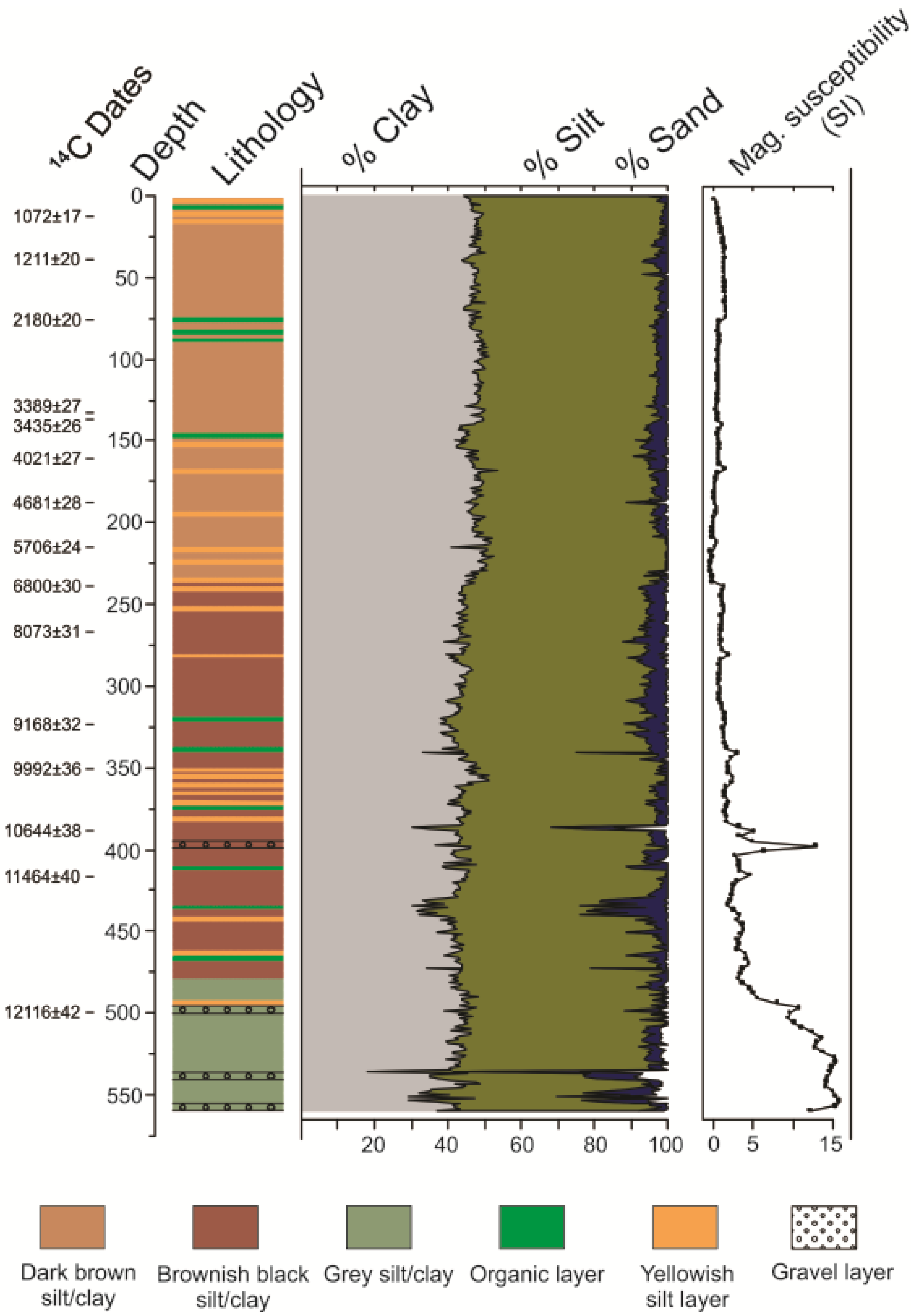

Figure 4.3. Radiocarbon ages (in ^{14}C yr BP ± 1 sd), lithology, grain size and magnetic susceptibility analyses of the correlated sediment section retrieved from Adelaide Tarn.

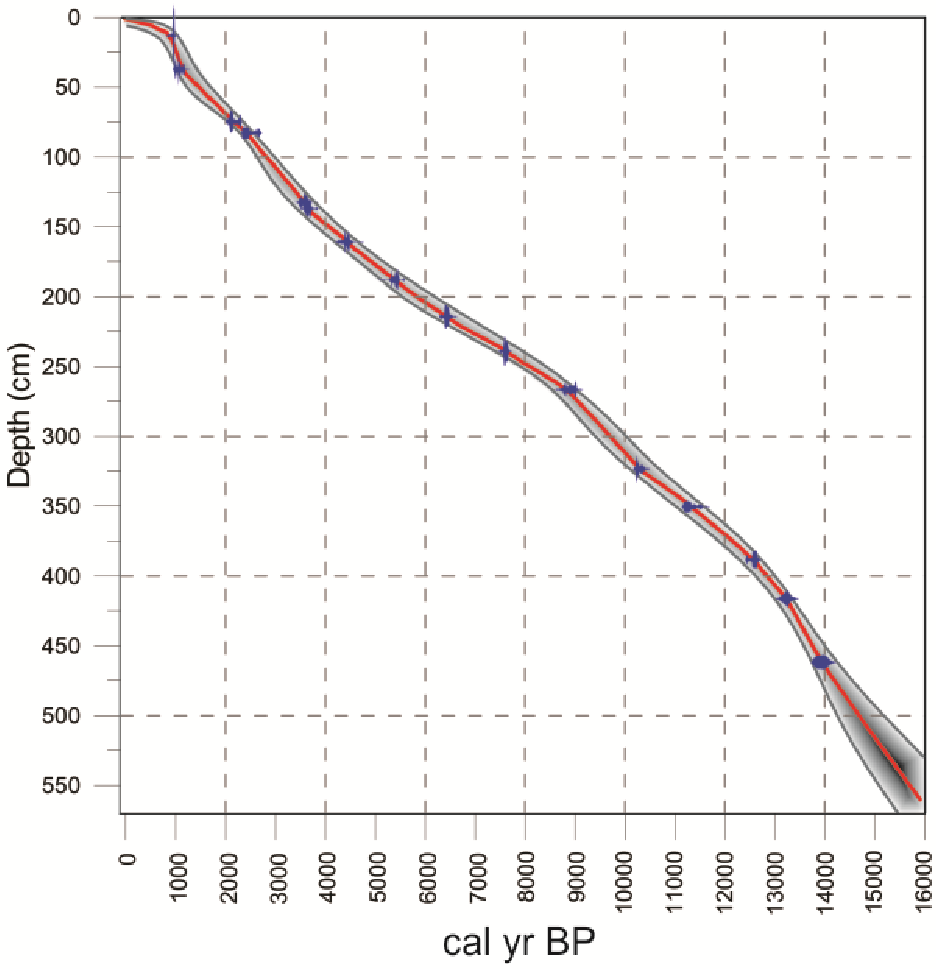

Figure 4.4. Bayesian age model based on the 16 radiocarbon dates from Adelaide Tarn. The model was developed using the Bacon package for the software R (Blaauw and Christen, 2011). Radiocarbon calibration was performed with the aid of the software CALIB 6.01 (Stuiver, 1993) using the SHCal13 calibration curve (Hogg et al., 2013). The image shows the 2 sigma calendar age range for each of the ages (blue), the modelled weighted mean age (red line), and the 95% confidence intervals (grey lines). The darker areas represent calendar ages with a high likelihood according to the model. The weighted mean age series is used to estimate an age for all pollen and plant macrofossil samples.

All calibrated radiocarbon ages are in chronological order (Figure 4.3; Table 4.2) which, together with the absence of any stratigraphic and visual evidence for significant break or disruption in the sedimentary sequence above the uppermost gravel layer at ~12,500 cal yr BP (11,464±40 ^{14}C yr BP), suggests that sediment accumulation was essentially continuous since that time. Because macroscopic organic material is absent from the lower unit, the oldest radiocarbon date was obtained at a depth of 463 cm, and the chronology below this point has been determined by extrapolation. The Bayesian age model derived from the calibrated ages (Figure 4.4) indicates sediment accumulation rates ranging from 9 to 98 years cm^{-1} with an average of 28 years cm^{-1}. The average temporal resolution of the pollen record is 147 years between samples. The weighted average for the maximal extrapolated age of the sequence is 16,100 cal yr BP (95% confidence range = 15,400–16,900 cal yr BP) and the maximal age for the pollen record is 15,800 cal yr BP (15,200–16,600 cal yr BP).

#	Laboratory code (CAMS#)	Depth (cm)	^{14}C date±1 σ (years)	calibration curve	youngest 2σ intercept (cal yr BP)	oldest 2σ intercept (cal yr BP)	Median probability (cal yr BP)
1	NZA 51077	13	1072±17	SHcal13	927	955	941
2	NZA999	37	1211±20	SHcal13	989	1155	1066
3	NZA998	75	2180±20	SHcal13	2086	2086	2126
4	NZA37637	83	2467±25	SHcal13	2359	2652	2459
5	NZA 50821	133	3389 ± 27	SHcal13	3514	3637	3586
6	NZA 50822	137	3435 ± 26	SHcal13	3591	3687	3637
7	NZA 50823	161	4021 ± 27	SHcal13	4417	4514	4463
8	NZA 50824	188	4681 ± 28	SHcal13	5314	5447	5406
9	NZA 50905	215	5706 ± 24	SHcal13	6408	6473	6444
10	NZA 50825	239	6800 ± 30	SHcal13	7582	7653	7614
11	NZA 51059	267	8073 ± 31	SHcal13	8785	9011	8900
12	NZA 51060	324	9168 ± 32	SHcal13	10,228	10,367	10,268
13	NZA 50826	351	9992 ± 36	SHcal13	11,254	11,403	11,357
14	NZA 50829	389	10,644 ± 38	SHcal13	12,557	12,646	12,596
15	NZA 50827	417	11,464 ± 40	SHcal13	13,202	13,311	13,259
16	NZA 50828	463	12,116 ± 42	SHcal13	13,823	14,000	13,917

Table 4.2. Summary of the radiocarbon dates from Adelaide Tarn.

4.5.2 Pollen record

I divided the pollen percentage record of Adelaide Tarn into six zones based on key changes observed in pollen composition and the CONISS ordinations. The main features of each zone are described in Table 4.3. Both pollen percentages (Figure 4.5) and influx (Figure 4.6) are presented. In summary, the pollen record shows the overall dominance of tree pollen (average 65%) over grass (18%) and shrub (13%) pollen throughout the record. The most common taxon is *Fuscospora*, which has maximum abundance at the beginning of the record between 15,800-14,800 cal yr BP, and later during the last 7000 years. In the interim, a series of other pollen taxa show significant changes in their abundance, starting with an interval of high shrub and grass abundance between 14,800-12,000 cal yr BP and followed by an increase in low- and midelevation conifers between 12,500-8500 cal yr BP (Figure 4.5).

4.5.3 Plant macrofossil record

I distinguished three distinctive zones in the plant macrofossil record of Adelaide Tarn (Figure 4.7). The lower zone, between 15,800-9,800 cal yr BP, is exclusively dominated by graminoids and bryophytes with their abundances ranging from rare to frequent. The appearance of *Lophozonia menziesii* at 9700 cal yr BP represents the first arboreal presence in the record and marks the beginning of the middle zone. *L. menziesii* abundance ranges from rare to uncommon between 9700-3000 cal yr BP, while *Fuscospora cliffortioides* ranges from rare to abundant across approximately the same time interval. Leaves of *Libocedrus bidwillii* are present but rare between 9300-8800 cal yr BP. Between 9700-2700 cal yr BP, graminoid and bryophyte abundances remain stable with values ranging from rare to uncommon. The upper zone spans the last 2700 years when the abundance of tree taxa declines significantly except for isolated appearances of rare *L. bidwillii*, whereas graminoid and bryophyte abundance remains comparatively stable throughout.

4.5.3 Temperature reconstructions

In broad terms, the temperature curves derived from the two different quantitative reconstructions (partial least squares and modern analogue technique) show similar long-term trends with MATs ranging between 6.0-8.5 °C (Appendix 1; Figure A1.1).

4.6. Discussion

4.6.1 Patterns of vegetation and climate change at Adelaide Tarn

The Adelaide Tarn pollen, plant macrofossil and sedimentological records provide a well-resolved history of vegetation and catchment conditions for the last ~15,800 years (Figures 4.5–4.7).

Zone	#Samples	depth (cm)	Age range (cal yr BP)	Dominant taxa (zone mean)	Additional information
AT 1	9	507-557	14,800-15,800	*Fuscospora* (52%), *Phylocladus* (11), Poaceae (11)	Minor contributions of *Lophozonia menziesii*, *Coprosma* and Asteraceae. High total tree percentages and low shrubs and percentages.
AT 2	25	387-502	12,500-14,800	*Fuscospora* (25), Poaceae (17), *Phylloladus* (14)	Abrupt drop of *Fuscospora* and increments in *L. menziesii*, *Prumnopitys taxifolia* and *Libocedrus*. Grassland taxa Apiaceae, *Astelia* and Poaceae reaching their record-maxima making the total tree percentage drop significantly
AT 3	13	313-382	10,000-12,500	Poaceae (14), *Lophozonia menziesii* (13), *Fuscospora* (12)	*Fuscospora* reaches minimum abundances while *L. menziesii* continues its increasing trend. *Dacrydium cupressinum* experience a significant increase throughout. Conifer-broadleaf taxa including *P. ferruginea*, *P. taxifolia*, *Libocedrus* and *Metrosideros* increase notoriously. Poaceae, *Astelia*, Apiaceae and Asteraceae show overall diminution.
AT 4	10	263-308	8700-10,000	*Dacrydium* (15), *Lophozonia menziesii* (14), *Fuscospora* (14)	*Fuscospora* recovers from minima while *L menziesii* high ambulances persist. *D. cupressinum* reaches a peak plateau. Prumnopitys *ferruginea*, *P. taxifolia*, *Libocedrus* and *Metrosideros* decrease with respect to the previous zone, while the shrub conifer *Halocarpus* shows a notable increment. All grass taxa decline in this zone
AT 5	10	213-258	6400-8700	*Fuscospora* (32), *Lophozonia menziesii* (13), *Dacrydium* (10)	*Fuscospora* continues recovering while *D. cupressinum* starts to decline. P. ferruginea, *P. taxifolia*, *Libocedrus* and *Metrocideros* show minimal abundances and *Halocarpus* decline considerable. The total shrub and herb abundances show considerable diminutions. Notably, this zone features a significant increment in the littoral macrophyte *Isoetes* (increment from 2% to 10%).
AT 6	43	1-208	Present-6400	*Fuscospora* (49%), *Isoetes* (15%), *Lophozonia menziesii* (10%)	Stable high abundances of *Fuscospora*, *L. menziesii* and *D. cupressinum* are the main features of this zone. Almost all the conifer-broadleaf taxa show minimal abundances except by *Halocarpus* that shows a gentle recovery. Total Shrubs and herbs do not show major changes, while *Isoetes* shows high magnitude oscillations superposed on an increasing trend. No exotic pollen is found in this or any previous zone.

Table 3. Summary of Adelaide Tarn pollen zones

Previous work has shown that pollen sites in such high-altitude setting are sensitive not just to the vegetation communities at that elevation, but also to those growing on lower slopes (Moar, 1970; McGlone and Basher, 2012) so they can provide insight into climate-related changes in altitudinal vegetation across a broad elevation range.

Between the extrapolated ages of 15,800-14,800 cal yr BP the pollen record is characterized by high levels of the forest tree taxon *Fuscospora*, the shrub-small trees *Phyllocladus*, *Coprosma* and *Myrsine*, and herb pollen. In contrast, the plant macrofossil record shows only non-arboreal taxa (Figure 4.5 and 4.7), suggesting local dominance of alpine grassland and a lowered treeline under relatively low temperatures. Cold conditions are also suggested by the low organic productivity, as indicated by the absence of brown organic sediments in the lake at that interval. The differences between the pollen and plant macrofossil records can be reconciled by considering that the pollen of *Fuscospora* and the other woody subalpine taxa were probably wind-transported both inland and upslope from distant sources across a relatively open landscape, a feature that has been observed in modern pollen rain studies (Bussell, 1988; McGlone and Basher, 2012).

Potential sources of *Fuscospora* pollen include the coastal regions of north-west South Island, to the west and south-west of the study site, where Last Glacial Maximum pollen assemblages dominated by *Fuscospora* (up to 80%) have been reported (Moar et al., 2008; Newnham et al., 2013). Further support for this interpretation comes from the comparatively low terrestrial pollen influx observed during this interval (Figure 4.6), consistent with sparse local vegetation and open landscape. Such conditions are likely to have existed during the earliest part of the Adelaide Tarn record when local vegetation communities were adjusting to recent deglaciation. The alternative explanation – that southern beech trees were established around the lake at ~14,000 cal yr BP – is not supported by our plant macrofossil evidence or by independent palaeoecological and palaeoclimatic records for this time (e.g. McGlone and Basher, 2012; Barrell et al., 2013).

Between 14,800-12,500 cal yr BP, *Fuscospora* declines rapidly from ~55 to ~25%, accompanied by a steady increase of *Lophozonia menziesii* and the appearance of several representatives of the conifer–broadleaf forest. During this period, herbs including Apiaceae, *Astelia* and Poaceae show significant expansions (Figure 4.5) while a lithological transition from the inorganic grey unit to a darker organic brownish black silt/clay occurs at 14,300 cal yr BP (Figure 4.3). There is still no trace of any arboreal elements in the macrofossil record (Figure 4.7), suggesting that a forest-free environment persisted around the lake. Whereas the appearance of conifer–broadleaf pollen taxa and the transition to a darker silt unit suggest a relative climate amelioration, the increments in *Lophozonia* and grass pollen suggest the opposite trend. Total terrestrial pollen influx underwent a five-fold increase from Zone 1 (900 grains*cm-2*yr^{-1}) to Zone 2 (4400 grains*cm^{-2}*yr^{-1}) and all major pollen taxa, including *Fuscospora*, experienced increases in their accumulation rates (Figure 4.6). The marked decrease in *Fuscospora* percentages therefore may reflect the proportionate increase of other terrestrial pollen, rather than a major decline in *Fuscospora* trees.

The pollen-derived climate signal is therefore ambiguous for this interval, although as discussed in the following sections, our preferred temperature reconstruction shows an attenuation of the warming trend that commenced before that period.

At ~12,500 cal yr BP, pollen levels of Poaceae and other herb taxa decline from their previous maxima while percentages of lowland to sub-alpine conifer–broadleaf tree taxa increase substantially. Prominent among these trees is the tall podocarp *Dacrydium cupressinum*, a lowland tree restricted to humid lowland areas below 600 m (Franklin, 1968). These changes suggest that conifer–broadleaf forest with prominent *D. cupressinum* expanded upslope to attain its present upper altitudinal limits or higher. Judging by the *D. cupressinum* curve (Figure 4.5), peak elevation may have been reached by 10,000 cal yr BP, close to the time that tree macrofossils first appear at Adelaide Tarn. I conclude that, from 12,500 cal yr BP and possibly earlier, forest communities expanded upslope across the region as a response to sustained warming. *Fuscospora* pollen abundances began to increase between 9800-7000 cal yr BP, along with the sub-alpine taxon *Halocarpus*, when other lowland to montane trees including *D. cupressinum* decline. This change signals the curtailment of the previous warming trend, although a plateau of relatively high abundance of *D. cupressinum* until 7600 cal yr BP indicates the persistence of comparatively mild and moist conditions.

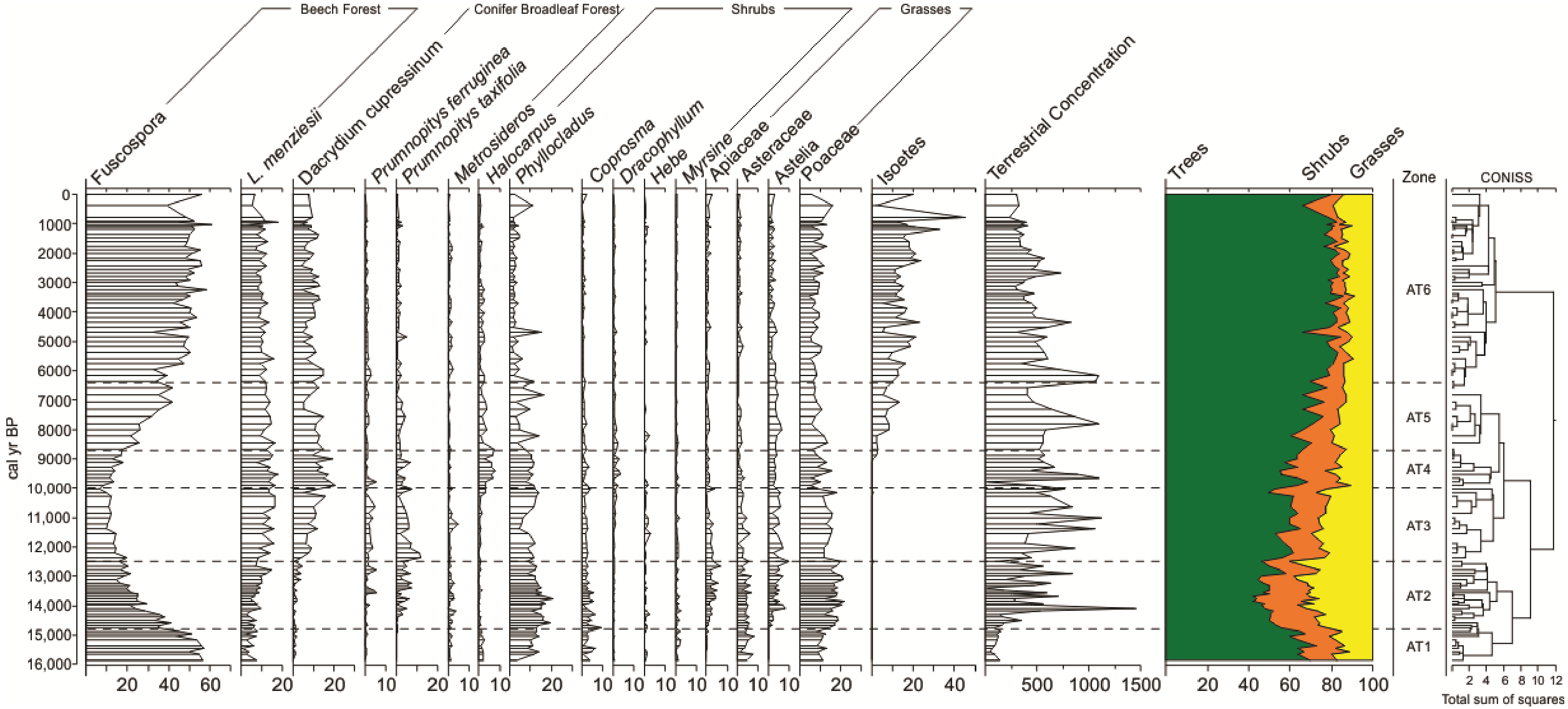

Figure 4.5. Adelaide Tarn pollen percentage diagram. Percent changes of the main pollen taxa are plotted against the time scale obtained from the age model. The diagram include the total concentration of terrestrial pollen and the total sum of trees, shrubs and grass taxa; as well as a stratigraphically constrained zonation of the pollen data using the statistic tool CONISS.

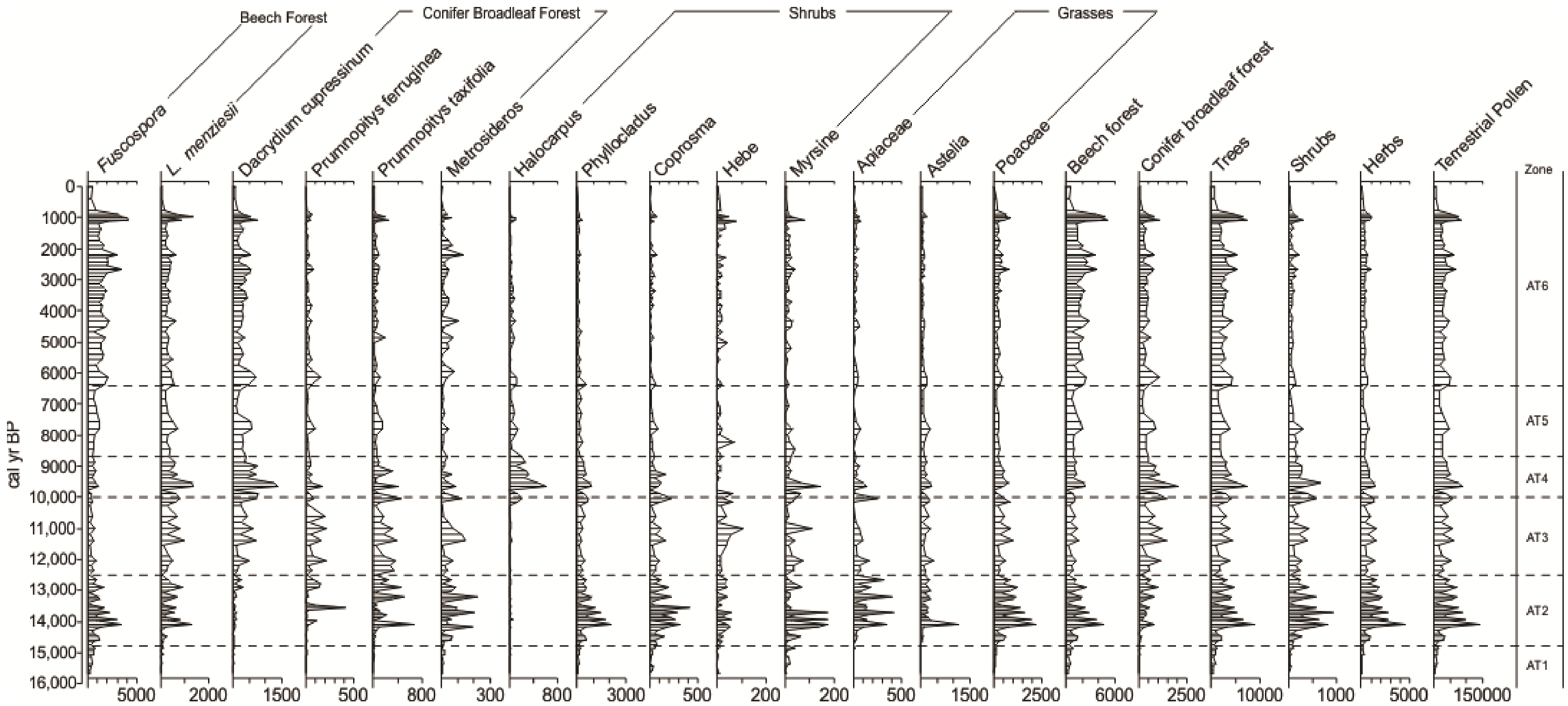

Figure 4.6. Adelaide Tarn pollen influx diagram. Pollen influx (grains*cm^{-2}*yr^{-1}) is plotted against the weighted mean calendar age indicated by the age model. The diagram include the total influx of trees, shrubs and grasses; as well as the sum of Beech and Conifer broadleaf forest taxa. Note that all values are divided by #100 except the values of Fuscospora, total Trees, Herbs, total Terrestrial pollen which are in turn divided by #1000.

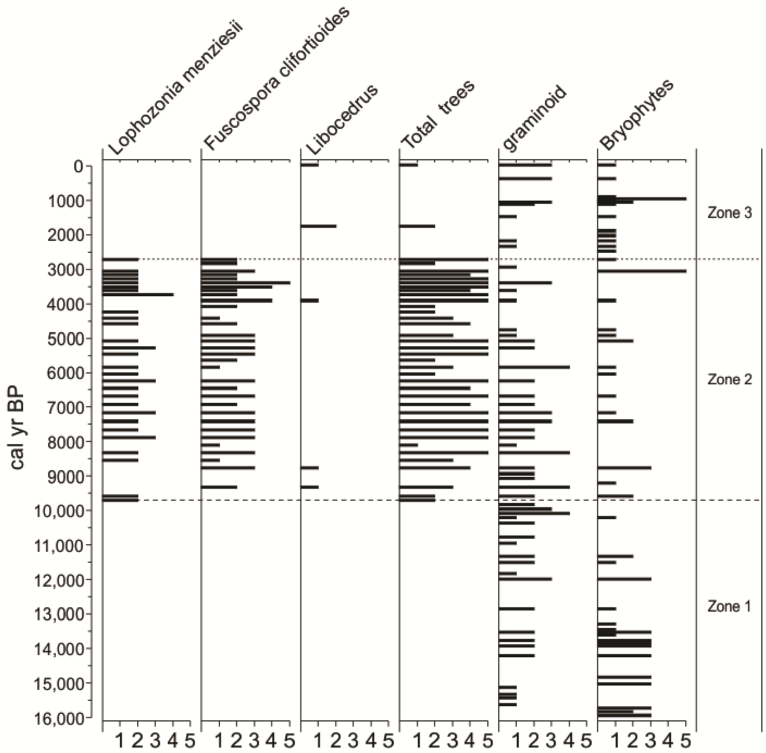

Figure 4.7. The Adelaide Tarn plant macrofossil record showing the major species identified and their variation with respect to a relative abundance scale (1) rare, (2) some, (3) many, (4) common and (5) abundant.

The plant macrofossil record shows the appearance of *Libocedrus bidwillii* together with *Fuscospora cliffortioides* and *Lophozonia* leaves. *L. bidwilii* is a conifer with a broad altitudinal range and is a common floristic element of lowland and montane conifer–broadleaf forest communities. However, its association with *L. menziesii* and *F. cliffortioides* occurs mainly above 700 m in the western South Island (Veblen and Stewart, 1982), and therefore their coexistence in the macrofossil record suggests a local development of high-elevation southern beech forest with minor presence of conifers, a similar vegetation pattern to that near the lake today. The increase in *Fuscospora* pollen therefore suggests the local establishment of *Fuscospora cliffortioides* trees. Although the overall decrease in the percentages of lowland to montane trees could be associated with a masking effect of the increase of local *Fuscospora* pollen, the influx of these former taxa decreases notably after 9000 cal yr BP (Figure 4.6), suggesting a genuine decline. Additionally, a lithostratigraphic change from dark brown to light brown clay/silt sediment at 7600 cal yr BP (Figure 4.3) suggests a decrease in the organic productivity of the lake as a response to lower temperatures. I therefore suggest a contraction of the conifer–broadleaf forest community in response to an overall cooling trend between 10,000-7000 cal yr BP, although this trend lacked the intensity or continuity to push the treeline below the Adelaide Tarn basin. This pollen–climate trend is more marked between 7600-7000 cal yr BP and subsequently reversed between 7000-6000 cal yr BP with an increase in *D. cupressinum* and a plateau of *Fuscospora*.

After ~6000 cal yr BP, *Fuscospora* pollen increased steadily again through to the present while most other terrestrial taxa remain relatively constant (Figure 4.5). The macrofossil record indicates the continuing presence of the tree taxa *Fusospora cliffortioides*, *Lophozonia menziesii* and *Libocedrus bidwillii* around the site during the mid- and late Holocene (Figure 4.7). At ~ 2700 cal yr BP there is a major change, with the disappearance of most trees from the macrofossil record. This event suggests a lowering of the treeline in response to a cooling trend starting at 2700 cal yr BP or before.

4.6.2 Regional palaeoclimate implications

A Lateglacial cooling interval, broadly corresponding to the Antarctic Cold Reversal (14,500–12,800 cal yr BP), has been recognized in palaeoecological (Newnham and Lowe, 2000; Vandergoes et al., 2008; Lowe et al., 2013), glacial geomorphological (Putnam et al., 2010; Kaplan et al., 2013) and speleothem (Hellstrom et al., 1998) records from New Zealand (see also Alloway et al., 2007; Barrell et al., 2013). The climate signal at Adelaide Tarn is ambiguous for this period in that both cool and warm climate indicators are observed. In particular, an increase in the abundance of alpine herbs is especially evident between 13,700-13,000 cal yr BP and implies cooler conditions at the site, whereas a minor increase in the lowland–montane tree taxon *Prumnopitys* implies warming at lower elevations. Interpretation of these signals is complicated by local site factors such as the catchment vegetation and hydrology were likely to be still adjusting to recent glacial retreat and by the changing ‘masking’ effect of the predominant pollen taxon during this zone, *Fuscospora*. Therefore, I refrain from conclusive assertions about this interval.

In contrast, unambiguous evidence for warming at Adelaide Tarn between 12,500-9800 cal yr BP is consistent with the assertion of an early Holocene (11,500–9000 cal yr BP) warm event widespread in New Zealand (Williams et al., 2005; McGlone and Moar, 1977; McGlone et al., 2004; McGlone et al., 2011). From a comparison of pollen and macrofossil data with a forest simulation model, McGlone et al. (2011) suggested that MATs in the central South Island between 11,500-9500 cal yr BP were at least 1.5°C higher than present, although they also indicated that summers could have been cooler and precipitation reduced by at least 30%. Vegetation patterns at this time were attributed to a combination of reduced seasonal extremes in temperature, warm oceans and reduced westerly wind flow. The argument of McGlone et al. (2011) for colder summers despite overall higher annual temperatures is supported by a series of records from sites at the present treeline that show minimal or no forest during the early Holocene. The plant macrofossil record at Adelaide Tarn, situated just below the modern treeline, is consistent with this scenario because the first unequivocal evidence for establishment of a treeline at this elevation is not observed until 9,700 cal yr BP, towards the end of this early Holocene warming interval. However, I acknowledge that the relatively late appearance of arboreal elements in the plant macrofossil record might also be the result of slow tree migration rates and not necessarily from cooler summers.

4.6.3 Adelaide Tarn temperature proxies

The quantitative pollen–temperature reconstructions derived for Adelaide Tarn using the modern analogue technique and partial least squares approaches differ fundamentally from that derived using the PTP index (Appendix 1; Figure A1.1). I question the applicability of both quantitative temperature reconstructions in light of these differences and several other observations (see Appendix 1, section A1.3). The quantitative temperature reconstructions are also fundamentally at odds with many of the temperature inferences drawn from the pollen and plant macrofossil records discussed above. In particular, the earliest part of the record (16,000–14,000 cal yr BP) is shown as warmer than most of the interval 12,000–9000 cal yr BP; and the late Holocene is shown as warmer than the early Holocene. Previous works (Wilmshurst et al., 2007; Newnham et al., 2013) have highlighted problems with the New Zealand pollen–climate transfer function approach when applied to cold climate reconstructions due to limitations in the modern training set. Further complications arise from the distorting influence of *Fuscospora,* a commonly over-represented and widely dispersed pollen type with an ambiguous temperature affinity. The qualitative PTP reconstruction, on the other hand, avoids both these limitations since it has been developed in the context of the known regional vegetation– climate relationships and is strongly correlated with MATs in the pre-deforestation pollen dataset (Figure A1.1). Although the PTP index is qualitative, I conclude that it can be used as a reliable temperature proxy at this site. I now turn to a comparison of other Southern Hemisphere climate records using the Adelaide Tarn PTP index.

4.6.4 Links with millennial-scale low- and high-latitude climate variations

The Adelaide Tarn PTP shows a pause in an ongoing warming trend between 13,700-13,000 cal yr BP (Figure 4.8). This pause overlaps with the later part of the Antarctic Cold Reversal and with a stalling or slight decline of the deglacial increase in global atmospheric CO_2 concentrations (EPICA community members 2004; Monnin et al., 2004; Figure 4.8). As the main source of cold and moist air masses in the Northwest Nelson region is the southern westerly wind (SWW) belt, then the implication for this attenuation at Adelaide Tarn is that the prevailing westerly circulation was positioned further northwards from its current position and consequently intensified at Adelaide Tarn. I emphasize that this particular assertion is tentative due to the difficulties in interpreting the early part of the Adelaide Tarn pollen record noted earlier. A warming trend observed in the PTP index between 12,500-10,000 cal yr BP (Figure 4.8), also observed elsewhere in New Zealand as discussed earlier, implies a weakening of the westerly circulation over Northwest Nelson because of a southward migration of the SWW belt. The warming trend includes a rapid phase between 13,000-12,000 cal yr BP and a plateau between 12,000-10,000 cal yr BP, and is well aligned with a rapid increase in Antarctic temperature between 12,500-11,500 cal yr BP and a peak warming between 11,500-9000 cal yr BP.

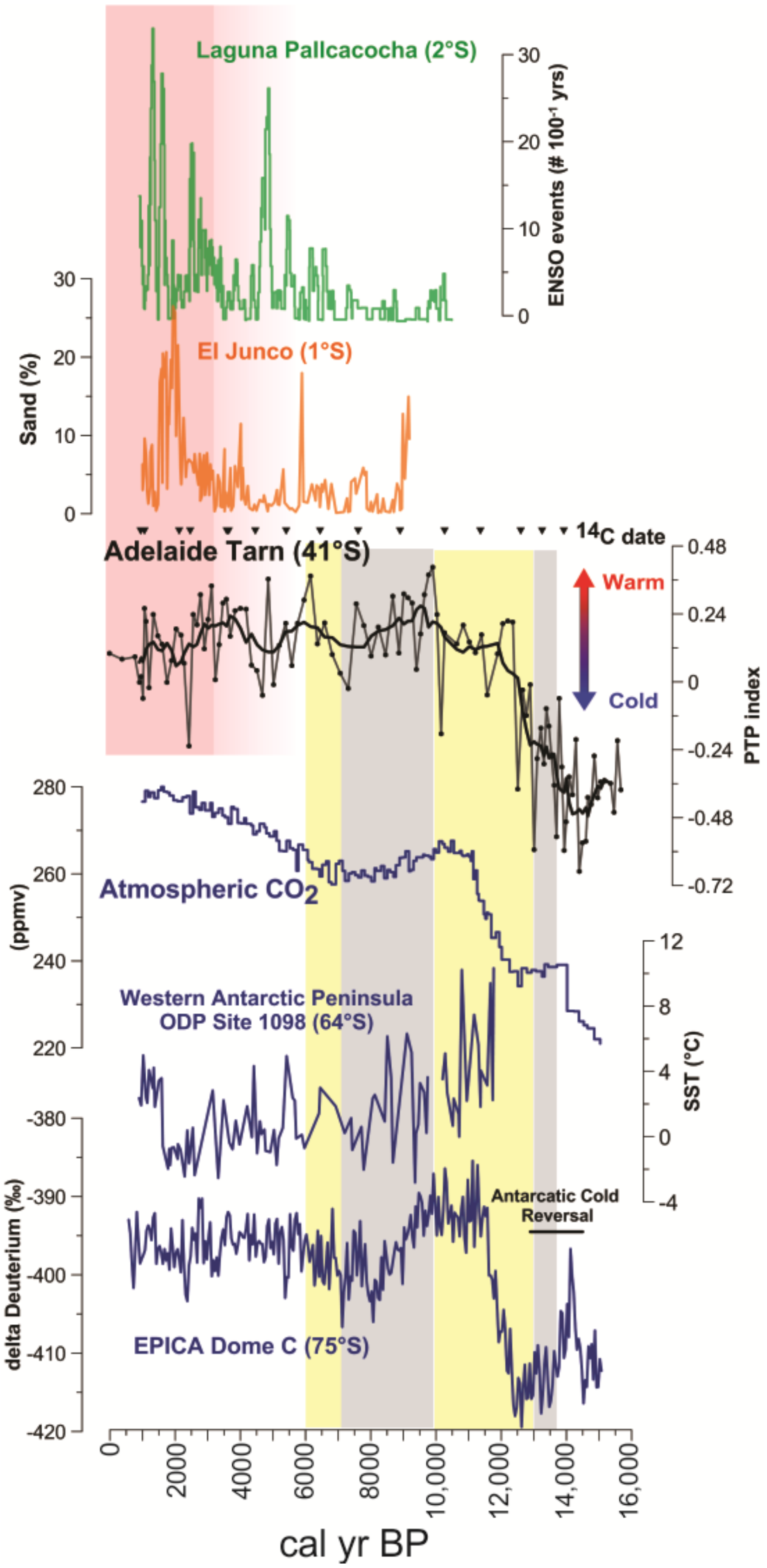

Figure 4.8. Adelaide Tarn PTP reconstruction (black curve) including all radiocarbon dates (black triangles) compared with climate proxies from the Tropical Pacific (Conroy et al., 2008; Moy et al., 2002), Antarctic Peninsula (Shevenell et al., 2011) and east Antarctica (EPICA Community Member, 2004). The grey rectangles indicate cooling or temperature ameliorations; while yellow rectangles indicates warming periods at Adelaide Tarn. The red rectangles indicates period of relative increased frequency/intensity of El Niño events.

These patterns at Adelaide Tarn concur with relatively high temperatures recorded in ocean records in the western margin of the Antarctic Peninsula (64°S) (Shevenell et al., 2011) as well as trends in global atmospheric CO_2 measured in Antarctic ice cores (Monnin et al., 2004; Figure 4.8). Further temperature co-variations between Adelaide Tarn and the Antarctic/Southern Ocean sector are evident in the form of: (i) a cooling trend accompanied by decreasing atmospheric CO_2 between 10,000-7000 cal yr BP, and (ii) a less intense warming in both these regions and increasing atmospheric CO_2 between 7000-6000 cal yr BP (Figure 4.8). The match between the Adelaide Tarn PTP index, Antarctica and the Southern Ocean records represents solid evidence for a continuing teleconnection between the high- and mid-latitudes of the Southern Hemisphere during the late glacial and early Holocene, an inference supported by the strong imprint of Antarctic temperature variability interpreted in pre- Holocene records from South Island, New Zealand (Vandergoes et al., 2005; Vandergoes et al., 2008; Newnham et al., 2012).

These co-varying temperature changes across the mid/high latitudes probably involved coupled ocean–atmospheric interactions modulated by latitudinal shifts of the SWW belt (Toggweiler et al., 2006; Moreno et al., 2010; Putnam et al., 2010). In this regard, warming intervals between 13,000-10,000 cal yr BP and between 7000-6000 cal yr BP in Northwest Nelson could have resulted from a significant reduction of the cold westerly air masses driven by a southward shift of the SWW belt, thereby increasing wind stress over the Southern Ocean around 60°S. Such a shift would have strengthened the Antarctic Circumpolar Current and stimulated the wind-driven upwelling of warmer circumpolar deep waters, warming the Southern Ocean, including the Antarctic Peninsula and promoting ocean CO_2 degasification (Toggweiler and Russell, 2008; Shevenell et al., 2011). Conversely, a northward migration of the SWW belt could have induced the opposite series of events, resulting in a relative cooling around Adelaide Tarn and the Antarctic margin and decrease in CO_2 concentration during the Antarctic Cold Reversal and, to a lesser degree, between 10,000-7000 cal yr BP.

To some extent the teleconnections between mid- and high-latitudes via south/north shifts of the SWW belt proposed here resemble the present-day climate variations expressed by the Southern Annular Mode (SAM). During persistent positive phases of the SAM, the westerly circulation weakens in the mid-latitudes and strengthens in the high-latitudes, resulting in a significant warming in New Zealand (Kidston et al., 2009; Figure 4.2), Patagonia (Garreaud et al., 2009) and the Antarctic Peninsula (Gillett et al., 2006), while most of the Antarctic mainland cools (Turner et al., 2005). Abram et al. (2014) showed this same set of temperature anomalies in their reconstruction of the SAM over the last millennium, which included a sustained positive trend since the 15th century. The millennial-scale warming observed in New Zealand, Patagonia and the Antarctic Peninsula during the early Holocene (13,000-10,000 cal yr BP) is consistent with an overall weakening of the westerly circulation in the mid-latitudes. However, the main difference between the present-day spatial pattern of temperature associated with a positive SAM and the pattern observed during the early Holocene is the intense millennial-scale warming experienced in mainland Antarctica between 12,500-9000 cal yr BP (Figure 4.8). One plausible explanation is that high Antarctic temperatures resulted from significantly longer summer duration between 12,000-8000 cal yr BP. Because summer duration exerts a dominant influence on Antarctic temperature at orbital timescales (Huybers and Denton, 2008), longer Antarctic summers during the first part of the Holocene could have overridden any cooling forcing associated with a positive SAM-like scenario. Thus, although there are some differences between the present-day spatial pattern of temperature anomalies associated with the SAM and the pattern observed during the early Holocene that may arise from differences in orbital configurations, the proxy evidence is still consistent with extended periods of atmospheric circulation analogous to the positive phase of the SAM, and to the negative phase of the SAM between 9500-7500 cal yr BP.

The Adelaide Tarn PTP shows high-amplitude oscillations between 6000-3000 cal yr BP and a sustained cooling during the last 3000 years. This latter signal is supported by the plant macrofossil record, yet it is not evident in the temperatures records of EPICA Dome C and the Antarctic Peninsula, which both show centennial-scale oscillations without a consistent longer-term trend. Moreover, the atmospheric CO_2 concentrations show a reversal of the previously declining trend from 7500 cal yr BP onwards and then a long-term steady rise for the remainder of the Holocene. Thus, a breakdown of the early Holocene millennial-scale coupling between Adelaide Tarn and the high-latitude proxies and their correspondence to global atmospheric CO_2 concentration seems evident. One potential mechanism explaining this disconnection emerges when the Adelaide Tarn temperature reconstruction is compared with climate proxies from the Tropical Pacific (Figure 4.8; Moy et al., 2002; Conroy et al., 2008). These low-latitude proxies suggest an increase in the frequency of El Niño events over the last 4000–5000 years, a trend that has been detected in Holocene lacustrine sediments from northern New Zealand (Gomez et al., 2013). Because present-day El Niño years are associated with a north-eastern displacement of the South Pacific Convergence Zone and an increase in cool westerly and south-westerly flow over New Zealand (Kidson and Renwick, 2002; Figure 4.2), more frequent El Niño states during the late Holocene are consistent with a long-term negative temperature trend over New Zealand. I suggest that this trend is discernible in the cooling PTP signal at Adelaide Tarn over the last 3000 years, and in the marked reduction in tree macrofossils from 2700 cal yr BP. Critical to our inference is that the development of frequent El Niño events in the Tropical Pacific can explain the downward temperature trend in Adelaide Tarn without necessarily requiring a sustained northward shift of the SWW belt. Such a shift would otherwise be associated with consistent cooling in the Antarctic Peninsula and decreases in atmospheric CO_2, but neither of these trends are observed in high-latitude proxy records (Figure 4.8). Stronger climate teleconnections between Adelaide Tarn and the Tropical Pacific for the late Holocene are also in agreement with a climate reconstruction from the eastern North Island that shows a switch from a stronger correlation with southern high-latitude records to a stronger influence of Tropical Pacific climate by 4900 cal yr BP (Gomez et al., 2012).

6.7 Conclusions

Integrated pollen and plant macrofossil records from Adelaide Tarn, a treeline site in mountainous Northwest Nelson, New Zealand, allowed a reconstruction of local and regional changes in vegetation and temperature for the last 16,000 years to be developed. Comparing the millennial- scale temperature trends of this record with other climate reconstructions from New Zealand, Antarctica, the Southern Ocean and the

Tropical Pacific provides key insights into the evolution of high- and low-latitude climate teleconnections manifested in New Zealand. A tight coupling between the temperature trends in Adelaide Tarn and climate proxies from Antarctica and the Southern Ocean suggests a strong teleconnection with the high latitudes for the interval 15,000–6000 cal yr BP, which subsequently weakens. The last 3000 years are marked by a cooling trend in Adelaide Tarn despite rising global atmospheric CO_2 levels, but consistent with other proxy evidence in New Zealand and records of stronger and more frequent El Niño events in the Tropical Pacific. This pattern suggests that the Northwest Nelson area developed stronger climate teleconnections with low-latitude ocean–atmospheric circulation systems from the late Holocene onwards. New highly resolved climate reconstructions from New Zealand should test for these changing climate controls, as well as refining their timing and elucidating the precipitation anomalies associated with them. Climate proxies from other terrestrial areas in the Southern Hemisphere mid-latitudes will help to understand the geographical extent of the climate controls proposed here.

Chapter Five

Continuous pollen-based temperature and precipitation records of the past 14,000 years in northern New Zealand (37°S) and their linkages with Southern Hemisphere atmospheric circulation

5. 1 Abstract

Continuous, 14,600-year pollen and charcoal records from an ombrogenous peatbog in northern New Zealand (37°S) are used to reconstruct regional and local vegetation histories and their association with temperature, precipitation and local water-table fluctuations. Two quantitative temperature reconstructions were developed based on a transfer function approach, whereas precipitation trends were inferred from a pollen ratio between taxa with different drought tolerances. A long-term warming trend observed between 14,600-10,000 cal yr, BP, is punctuated by two brief plateaux between 14,200-13,800 and 13,500-12,000 cal yr BP. Periods of persistent dry conditions are recorded between 14,000-13,400 and 12,000-10,000 cal yr BP, while a long-term wet period is observed between 10,000-6000 cal yr BP. The last 7000 years feature relatively stable temperatures, a long-term drying that culminates with persistent drier conditions over the last 3000 years, and cyclical fluctuations in the bog's water table and fires. Present-day climate controls and comparisons with other climate reconstructions from New Zealand and the Tropical Pacific suggest complex and temporally-variable teleconnections between northern New Zealand and the Southern Hemisphere low- and high-latitude circulation.

5.2. Introduction

Palynological records have valuable potential for reconstructing temperature and rainfall variability at timescales that extend well beyond the instrumental record. Pollen-climate reconstructions from New Zealand, positioned in the mid-latitudes of the South Pacific Ocean, can additionally provide insight into past teleconnections with the low- and the high-latitude circulation systems. Pollen-based studies have helped to constrain the timing and structure of climate fluctuations during the late-Quaternary glacial cycles

(Newnham et al., 2007; Vandergoes et al., 2005) and the transition from the last glacial to the Holocene (McGlone et al., 2010; Newnham et al., 1995; Newnham and Lowe, 2000). The integration of these and other proxy records has resulted in the characterization of a sequence of climate events for New Zealand for the last 30,000 years (Alloway et al., 2007; Barrell et al., 2013). This classification has largely been based around temperature proxies and much less in known about precipitation variability. The relative absence of pollen-based precipitation reconstructions may be explained by two general reasons: (1) because precipitation constraints on vegetation occur in a very limited areas of New Zealand (e.g. McGlone and Moar, 1998) as the oceanic setting imposes a climate regime without pronounced rainfall minima, and (2) because precipitation anomalies, and their relationship with hemispheric circulation, are rather complex and heterogeneous, especially in northern New Zealand where precipitation regimes are associated with both extra-tropical (westerly) and sub-tropical (easterly) circulation (Ummenhofer and England, 2007).

New detailed pollen reconstructions located athwart rainfall-sensitive vegetation setting will not only increase the limited number of precipitation reconstructions, but may also help to resolve specific questions regarding New Zealand paleo-climate. For instance, the existence of a late glacial cold episode has been recognized in northern and southern New Zealand between 13,700-12,500 and 15,000-13,000 cal yr BP respectively (Newnham and Lowe, 2000; McGlone et al., 2004; Newnham et al., 2007; Barrell et al., 2013). In southwest New Zealand, a northward shift of the Southern Westerly Winds (SWW) and associated increase in precipitation has been proposed (Putnam et al., 2010; Vandergoes and Fitzsimons, 2003). However, the timing and direction of precipitation changes in northern New Zealand are mostly unknown; which prevent testing the spatial extent of this proposed expansion, and hence potential drivers and controls.

There are also uncertainties regarding the role of climate teleconnections in the spatial differences observed in paleo-climate trends across the country. For instance, while vegetation modelling using pollen data suggests that precipitation was substantially lower in southern New Zealand between 11,500-9500 cal yr BP (McGlone et al., 2011); the expansion of drought-intolerant taxa in northern New Zealand indicates a period of relatively moister conditions between 12,000-9000 cal yr (Augustinus et al., 2011; Newnham et al., 1995; Newnham et al., 1989; Sandiford et al., 2003). Whether or not these differences arise from problematic interpretations of the proxy data or from the influence of different sources of precipitation has yet to been explored.

New pollen records aimed at advancing understanding of precipitation variability across New Zealand during the Late-glacial and Holocene periods will help to resolve these and other important questions, contextualize the instrumental record of precipitation variability in a longer-term timeframe, and develop a stronger basis for exploring past teleconnections between New Zealand and the Southern Hemisphere circulation systems. Here I use a highly-resolved pollen and microscopic charcoal record from a peatbog in the Waikato region in northern New Zealand to reconstruct the local vegetation history and its association with temperature and rainfall changes over the last 14,600 years. The vegetation setting of the Waikato region has two key advantages for developing regional temperature and precipitation proxies. First, the dominance of mixed conifer-broadleaved forest over beech forest offers the possibility of applying the transfer function approach to develop quantitative temperature reconstructions without distortions arising from the masking effect of beech pollen (Newnham et al., 2013; Wilmshurst et al., 2007). Second, the relative abundance among the dominant podocarp trees can be related to precipitation changes (McGlone and Topping, 1977). I took advantage of these features to develop pollen-based temperature and moisture reconstructions using quantitative methods and a podocarp pollen ratio, respectively. The integration of these reconstructions with other terrestrial and marine proxies is used to provide insights into large-scale atmospheric controls.

5.3 Study Region

5.3.1 The physical setting

The Waikato region (18,000 km^2) comprises two main alluvial basins (100-200 masl) surrounded by a series of mountain ranges (600-900 masl). The lowland basins have been infilled by fluvial aggradation and by volcanic deposits derived from the North Island volcanic centres (Lowe et al., 1987; Lowe, 1988; Selby, 1992). Much of the

Waikato lowlands today are occupied by small lakes and wetland areas where the deposition of volcanic and fluvial sediments impeded the drainage of subsidiary riverine valleys (Lowe, 1988).

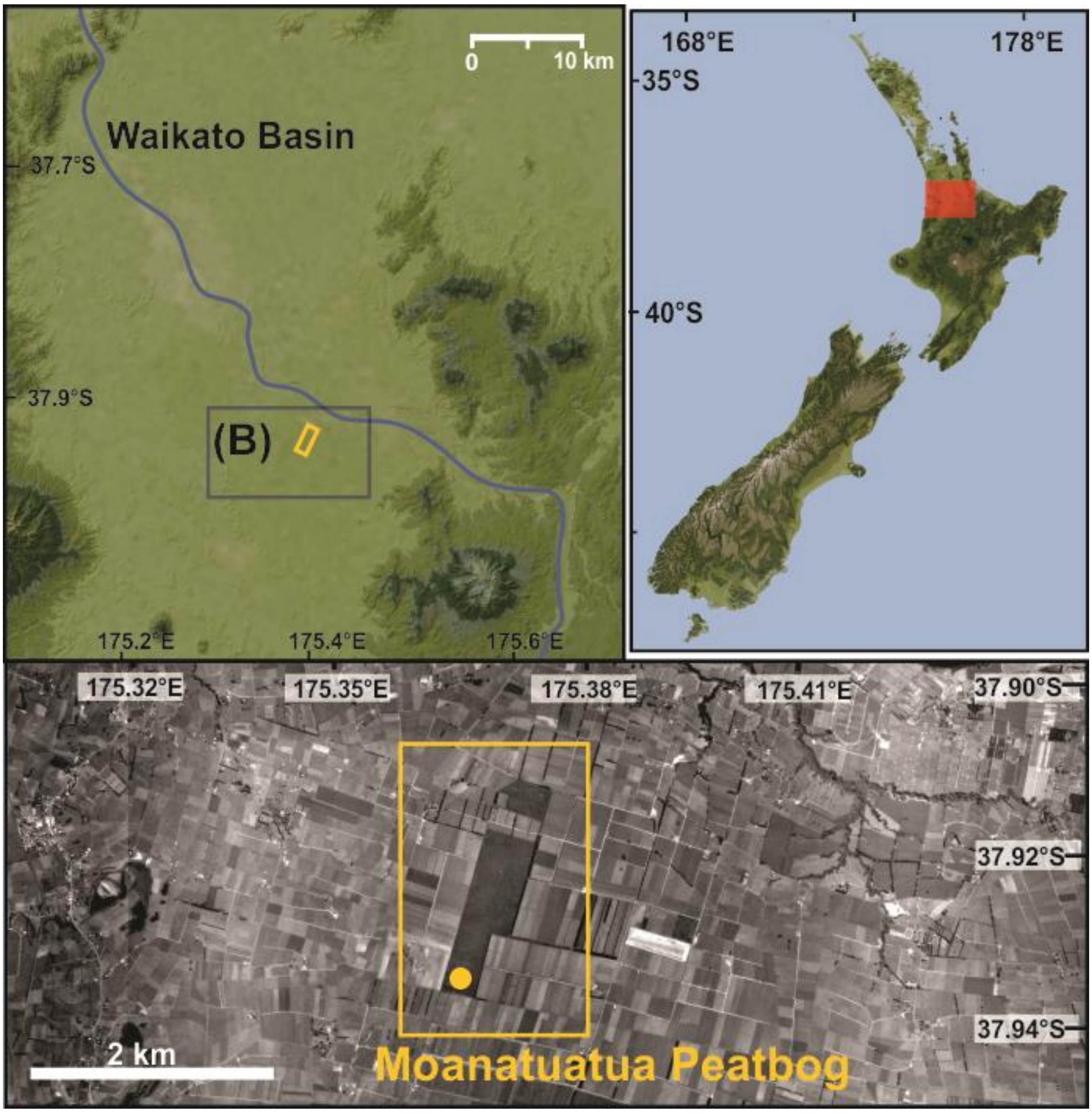

Figure 5.1. (A) Digital elevation model of the Waikato Basin. (B) Aerial photograph showing Moanatuatua Peatbog. The yellow dot demarks the coring area (C) Correlation (1979-2014) between New Zealand summer (DJF) surface temperature (2 m above ground level), precipitation, and the SAM and ENSO index. The SAM corresponds to the Antarctic Oscillation Index from the National Oceanic and Atmospheric Administration (NOAA) while ENSO corresponds to the Southern Oscillation Index (SOI). Contour intervals are at 0.1 values of a detrended correlation coefficients. 2-tailed Student's t test is used to calculate significance values (colored contours). Atmospheric data correspond to monthly mean ERA-Interim global atmospheric reanalysis (1979-present) employed at 1.5x1.5° latitude-longitude resolution.

Some of these, including the study site, have developed into peat bogs during post-glacial times (McGlone, 2009). Sedimentary records recovered from these lakes and bogs have included a series of Quaternary tephra layers from the Central North Island volcanic zone, the Egmont-Taranaki volcanic complex, and offshore volcanic islands (Lowe et al., 1980).

5.3.2 Climate controls

Situated around the 37-38°S boundary, the Waikato region has a warm-temperate climate with prevailing westerly and south-westerly wind flow. Data from the National Climate database (www.cliflo.niwa.co.nz) shows that mean annual temperatures are around 14°C in the lowland but they can drop to less than 9°C in the few areas above 900 masl. During austral summer months (December, January and February) lowland mean temperatures can reach above 18°C, while winter (June, July and August) temperatures are about 10°C. The geographic distribution of precipitation in the Waikato region is largely a result of the prevailing westerly flow and the regional physiography. Peak annual precipitation in the western uplands (2300 mm*yr^{-1}), while annual precipitation in the lowlands is considerably lower, oscillating between 1100-1500 mm. Overall, the whole region experiences a slight rainfall peak during winter months (30% of the annual amount) when south-westerly storms are stronger and more frequent (Ummenhofer and England, 2007). However; summer precipitation may also be significant (20%) and highly variable on an inter-annual basis, especially when sub-tropical storms reach the region.

New Zealand climate variability is explained to a significant extent by modes of climate variations such as the El Niño Southern Oscillation (ENSO) and the Southern Annular Mode (SAM) (Kidson and Renwick, 2002; Kidston et al., 2009; Ummenhofer and England, 2007). El Niño conditions and negative phases of SAM are associated with anomalous westerly and southwesterly flow, bringing colder temperatures to most of the country (Figure 5.1) (Salinger and Mullan, 1999; Thompson et al., 2011). During La Niña years and positive phases of SAM these patterns are reversed overall, with generally warmer temperature over the country. In Northern New Zealand including the Waikato region, El Niño conditions produce strong negative anomalies in summer precipitation (Figure 5.1), which result from a reduced input of easterly and northwesterly precipitation fronts (Kidson and Renwick, 2002).

5.3.3 Modern vegetation trends

The native vegetation of the Waikato lowlands has been almost completely destroyed by anthropogenic fires and clearance and replaced by an agricultural landscape. Soil and pollen analyses suggest that this region was densely covered by mixed conifer-broadleaf forest prior to human settlement in the 13th century (Newnham et al., 1995; Newnham et al., 1989). Small relict stands and tree stumps indicate the abundance of the emergent conifers *Dacrydium cupressinum*, *Podocarpus totara* and *Prumnopitys taxifolia*. While *D. cupressinum* is the dominant conifer tree in low rolling areas from well drained to waterlogged soils (Franklin, 1968), *Podocarpus totara* and *Prumnopitys taxifolia* tend to become dominant species in relatively drier, exposed areas such as scarps and gullies where sandy and gravel soils prevails. On the slopes of the mountainous areas, where bigger patches of lowland native forest are better preserved, these emergent conifers are accompanied by broadleaved species such as *Beilschmiedia tawa*, *Alectryon excelsus*, *Eleaocarpus dentatus*, *Metrosideros robusta* and *Knightia excelsa*. Other conifers and angiosperms such as *Beilschmiedia taraire*, *Dysoxylum spectabile*, *Rhopalostylis sapida*, *Laurelia novae-zelandiae* and *Dacrycarpus dacrydioides* are also common elements of the canopy of this forest community. The understory is unusually complex and diverse in small trees and shrubs such as *Melicytus ramiflorus*, *Hedycarya arborea*, many other vascular species and also ferns such as *Cyathea dealbata*. Stumps and logs preserved in bogs indicate that the lowland plains north of 38°S once sustained multiple stands of the conifer *Agathis australis* (Clayton-Greene, 1978; Ogden et al., 1992), which apart from isolated relict individuals, is now restricted to the mid-elevations of the surrounding eastern and western ranges following 200 years of European logging. In these areas it appears together with *Fuscospora truncata* and *Phyllocladus trichomanoides* in drier ridges (Newnham et al., 1989).

5.3.4 Study site

Moanatuatua (Figure 5.1) (37°55’33’’S; 175°22’04’’E; 60 masl) is a raised ombrogenous (rain-fed) bog, formed by the progressive accumulation of post-glacial organic-rich material over poorly-drained Pleistocene alluvial terraces (Selby and Lowe, 1992). Today most of the bog has been converted to agricultural land, following extensive drainage over the past ~100 years. The current areal extent (1.15 km^2) is less than 2% of its original expanse (Clarkson, 1997) and the height of the peat surface has also sunk considerably (Gehrels, 2009). The bog vegetation is dominated by two species of the Restionaceae family (restiads or jointed rushes), i.e. *Empodisma robustum* (hereafter referred as *Empodisma*) and *Sporadanthus traversii* (*Sporadanthus*). The dense root system formed by these two species provides the main constituent of peat formation although other plant remains are also well preserved (Haenfling et al., 2016). Other common plants are the shrubs *Leptospermum scoparium* and *Epacris pauciflora*, herbs such as *Baumea teretifolia* and *Schoenus brevifolius*, the ferns *Gleichenia circinnata* (umbrella fern) and *Lycopodium laterale*. Moanatuatua peatbog has been the focus of several ecology, paleoecology and paleoclimate studies in the last 30 years (Appendix 2).

5.4. Methods

5.4.1 Coring, stratigraphy and chronology

Two overlapping 8-m-long cores were obtained from the modern southern edge of the bog in November, 2012. The cores included 0.5-m-long and 1-m long sections obtained with a Russian D-section corer (Jowsey, 1966) and a square-rod piston corer (Wright, 1967), respectively. Correlation between the two cores was based on the identification of corresponding organic and inorganic core horizons that facilitated the construction of a single, composite section. The stratigraphy of the composite section was reconciled through a combination of visual core inspection and photographs. Glass shard constituents of macroscopically visible tephra were geochemically characterized using the electron microprobe (EMP) housed at Victoria University (see Appendix 2). The identification of Waiohau Tephra (14,000 cal yr BP., Lowe et al. 2013) at the base of the composite core was affirmed by a combination of glass shard major element chemistry in conjunction with radiocarbon chronology (Appendix 2; Figure A2.1 and Table A2.1). The chronology of the composite section was constrained by 13 AMS radiocarbon dates obtained from plant macrofossil debris, including wood and charcoal remains. A Bayesian age-depth model was developed using the BACON statistical package (Blaauw and Christen, 2011) in the R platform (https://www.r-project.org/).

5.4.2 Pollen and charcoal analysis

A total of 149 samples taken from 1-cm thick slices spaced at continuous 5-cm intervals were analyzed for pollen and charcoal content. A constant volume of 1 cm^3 of sediment was taken at each slice and then processed for pollen following standard procedures for peat deposits (including KOH and HCL treatments and acetolysis reaction; excluding HF treatment; see Chapter Three). Exotic *Lycopodium* marker spores were added to each sample to enable the calculation of pollen concentration and pollen influx rate. Pollen identification was conducted with the aid of the pollen atlas presented by Moar (1993) and modern reference slides. Since the pollen slides typically revealed a considerable amount of deteriorated saccate conifer pollen specimens (see Appendix 2), three additional morphologic groups were assigned to accommodate the varying levels of taxonomic precision that were achievable. "*Prumnopitys spp"* includes grains of *P. taxifolia and P. ferruginea* that could not be differentiated. "*Podocarpus/Prumnopitys"* includes specimens that can be from either genus. Highly deteriorated saccate conifer grains were further grouped as "Podocarpoids" which includes all members of New Zealand Podocarpaceae. All pollen diagrams were created with the software Tilia version 1.7.16. (E. Grimm, Illinois state Museum, Spingfield, Illinois). A zonation of the pollen diagrams was established based on visual identification of the main transitions and with the assistance of cluster analysis (CONISS) provided by Tilia. Additionally, I calculated microscopic charcoal accumulation rate (#particles*cm^{-2}*yr^{-1}, hereafter referred to as "CHAR") based on charcoal count in pollen slides, their corresponding number of *Lycopodium* markers and the depositional time obtained in the age model. The main trends in pollen, fern spore and CHAR were also examined by Principal Component Analysis (PCA) using the R platform with the Rioja package (Juggins, 2015; see Chapter Three). The analysis excluded all taxa that were <3% in abundance in at least one sample. A square root transformation was applied to the percentage data to minimize the statistical weight of the main pollen taxa.

5.4.3 Temperature and precipitation reconstructions

I applied the modern analogue technique and partial least squares regression models using the New Zealand pre-deforestation pollen dataset published by Wilmshurst et al. (2007) to develop two quantitative temperature reconstructions. Additionally, I estimated the main changes in precipitation around the site by developing a qualitative Pollen Moisture Index (PMI). The PMI is calculated as the normalized base-10 logarithm of the ratio of *Dacrydium cupressinum* (hereafter referred to as *Dacrydium*) pollen percentage to the percentage of *Prumnopitys taxifolia*, *Podocarpus/Prumnopitys and Podocarpus.* This pollen ratio has been used previously for describing past moisture conditions in central North Island (McGlone and Topping, 1977) and in Waikato (Newnham et al., 1989; Newnham et al., 1995) based on the documented drought intolerance of *Dacrydium* compared to the other tree podocarps (Wardle, 1991). The use of this ratio is further supported by the strong negative correlation between *Dacrydium* and humidity in austral spring, measured as the October vapor pressure deficit (OCT-VPD) in the pre-deforestation pollen dataset (Wilmshurst et. al., 2007), and the strong positive correlation showed by *P. taxifolia* (Table 5.1). To describe precipitation changes based on variations in the PMI I normalized the index by its record mean. Thus, positive (negative) values of PMI will indicate the relative dominance (subordination) of the drought-intolerant *Dacrydium* over the other more drought-tolerant podocarp trees under above-average (below-average) rainfall with respect to the average of the last 14,000 years.

Species	MAT	OCT-VPD
Dacrydium cupressinum	0.51	-0.26
Prumnopitys taxifolia	0.06	0.23
Prumnopitys ferruginea	-0.09	-0.44
Phyllocladus trichomanoides	0.64	0.23
Ascarina lucida	0.46	-0.02
Agathis australia	0.59	0.19

Table 5.1. Mean annual temperature (MAT) and October water vapour deficit (OCT-VPD) of selected taxa from the pre-deforestation pollen dataset. Significant correlations are highlighted in yellow (Wilmshurst et al., 2007).

5.5 Results

5.5.1 Stratigraphy and chronology

The Moanatuatua sedimentary sequence features two basal tephra: a 38 cm-thick, fine-graded-to-coarse grey tephra between 731-768 cm, and a 9 cm-thick fine orange tephra at 675-683 cm. Glass major element determination on the fine orange tephra and comparison against major elements data from reference tephras confirms correlation with the Waiohau tephra (14,000 ± 155 cal yr BP; Lowe et al., 2013) (Appendix 2). The Waiohau tephra is overlain by homogenous black, well-humified peat sediments until the top of the section (Figure 5.3). No evidence of other macroscopic tephra is found throughout the section, although several pollen slides show abundant glass shards indicating the likely presence of cryptotephra. There are no marked changes in peat composition in the section although several woody, root and charcoal layers were observed. The uppermost 75 cm of the peat sequence consists of very moist, unconsolidated material comprising mostly root matting, which was unable to be recovered. Ten of the thirteen dated levels yield ages in chronological/stratigraphic order but three samples (NZA 58261, NZA 58253 and NZA 58261) in the upper section show reversed ages (Figure 5.3; Table 5.2). The most basal level dated (730-731 cm) represents the beginning of peat accumulation over the grey tephra and has a 95% confidence range of 15,060-14,250 cal yr BP with a weighted mean of 14,650 cal yr BP. The most basal pollen sample is located one centimeter above the basal-most date level. The upper-most dated level corresponds to the first centimeter of the sediment section and yielded a modern radiocarbon age. The average peat accumulation rate is 0.05 cm*yr^{-1}, and the average resolution for the pollen record is 103 years per sample.

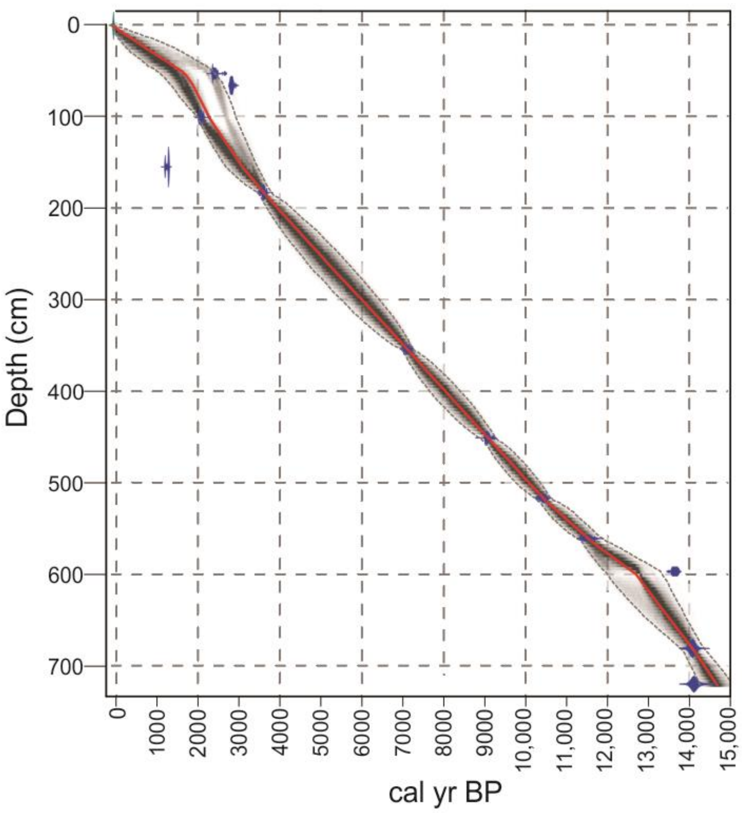

Figure 5.2. Bayesian age-depth model based on the 13 AMS radiocarbon dates from Moanatuatua peatbog. Age modelling was performed with the Bacon package (Blaauw and Christen, 2011) in the R software platform (R core team, 2014). The Southern Hemisphere terrestrial curve (SHCal13) was used to calibrate the radiocarbon dates (Hogg et al., 2013). All calibrated dates with their 95% confident interval are showed in blue. The red line corresponds to the modelled weighted mean and the dotted grey lines demark the modelled minimum and maximum 95% confidence ranges for each centimeter.

5.5.2 Pollen record

The pollen record shows persistent high levels of trees (>80% throughout), dominated by the lowland trees *Dacrydium* and *Prumopitys taxifolia*. Minor terrestrial taxa show successive expansions including *Coprosma* between 14,500-12,500 cal yr BP, *Ascarina* between 12,500-7000 cal yr BP and *Phyllocladus* over the last 7000 years. This latter period feature a series of semi-regular ~ 1000-year peaks in *Prumnopitys taxifolia*, *Podocarpus* and *Podocarpus/Prumnopitys*. The wetland taxa *Empodisma* and *Sporadanthus* show average abundances of 16% relative to the total amount of terrestrial pollen; whereas the fern taxa *Cyathea* and *Gleichenia* average 10 and 4% respectively. Six formal pollen zones were established following these changes (Figure 5.3; Table 5.3).

#	Laborator y code (CAMS#)	Dept h (cm)	14C date ± 1 σ (years)	Calibration curve	youngest 2σ intercept (cal yr BP)	oldest 2σ intercept (cal yr BP)	Median probability (cal yr BP)
1	NZA60455	1	0	SHCal12	0	0	0
2	NZA60344	53	2418±24	SHCal13	2338	2676	2403
3	NZA 58253	66	2776±23	SHCal13	2761	2918	2823
4	NZA 60343	101	2141±25	SHCal13	2008	2149	2073
5	NZA 58261	157	1383±23	SHCal13	1185	1304	1277
6	NZA 58257	185	3399±25	SHCal13	3483	3690	3599
7	NZA 58256	354	6251±28	SHCal13	7004	7243	7098
8	NZA 58255	451	8173±33	SHCal13	8996	9244	9069
9	NZA 58258	517	9294±36	SHCal13	10,226	10,554	10,426
10	NZA 58262	561	10,068±38	SHCal13	11,319	11,749	11,518
11	NZA 58254	597	11,867±46	SHCal13	13,490	13,765	13,651
12	NZA 58256	692	12,230±39	SHCal13	13,943	14,251	14,078
13	NZA 58263	731	12,267±47	SHCal13	13,952	14,324	14,121

Table 5.2. Core, length, calibration curve and sampled material for all radiocarbon date at Moanatuatua. Calibration was performed with the Software Calib 7.02.

5.5.3 Principal Component Analysis

Principal Component Analysis axes one and two (thereafter referred to as PCA 1 and PCA 2) explained 14 and 13 percent of the total variance of the data respectively. In term of taxon scores, PCA 1 is positively related to variations in *Prumnopitys taxifolia* and negatively related to the other non-specific podocarp groups *Prumnopitys* spp, *Podocarpus*/*Prumnopitys* and *Podocarpoid* (negative). PCA 2 distinguishes between positive relationships with *Ascarina*, *Empodisma*, *Sporadanthus* and *Gleichenia* and negative relationships with *Coprosma* and *Prumnopitys ferruginea*. The stratigraphic arrangement of the first two principal components show that sample scores for pollen zones MT 1 and MT 2 have distinctive negatives values for PCA 2 and positive values for PCA 1; while the samples from all the other zones form a denser cluster with comparatively high positive values for PCA 2 (Figure 5.4).

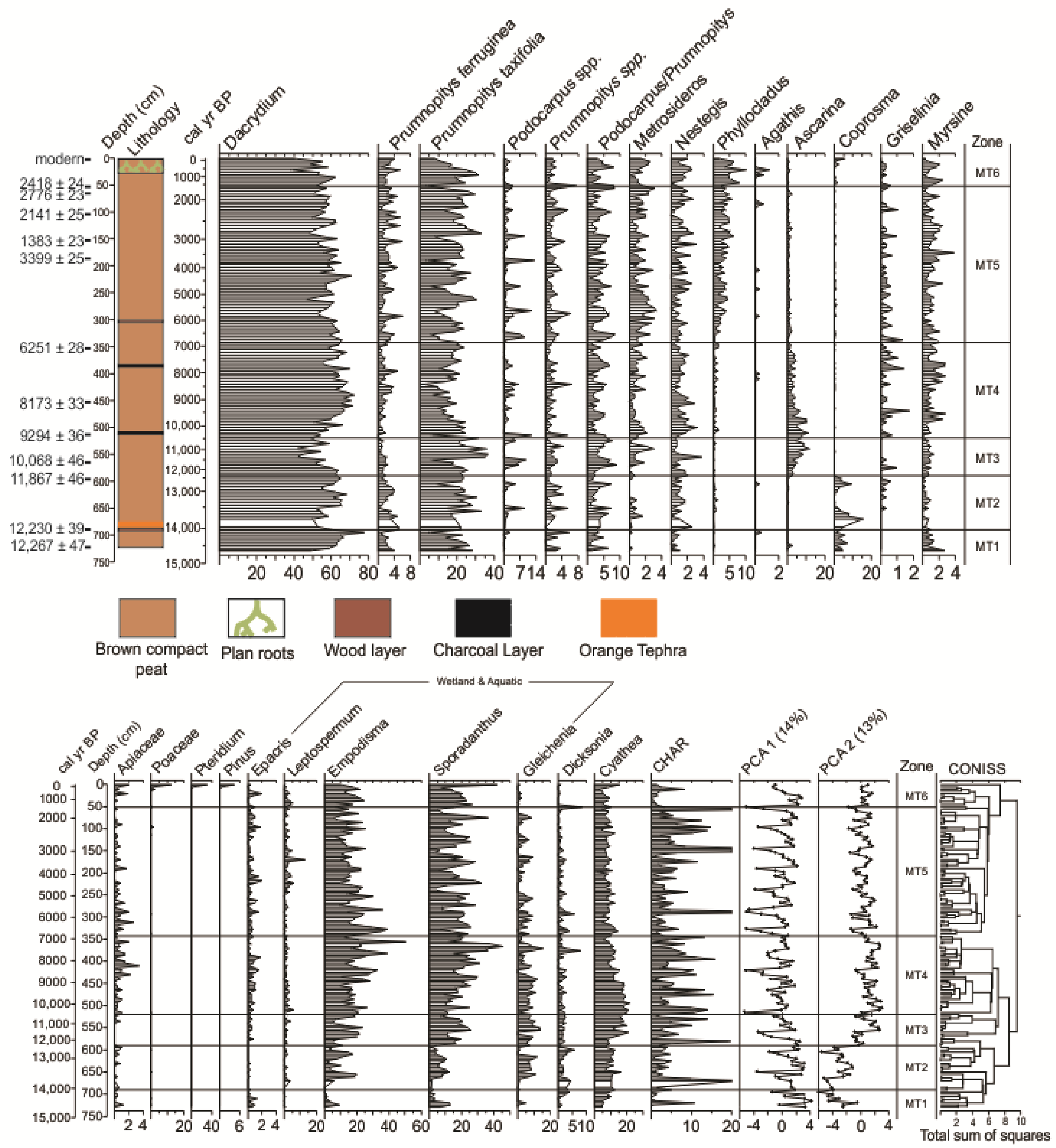

Figure 5.3. Sediment sequence and pollen stratigraphy. The percent abundance of main pollen and spore types are potted against the modelled age and lithology. The upper panel includes the dryland tree and shrub taxa, while the lower diagram shows grass, introduced, wetland, aquatic and fern taxa. The lower panel also shows the sample scores for the first two principal components of the PCA and a stratigraphically-constrained zonation of the pollen data using CONISS analysis. Note the changing scale for certain taxa. Microscopic CHAR vales are divided by 1000 and the curve has been truncated to 20 particle*cm^{-2}*yr^{-1}.

Zone	#Samples	Depth (cm)	Age (cal yr BP)	Dominant taxa (zone mean)	Additional information
MT1	8	749-690 cm	14,600-14,000	*Dacrydium* (63%), *Prumnopitys taxifolia* (19), *Coprosma* (3)	All other main terrestrial taxa show minimal values. Similarly, the restiads *Empodisma* (3%) and *Sporadanthus* (5%) and the tree fern *Gleichenia* (1%) remain sparse throughout this zone. Apart from a prominent peak at the base of the record, CHAR values are minimal during this zone.
MT2	18	690-590 cm	14,000-12,400	*Dacrydium* (58), *Prumnopitys taxifolia* (21), *Coprosma* (4)	*Coprosma* shows two well-defined expansion pulses peaking at 13,900 and 12,700 cal yr BP. The bog taxa, *Empodisma* (7%), *Sporadanthus* (6%) and *Gleichenia* (5%) show slightly higher levels than for the previous zone. CHAR displays higher values compared to the previous zone and a marked peak at 13,900 cal yr BP.
MT3	29	590-520 cm	12,400-8900	*Dacrydium* (56), *Prumnopitys taxifolia* (20), *Ascarina* (5)	Short-lived expansion of *P. taxifolia* (20%), followed by recovery of *Dacrydium* to the previous levels. While *Coprosma* disappears at the beginning of this zone, other broad-leaf taxa such *Griselinia* (<1%), *Nestegis* (1%) and *Metrosideros* (1%) show higher abundances relative to the previous zone. *Empodisma* (15%), *Sporodantus* (16%), *Gleichenia* (7%) and the tree fern *Cyathea* (16%) experience all notable expansion, while *Dicksonia* (2%) shows overall lower abundances. The bog taxa *Epacris* (0.6%) and *Leptospermum* show minor, albeit noticeable increments in this zone. CHAR displays similar background values as the previous zone and several noticeable peaks throughout this zone.
MT4	18	520-342 cm	8900-7100	*Dacrydium* (62), *Prumnopitys taxifolia* (14), *Ascarina* (3)	*Ascarina* (3%) shows progressive decline during this entire zone as does *Cyathea* (14%). This interval also features further increments in the wetland taxa including *Epacris* (1.1%), *Sporadanthus* (20%) and *Empodisma* (22%), the latter two culminating in maxima for the entire record between 7600-7300 cal yr BP. CHAR displays relatively high background values and two peaks centered at 8600 and 7900 cal yr BP.
MT5	63	342-52 cm	7100-1000	*Dacrydium* (56), *Prumnopitys taxifolia* (18), *Gleichenia* (3)	The conifer taxon *Phyllocladus* (3%) and the broad-leaf *Metrosideros* (1%) both show higher abundances than in the previous zone, with the former featuring a persistent increasing trend throughout. After peak abundances in the previous zone, *Empodisma* (18%) and *Sporadanthus* (16%) show overall lower percentages with the latter exhibiting the same distinctive semi-regular cycles mentioned above. CHAR shows relatively low background levels although several high-magnitude peaks including the record-maxima values are observed in this zone.
MT6	10	52-1 cm	1000-present	*Dacrydium* (53), *Prumnopitys taxifolia* (20), *Phyllocladus* (7)	Marked increments in *Phyllocladus* (5%) and the restiads *Empodisma* (19%) and *Sporadanthus* (19%). The end of this zone features a rapid expansion of Poaceae (2%), the fern *Pteridum* (3%) and the exotic *Pinus* (0.5%). CHAR throughout this zone is characterized by increasing values and by the presence of a prominent peak at 200 cal yr BP

Table 5.3. Summary of Moanatuatua Pollen Zones

5.5.4 Temperature and precipitation reconstructions

The temperature reconstructions obtained by the modern analogue technique and partial least squares show little difference from one another (Figure 5.5), the exception being that the modern analogue technique presents overall slightly higher mean annual temperatures with an average of 13.5°C (averaged standard error = 1.54°C); versus 12.7°C (1.55°C) for the partial least squares. In this regard, the modern analogue technique better reproduces the present-day mean annual temperature of the Waikato lowlands (14°C). Although both reconstructions show continuous long-term warming between 14,600-10,000 cal yr BP, the partial least squares reconstruction shows a more marked early Holocene temperature peak and overall more pronounced variability than the modern analogue technique during the late Holocene, including a more defined temperature peak between 12,000-9000 cal yr BP (Figure 5.5).

Three phases of relatively dry conditions can be distinguished from the Pollen Moisture Index based on intervals with below-average values (Figure 5.5). These phases are recorded between 14,000-13,400; 12,000-10,000 cal yr BP; and during the last 3000 years of the record. One marked long-term wet phase is recorded between 10,000-6000 cal yr BP, while less pronounced short-term wet conditions are also observed between 12,500-12,000 and 5000-4200 cal yr BP (Figure 5.5).

5.6 Discussion

5.6.1Vegetation and climate

The pollen record from Moanatuatua indicates that the Waikato lowlands have been extensively forested for at least 14,600 years, in consistent with previous studies from this region (McGlone et al., 1984; Newnham et al., 1989; Newnham et al., 1995). The dominance of *Dacrydium* and *Prumnopitys* throughout the record indicates that lowland conifer-broadleaved forest was the dominant forest formation; whereas minimal abundances of *Fuscospora*/*Lophozonia* indicate that beech forest was essentially absent.

The period between 14,600-14,000 cal yr BP (pollen zone MT1; Table 5.3) shows increasing *Dacrydium* values when all other main terrestrial taxa either do not vary much or show overall declines. From these trends I infer a period of climate amelioration with increasingly warmer and moister conditions. Relatively low levels of CHAR (microscopic charcoal accumulation rate), apart from a single peak, suggests low fire activity and, by inference, relatively wet conditions. The early fire history of the bog must be interpreted with caution however because Haenfling et al. (2016) show that burning of the bog surface was probably not common until raised bog status was achieved in the early Holocene, which made the bog more susceptible to periods of drying. Minimal abundances of *Empodisma* and *Sporadanthus* pollen suggest that raised peat bog conditions were not yet developed around the core site and Haenfling et al. (2016) suggest local swamp forest persisted during this period.

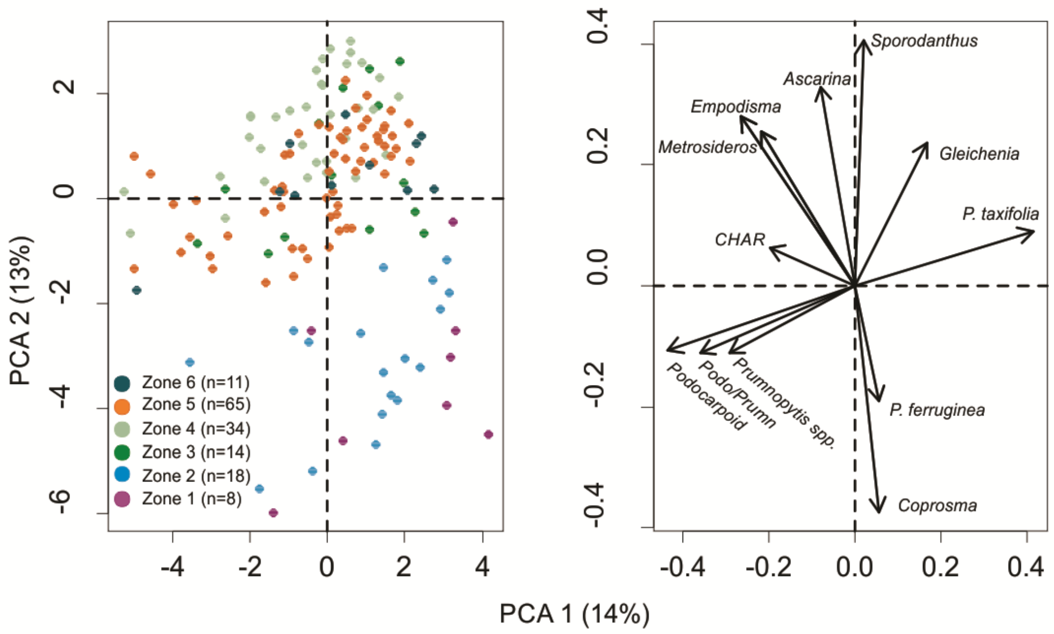

Figure 5.4. Principal Component Analysis (PCA) plot of the two principal axes including pollen and charcoal data from Moanatuatua peatbog. The ordination was carried out in the R software. The results of the analysis are plotted in biplot graphs where the two principal components explaining the largest amount of variation are the main axes. I have added the values of each pollen sample (sample scores) with the pollen zone in different colour labels (left panel) (Table 5.3), and the specific values for the main taxa including CHAR (taxa loadings; right panel). Additionally, the sample scores were added to the pollen diagrams on Figure 5.3.

Between 14,000-12,400 cal yr BP (zone MT2; Table 5.3) the record features two expansion pulses of *Coprosma* peaking at 13,800 and 12,800 cal yr BP, interrupted by increases in *Dacrydium* and *Prumnopitys taxifolia*. The shrub and small tree species included in the genus *Coprosma* are present in a wide range of vegetation communities, including lowland forest, montane beech forest, poorly drained swamp forest and wetlands, and in the margins and gaps of recently disturbed forest (Clarkson, 1997; Wilmshurst and McGlone, 1996). Hence, their expansion at Moanatuatua may support at least two different, but not necessarily exclusive interpretations: the downslope spread of montane *Coprosma* species responding to colder conditions; and the colonization of open *Dacrydium/P. taxifolia* patches by light-demanding *Coprosma* species in response to forest succession or disturbance. I note that the first of these pulses occurs in association with a prominent peak in CHAR at 13,900 cal yr BP, immediately above the Waiohau Tephra (Figure 5.4). This pattern suggests a response to volcanic disturbance (Wilmshurst and McGlone, 1996), although I note that no other taxa indicative of forest disturbance (e.g *Leptospermum*) show noticeable increases. The second *Coprosma* pulse shows neither volcanic nor fire association, suggesting the possibility of an underlying climate signal. The timing and structure of this sequence of pollen and stratigraphic changes display a strong resemblance to the pollen dynamics documented at the upland site, Kaipo Bog, ~180 km southeast from Moanatuatua (Newnham and Lowe, 2000). At this site, the deposition of the Waiohau Tephra is followed by (i) a short-lived (>50 yr) peak of herb pollen, (ii) a transient recovery of tree pollen, and finally by (iii) a second and longer expansion of herbs starting 100-200 years after the tephra deposition and persisting for the next 900-1000 years. This latter long-term persistence of herb pollen relative to arboreal taxa has been interpreted as a late-glacial cooling interval in northern New Zealand (Newnham and Lowe, 2000). Although *Coprosma* is a diverse genus that includes species with low climate sensitivity, the correlation with the Kaipo Bog pattern suggests that the second expansion of *Coprosma* at Moanatuatua between 13,100-12,500 cal yr BP might also be an expression the same cooling interval.

At a local scale, notable increases in *Empodisma*, *Sporadanthus* and *Gleichenia* between 14,000-12,500 cal yr BP suggest a period of sustained peatbog development, although the presence of macroscopic vascular tissue and Cyperaceae cuticles in the plant macrofossil record suggests that the area in the immediate vicinity of the core site lacked bog vegetation and was instead experiencing a transition from swamp forest to fen conditions (Haenfling et al., 2016). This result highlights the fact that peatbog development was patchy at first with extensive peatbog growth likely to have arisen through coalescence of initially discrete patches where drainage impedance was greatest.

The disappearance of *Coprosma* and the expansion of several broadleaf taxa such as *Metrosideros*, *Nestegis* and most notably *Ascarina* between 12,500-10,000 cal yr BP signal an increase in understory diversity beneath a podocarp-dominated canopy as a response to sustained warming and relative moist conditions. This transition is represented by a positive shift in PCA 2, indicating that this component of the PCA analysis is positively correlated to temperature. Between 11,500-11,000 cal yr BP, *Prumnopitys taxifolia* shows a pronounced rise at the expense of *Dacrydium*. The higher drought tolerance of *P. taxifolia* over *Dacrydium* suggests that the 500-year expansion of the former likely represents a trend towards decreasing precipitation. Increasing CHAR values further support this inference, indicating a rise in fire frequency and/or intensity that more likely resulted from drier conditions (Figure 5.5).

Between 11,000-9000 cal yr BP, a shift to warmer and moister climate is indicated by a persistent increase in *Dacrydium*, maximal abundances of *Ascarina* and decreasing abundances of *P. taxifolia*. This period is marked by a rapid increment in PCA 3, manifesting the close relationship beween this compoment and *Dacrydium* abundances (Figure 5.3). Other taxa such as the broadleaf trees *Metrosideros*, *Nestegis*, *Griselinia*, *Myrsine* and the tree-fern *Cyathea* show noticeable expansions suggesting an increase in floristic diversity at the canopy and sub-canopy level. The presence of considerable amounts of CHAR suggests, however, that such conditions did not prevent the occurrence of periodic fires. The plant macrofossil record of Haenfling et al. (2016) indicates the development of raised bog conditions at the core site during this interval. Haenfling et al. (2016) also argue that local peat burnings accompanied the development of raised bog conditions because water table drawdown during dry summers could not be replenished by other moisture sources. The CHAR record presented here supports this assumption by showing a period of high fire activity between 12,500-9500 cal yr BP, despite a trend towards overall moister conditions indicated by the dryland vegetation.

The period between 9000-7000 cal yr BP features a reversal of this pattern. There is a sustained increase in *P. taxifolia*, a decreasing trend in *Dacrydium* and reduced presence of *Ascarina*. Taken together, this evidence likely implies a decrease in regional precipitation and probably decreasing temperatures. CHAR, on the other hand, shows high basal values and at least two prominent peaks, although there is no discernible increase from the previous period (Figure 5.5). These results suggest that the inferred drier trend lacked the intensity or duration to significantly increase the risk of fire. All wetland/bog taxa show notable expansions and record-maxima by the end of this period. This palynological trend concurs with plant macrofossil evidence in showing extensive bog development at this point (Haenfling et al., 2016), almost certainly extending beyond its present-day artificial limits.

The period between 7000-800 cal yr BP features a slow decrease in *Dacrydium*, minima in *Ascarina* and a long-term increase of *Phyllocladus* followed by an expansion in *Agathis* starting at 2100 cal yr BP. In this regional setting, *Phyllocladus* pollen almost certainly represents the northern species *P. trichomanoides* and *P. glaucus* rather than the southern upland species *P. alpinus* (Newnham et al., 1989). The modern occurrence of the northern *Phyllocladus* and *Agathis* shows they are able to tolerate a range of different precipitation conditions including drought (McGlone et al., 1984; Newnham et al., 1989, Ogden et al., 1992), unlike *Ascarina* and *Dacrydium*. This ecological observation is supported in the pre-deforestation pollen dataset which shows strong positive correlations with October vapour pressure deficit (spring air dryness) for both *P. trichomanoides* and *Agathis australis* but near-zero or negative correlations with *Ascarina* and *Dacrydium* (Table 5.1; Wilmshurst et al., 2007). Together this evidence suggests the onset of a multi-millennial trend towards drier conditions and or more variable rainfall regimes in the Waikato lowlands from ~7000 cal yr BP.

A sharp rise of taxa indicative of more open vegetation and forest disturbance (i.e. Poaceae, *Pteridium* and *Pinus*) occurs simultaneously at the top 10 cm of the sediment section (Figure 5.4). The standard palynological sequence for anthropogenic forest disturbance in northern New Zealand features two distinctive phases marked by (1) a decrease in *Agathis* and other forest trees and increase in both charcoal accumulation and *Pteridium* – a fern genus that has been documented as a regional marker for human clearance – by about 800 cal yr BP (McGlone and Wilmshurst, 1999), and (2) a second expansion of *Pteridum* together with exotic elements such as *Pinus* and *Plantago* by

150 cal yr BP (McGlone, 1983; Newnham et al., 1989). The Moanatuatua pollen record shows the two phases of the anthropogenic sequence merged into the two topmost samples (Poaceae expands in the 2 top samples; whereas *Pteridium*, and *Pinus* appear exclusively in the topmost sample) (Figure 5.3), suggesting the effect of sediment mixing or an incomplete stratigraphy. Despite a radiocarbon date from a root sample from the top of the sediment section yielding a modern radiocarbon age (Table 5.2), I consider that this age is likely underestimated because the first 30 cm of the section are disturbed by the penetration of root systems from surface vegetation. This alternative could explained the presence of *Pinus* pollen in samples that might be considerably older than 150 cal yr BP, as the penetration of modern roots could cause the downward translocation of exotic pollen. Alternatively, an incomplete stratigraphy of the top portion of the sediment section might result from the recent drainage or burning of the bog, which could have reduced or removed the uppermost sediments; or by failure to capture these most recent sediments when coring. More details about the first portion of the sediment sections are provided in Appendix 2. A further discussion about the human impact over the vegetation around Moanatuatua is not provided here because it is out of the scope of this study.

5.6.2 Holocene water table fluctuations and fire

A series of ~ 1000-year spaced peaks in *Prumnopitys taxifolia* percentages are centered at 7100, 6200, 5200, 4300, 3300, 2400 and 1400 cal yr BP (Figure 5.3). Based on the reported maximal age range for this species of 800-900 years (Norton et al., 1987; Smale et al., 1997), a straightforward interpretation would attribute those peaks to an ecologically-driven dieback and replacement of *P. taxifolia* cohorts. Cyclical fluctuations between *P. taxifolia* and *Podocarpus* have also been observed at shorter timescales in a lake sequence from north-eastern New Zealand between 1350-850 cal yr BP (Wilmshurst et al., 1997), where seasonal fluctuations in pollen deposition or regular masting cycles has been proposed as potential causes. At Moanatuatua, these cycles occur at considerable longer timescales and extend back until at least 7000 cal yr BP. Critically, a strong negative correlation with the percentages of corroded pollen indicates that the ~1000-year peaks in *P. taxifolia* are likely driven by changes in pollen preservation (Figure 5.3; see Appendix 2 for more details). If so, then these cycles are an artefact of the varying pollen preservation conditions in the peat which governed the ability to identify grains to species rather than generic level. This conclusion is supported by observing that the cycles of *P. taxifolia* are generally in antiphase with the other generic pollen groups that include this species (*Prumnopitys*, *Prumnopitys/Podocarpus*, *Podocarpoid* in Figure 5.3), indicated by the opposing directions between *P. taxifolia* and these other gropus in the PCA plot (Figure 5.4). In other words, when pollen is well preserved, it can be more reliably identified to species level such as *P. taxifolia*; whereas during phases of poor preservation, only general grouping is possible. In this regard, PCA 1 is correlated with the degree of corrosion experienced throughout the record.

In accumulating peat deposits, pollen preservation is most likely controlled by water table variability. Phases of lower/higher water table will encourage/discourage aerobic biological activity in the peat surface, leading to greater/lower levels of pollen corrosion (Lowe, 1982). Thus the quasi-regular fluctuations in *P. taxifolia* pollen levels and the compensating changes in the other groups point to the possibility of millennial-scale cycles of water table fluctuation. In a rain-fed bog complex such as Moanatuatua Bog, these fluctuations must be driven by changes in potential evapotranspiration, which are in turn linked to precipitation. Additionally, there is a positive (although weak) correlation between periods of high corrosion and CHAR, which links fires events with periods of low water table (Table 5.4). The lack of a strong relationship might be related to the fact that fire is more likely to occur during periods of low water table, although other variables such as ignition source and accumulation of fuel might also be critical. A key element to this puzzle is *Gleichenia*. This fern genus also shows quasi-regular 1000-yr cycles, although these cycles are not correlated with corroded pollen or CHAR fluctuations (Table 5.4). Moreover, the *Gleichenia* and the *P. taxifolia* vectors show similar directions in the PCA plot, suggesting a close relationship. I note that the expansion/contraction of *Gleichenia* occurs “out of phase” with the water table and fire cycles discussed above. *Gleichenia* is a usual element in the early post-fire recovery in bogs, where it can resprout from underground rhizomes or burnt bases (Clarkson, 1997). Nevertheless, its post-fire recovery is slow in comparison with other bog species and therefore it might take up to several years to reach its pre-fire abundances (Timmins, 1992; Clarkson, 1997). Thus, a slow recovery of *Gleichenia* might explain the lack of direct positive relationship with CHAR.

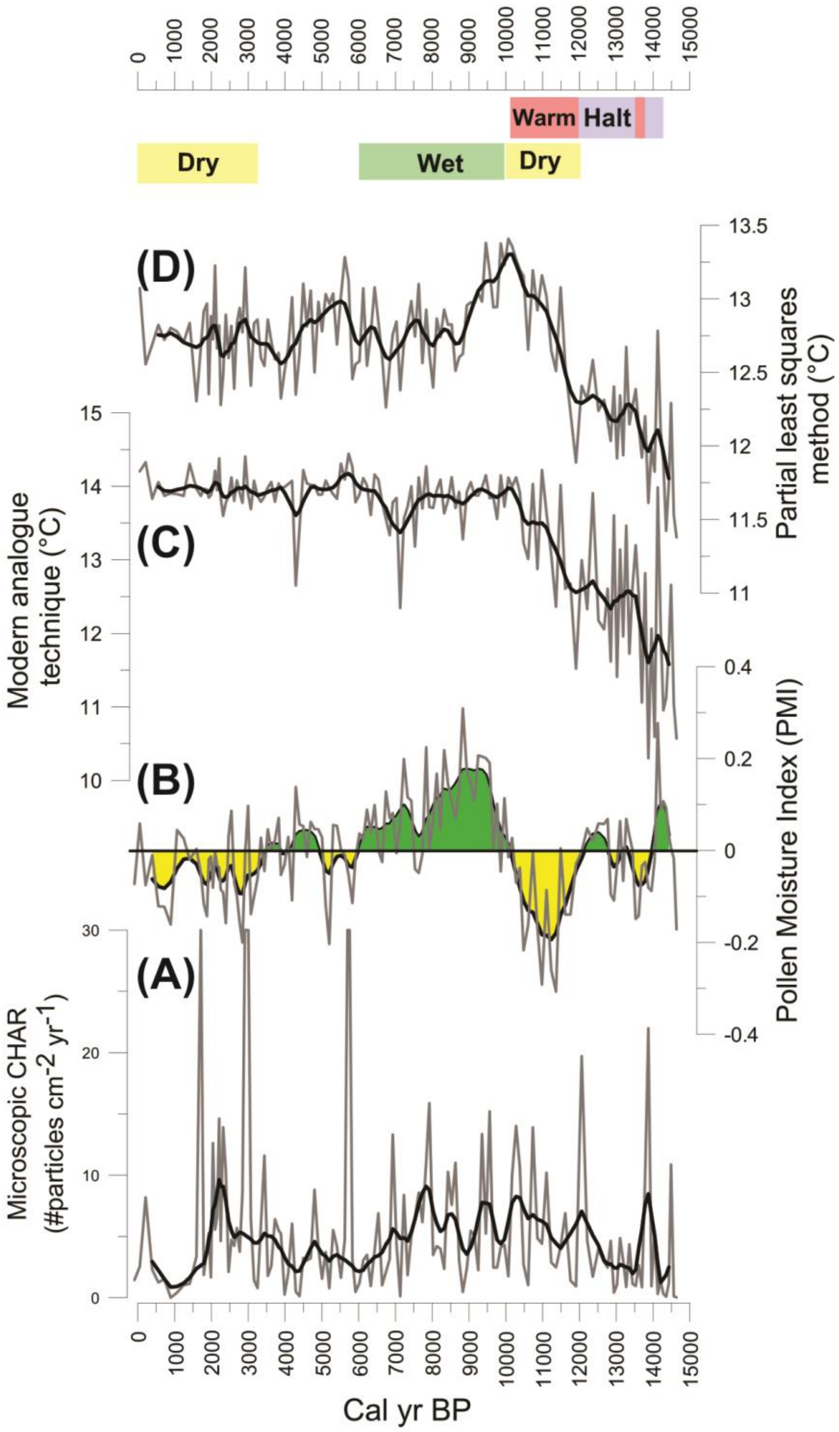

Figure 5.5. Temperature and precipitation reconstructions. Both temperature reconstructions were constructed with the pre-deforestation pollen dataset (Wilmshurst et al. 2007). (A) Microscopic CHAR, (B) Pollen Moisture Index (PMI) calculated as the normalized base-10 logarithm of the ratio of *Dacrydium cupressinum* pollen percentage to the percentage of *Prumnopitys taxifolia*, *Podocarpus/Prumnopitys* and *Podocarpus spp*, (C-D) Temperature reconstructions obtained by the modern analogue technique (C) and the partial least squares (D).

variables compared	correlation	p value regression
corroded restiads vs corroded total pollen	0,71	4,8E-06
corroded total pollen vs *P. taxifolia*	-0,41	0,02
corroded total pollen vs *Gleichenia*	-0,29	0,11
corroded total pollen vs micro CHAR	0,23	0,20
corroded total pollen vs Pollen Moisture Index	-0,03	0,88
P. taxifolia vs microscopic CHAR	-0,42	0,02
Pollen Moisture Index vs micro CHAR	0,06	0,74
Gleichenia vs Microscopic CHAR	-0,24	0,19
Gleichenia vs Pollen Moisture Index	-0,03	0,88

Table 5.4. Correlation coefficients (Pearson Product-Moment) for the result of the pollen corrosion analysis. Significant correlations are highlighted in yellow.

5.6.3 Climate reconstruction and regional atmospheric circulation

In order to characterize regional climate variability pollen data were used to develop temperature and precipitation reconstructions. Figure 5.5 shows these reconstructions with a 7-point weighted average applied to each of them. The two approaches employed for developing the temperature reconstructions have different strengths and limitations, and therefore both of them were used in this discussion (see Appendix 2).

Both temperature reconstructions feature a long step-wise warming trend between 14,600-10,000 cal yr BP separated by plateaux between 14,200-13,800 and 13,500-12,000 cal yr BP. Whereas the earlier of these pauses is possible an artefact generated by the expansion of *Coprosma* after volcanic disturbance, the latter falls within the range of the late-glacial cooling episode as it has been recognized in northern New Zealand (between 13,700-12,500 cal yr BP; Hajdas et al., 2006; Newnham and Lowe, 2000). The lack of a single, well-defined cooling episode at Moanatuatua can be explained by several factors including (1) a comparatively weak expression of the late-glacial cooling episode in northern New Zealand (Carter et al., 2008; Newnham, et al., 2012), (2) little temperature sensitivity of lowland vegetation compared to sub-alpine communities (e.g. Newnham and Lowe, 2000), (3) a seasonal expression unable to be captured by pollen data (Sikes et al., 2013). Alternatively, the two plateaux amidst the long term warming trend at Moanatuatua might each represent minor cooling intervals during late-glacial times or a single, longer cooling episode. Both these scenarios have been previously reported from multi-proxy limnological reconstructions from Onepoto maar, 135 km to the north of Moanatuatua (Augustinus et al., 2012; Sikes et al., 2013).

The late-glacial cooling episodes recorded in proxy records from northern and southern New Zealand have been linked to the Antarctic Cold Reversal (ACR; 14,700-13,000 cal yr BP) (Newnham et al., 2012; Vandergoes et al., 2008). A northward shift of the Southern Westerly Winds (SWW) has been proposed to account for the decrease in temperature (Putnam et al., 2010) and for the increase in precipitation in southern New Zealand (Vandergoes and Fitzsimons, 2003; Sikes et al., 2013). At Moanatuatua, the Pollen Moisture Index (PMI) indicated below-average precipitation between 14,000-13,000 cal yr BP, which is inconsistent with enhanced westerly flow over northern New Zealand. Even though drier conditions at Moanatuatua could have resulted from decreasing westerly flow, this scenario is unlikely considering the aforementioned evidence for northward-shifted westerly winds during the Antarctic Cold Reversal (ACR). Alternatively dry conditions could have resulted from a significant decrease in sub-tropical precipitation. This alternative is only tentative as it cannot be tested with our reconstruction. However, it is consistent with proxy-inferred drier conditions in Northern Australia during the ACR (Denniston et al., 2013), which has been attributed to a northward migration of the tropical circulation belt during that period (Pedro et al., 2016).

The PMI shows the late-glacial warming and the peak temperature observed at Moanatuatua occur together with a distinctive earlier (12,000-10,000 cal yr BP) below-average and a later (10,000-6000 cal yr BP) above-average precipitation anomaly (Figure 5.5). These results are partially supported by other pollen records from northern New Zealand which, in their majority, show persistent warm and moist conditions between 12,000-9000 cal yr BP based on the expansion of the sub-canopy tree *Ascarina* (Augustinus et al., 2011; McGlone et al., 2011; McGlone and Moar, 1977; Newnham et al., 1995; Newnham et al., 1989). Although this expansion is also recorded at Moanatuatua, critical in our interpretation is the increase of the canopy taxa *Podocarpus spp*. and *Prumnopitys spp*, and the reduction in *Dacrydium* abundance. This dry phase coincides with the first period of a documented southward shift of the northern margin of the SWW which resulted in significantly drier conditions in terrestrial mid-latitudes, including New Zealand between 12,000-8000 cal yr BP (Fletcher and Moreno, 2012; Lamy et al., 2010; McGlone et al., 2010). That the pronounced dry phase at Moanatuatua was likely the result of a sustained decrease in the SWW flow is consistent with modern climate observations in the region (De Lisle, 1967).

Interestingly, the first part of the subsequent wet phase at Moanatuatua overlaps with the proxy-inferred period of persistent southward shifted SWW. Under a scenario of reduced SWW over most of New Zealand, an intensification of the sub-tropical eastery circulation offers a potential explanation for the wet conditions in the northern region. Based on pollen records from bog sequences in central New Zealand, Rogers and McGlone (1989) proposed reduced westerly influence and increase in the frequency of northerly wind flow during the early-Holocene. Although this scenario is difficult to corroborate because of the scarcity of proxies from tropical areas, sea surface temperature (SST) reconstructions indicate peak warming in the western Tropical Pacific between 10,000-6000 cal yr BP (Stott et al., 2004) at the same time that SSTs were relatively colder in the eastern Tropical Pacific (Lamy et al., 2010). This pattern resembles the present-day La Niña state, which is consistent with anomalous easterly and northwesterly flows and positive precipitation anomalies in northern New Zealand (Kidson and Renwick, 2000). Clearly, these inferences need to be substantiated by other precipitation reconstructions from the northern New Zealand region.

After 7000 cal yr BP both temperature reconstructions show more stable values, with minor warming between 7000-6000 cal yr BP and cooling between 6000-4000 cal yr BP, both more pronounced in the partial least squares reconstruction. The PMI index shows a long-term drying trend although persistent below-average values are not observed until 3500 cal yr BP. This drying trend is interesting in relation to the downward sloping trend in the $\delta^{18}O$ values of a speleothem record from the Waitomo Cave in western North Island, just 45 km southwest from Moanatuatua (Williams et al., 2010). Although the isotope curve has mostly been interpreted as a cooling signal, Williams et al. (2010) links this cooling with reduced penetration of sub-tropical precipitation fronts. This climate inference might certainly explain the drying trend at Moanatutua. In addition to the PMI index, the disappearance of *Ascarina* and the increase in *Phyllocladus* occurring both from 7000 cal yr BP onwards are consistent with an increase in the frequency of drought and frost events (McGlone & Moar, 1977; Newnham et al., 1995). Thus, I interpret the Moanatuatua pollen record as a predominantly multi-millennial drying signal starting at 7000 cal yr BP, in agreement with other pollen evidence from this area (Newnham et al., 1989; 1995).

The last 3300 years are marked by persistent below-average precipitation in the PMI index, indicating a period of relative dryness. This inference is also evidenced by peak *Phyllocladus* abundances and the latter appearance of *Agathis*. Drier conditions at Moanatuatua is in relative agreement with similar trends inferred from high $\delta^{13}C$ values in the Waitomo speleothem record after 3000 cal yr BP (Williams et al., 2010); and by sediment and pollen records from the North Island suggesting overall drier condition after 4000 cal yr BP (McGlone et al., 1984; Newnham et al., 1995; Gomez et al., 2013). At present day, dry conditions in northern New Zealand are strongly associated with El Niño states (Figure 5.1), when a northward migration of the South Pacific Convergence Zone results in a decrease in the penetration of sub-tropical precipitation fronts (Ummenhofer & England 2006; Kidson and Renwick, 2002). Critical for supporting this scenarios is the evidence for an increase in the frequency and intensity of El Niño events in the Tropical Pacific over the last 5000 years (Conroy et al., 2008; Moy et al., 2002); and the positive relationship found between past El Niño events and *Agathis australis* growth in tree-ring chronologies from northern New Zealand (Fowler et al., 2012). Together, this evidence suggests that climate variability in northern New Zealand has been strongly associated with the El Niño Southern Oscillation for at least the last 3300 years. Further, the quasi-regular water-table fluctuations after 7000 cal yr BP discussed above (Figure 5.3) may also reflect periodic oscillations between El Niño-like and La Niña-like conditions.

5.7 Summary and Conclusions

The Moanatuatua vegetation reconstruction covering the last 14,600 years is used to reconstruct millennial-scale regional temperature and precipitation trends, and also provides evidence for past bog's water table fluctuation. Progressive warming is recorded between 14,600-10,000 cal yr BP, interrupted by two plateaus between 14,200-13,800 and 13,500-12,000 cal yr BP. Warm conditions during the early Holocene occur under an early dry phase between 12,000-10,000 and a wet phase between 10,000-6000 cal yr BP respectively. While temperature proxies remain more or less stable after 7000 cal yr BP, precipitation trends show a long-term drying trend. Based on the present-day regional climate controls and the comparison with other climate reconstruction from New Zealand and the tropical sector of the Pacific Ocean, I propose that the millennial-scale temperature and precipitation changes in northern New Zealand since ca 14,600 years BP have resulted from complex and temporally-variable connections between New Zealand and the Southern Hemisphere low- and high-latitude circulation systems. The precipitation trends presented in this study represent a contribution not only to the temperature-dominated climate stratigraphy of New Zealand, but also to a better understanding of the New Zealand past teleconnections with the hemispheric climate circulation.

Chapter Six

Vegetation, fire and climate links in the Andean *Nothofagus*-forest of Northwestern Patagonia over the last 16,000 cal yr BP (43°S)

6.1 Abstract

A 16,000-year long pollen and charcoal record from a small lake in the Andes of Northwestern Patagonia (43°S) is presented with the aim of reconstructing long-term vegetation, fire and climate linkages. Deposition of inorganic glacial silts, dominance of a high-Andean grassland and absence of local fires prior to 13,600 cal yr BP indicates a glaciolacustrine environment under hyper cold and moist conditions resulting from intense Southern Westerly Winds (SWW). An abrupt transition to organic sedimentation accompanied by rapid forest colonization occurred at 13,600 cal yr BP, and since that time a closed canopy *Nothofagus* forest dominated the immediate environment surrounding the lake. Cold-resistant taxa expand between 13,600-12,000 cal yr BP, indicating that, despite forest expansion, overall cold/moist conditions prevailed. Decline of cold-resistant elements and high charcoal accumulation suggests a trend towards warmer and drier conditions as a result of a weakening and/or southward-shifted SWW between 12,000-10,000 cal yr BP. Increasing seasonality superimposed on a long-term trend towards cold and wet conditions over the last 10,000 years were likely the drivers of persistent closed canopy *Nothofagus* forest, the introduction of cold-tolerant conifers by 6000 cal yr BP, a relatively open forest by 4000 cal yr BP, and steadily increasing fire activity until present time. Local *Nothofagus* dominance is only interrupted by the expansion of non-arboreal elements associated with European settlement over the last 130 yr BP, showing that this recent anthropogenic disturbance was the most significant driver of vegetation change over the last 13,600 years. The reconstruction from Lago Espejo shows that forest expansion predates the onset of high charcoal accumulation by at least 700 years, whilst significant variability in charcoal accumulation occurs under invariant *Nothofagus* forest. These observations indicate that climate variability, and not woody vegetation, was the main driver of fire regimes in the Andes of Northwestern Patagonia. The long-term increase in the difference between

summer and winter temperatures during the Holocene seems to have played an important role in maintaining the dominance of *Nothofagus* forest over lowland broad-leaved forest communities in these mountainous environments.

6.2 Introduction

The Andes of Northern Patagonia (38-43°S) are characterised by a continental climate with well-defined warm/dry summers and cold/wet winters. Along with frequent disturbance from volcanic activity and fire, these climatic patterns exert a strong environmental control that underpins the dominance of closed-canopy *Nothofagus* forest over other lowland (<300 masl) broad-leaved forest communities (Veblen and Ashton, 1978). In this region, fires are generally considered to be the most prevalent disturbance agent able to generate widespread tree mortality and extensive even-aged trees stands (Veblen et al., 1992). In the humid *Nothofagus* forest on the western flanks of the Andes, inter-annual fire regimes seem to be directly associated with moisture deficits, whereas in the drier *Nothofagus*/*Austrocedrus* woodlands on the eastern Andean slopes, precipitation variability controls fire occurrence by favouring the production and accumulation of ignitable fuel (Kitzberger et al., 1997). Wildfire mapping on these eastern slopes showed that historical fires have effectively controlled the spatial extent of *Nothofagus* forests by promoting their replacement by fire-adapted shrubland (Mermoz et al., 2005). On top of these geographic patterns, changes in atmospheric circulation contribute to the impact upon the composition and structure of the Andean *Nothofagus* forest and they also alter fire regimes. Years of widespread fires on both sides of the Andes have been found to be associated with the positive phase of the Southern Annular Mode (SAM) and, on the *Austrocedrus* woodland on the eastern Andean foothills, years of widespread fires have been associated with La Niña conditions (Holz and Veblen, 2011; Kitzberger and Veblen, 1997). The interplay between climate and fire disturbances and its impact over modern Andean vegetation from seasonal to inter-annual timescales have been addressed by these and several other ecological studies (e.g. Kitzberger and Veblen, 2003; Lara et al., 2005), however, their interactions at longer timescales are still poorly understood.

The combination of high-resolution pollen and charcoal reconstructions offers an opportunity to explore causal links between climate, vegetation, and disturbances at longer timescales than classical ecological studies. In Northwestern Patagonia, detailed pollen records have reconstructed past fire activity associated with variations in the position/intensity of the Southern Westerly Winds (SWW) (e.g. Moreno 2004; Pesce and Moreno, 2016); whereas pollen and charcoal reconstructions from lacustrine sequences with multiple tephra layers have been employed to investigate the interplay between volcanism, vegetation and fire regimes (Jara and Moreno, 2014; Henriquez et al., 2015). These and several other post-glacial reconstructions have, however, revealed divergences between sites from the western and eastern sides of the Andes. In the forest-steppe ecotone of the eastern Andean flanks, the absence of woody vegetation has arguably prevented fire occurrence prior to regional *Nothofagus* forest expansion between 16,000-10,000 cal yr BP (Iglesias and Whitlock, 2014). After postglacial forestation, biomass burning seems to have been controlled by fuel availability dictated, in turn, by forest coverage. In the western lowlands, on the other hand, postglacial forest expansion occurred as early as 17,800 cal yr BP and predated the onset of high-magnitude fires by several millennia (Moreno 1999; Moreno and Leon, 2003; Pesce and Moreno, 2014). As mentioned above, past changes in fire regimes in Northwestern Patagonia are not strongly linked to vegetation change but tightly coupled with precipitation variability ultimately controlled by the position and/or intensity of the SWW. Yet, the limited number of sites that extend well beyond the period of regional forest expansion in the Andean sector of Northwestern Patagonia has prevented a closer examination of the relationship between forest expansion, fire and climate in this region.

In this study we present a new 16,000-year long vegetation and fire reconstruction based on high-resolution pollen and charcoal analysis from a postglacial sediment section of Lago Espejo (43.19°S; 71.86°W; 340 masl), a small closed-basin lake in the town of Futaleufú in the Andean sector of Chiloé Continental. This study seeks to clarify the relationship between vegetation change and fire activity changes in this region in the context of millennial-scale climate variability.

6.3 Study Area

Northwestern Patagonia (Figure 6.1) straddles the southwest coast of South America between 39-44°S. It is bordered by the Pacific Ocean and the Coastal Cordillera to the west and by the Southern Andes and eastern Patagonian plains to the east. Athwart these two mountain systems, a central depression extends north-south decreasing in elevation southwards until it descends beneath the ocean at 41°S. South from that latitude, the Coastal Cordillera is represented by the western part of Isla Grande de Chiloé (41-43°S); and the Andes by the Chiloé Continental region (42-44°S). South of Isla Grande de Chiloé, the Coastal Cordillera terminates and instead, the Andes extend to the Pacific coast which is typically characterised by an archipelego of mountainous bedrock islands separated from the Continental Andes by an intricate network of fiords.

Within the Southern Hemisphere mid-latitudes, the spatial climate gradients in Northwestern Patagonia are established following the continuous flow of the Southern Westerly Winds (SWW) and their interaction with the axial mountain systems (Seluchi et al., 1998). Orographic lift of rain-bearing westerly air masses brings abundant precipitation to the west-facing slopes; whilst a rain shadow effect diminishes precipitation in the central depression. Data from climate stations derived from Dirección Meterológica de Chile (http://www.meteochile.gob.cl/climatologia.php) reflect this pattern showing >2000 mm*yr^{-1} of precipitation in stations located on the western slopes of the Coastal and Andes ranges; and around 1000 mm*yr^{-1} in the central depression. Blocking of precipitation fronts by the Andes is even more extreme, generating an abrupt drop in annual precipitation from up to 3000 mm*yr^{-1} in the western flanks to less than 300 mm*yr^{-1} in the eastern side in less than 60 km (Paruelo et al., 1998). Mean annual temperature decreases southwards from 11.5°C at 38°S (e.g. Temuco; 114 masl) to 9.5°C at 43°S (e.g. Futaleufú; 330 masl) and annual precipitation increases southwards from 900 mm*yr^{-1} at 38°S to >1600 mm/yr at 43°S. A maritime climate with relatively low seasonal variation prevails at low elevation (e.g. Puerto Montt area; 41°S, 85 masl), whereas a more continental climate develops in the Andean sectors of Chiloé Continental (e.g. Futaleufú area), where austral summer months (December, January and February) feature prolonged droughts and temperatures well above 20°C and frosts are common during winter months (June, July and August) (Table 6.1).

Changes in the relative position of the South Pacific high-pressure belt and the SWW from seasonal to decadal timescales impact significantly upon regional climate trends of Northwestern Patagonia. For instance, a southward extension of the high-pressure cell and the westerly belt during the austral summer produces a marked drop in precipitation, with less than 15% of the total annual precipitation falling during summer months in the lowlands. Over longer timescales, a sustained decrease in annual precipitation in Northwestern Patagonia over the last decades has been linked to a progressive southward shift of the SWW belt (Garreaud et al., 2013). This trend has been characterised as a tendency towards the positive phase of the Southern Annular Mode (SAM; Thompson and Solomon, 2002).

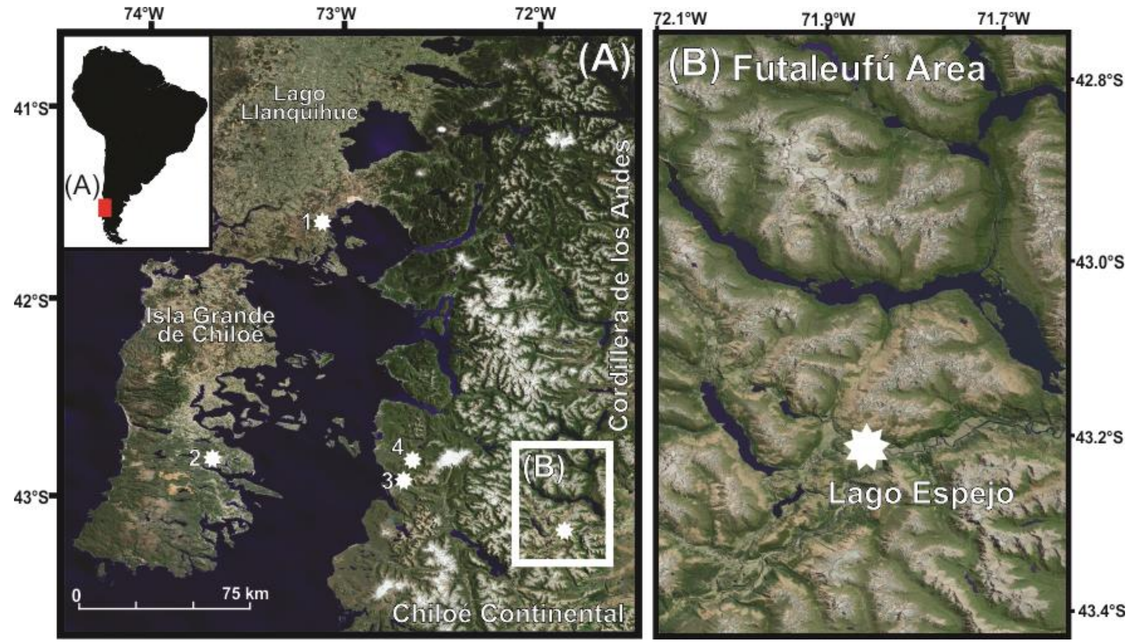

Figure 6.1. Composite map of Northwestern Patagonia (A) and the Futaleufú area (B), showing the location of the study site, nearby palynological sites and physiographic units mentioned in the text. 1. Huelmo site (41.51°S, 73.0°W; 10 masl; Moreno and Leon, 2003), 2. Lago Lepué (42.80°S, 73.71°W; 124 masl; Pesce and Moreno; 2014), 3. Lago Teo (42.90°S, 72.70°W; 45 masl; Henriquez et al., 2015), 4. Volcán Chaitén (42.83°S, 72.65°W; 1122 masl).

Climate station	period (AD)	Location	Elevation (masl)	Summer max T (°C)	Winter min T (°C)	Summer mean T (°C)	Winter mean T (°C)
Puerto Montt el tepual	2010-2014	41.42°S; 73.08°W	85	19.5	3.7	13.8	6.4
Futaleufu Aeropuero	2010-2014	43.20°S; 71.86°W	330	21.3	0.8	15.0	3.5

Table 6.1. Climate data from two stations in Northwestern Patagonia. The data were retrieved from the climate yearbook of the Dirección General de Aeronaútica Civil, Dirección Metereológica de Chile.

The regional climate patterns summarized above determine the broad distribution of the main forest communities of Northwestern Patagonia (Schmithüsen, 1956; Oberdorfer 1960; Villagran 1980; Veblen et al., 1983, Heusser, 2003). Prior to European settlement, the Pacific coast, the Central Depression and the flanks of both mountain ranges sustained dense evergreen rainforest. In the few remnants of native forest left on the mountain slopes today, deciduous *Nothofagus* forest communities supersede evergreen forest at higher elevation. *Valdivian evergreen rainforest* is the predominant formation in the lowland of the central depression and the northern portion of Isla Grande de Chiloé. In well-drained areas, this forest formation is dominated by several emergent trees including *Eucryphia cordifolia*, *Aextoxicon punctatum*, *Weinmannia trichosperma*, *Laureliopsis philippiana*, *Drimys winteri* and several tree and shrub species of the Myrtaceae family. This forest community features the highest diversity of trees and sub-canopy taxa. Species such *Tepualia stipularis* and the conifer *Pilgerodendron uviferum* become increasingly abundant in poorer drained areas. *North Patagonian evergreen rainforest* gradually replaces Valdivian ensembles in the mountain slopes from around 400 masl at 40°S, although the elevation of this transition decreases significantly in the southern part of Northwestern Patagonia. *Nothofagus dombeyi* reaches its maximum development in the North Patagonian communities in the western flanks of the Andes, where it is accompanied by several of the Valdivian trees mentioned above. Other important trees of this community include the conifers *Saxegothaea conspicua*, *Podocarpus nubigena* and *Fitzroya cupressoides*; and other evergreen southern beech species (*Nothofagus nitida* and *N. betuloides*). The bamboo *Chusquea quila* is an abundant element of North Patagonian forest sub-canopy, especially in forest gaps generated by fire or logging (Gonzalez, 2002). The deciduous *Nothofagus pumilio* and *N. antarctica* species become dominant above 1000 masl in the western Andean slopes, and above 600 masl in western Isla Grande de Chiloé. These species form the deciduous sub-Antarctic forest community which extends up to the treeline which, in Northwestern Patagonia, ranges from ~1600 masl at 38°S to 1250 at 43°S (Lara et al., 2005). Above this boundary, open shurbland and grassland vegetation establishes, dominated by high-Andean taxa with several species of the Poaceae, Asteraceae and Ericaceae families among others.

6.4 Methods

6.4.1 Stratigraphy and chronology

Four overlapping sediment cores were taken from a platform anchored over the deepest portion of Lago Espejo (1080 cm depth) using a modified square rod Livingstone Piston Corer (Wright, 1967). An additional corer, modified with a transparent plastic chamber, was used to capture a single core containing the top part of the section with the water-sediment interface. The cores taken with the Livingstone corer were wrapped in cellophane and transported for storage; whereas the short core was sampled and bagged in the field. All the sediments were stored at 5°C in the Laboratory of Quaternary Paleoecology at Universidad de Chile. The main lithological features of the core were described in situ during core-retrieval. The weight percent of organic, carbonaceous and siliciclastic content of all cores was estimated by Loss on Ignition Analysis (LOI; Heiri et al 2001; see Chapter Three). LOI was also used for inter-core correlations and to assist in the identification of tephra layers (identified as samples with inorganic density values >0.4 g/cc in the LOI).

Major element composition of glass shards was conducted on selected tephra layers and compared against equivalent-aged distal tephra sequences from Chile (section Pumalin-4) and Argentina (Alérce-6 and La Zeta, Esquel) (B.V. Alloway - *unpublished data*). These analyses, in conjunction with stratigraphic data from surface deposits, permit comparison and correlation of tephra and their associated chronologies between these sites (see Table 6.2 and Appendix 3).

The chronology of the Lago Espejo cores was constrained by accelerator mass spectrometry radiocarbon measurements of samples taken at different positions throughout the core series (Table 6.3). Changes in the rate of sediment deposition were modelled by a Bayesian age-depth model using the calibrated radiocarbon dates. Tephra deposition was assumed to be instantaneous and so tephra thicknesses were subtracted from the depth scale for age modelling.

Radiocarbon calibration was performed with the SHCal13 calibration curve (Hogg et al., 2013) for the dates younger than 11,000 ^{14}C yr BP, and the IntCAL13 calibration curve (Reimer et al., 2013) for older samples. Age modelling was performed using the

BACON statistical package (Blaauw and Christen, 2011) with the aid of R software (R core team, 2014).

6.4.2 Pollen and charcoal analysis

Pollen processing was conducted on 1-cc samples taken at 3-cm intervals excluding tephra layers. Pollen processing followed standard procedures for lake sediments (Faegri and Iversen, 1989; see Chapter Three for more details), which include KOH digestion, HCl (10%) and HF (33%) treatments, Acetolysis reaction, and silicone oil mounting (see Chapter Three). A minimum of 300 dryland pollen grains was counted in the upper 750 cm, but below that depth pollen concentrations dropped drastically so that no more 100 grains were counted. Pollen counting was performed with a stereomicroscope at 400X magnification. Identification of key pollen taxa was conducted with the aid of Heusser (1971). Pollen data are plotted as percentage data and pollen influx (grains*cm^{-2}*yr^{-1}). A zonation of the pollen record was based on a Constrained Incremental Sum of Squares (CONISS) ordination performed with Tilia Software (Grimm, 1987). The palynomorph "Cupressaceae" includes *Fitzroya cupressoides*, *Pilgerodendron uviferum* and *Austrocedrus chilensis*; "*Nothofagus dombeyi*-type" (hereafter referred as "*Nothofagus"*) includes *N. dombeyi, N. betuloides, N. pumilio, N. antarctica* and *N. nitida*. Climate inferences from pollen data are based on the relationship between the modern distribution of native plant communities and the regional climate gradients described in the previous section. Additionally, the main trend in pollen and CHAR were further investigated with a Principal Component Analysis (PCA) carried out on the percentage pollen (>3%) and charcoal data.

Charcoal analysis is based on the counting of microscopic particles (<125 μm) in the pollen slides and macroscopic particles (>125 μm) from 1-cc of samples taken at contiguous 1-cm intervals. Macroscopic charcoal processing and tallying followed the methodology described in Whitlock and Larsen (2001). General charcoal trends are described based on changes in the charcoal accumulation rate (CHAR; particles*cm^{-2}*yr^{-1}). The time series analysis of macroscopic charcoal records was further analysed using the software CharAnalysis (Higuera et al., 2009). This software is designed to identified fire peaks in CHAR time series through modelling and removing a *peak charcoal* signal (high-frequency CHAR variations assumed to be related to fire events) from a *background signal* (low-frequency variations assumed to be unrelated to local fire events). For Lago Espejo, the macroscopic CHAR time series was initially interpolated at regular time intervals corresponding to the median sample resolution of the record. The *background charcoal* was modelled using a LOWESS robust to outliers smoothing with a 1000-yr window width. Individual peaks were identified as interpolated CHAR values that surpass a locally-determined threshold defined as the 99 percentile of a Gaussian distribution of the *peak charcoal* time series.

The effect of tephra deposits on the vegetation and fire activity was tested by performing a Superimposed Epoch Analysis (SEA) (Prager and Hoening, 1992) on influx series of selected pollen types and macroscopic CHAR. SEA allows the identification of consistent responses to a set of recurrent events (e.g. tephra deposition) in long time series. The methodology consists of identifying the variations around a fixed time window centred at each event, to then synchronize and average all the individual responses (Prager and Hoening, 1992). For this study I analysed the responses of *Nothofagus*, Poaceae and macroscopic CHAR to the deposition of tephra identified in Lago Espejo. Other species documented as shade-intolerant, fast-growers or colonizers of recently disturbed areas such as *Weinmannia trichosperma* or *Eucryphia cordifolia* were not included in the analysis because their abundances at Lago Espejo were minimal and/or because their presence did not encompass a significant number of tephra deposits. I followed the methodology adopted by Jara and Moreno (2014), which includes the interpolation of the data to fixed-time intervals corresponding to the median sample resolution of the pollen and CHAR records. The interpolated data were normalized and scaled in order to minimize the effect of long-term trends and to express the data as departures ranging from -1 to +1 from a zero-centred mean (Adams et al., 2003). Individual responses were analysed through a temporal window of 300 (-150 yr to +150) years for the pollen data and 180 (-90 to +90) years for CHAR. Consistent responses were tested using 95% confidence intervals calculated from a Monte Carlo randomization using 3000 replications. Additionally, the averaged values of the intervals immediately after and before the tephra were compared using a nonparametric Wilcoxon test with a null hypothesis of equal pre and post tephra averages.

6.5 Results

6.5.1 Stratigraphy and chronology

The Lago Espejo sedimentary sequence extends for 950 cm and consists of two main units: (1) a basal ~200 cm thick inorganic (0-10% organic matter) bluish-grey silt unit, and (2) an upper ~750 cm-thick organic (20-60%) yellowish-brow lacustrine unit (Figure 6.2). The transition between the two units is sharp and concordant. Carbonate content is very low, fluctuating from less than 1 percent in the lower unit, to 2-6% throughout the upper unit. A total of 28 tephra layers are recognized with a cluster between 800-550 cm (14) and in the top 150 cm (4; Table 6.2). Tephra thickness ranges from 1 to 9 cm.

Glass shard major element determination of tephra horizons allowed the correlation of 5 tephras from Lago Espejo (Table 2) with corresponding deposits from other distal sections in both Chile and Argentina (see Appendix 3 for more details). The lowest of the correlated tephra at Lago Espejo (LE-28; 950 cm) has a correlative deposit (T1) at La Zeta sequence, 80 km northeast from Lago Espejo. T1 has an associated radiocarbon age of 12,935 ± 50 ^{14}C years B.P (LLNL-158297) (Figure 6.2). This radiocarbon age is directly applied to date LE-28 within the Lago Espejo record, an interval where coincidentally there is a paucity of radiocarbon chronology.

All radiocarbon dates are in stratigraphic order, suggesting the absence of age reversal and thus overall continuous undisturbed accumulation (Table 6.3; Figure 6.3). However, the most basal radiocarbon date (UCIAMS-156599; 13,440 ±160) at 775 cm presents an anomalously old age considering the basal correlation with La Zeta sequence described above. This latter correlation is strongly supported by glass shard major element determinations, and therefore we consider the basal-most date from the Lago Espejo section as being erroneous and have removed it from the age model calculations. The basal ages from the site is thus constrained by LAZ-T1 12,935 ± 50 ^{14}C yr BP, which gives a 2-sigma calendar range of 15,620-15,450 cal yr BP with a median probability of 15,456 cal yr BP. The age model indicates a median deposition time of 15 yr*cm^{-1} for the sediment sequence and median sample resolution of 50 years for the pollen record and 15 years for the macroscopic charcoal record.

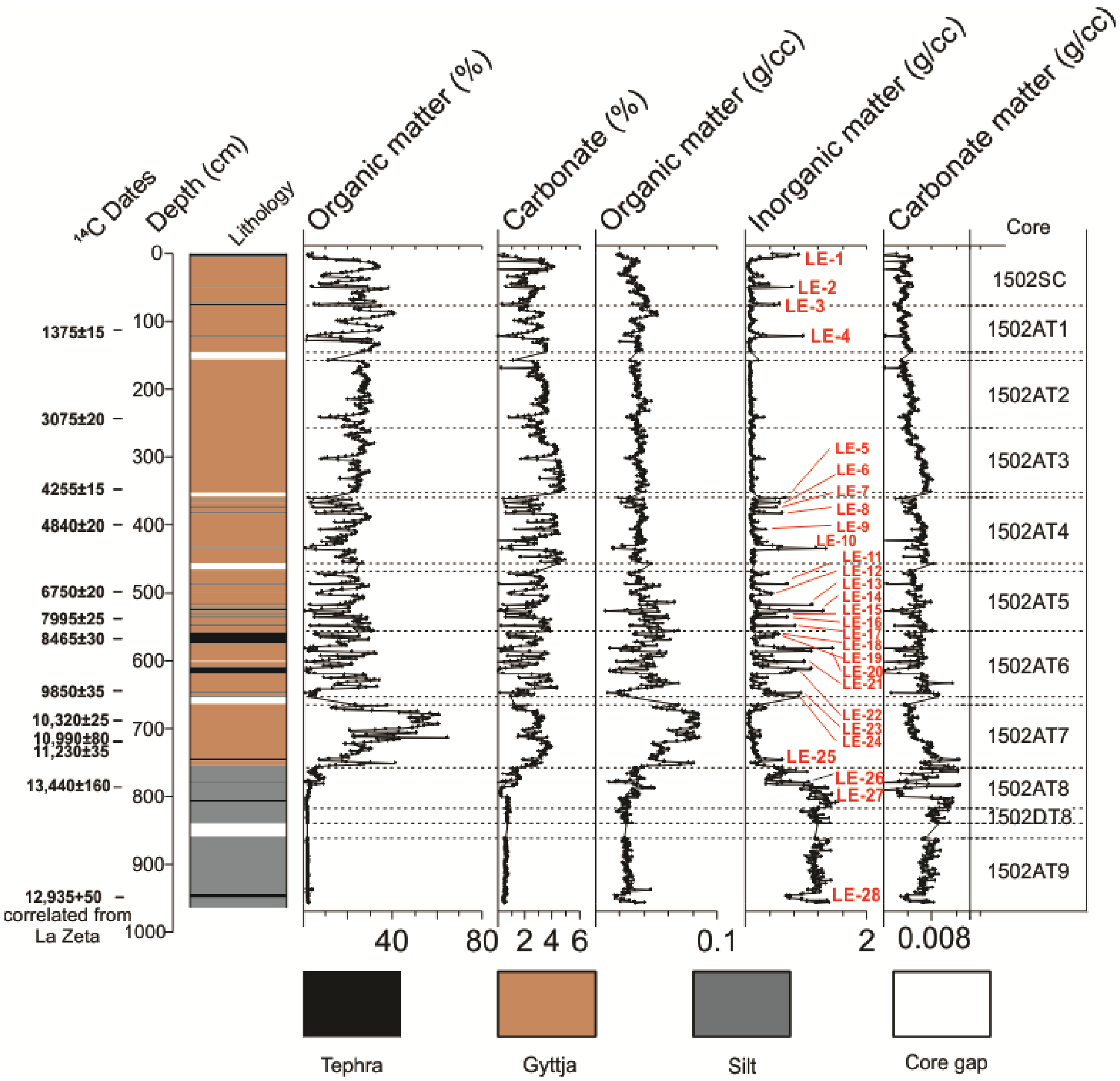

Figure 6.2. Stratigraphy of Lago Espejo including AMS radiocarbon ages (expressed as ^{14}C age), the Loss on Ignition Analysis and the relative position of the individual core sections. Tephra layers identified in the cores are labelled (following Table 6.4 nomenclature) adjacent to their corresponding peak in inorganic matter.

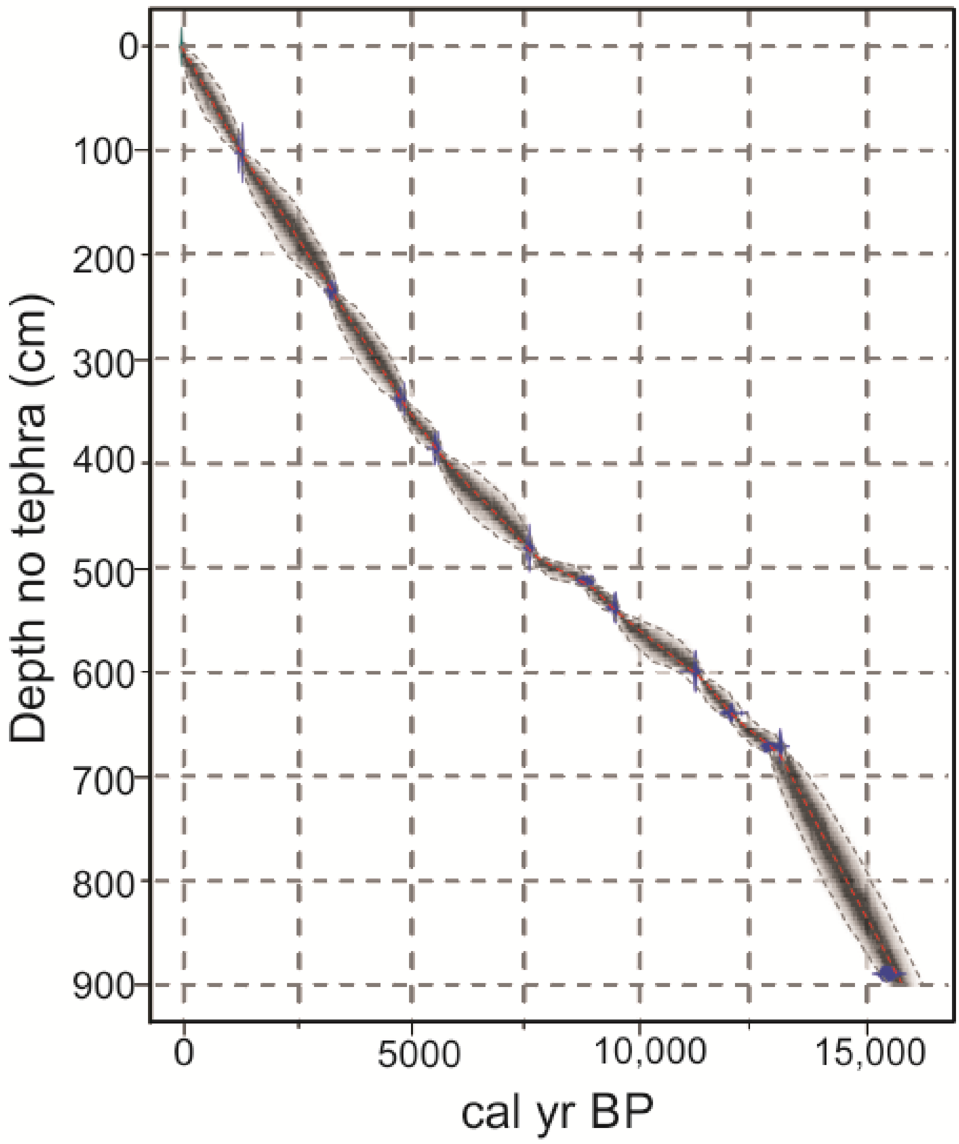

Figure 6.3. Bayesian age model based on 12 dated levels from Lago Espejo. The figure shows each of the calendar ranges (blue), the modelled 95% confidence intervals (dotted grey lines) and the median probability (red curve). The model was developed using the BACON package for the R software (Blaauw and Christen, 2011). The grey scale encompassed by the confidence intervals represent the age probability according to the model.

6.5.2 Pollen and charcoal analysis

The pollen record of Lago Espejo comprises a total of 267 samples largely dominated by *Nothofagus* (mean abundance 80%) followed by Poaceae (7%) (Figure 6.4). High values of Poaceae, several other non-arboreal elements and the fern *Blechnum* type are observed between 16,000-13,600 cal yr BP. At 13,600 cal yr BP *Nothofagus* expands to over 80%, and after this time it persists with little variation until 220 cal yr BP, when non-arboreal taxa expand abruptly (Figure 6.4). Pollen influx values are negligible abundances for all taxa before 13,500 cal yr BP. After this time total pollen influx fluctuates between 5000-25,000 grains*cm^{-2}*yr^{-1} (Figure 6.5). Seven zones were identified from a visual inspection of the pollen stratigraphy and supplemented with CONISS ordination (Table 6.4).

Tephra #	Core	Core length (cm)	depth (cm)	Thickness (cm)	Age (cal yr BP)	95% age range (cal yr BP)	Correlative with external sequence
LE-1	1502SC	0-4	0-4	4	-55	-63-29	
LE-2	1502SC2	49-50	49-50	1	510	226-820	
LE-3	1502SC2	74-76	74-76	2	800	425-105	
LE-4	1502AT1	64-65	122-123	1	1420	1257-1658	
LE-5	1502AT4	3-4	361-363	2	4950	4761-5174	
LE-6	1502AT4	9-10	367-368	1	5020	4810-5246	
LE-7	1502AT4	16-17	374-375	1	5130	4881-5406	
LE-8	1502AT4	25-26	383-384	1	5260	4973-5520	CHA-2
LE-9	1502AT4	50-51	408-409	1	5670	5532-5812	
LE-10	1502AT4	75-77	434-436	2	6200	5772-6732	
LE-11	1502AT5	29-30	487-488	1	7310	6864-7601	
LE-12	1502AT5	42-44	501-503	2	7600	7443-7719	
LE-13	1502AT5	60-61	518-519	1	8070	7719-8541	
LE-14	1502AT5	65-69	524-528	4	8290	7876-8732	
LE-15	1502AT5	73-74	531-532	1	8420	7940-8800	
LE-16	1502AT5	78-79	536-537	1	8600	8058-8976	
LE-17	1502AT5	91-92	549-550	1	9040	8836-9246	
LE-18	1502AT6	3-4	561-562	1	9290	9052-9531	
LE-19	1502AT6	8-9	566-567	1	9380	9151-9546	
LE-20	1502AT6	22-28	581-587	6	9640	9510-10080	LAZ-T13
LE-21	1502AT6	44-45	602-603	1	10,190	9721-10745	
LE-22	1502AT6	52-61	611-620	9	10,420	9903-10,976	LAZ-T10
LE-23	1502AT6	88-90	647-649	2	11,230	10,906-11,416	LAZ-T7
LE-24	1502AT6	95-96	653-654	1	11,330	11,024-11,470	
LE-25	1502AT7	87-89	746-748	2	13,300	12,989-13,666	
LE-26	1502AT8	21-22	779-780	1	13,680	13,251-14,136	
LE-27	1502AT8	46-50	805-809	4	13,980	13,521-14,472	
LE-28	1502AT9	86-91	945-950	5	15,640	15,280-16,109	LAZ-T1

Table 6.2. Core, length range, thickness and age of the tephra deposits identified at Lago Espejo

Principal Component Analysis axes one and two (thereafter referred as PCA 1 and PCA 2) explained 33% and 15% of the total variance of the data, respectively (Figure 6.6). The taxa loadings plot arrange pollen taxa into 4 distinct groups: (1) non-arboreal taxa plus Myrtaceae with high negative PCA1 values, *Nothofagus* with high positive PC1 values, (3) *Podocarpus nubigena* with negative PCA 2 values and Cupressaceae, *Rumex* and *Plantago* with positive PCA 2 values (Figure 6.6). In the sample score plot, PCA 1 contrasts negative values of basal zones Espejo-1 and Espejo-2 with positive values in all other zones; PCA2 distinguishes zones Espejo-6 and Espejo-7 with positive values whereas all other zones have negative or near zero PCA2 values (Figure 6.6).

#	Laboratory Code (CAMS#)	Depth (cm)	^{14}C age± 1σ (years)	calibration curve	youngest 2σ intercept (cal yr BP)	oldest 2σ intercept (cal yr BP)	Median probability (cal yr BP)
1	UCIAMS -171564	110	1375±15	SHCal13	1186	1299	1275
2	UCIAMS -171565	243	3075±20	SHCal13	3084	3348	3234
3	UCIAMS -156601	347	4255±15	SHCal13	4644	4849	4745
4	UCIAMS -171566	399	4840±20	SHCal13	5471	5596	5516
5	UCIAMS -171567	498	6750±20	SHCal13	7508	7622	7579
6	UCIAMS -171568	538	7995±25	SHCal13	8649	8982	8834
7	UCIAMS -171569	567	8465±30	SHCal13	9321	9526	9460
8	UCIAMS -171570	644	9850±35	SHCal13	11,175	11,268	11,224
9	UCIAMS -156600	687	10,320±25	SHCal13	11,830	12,357	12,005
10	UCIAMS -171572	719	10,990±80	SHCal13	12,706	13,008	12,826
11	UCIAMS -171571	719	11,230±35	SHCal13	12,980	13,137	13,062
12	UCIAMS -156599	775	13,440±160	IntCal13	15,714	16,676	16,178
13	LLNL-158297		12,935±50	IntCal13	15,252	15,686	15,456

Table 6.3. Lago Espejo radiocarbon date details. All dates were obtained using AMS dating technique. Radiocarbon calibration was performed using the software CALIB 7.01 with the SHCal13 calibration curve (Hogg et al., 2013).

The microscopic and macroscopic charcoal record features very similar multi-millennial trends, including virtually no charcoal accumulation before 13,000 cal yr BP and fluctuations at millennial timescales superimposed on multiple short-lived peaks after that time (Figure 6.4). Four main periods are recognized: (1) persistent accumulation between 13,000-10,000 cal yr BP; (2) low values with several high intensity peaks between 10,000-4000 cal yr BP; (3) persistent high values between 4000-1000 cal yr BP; and (4) three well defined centennial-scale peaks in the last 1000 years (Figure 6.4). Time series analysis of the macroscopic CHAR record with CharAnalysis identified 53 statistically significant peaks occurring after 13,900 cal yr BP. Peak magnitude ranges from 1 to 2300 particles cm^{-2} yr^{-1}, with intervals of high peak frequency between 11,500-9000 and 4000-1000 cal yr BP (Figure 6.7).

Superposed Epoch Analysis show that none of the variables analysed, macroscopic CHAR, *Nothofagus* and Poaceae, presented responses to tephra deposition falling outside of the 95% confidence band. Similarly, the median values of the intervals preceding and following tephra deposition do not present statistically significant differences (Figure 6.8).

6.6 Discussion

6.6.1 Vegetation, fire and climate

Lago Espejo provides a 15,700-year reconstruction of the vegetation and fire regimes in the Chiloé Continental area (43°S) of Northwestern Patagonia. The result of SEA analysis indicates the lack of a consistent response of the two major pollen taxa and macroscopic CHAR to tephra deposition. Additionally, we note that the onset of expansion of other important taxa such as *Weinmannia trichosperma*, *Saxegothaea conspicua*, *Podocarpus nubigena* and *Blechnum-type* (discussed in the following paragraphs) are not associated with tephra deposition. Without a discernible effect of volcanic disturbance over pollen assemblages at the time resolution investigated here, we assume that climate and fire activity were the main drivers of vegetation changes. The following discussion of the record focuses on these factors.

Increasing abundances of *Nothofagus* and Myrtaceae and decreasing values of Poaceae are observed between 15,700-15,100 cal yr BP, suggesting a centennial-scale expansion of North Patagonian forest (Figure 6.4). Yet, the absence of the *Nothofagus*-specific mistletoe *Misodendrum* suggests that such expansion did not occur locally. This inference implies that the bulk of *Nothofagus* pollen deposited during this time was transported from an extra-local source, reflecting the extra-local expansion of forest. This interpretation is consistent with the disappearance of high-Andean vegetation and an expansion of North Patagonian forest recorded in the Huelmo site (200 km northwest from Lago Espejo; Figure 6.1) during this same time interval (Moreno and Leon, 2003); and it is in partial agreement with the Lago Lepué record (Isla Grande de Chiloé 150 km west from Lago Espejo) which shows the expansion of thermophilic North Patagonian elements between 16,100-14,600 cal yr BP (Pesce and Moreno, 2014).

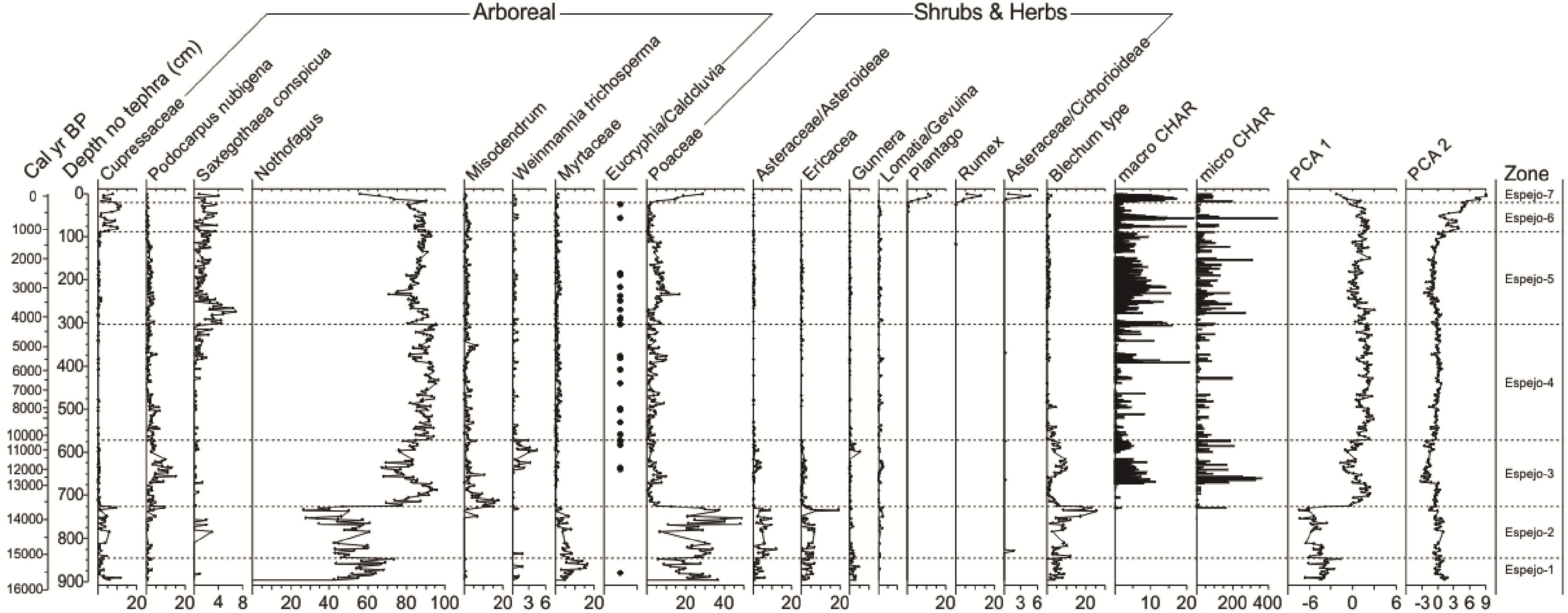

Figure 6.4. Lago Espejo pollen percentage diagram. The percentage changes of selected arboreal, non-arboreal and fern taxa are presented relative to the calendar age provided by the age model. The diagram also includes the sample scores for the first two principal axes from the Principal Component Analysis (Figure 6.8).

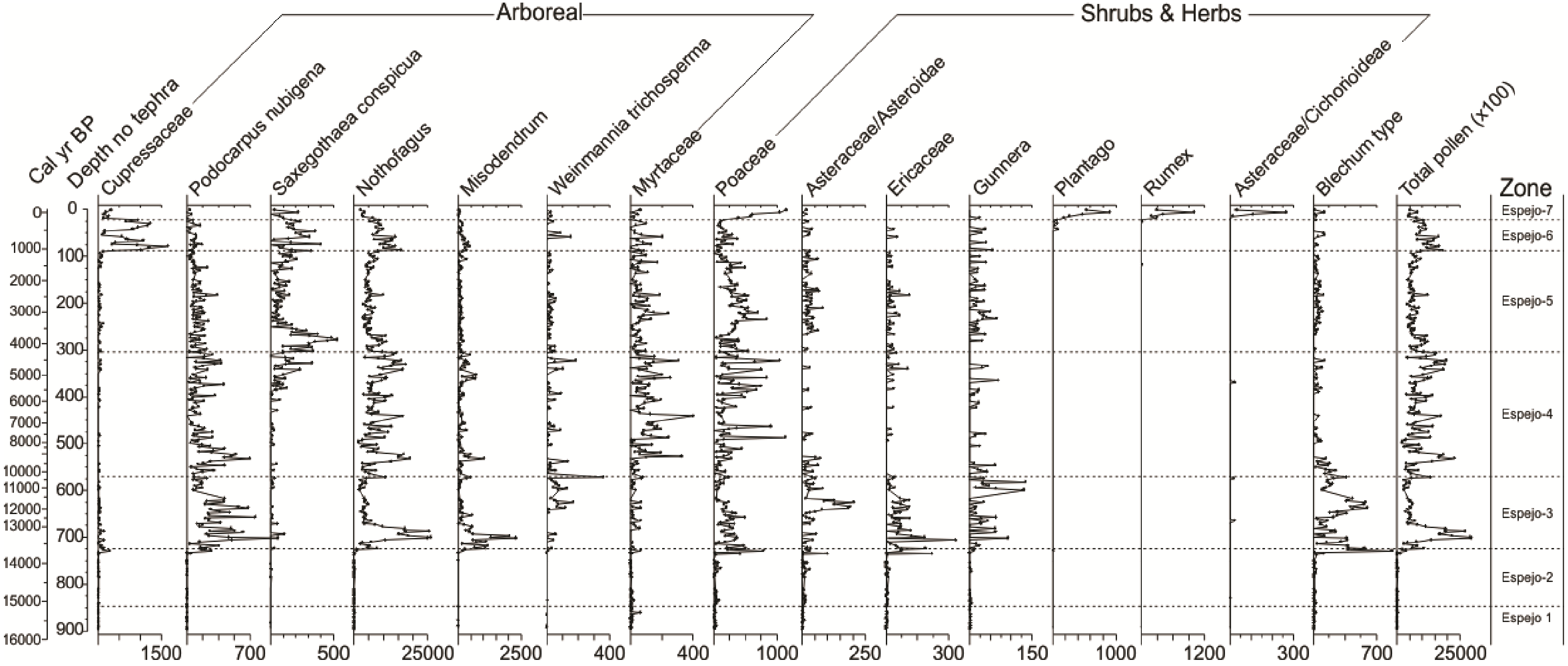

Figure 6.5. Lago Espejo Pollen influx (grains*cm^{-2}*yr^{-1}) diagram including main arboreal, non-arboreal and fern taxa. Note different scales.

Zone name	Depth no tephra (cm)	Age (cal yr BP)	Summary
Espejo-1	895-847	15,700-15,120	Increasing trends in *Nothofagus* (58%) and Myrtaceae (9) and declining Poaceae (20). Other important taxa are *Ericaceae,* (3), *Gunnera* (2) and the fern *Blechnum-type* (5). All taxa feature near-zero pollen accumulation rates.
Espejo-2	847-725	15,120-13,640	*Nothofagus* (47) and Myrtaceae (4) decline while Poaceae (28), Asteraceae/Asteroideae (5), Ericaceae (4) and Blechnum-type (9) all increase. Pollen accumulation rate of all taxa remains near-zero
Espejo-3	725-571	13,640-10,300	Abrupt increase in *Nothofagus*(82) and expansion of *Misodendrum* (4), *Podocarpus nubigena* (5) and *Weinmannia trichosperma* (1), and the aquatic Cyperaceae (2). Conversely, Poeaceae (3), Myrtaceae (1), unknown-1 (5), Ericaceae (1) and *Blechnum*-type (4) decrease markedly. Pollen accumulation rates of all terrestrial taxa show significant increments at various stages.
Espejo-4	571-303	10,300-4230	*Nothofagus*(90) reaches a long-term peak whereas all major pollen taxa attain minimal values. Pollen accumulation rates of arboreal taxa are higher than for the previous zone and markedly lower for non-arboreal taxa.
Espejo-5	303-88	4230-1050	Minor decline in *Nothofagus* (86) and increases in Poaceae (5), *Saxegothaea*(2) and a re-expansion of unknown-1 (6). Pollen accumulation rates decrease for tree taxa and increase for non-arboreal groups.
Espejo-6	88-22	1050-220	Invariant *Nothofagus* abundances (86), and expansion of Cupressaceae (6) and decreasing in Poaceae (1). Pollen accumulation rates of all terrestrial taxa are similar to the previous zone except for Cupressaceae which shows a notable increase.
Espejo-7	22-1	220- -50	Notable decline of *Nothofagus* (72) and rapid increases in Poaceae (17), Plantago (8) and *Rumex* (7) and Asteraceae/Cichoriodeae (1). Pollen accumulation rates of arboreal taxa drop markedly whereas Poaceae, Asteraceae/Cichoriodeae and introduced herbs show notable increases.

Table 6.4. Lago Espejo pollen zone details including depth, age and main pollen trends.

These relative correlations suggest that Lago Espejo is recording a period of regional forest expansion more likely driven by sustained warming. Based on these results I infer a southward shift/weakening of the SWW started at least by 15,700 cal yr BP. At Lago Espejo, relatively high abundances of non-arboreal elements common to high-Andean environments such as Ericaceae, Asteraceae/*Asteroideae* and *Gunnera* suggest that, in the absence of forest, a low-growing grassland and shrubland community developed around the site. The coverage of this plant community must have been minimal as near-zero pollen influx indicates a landscape scarcely vegetated (Figure 6.5). The deposition of inorganic glaciolacustrine silts indicates marginal organic productivity in the lake (Figure 6.2). In summary, the pollen record shows that, despite regional forest expansion/warming, cold conditions persisted around the site. We note that present-day annual precipitation above the treeline in the Andes of Northwestern Patagonia exceeds significantly the values of the mid-elevation areas where Lago Espejo is situated, and therefore we infer of increasing precipitation relative to modern values during this interval. Zero charcoal accumulation during this period might be explained by the lack of vegetation continuity and/or by the persistence of humid conditions.

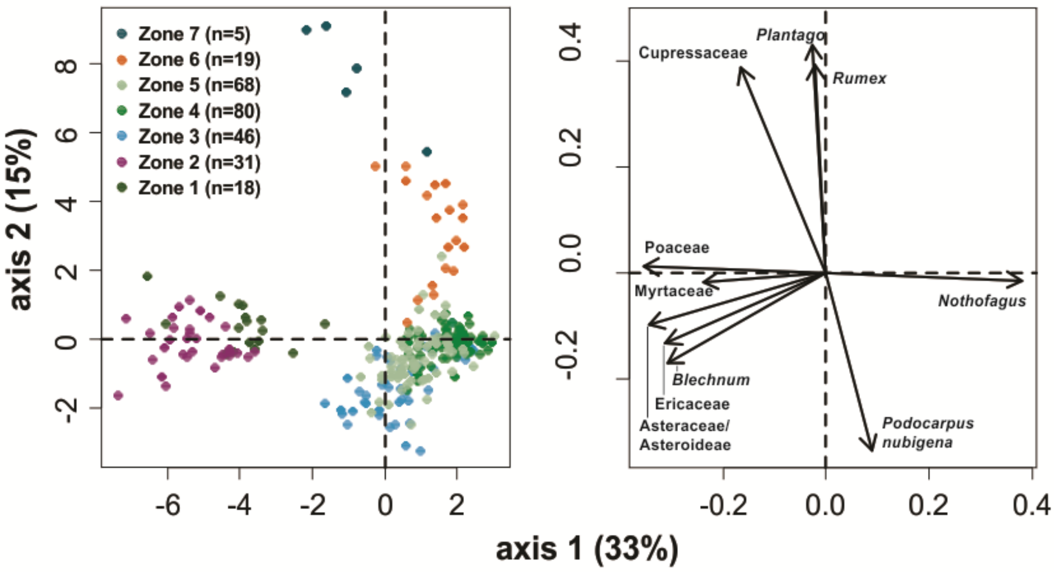

Figure 6.6. Principal Component Analysis biplots of the pollen percentage data of Lago Espejo. The two principal components explaining the largest amount of variability (PC 1 and PC 2) correspond to the main axes. The left plot shows samples scores arranged in relation to the pollen zones. The right plot shows the relationship between the first two PCA axes and the main taxa of the record. The samples scores are also plotted in stratigraphic order in the pollen percentage diagram (Figure 6.4).

Between 15,100-13,600 cal yr BP the previous pollen trend is reversed as arboreal elements (*Nothofagus* and Myrtaceae) decline while Poaceae and other high-Andean non-arboreal elements increase (Figure 6.4). There is still no trace of *Misodendrum* suggesting that the source of *Nothofagus* is predominatly extra-local. Notably, this period features an expansion of the fern taxon *Blechnum*. Two fern species of this genus are common understory elements of the closed-canopy Valdivian and North Patagonian forest (*Blechnum chilense; B. magellanicum*), while another -*B. penna-marina*- is present in the relatively more open deciduous *Nothofagus* forests and as part of the plant succession in recently glaciated areas (Heusser, 2003).

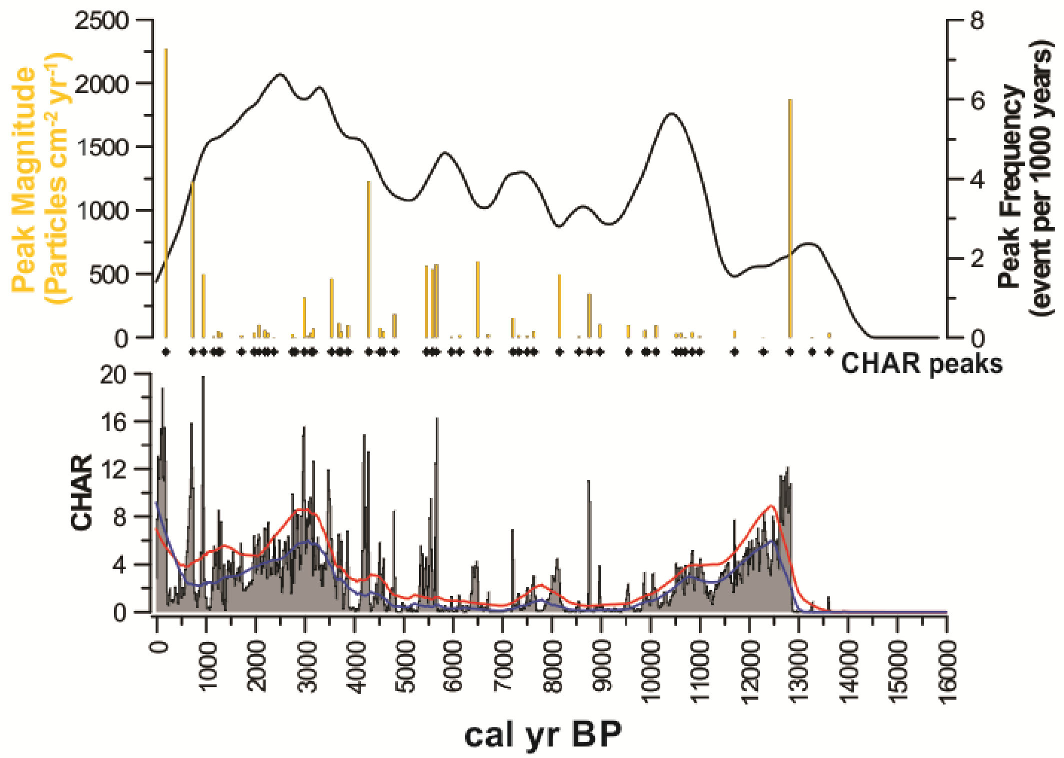

Figure 6.7. Time series analysis of macroscopic CHAR performed with the software CharAnalysis (Higuera et al., 2009). The bottom panel superposes the interpolated (15 years) CHAR series (grey graph), the background signal (blue line) modelled using a LOWESS robust to outliers smoothing with a 1000-yr window, and the locally-determined threshold values (red line). The upper panel shows the position of the statistically significant CHAR peaks detected by the analysis (black diamonds), as well as their frequency per 1000 years (black line) and intensity (black columns).

At Lago Espejo, peak *Blechnum* changes occur largely in antiphase with *Nothofagus* and parallel peaks in high-Andean taxa (Figure 6.4). This relationship indicates an expansion of high-Andean shrubland-grassland environment and a regional contraction of North Patagonian forest as a response to a peak in cooling during this interval. Inorganic sedimentation is consistent with this interpretation (Figure 6.2), whereas zero charcoal accumulation suggests hyper-humid conditions prevailed during this interval (Figure 6.4). The timing of these patterns at Lago Espejo matches the early part of the cold reversal identified at the Huelmo site (Moreno and Leon, 2003) and is in partial agreement with the expansion of cold-resistant hygrophilous conifers at Huelmo between 14,600-12,700 (Pesce and Moreno, 2014), suggesting that Lago Espejo is recording an interval of regional climate deterioration, probably the result of a northward shift/intensification of the SWW (Moreno et al., 2015).

An abrupt expansion of *Nothofagus* and *Misodendrum* occurs at 13,600 cal yr BP at the same time that non-arboreal taxa and Myrtaceae plummet to their minima (Figure 6.4). This change signals the establishment of a closed-canopy *Nothofagus* forest around Lago Espejo, a transition that took less than 100 years. In PCA terms, this is the most important transition of the record with a rapid shift from negative to positive values for PCA 1 (Figure 6.4 and Figure 6.6). In other words, PCA 1 is correlated to overall tree cover and thus this axis is indirectly associated with temperature.

The establishment of a closed *Nothofagus* forest is accompanied by an equally sharp lithological transition from inorganic silts to organic gytjja, suggesting an abrupt rise in organic productivity coinciding with forest colonization. We interpret the replacement of high-Andean vegetation by *Nothofagus* forest as evidence of warming that brought temperature above the threshold levels for forest establishment. This warming was likely the result of a southward shift and/or weakening of the westerly circulation.

During the last glacial termination (18,000-11,000 cal yr BP), North Patagonian rainforest expansion occurred in close association with the retreat of Andean ice sheets driven by warmer conditions generated by southward shift/weakening of the SWW (Denton et al., 1999; Moreno et al., 1999). At Huelmo site, forest expanded rapidly at 17,800 cal yr BP (Moreno and Leon, 2003); whereas forest colonization occurred at around 17,000 cal yr BP in the Lago Lepué (Pesce and Moreno, 2014). At Lago Espejo forest expansion along with a transition from glaciolacustrine to organic sediments is recorded considerably later at 13,600 cal yr BP. This correlation implies that a cold glacial environment, more likely induced by the proximity of glacier margins, persisted several millennia later in the Andean sector of Chiloé Continental than in the lowlands of Northwestern Patagonia.

Between 13,000-12,000 cal yr BP the record features decreasing *Nothofagus* and the expansions of *Podocarpus nubigena* and Poaceae (Figure 6.4). The influx diagram reveals that these two taxa expand as early as 13,600 cal yr BP (Figure 6.5), indicating a masking effect caused by the rapid increase in *Nothofagus* percentages. *P. nubigena* is a cold-tolerant conifer that grows as an understory tree in areas with maritime climate under high humidity conditions (Donoso, 2006), and therefore its expansion along with Poaceae suggests that cold and humid conditions prevailed between 13,600-12,000 cal yr BP.

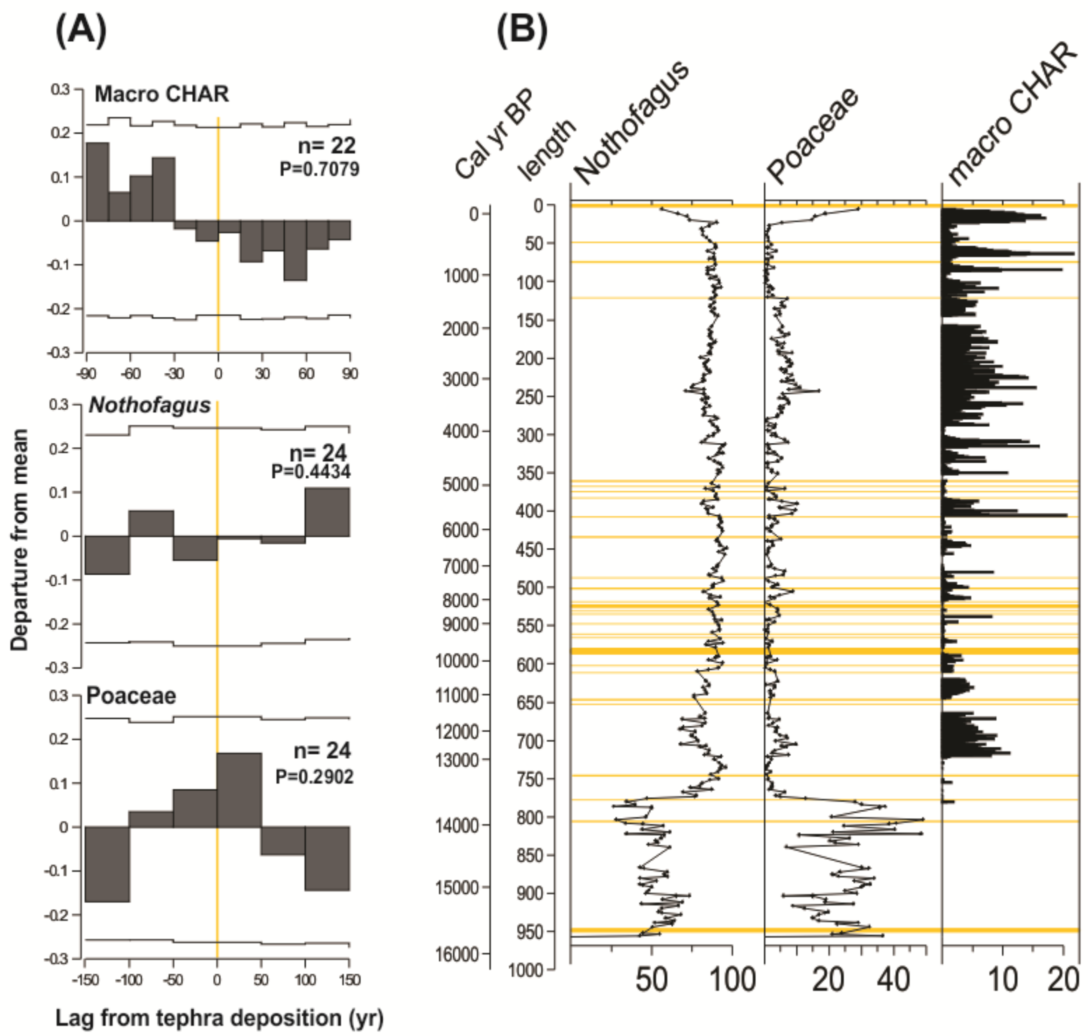

Figure 6.8. (A) Averaged response of selected pollen taxa and macroscopic CHAR to the deposition of tephra layers calculated with Superposed Epoch Analysis (Jara and Moreno, 2014). Tephra deposition corresponds to time "0" (vertical yellow bar). The 95% confidence interval (horizontal black lines) were calculated by a Monte Carlo randomization using 3000 replications. "N" indicates the number of tephra layers analysed for each variable and "P" indicates the p-values for the Wilcoxon test used to compare the averaged values immediately before and after tephra deposition. (B) Percentage variation of the selected taxa and Macroscopic CHAR in relationship to the stratigraphic position of the tephra layers identified in the Lago Espejo record.

Several palynological studies in Northwestern Patagonia document the expansion of cold-tolerant conifers including *P. nubigena* as indicative of a climate cooling between 14,500-12,500 cal yr BP (Moreno and Leon, 2003; Pesce and Moreno, 2014; Jara and Moreno, 2014). At Lago Espejo, this expansion occurs several centuries later. This difference might be attributed to different climate sensitivities of the local vegetation in the Andean sector relative to the lowlands of Northwestern Patagonia. We further note that this expansion occurs during an interval of minimal summer and maximal winter insolation at 30°S (Figure 6.9), suggesting that low seasonality (with colder summers) could have been a key factor.

Along with *P. nubigena*, Lago Espejo shows the onset of a period of high macroscopic and microscopic CHAR values (Figure 6.4) and marked increase in charcoal peaks (Figure 6.7) between 12,900-10,000 cal yr BP. Although local fire activity and forest expansion are related at a multi-millennial timescales, we note that the onset of charcoal accumulation postdates forest establishment by more than 700 years, and that high magnitude variations in macro and microscopic CHAR occurs during periods of invariant forest coverage afterwards. Collectively, this evidence indicates that, unlike the eastern Andean slopes (Iglesias et al., 2014), the development of woody vegetation was not the limiting factor for the emergence and variation of fire regions at western Andean slopes. We propose that fire activity at Lago Espejo is associated with relative changes in precipitation ultimately driven by variations in the position/intensity of the SWW (Abarzua and Moreno, 2008; Whitlock et al., 2007). In particular, a sustained decrease in summer precipitation is the most plausible interpretation to explain the increase in fire activity between 12,900-10,000 cal yr BP. Under this scenario, overall cold/wet conditions and reduced seasonality allowed the establishment of a dense, closed-canopy *Nothofagus* forest with cold-resistant trees and the resulting accumulation of continuous woody material; whereas summers started to become sufficiently dry as to support widespread fires.

By 12,000 cal yr BP, *P. nubigena* starts to decline whereas *W. trichosperma* expands rapidly from basal values. CharAnalysis shows a rapid increase in CHAR peak frequency by 11,500 cal yr BP (Figure 6.7). Unlike *P. nubigena, W. trichosperma* does not have a distribution limited to hyper-humid/cold North Patagonian forest but extends more widely and is present in Valdivian and North Patagonian communities. Additionally, it has the ability to colonize recently disturbed areas due to its intolerance to shade and rapid seed dispersal (Lusk, 1999; Donoso, 2006). Thus, the decline of *P. nubigena* and the expansion of *W. trichosperma* reflect a period of relatively warmer/drier conditions and increasing fire disturbances. These interpretations are aligned well with other regional reconstructions suggesting the establishment of a cold, seasonal dry climate during this interval based on decreasing *P. nubigena* and increasing *W. trichosperma* and CHAR between 12,900-11,100 cal yr BP (Moreno and Leon, 2003 Pesce and Moreno, 2014; Jara and Moreno, 2014). Furthermore, this interpretation aligns well with the evidence for the onset of drier, albeit warmer, summers associated with a southward migration of the SWW around 13,000 cal yr BP, based on glacial retreat in the South Island of New Zealand (43°S) (Putnam et al., 2010).

Between 10,000-4000 cal yr BP, consistently high *Nothofagus* values (85-95%) are observed at Lago Espejo while all other arboreal and non-arboreal taxa occur in very low abundances, suggesting the persistence of a closed-canopy forest (Figure 6.4). Low CHAR values relative to the previous period (12,900-10,000 cal yr BP) and the drop in CHAR peak frequency (Figure 6.7) can be interpreted as resulting from less regular ignition events or the lack of droughts which might otherwise desiccate woody material that was available.

Several records from Northwestern Patagonia, including Isla Grande de Chiloé and Chiloé Continental show evidence of the expansion of thermophillous and drought-tolerant Valdivian taxa between 11,000-8000 cal yr BP (Villagran, 1990; Moreno and Leon, 2003; Moreno 2004; Pesce and Moreno, 2014; Jara and Moreno, 2014; Henriquez et al., 2015). This evidence has been interpreted as the establishment of a warm/dry conditions resulting from a weakening/southward-shift of the SWW. With invariant *Nothofagus*, Lago Espejo lacks any significant vegetation change that can be interpreted as such, although we note that traces of the thermophilous and drought-tolerant *Eucryphia/Caldcluvia* start to appear consistently between 12,000-8000 cal yr BP (Figure 6.4). In the Andean region of Chiloé Continental where North Patagonian *Nothofagus* forest dominates, winters typically feature frosts and are considerably colder than the adjacent lowlands where Valdivian forest tends to prevail. Summer temperatures, on the other hand, tend to be more similar between these two regions (Table 6.1), implying that winter minima are likely to be the key factor underpinning the different distributions of these plant communities. The insolation curves for 45°S show sustained increased seasonality, with a trend towards colder winters and warmer summers starting at 11,000 cal yr BP (Figure 6.7). My interpretation based on these observations is that winters were likely cold enough at 11,000 cal yr BP, and increasingly colder afterward, to prevent the establishment of thermophilous Valdivian rainforest in the Andes of Chiloé Continental between 11,000-8000 cal yr BP.

Between 6000-1500 cal yr BP the record shows the expansion of the conifer *Saxegothaea conspicua* followed by an increase in Poaceae and microscopic and macroscopic CHAR by 4000 cal yr BP (Figure 6.4). Similar to *P. nubigena*, *Saxegothaea conspicua* is a shade-tolerant and cold-resistant tree commonly found in the Valdivian and North Patagonian forests under cold and humid maritime climates (Donoso, 2006). This association suggests the persistence of relatively cool and wet conditions around the site, an inference supported by the documented expansions of this and other hygrophilous/cold-resistant North Patagonian taxa in several sites after 7000 cal yr BP (Moreno 2004; Pesce and Moreno, 2014; Henriquez et al., 2015). Nonetheless, unlike *P. nubigena*, *S. conspicua* is able to extend its modern distribution into the mountain ranges of south central Chile where it is capable of withstanding more continental conditions with colder winters and warmer/dryers summers. Thus we interpret this pollen expansion as responding to a combination of a multi-millennial cooling superimposed with a trend towards increasing seasonal differences after 6000 cal yr BP. These inferred trends, consistent with the increase in seasonally inferred from summer and winter insolation curves, could have explained the expansion of *S. conspicua* relative to other cold-resistant trees that have distributions limited to maritime environments (Figure 6.9).

At 4000 cal yr BP *S. conspicua* and *Nothofagus* show noticeable decreases whereas Poaceae expands rapidly. Microscopic and macroscopic CHAR show persistently high values (Figure 6.4) along with a notable increase in the frequency of CHAR peaks (Figure 6.7). This set of changes indicates a pulse of forest opening and an increase in fire activity adjacent to Lago Espejo. The two are likely to be related as more fires could have generated the forest gaps necessary to promote the proliferation of the Poaceae bamboo *Chusquea*, a documented fast colonizer of gaps in *Nothofagus* forest after disturbance (Veblen et al., 1992). Persistent fires are indicative of persistent drier conditions and/or the establishment of a more variable precipitation regime. Significant percentages of *S. conspicua* after 4000 cal yr BP suggests, however, an overall cold and wet climate; and therefore rainfall variability is the most likely driver of the intense fire activity witnessed during this period. This fire-climate relationship shows similarities with the open *Nothofagus*/*Austrocedrus* parkland where rainfall variations promote fire via production and accumulation of desiccated material (Kitzberger et al., 1997).

Centennial-scale changes in precipitation have been attributed to the emergence of the Southern Hemisphere modes of climate variability such as the Southern Annular Mode (SAM), El Niño Southern Oscillation (ENSO), and their teleconnection with the

Southern mid-latitudes (Fletcher and Moreno, 2012; Moreno et al., 2014). Yet, the pollen and charcoal records from Lago Espejo do not show well-defined centennial-scale oscillations that can be linked with these modes of climate change. Alternatively, the insolation curves for 45°S show peak seasonal differences after 4,000 ca yr BP, suggesting warmer summers and colder winters (Figure 6.9). Considering that precipitation in Northwestern Patagonia is concentrated during winter months, divergent seasonal insolation curves could have resulted in increased seasonal rainfall differences as well as a net increase in annual means. Taken together, we interpret this evidence as a continuation of the climate trends started around 6000 cal yr BP, i.e., long-term cooling and increasing precipitation variability and seasonality.

The upper-most section of the record features the expansion of Cupressaceae by 1500 cal yr BP, followed by the expansion of Poaceae and other non-arboreal taxa commonly associated with European deforestation such as *Rumex* and *Plantago* by 150 cal yr BP (Figure 6.4). Meanwhile the continued dominance of *Nothofagus* forest with minor presence of *Saxegothaea* between 1500-150 cal yr BP is evidence of the persistence of a closed canopy North Patagonia forest under cold temperatures and abundant precipitation. Prominent centennial-scale peaks in CHAR over the last 1000 years are likely to indicate longer-term precipitation variability with alternation of wet and dry periods of sufficient intensity and duration to effectively accumulate and desiccate woody material and promote long periods of widespread fire events. These changes are represented by a marked shift towards positive values in PCA 2 (Figure 6.6), indicating that this PCA component is associated with precipitation variability (contrast between *P. nubigena* and Cupressaceae) along with with the introduction of exotic taxa.

The three Cupressaceae species present in Patagonia show different climate associations. While *Fitzroya cupressoides* and *Pilgerodendron uviferum* are hygrophilous trees present in the hyper-humid evergreen rainforest communities of western Patagonia, *Austrocedrus chilensis* develops over the dry forest-steppe ecotone in the eastern Andean slopes as well as northward in the western Andes within the summer-drought region of south central Chile.

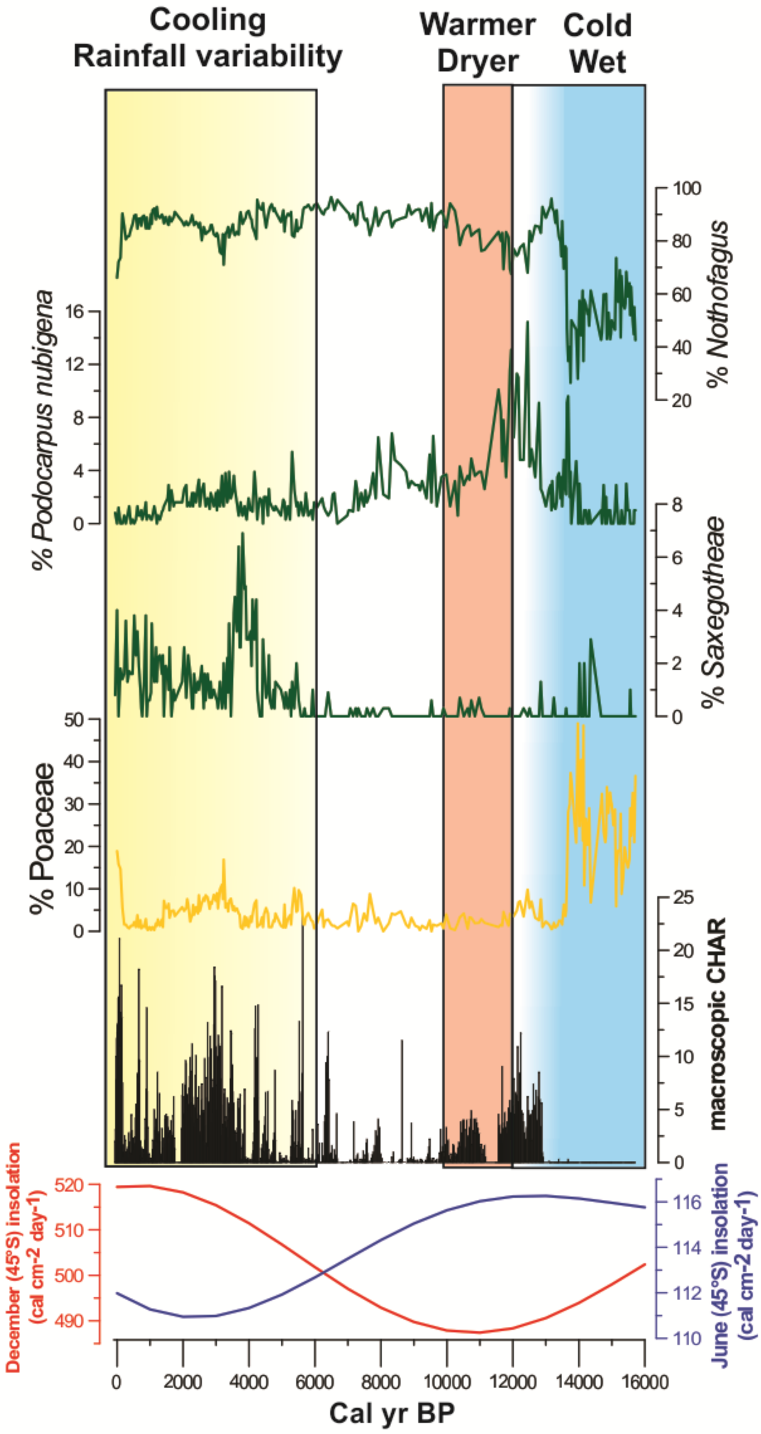

Figure 6.9. Summary panel with the key climate features inferred from Lago Espejo, including selected pollen percentage taxa along with macroscopic CHAR. The data are plotted against changes in Southern Hemisphere (45°S) summer (December) and winter (June) insolation (Berger and Loutre, 1991).

Unfortunately, these vegetation-climate distinctions cannot be routinely made from Chilean pollen assemblages because it has not been possible to divide Cupressaceae pollen into more than one single morphological group (see Appendix 3 for more details). Finally, the increase in Poaceae and non-arboreal taxa associated with European disturbance drove a notable drop in *Nothofagus* abundance (from 90% to 50%), leading to values comparable to the ones observed prior to 16,000 cal yr BP. Arboreal demise and expansion of non-arboreal elements have been widely recorded in the Lake District and Central Patagonia (Jara and Moreno, 2014; Henriquez et al., 2015; Villa-Martinez et al., 2012). The timing at Lago Espejo matches the documented time of European settlement of the Chiloé Continental area (Martinić, 2004) and suggests that European settlement was the most significant disturbance event for native vegetation in the Futaleufú area since the forest expansion during the last deglaciation.

6.7 Conclusions

1. Lago Espejo (43°S) provides a detailed record of the interactions between climate variations, vegetation and fire regimes at millennial-timescales in the Andean sector of Chiloé Continental area at the southern margin of Northwestern Patagonia.

2. An open, treeless landscape dominated by high-Andean grasses with minimal organic productivity and zero CHAR between 16,000-13,600 cal yr BP was likely associated with cold and hyper humid conditions resulting from intense SWW flow.

3. Rapid *Nothofagus* expansion along with a sharp transition from glaciolacustrine to organic sedimentation indicates a warming at 13,600 cal yr BP. The expansion of cold-resistant taxa suggests, however, that a cold/humid climate prevailed until 12,000 cal yr BP. Comparison with regional pollen records shows that post-glacial forest expansion of the Andean sectors of Chiloé Continental postdated forest development in the lowlands, suggesting that cold glacial conditions persisted several millennia later in the Andean sector of Chiloé Continental.

4. The decline of cold-resistant elements, the expansion of shade-intolerant trees with broader distributions, and high CHAR between 12,000-10,000 cal yr BP signal a period of warmer/drier conditions and increasing fire disturbances as a result of a weakening/southward migration of the SWW.

5. Closed-canopy *Nothofagus* forest dominates continuously after 10,000 cal yr BP. The expansion of cold-tolerant taxa, grasses and persistent high CHAR after 4000 cal yr BP suggest increasing rainfall variability superimposed on a long-term trend towards colder/wetter conditions. These changes occur during a period of increasing difference between summer and winter insolation at 45°S, suggesting that seasonality and intense fire activity could have played an important role in maintaining the dominance of *Nothofagus* over other broad-leaved forest trees during the late Holocene.

6. The rapid decrease in *Nothofagus* and the expansion of grass and exotic taxa by 150 cal yr BP shows that European settlement of the region represents the most significant vegetation change over the last 16,000 years.

7. The onset of charcoal accumulation lagged local forest expansion by at least 700 years and significant variations in CHAR, and CHAR peak frequency and magnitude are observed under continuous forest coverage, suggesting that climate and not arboreal coverage has been the key modulator of fire activity in the western Andean flanks of Northern Patagonia.

8. Finally, we note that key pollen transitions at Lago Espejo between 16,000-8000 cal yr BP lagged by several centuries -if not millennia- similar trends documented in palynological sites northward and westward from the site. These variations might be attributed to differences in the timing of glacial abandonment during the Last Termination and to different climate sensitivity of Andean vegetation relative to lowland communities. The replication at Lago Espejo of the vegetation trends observed in lowland sites, seems ultimately to depend upon the intensity of the underlying climate trend relative to the environmental controls imposed by the continental climate and the disturbance regime of the Andes.

Chapter Seven

Synthesis

7.1 Research aims and rationale

This final chapter synthesises and discusses the main results of this research to address the thesis aims, followed by discussion of the key scientific contributions and a consideration of some future research investigations that could be informed by this work.

As discussed in Chapter One, this thesis has two general research aims:

(1) To develop three new pollen-based climate reconstructions that document millennial-scale changes in temperature and precipitation in New Zealand and Northwestern Patagonia over the last 15,000 years
(2) To compare and contrast these reconstructions to elucidate general past trends in the atmospheric circulation of the Southern Hemisphere.

To achieve these aims, the research strategy has exploited similarities and differences between the climate regimes of New Zealand and Northwestern Patagonia. As discussed in Chapters One and Two, both study regions lie at the northern edge of the Southern Westerly Wind belt (SWW), which implies that their patterns of atmospheric circulation are governed by changes in the intensity and latitudinal position of the westerly belt (Figure 7.1). Due to the oceanic character of the Southern Hemisphere, the SWW are highly symmetric in their latitudinal flow. Thus paleo-climate trends of the same timing and direction (cooling/warming, increase/decrease in precipitation) between the two study areas will be interpreted as resulting from zonally-symmetric changes in the strength and position of the SWW. The paleo-climate inferences that arise from this rationale are further tested against other published SWW reconstructions.

Chapters One and Two also highlight that northern New Zealand lacks a prominent topographic barrier such as the Southern Andes in Northwestern Patagonia. Due to the presence of this prominent axial cordillera, the latter region is isolated from easterly sources of precipitation. In contrast, the northern and eastern parts of New Zealand are directly exposed to the sub-tropical circulation of the Pacific Ocean. Therefore, divergent paleo-climate signals between this region and Northwestern Patagonia are expected to result from the effect of a stronger sub-tropical circulation over Northern New Zealand. The paleo-climate inferences that arise from this rationale are also further tested via comparison with proxy evidence from the Tropical Pacific. In sum, the similarities and differences between the modern climate regimes of New Zealand and Northwestern Patagonia provide a basis for reconstructing past changes in Southern Hemisphere atmospheric circulation using pollen-based climate reconstructions and appropriate hemispheric comparisons.

This final chapter is divided into three broad sections. Firstly, key paleo-climate trends presented in Chapter Four, Five and Six will be summarised. Second, these findings are integrated to put forward a general scheme of paleo-circulation of the Southern Hemisphere over the last 15,000 years. The final section raises some important research questions arising from or linked to this research and that could lead to further fruitful advances of knowledge.

7.2. Summary of three new pollen-climate reconstructions

Chapter Four presents a 16,000-year pollen and plant macrofossil reconstruction from Adelaide Tarn (41°S), a small lake at 1250 masl located in central New Zealand (Figure 7.1). A qualitative index for annual temperatures termed Pollen Temperature Proxy (PTP) was developed for this site, based on the relative abundance of lowland to highland vegetation. The PTP from Adelaide Tarn shows evidence for rapid warming between 13,000-10,000 cal yr BP with a brief plateau between 13,700-13,000 cal yr BP. Peak temperatures are reached between 10,000-9000 cal yr BP and then a long-term cooling trend sets in, culminating with minimal temperatures and a lowering of the treeline over the last 3,000 cal yr BP.

A 14,500-year reconstruction from Moanatuatua peatbog in Northern New Zealand (37°S; 60 masl) is presented in Chapter Five (Figure 7.1) with the aim of reconstructing regional temperature and precipitation over a similar age interval to Adelaide Tarn situated 450 km to the southwest. A qualitative precipitation proxy, termed Pollen Moisture Index (PMI), was produced based on the relative dominance of conifer trees with different drought tolerances; whereas two quantitative temperature reconstructions with the modern analogue technique and the partial least squares method using the New

Zealand pre-deforestation pollen dataset were developed (Wilmshurst et al., 2007). These reconstructions show a mostly continuous warming trend between 14,500-10,000 cal yr BP, accompanied by an early dry phase between 12,000-10,000; and a later wet phase between 10,000-6000 cal yr BP. Holocene temperature remains mostly unchanged, and the last 7000 years feature a long-term trend towards drier conditions.

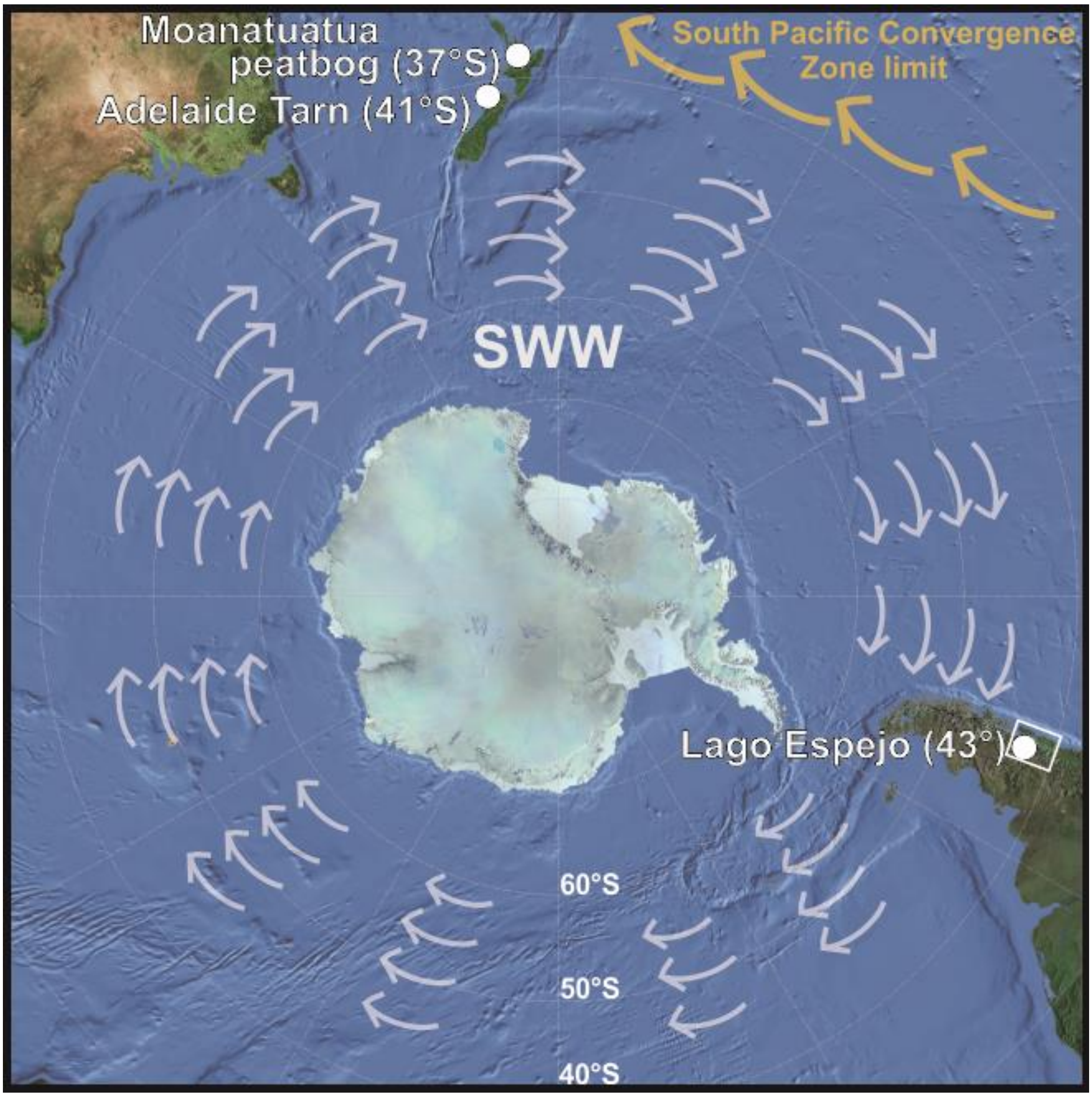

Figure 7.1. Sketch map of the Southern Hemisphere mid- and high-latitudes showing the Southern Westerly Wind belt (SWW) and the northern limit of the South Pacific Convergence Zone and associated circulation. The figures also show the position of the study sites presented in this thesis. The black rectangle encompasses the location of Northwestern Patagonia.

In Chapter Six, a 16,000-year pollen and charcoal accumulation rate (CHAR) record from Northern Patagonia (43°S; 330 masl) is presented with the aim of reconstructing regional vegetation and fire activity; and their association with variation in the intensity and/or position of the Southern Westerly Winds (SWW; Figure 7.1). The pollen record reveals the dominance of high-Andean elements prior to 13,600 cal yr BP, suggesting persistent cold and moist conditions under stronger/northward-shifted SWW. Rapid expansion of *Nothofagus* forest and the transition from glacial silts to organic sediment at 13,600 cal yr BP reflect a warming trend, although the expansion of cold-resistant hygrophilous trees between 13,600-12,000 cal yr BP suggest that, despite overall warming, conditions remained cold and wet. The decrease of cold-tolerant elements, the expansion of a shade-intolerant taxon with a broader climate distribution, and high fire activity indicate warmer conditions and a trend towards drier summers between 12,000-10,000 cal yr BP. The last 10,000 years of the record are marked by persistence of a closed-canopy *Nothofagus* forest. The re-expansion of hygrophilous, cold-tolerant taxa at 6000 cal yr BP is interpreted as a long-term cooling with increases in precipitation resulting from a northward shift and/or intensification of the SWW. The subsequent expansion of grasses and increases in CHAR after 4000 cal yr BP is interpreted as reflecting increasing precipitation variability which is superimposed on a long-term cooling trend. Peak differences in summer and winter insolation at 45°S after 4000 cal yr BP suggest that this variability could have been linked to increasing seasonality.

7.3. Discussion

7.3.1 Late-glacial climate trends

The late-glacial to Holocene transition covered by the three records presented in this thesis (15,000-11,000 cal yr BP) is characterized by sustained warming trends. At Adelaide Tarn, this warming is indicated in the Pollen Temperature Proxy as lowland trees progressively expand in the pollen diagram (Figure 7.2E). At Moanatuatua, both quantitative reconstructions show sustained increases in temperature as thermophilous taxa expand or increase their abundances in the pollen record (Figure 7.2B). At Lago Espejo, abrupt warming is indicated by a transition from high-Andean vegetation to a *Nothofagus* forest. Overall, these results are consistent with multiple other independent climate reconstructions from the Southern Hemisphere mid-latitudes which show prominent warming pulses during the Last Glacial Termination (18,000-11,000 cal yr

BP), indicating a southward shift of the SWW with respect to their glacial position (Denton et al., 2010).

Both New Zealand sites show either a cessation or a subtle reduction in their late-glacial warming trends at different times. At Adelaide Tarn, a small reduction in the Pollen Temperature Proxy is observed between 13,700-13,000 cal yr BP (Figure 7.2E), reflecting the expansion of alpine vegetation. Nonetheless, this climate inference is ambiguous because lowland-montane trees experience noticeable increases along with alpine taxa. As discussed in Chapter Four, local factors affecting the palynological signal such as the masking effect of *Fuscospora* pollen or the constraints on vegetation development imposed in a recently deglaciated landscape might explain these complex patterns. Thus, the timing and signature of the New Zealand late-glacial cooling cannot be assessed with confidence from the Adelaide Tarn record.

At Moanatuatua, rapid warming seen in both temperature reconstructions is punctuated by cessations between 14,200-13,800 and 13,500-12,000 cal yr BP, reflecting the expansion of non-arboreal taxa. While the earlier of those expansions may be attributed to the effects of volcanic disturbance on vegetation; the second expansion appears to represent a climate expression which is in broad agreement with a cold reversal recognised elsewhere in northern New Zealand, which has been linked to the Antarctic Cold Reversal (ACR; 14,700-13,000 cal yr BP, light blue bar in Figure 7.2) (Newnham & Lowe, 2000; Newnham et al., 2012; Barrell et al., 2013).

A northwards shift of the SWW has been proposed to account for the decrease in temperature (Putnam et al., 2010) and also for increased precipitation observed in some of these New Zealand Late-glacial records (Vandergoes and Fitzsimons, 2003; Sikes et al., 2013). However, when pollen sites from northern and southern New Zealand are compared, the southern sites show more pronounced cooling signatures that clearly align with the ACR, whilst the northern records evidence a weaker cooling lagging the Antarctic signature by several centuries (13,600-12,600 cal yr BP) (Newnham and Lowe, 2000; Newnham et al., 2012). The pattern of a minor temperature reversal observed at Moanatuatua at around the time of deposition of Waiohau Tephra is consistent with a weaker and delayed expression of the ACR in northern New Zealand (Newnham et al., 2012).

Although the pollen record from Lago Espejo in Northwestern Patagonia does not provide evidence for a well-defined cold period during the Late-glacial to Holocene transition, it shows that cold/and wet conditions persisted until ~12,000 cal yr BP, well beyond the ACR Chronozone. Nevertheless, this timing might not necessarily represent a regional climate signal because, due to the Andean position and the relative high elevation of Lago Espejo, deglacial conditions were reached later (13,600 cal yr BP) than at other lowland sites from Northwestern Patagonia such as Huelmo mire or Lago Lepué (Moreno and Leon, 2003; Pesce and Moreno, 2014); Additionally, Andean vegetation was likely adjusting to the recent forest expansion (*Nothofagus* increase in Figure 7.2I). Thus, I refrain from making any conclusive inferences regarding this climate episode from the Lago Espejo record. However, evidence from the well-dated lowland pollen sites of Huelmo mire, Lago Lepué, and Lago Pichilafquén in Northwestern Patagonia show a clear interval of decreased temperature and increased precipitation well aligned with the ACR (Hajdas et al., 2003; Moreno and Leon, 2003; Pesce and Moreno, 2014; Jara and Moreno 2014). The close control exerted by the SWW over the modern climate of Northwestern Patagonia implies that a northward shift and/or intensification of the westerly circulation were the most likely scenarios during this interval (Moreno et al., 2015).

In summary, the integration of Patagonian and New Zealand records suggest a symmetric equatorward migration of SWW across the mid-latitudes during ACR times. The weak expression of this apparent zonally-symmetric cooling in northern New Zealand including Moanatuatua might be explained by means of an enhanced inflow of warm subtropical waters from the equatorial Pacific Ocean, as suggested by a stable isotope record of foraminifera deposited in marine cores offshore of northeast New Zealand (Carter et al., 2008). Alternatively, an attenuated cooling in Northern New Zealand could have resulted from southward atmospheric heat transport from the tropics during the ACR, as indicated by recent climate simulations (Pedro et al., 2015).

7.3.2 Vegetation and climate change, 12,500 – 10,000 cal yr BP

Temperature reconstructions from both New Zealand sites show rapid warming between 12,500-10,000 cal yr BP (Figure 7.2 yellow area). At Adelaide Tarn this warming is evident in the expansion of lowland conifers (e.g. *Dacrydium cupressinum*; Figure 7.2G) and decline of *Fuscospora/Lophozonia* forest forest (Figure 7.2F); whereas at Moanatuatua it is marked by the expansion of lowland conifer and thermophilous broadleaf species (e.g. *Ascarina lucida;* Figure 7.2D), along with the decline of cold-tolerant shrubs and herbs. The overall dominance of drought-tolerant over hygrophilous conifer trees, as shown by below-average values in the Pollen Moisture Index between 12,000-10,000 cal yr BP (Figure 7.2A), indicates relatively low rainfall, although not sufficient to suppress the rise of drought- and frost-intolerant *Ascarina* (Figure 7.2D). These results suggest that temperature and precipitation trends in New Zealand after 12,500 cal yr BP were likely to have been modulated by a southward contraction of the SWW.

At Lago Espejo warming is inferred based on the disappearance of cold-tolerant taxa and the expansion of tree species with broader climate affinities by 12,000 cal yr BP. This record also shows an abrupt rise of fire activity between 12,900-10,000 cal yr BP (Figure 7.2J), which is interpreted as resulting from increasing dry conditions during summer time. Regular fire could have certainly resulted from anthropogenic activities as human population of Northwestern Patagonia started as early as 14,000 cal yr BP (Dillehay et al., 2008). However, at least two independent lines of evidence suggest that, despite the undeniably anthropogenic influence on past fires, periods of regional fires has been ultimately controlled by climate variations modulated by changes in the SWW: (1) several sites in Northwestern Patagonia experience prominent rise in charcoal accumulation along with the expansion of thermophilous and drought-resistant taxa between 12,000-8000 cal yr BP (Moreno and Leon, 2003; Pesce and Moreno, 2014; Jara and Moreno, 2014), suggesting that warm and dry conditions generated by a southward migration of the SWW promoted synchronous fires at the beginning of the Holocene, and (2) tree-ring fire chronologies from Northern Patagonia reveal a close association between historical years of widespread fires and warm and dry conditions resulted from reduced westerly flow (Holz and Veblen 2011; Kitzberger et al., 1997). Based on these evidences, I inferred relative warm and dry conditions resulting from decreased SWW flow at Lago Espejo between 12,900-10,000 cal yr BP.

Similar warming and relatively dry conditions in New Zealand and Patagonia between ~12,000-10,000 cal yr BP suggests a zonally symmetric polar contraction of the SWW (yellow area in Figure 7.2), in general agreement with the onset of a southwards shift of the SWW by 12,500 cal yr BP proposed by Fletcher and Moreno (2011), and with the interpretation made by Putnam et al. (2010) based on exposure dating of moraine deposits in southern New Zealand.

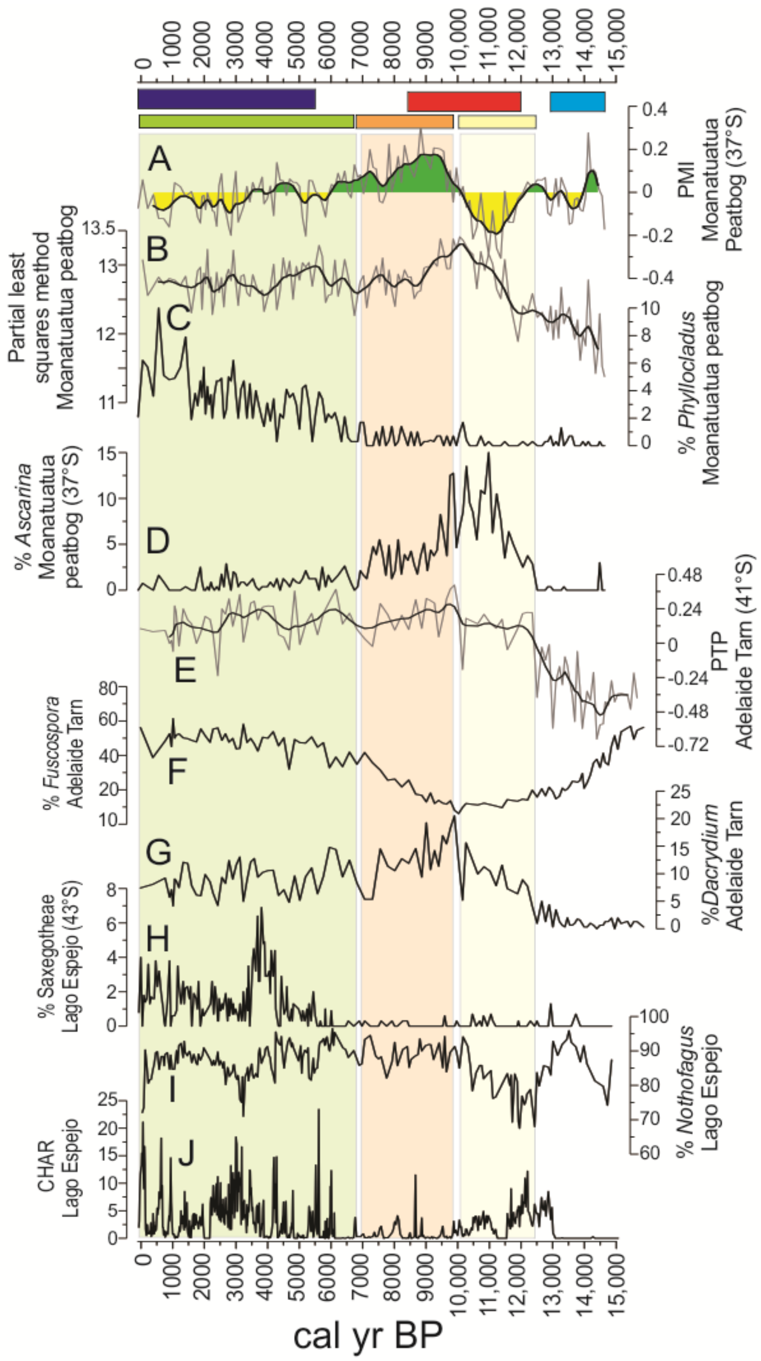

Figure 7.2. **A:** Moanatuatua Pollen Moisture Index (PMI). Green areas indicate above-average moisture, whereas yellow areas indicated below average moisture. **B:** Moanatuatua quantitative temperature reconstruction using the partial least squares technique (dataset from Wilmshurst et al. (2007)). **C:** *Phyllocladus spp.* percentage from Moanatuatua peatbog. **D:** *Ascarina lucida* percentage from Moanatuatua peatbog. **E:** Adelaide Tarn Pollen Temperature Proxy. **F:** *Fuscospora* percentage from Adelaide Tarn. **G:** *Dacrydium cupressinum* percentage from Adelaide Tarn. **H:** *Saxegothaea conspicua* percentage from Lago Espejo. **I:** *Nothofagus* from Lago Espejo. **J:** Macroscopic charcoal accumulation rate (CHAR) from Lago Espejo. The intervals discussed in section 7.3 are represented with coloured bars in the top of the figure with yellow (12,500-10,000 cal yr BP), orange (10,000-7000) and green (last 7000 years). The blue (red) bars represent the period of intensified (weakened) Southern Westerly Wind intensity according to Lamy et al. (2010). The light blue bar marks the Antarctic Cold Reversal interval (14,700-13,000 cal yr BP).

In summary, the empirical evidence presented in this thesis supports a unified expression of late-glacial early-Holocene climate oscillations across the Southern Hemisphere mid-latitudes.

7.3.3 Vegetation and climate change, 10,000 - 7000 cal yr BP

Peak warming is observed in New Zealand at 10,000 cal yr BP, as represented by maximum abundance of lowland vegetation at both sites. At Moanatuatua warm conditions are accompanied by the onset of a long-term period of relative high precipitation as indicated by above-average values of the Pollen Moisture Index (Figure 7.2A) and persistence of drought-intolerant *Ascarina lucida* between 10,000-7000 cal yr BP (Figure 7.2D).

At Lago Espejo, CHAR declines to minimal values by 10,000 year BP, indicating a marked drop in fire activity that persists with isolated high-magnitude peaks until 5000 cal yr BP. At this site, a closed-canopy *Nothofagus* forest persists with minimal occurrence of other taxa between 10,000-6000 cal yr BP, which prevents further inferences regarding regional vegetation/climate variability being made from the pollen data. However, several pollen records from Northwestern Patagonia such as Lago Condorito, Lago Pichilafquén, Lago Lepué and Lago Teo show the expansion of thermophilous and drought-tolerant trees between 11,000-7000 cal yr BP, an indication of a multi-millennial dry phase attributed to a southwards migration of the SWW (Henriquez et al., 2015; Jara and Moreno, 2014; Moreno 2004; Pesce and Moreno, 2014). Reduced westerly influence and reduced rainfall at this time are also reported from several additional reconstructions from the western regions of the Southern Hemisphere mid-latitudes (Lamy et al., 2010; Fletcher and Moreno, 2011).

Together, this evidence reveals clear divergent precipitation trends: increasing in New Zealand and decreasing in Northwestern Patagonia (orange area in Figure 7.2). Two key observations point to changes in atmospheric configuration to explain this divergence. First, sites located in regions exposed to easterly-circulation in eastern Patagonia and central Tasmania feature increased lake levels (Ariztegui et al., 2010) and high precipitation and detrital input (Rees et al., 2015) between 12,000-8000 cal yr BP, suggesting that, under reduced westerly flow, these regions received precipitation from easterly sources. Second, at present, easterly and northeasterly fronts sourced in the sub-tropical Pacific Ocean intersect the northern portion of New Zealand much more frequently during periods of weaker westerly flow (Salinger and Mullan, 1999). Hence, divergent precipitation signals between northern New Zealand and Northwestern Patagonia points towards increasing easterly precipitation in northern New Zealand. In this regard, the New Zealand evidence presented here is analogous with the scenario for eastern Patagonia and central Tasmania, and supports earlier interpretations made by Rogers and McGlone (1989) for New Zealand and more recently by Fletcher and Moreno (2011) more generally for the mid-latitudes of the Southern Hemisphere. Warmer temperatures, reduced westerly and southwesterly flow and positive easterly and northeasterly wind anomalies are common features of present-day New Zealand circulation during the positive phase of the Southern Annular Mode and La Niña conditions (Ummenhofer and England, 2007).

7.3.4 Vegetation and climate change, the last 7000 years

Over the last 7000 years, millennial-scale temperature trends are less marked and less variable at both New Zealand sites than for the late-glacial and early Holocene (green area Figure 7.2). At Adelaide Tarn, a long-term cooling, inferred from a decrease in lowland conifers and a lowering in treeline elevation, is observed after 3000 cal yr BP. At Moanatuatua, the Pollen Moisture Index reveals a long-term drying arising from increments in drought-tolerant conifers after 7000 cal yr BP (Figure 7.2A). Additionally, this pollen record shows a multi-millennial trend towards drier conditions and/or more variable rainfall regimes indicated by the demise of *Ascarina lucida* and the expansion of the drought tolerant conifer *Phyllocladus* (Figure 7.2C).

At Lago Espejo, the last 5000 years are marked by the expansion of the cold-resistant conifer *Saxegothaea conspicua* (Figure 7.2H), superimposed on a trend towards increasing rainfall variability as inferred from the high CHAR values (Figure 7.2J). The long-term cooling with increased precipitation inferred from these data are explained by a strengthening of the westerly circulation, in broad agreement with stronger SWW inferred from increasing rainfall in western regions of the Southern Hemisphere mid-latitudes (Lamy et al., 2010). Increasing rainfall variability might in turn be related to high-amplitude changes at inter-annual timescales associated with the emergence of the modern variability of El Niño Southern Oscillation and the Southern Annular Mode and their mutual interaction. Alternatively, high fire activity could have resulted from increasing seasonal differences in temperature and precipitation, as suggested by the strong difference between December and June insolation at 45°S (Chapter Five).

A long-term cooling at Adelaide Tarn is coherent with stronger SWW during the Late Holocene as the westerly circulation brings cold and moist air masses to most of the New Zealand territory (Salinger, 1980). In this context, the drying at Moanatuatua is again distinct from the trends observed in central New Zealand and Northwestern Patagonia, yet it is supported by other pollen reconstructions from northern New Zealand indicating drier conditions during the middle and late Holocene (green area Figure 7.2) (McGlone et al., 1984; Newnham et al., 1995). At present, lower rainfall in northern New Zealand under enhanced westerly flow occurs as a result of an eastward shift of the South Pacific Convergence Zone in the subtropical Pacific during El Niño conditions (Figure 7.1; Salinger and Mullan 1999). This modern climatological correlation suggests that an analogous scenario could have occurred after 4000 years BP (Gomez et al., 2013). This interpretation is in-turn consistent with proxy reconstructions from the Tropical Pacific region which show increased frequency of El Niño events over the last ~5000 years (Moy et al., 2002; Conroy et al., 2008). In summary, these proposed climate interpretations and their associations with other climate proxies and modern climatology are consistent with sustained northward expansion/intensification of the SWW, and a distancing of the South Pacific Convergence Zone from northern New Zealand.

7.4 Outcomes regarding research hypothesis

The relative influence of the sub-tropical and extra-tropical circulation systems over New Zealand vegetation and climate during the last 14,000 years was tested with the research hypothesis proposed in Chapter One. The working hypothesis for this thesis was:

H_0 = *There is no difference in the timing and direction of the major pollen-based climate trends between New Zealand and Patagonia in the last 14,000 years.*

If H_0 cannot be rejected, then changes in the position and strength of the extra-tropical SWW have been the main drivers of vegetation change in New Zealand. If, on the other hand, there is sufficient evidence to rejected H_0, then the alternative hypothesis H_1 is proposed as:

H_1 = *There are significant differences at millennial timescales between the pollen-based climate trends of New Zealand and Patagonia.*

Based on the results discussed in section 7.3, $\mathbf{H_0}$ cannot be rejected during the interval between 14,000-10,000 cal yr BP, where pollen trends in New Zealand and Northwestern Patagonia show a similar timing and direction, suggesting a strong climate control exerted by the extra-tropical circulation over the climate and vegetation in New Zealand. $\mathbf{H_0}$ can effectively be rejected after 10,000 cal yr BP, when the pollen changes from New Zealand and Northwestern Patagonia point toward divergent climate trends between these two regions. These divergences confirm $\mathbf{H_1}$, indicating that the sub-tropical circulation has been the driver of vegetation change in New Zealand.

7.5 Scientific contributions of this thesis

As reviewed in Chapter Two, Quaternary studies have a long tradition in both New Zealand and Patagonia. Historical and recent investigations have shown potential for comparing these two regions through the lenses of botany, ecology, and paleo-climatology (Schmithüsen, 1966; Wardle et al., 2001; Fletcher and Moreno, 2011). Considerable international scientific interest has emerged, largely as New Zealand and Patagonia are two of only a few terrestrial areas extending well into the Southern Hemisphere mid-latitudes, as well as the only landmasses outside Antarctica that experienced extensive Quaternary glaciations. Amongst the different fields of Quaternary sciences, pollen-based climate reconstructions from New Zealand and Patagonia have proven to be an outstanding tool for deciphering key aspects of the paleo-circulation of the Southern Hemisphere (e.g. Moreno et al., 2001; Vandergoes et al., 2005; McGlone et al., 2010; Moreno et al., 2010; Newnham et al., 2012). The bulk of investigations have been focused either on evidence from single sites, or from multiple sites within a single region, whilst inter-regional comparisons, despite their potential for reconstructing hemispheric-scale patterns, remain uncommon (e.g. Markgraf et al., 1992; Fletcher and Moreno, 2011). This thesis has taken this latter approach by presenting new highly-resolved pollen-derived reconstructions from New Zealand and Northwestern Patagonia, and comparing them to deduce regional and hemispheric-wide changes in atmospheric circulation for the past 15,000 years.

In addition to these major contributions, each of the three sites investigations has revealed valuable information. For instance, Chapter Four presented one of the most comprehensive post-glacial reconstructions from a high-alpine site in New Zealand, providing solid evidence for changes in the treeline position over the last 14,000 years, a topic rarely addressed by previous vegetation reconstructions in New Zealand and many other regions. Chapter Five provided what is perhaps the first pollen-based continuous precipitation reconstruction from New Zealand, a region where palynological investigations have largely relied on temperature variability. This record also demonstrated potential for pollen degradation to be used as a proxy for water table and hence precipitation variability in raised bog settings. In addition to providing new paleoclimate insights, these new proxies may be used to provide long term background information for land management or climate mitigation plans for northern New Zealand, a region that relies heavily on precipitation as the main water supply for its agricultural and forestry industries. Chapter Six presented new insight into the interplay between climate, post glacial vegetation and fire, a research topic that has been studied in detail in the eastern part of Patagonia but not on the western flanks of the Andes. In particular, it provided solid evidence to show that climate variations have played a major role in controlling long-term changes in fire regimes in the *Nothofagus* forest of the Patagonian Andes**.**

7.6 Topics of future research interest

7.6.1 Pre-deforestation pollen dataset for Patagonia

The application of modern pollen-climate relationships to fossil data was implemented in Chapter Four and Five, where quantitative temperature reconstructions were calculated using a pre-deforestation pollen dataset (Wilmshurst et al., 2007). Quantitative climate estimates from proxy data are a significant advance over traditional qualitative approaches because they allow direct comparisons with modern climatology and the numerical estimations of future climate trends; as well as a tool for validating atmospheric circulation and other types of climate models (Birks et al., 2010). These advantages have been recognized and have prompted quantitative analyses in New Zealand, and more recently in other terrestrial regions of the Southern Hemisphere mid latitudes such as Tasmania (Fletcher and Thomas, 2010).

In Patagonia this approach was initially used by Heusser and Streeter (1980) to reconstruct summer temperatures and annual precipitation means. Despite showing well-defined quantitative trends, the climate values generated for the fossil ensembles exceeded considerably the range of the modern dataset, suggesting limitations arising from the lack of modern analogues. A more comprehensive modern pollen-climate dataset was presented in Markgraf et al. (2002), which allowed the reconstruction of seasonal temperature and precipitation at three postglacial pollen sites from northern Patagonia. However, with few exceptions (e.g. Haberle and Bennett, 2001) modern pollen-climate studies have been focused in the eastern side of Patagonia (e.g. Paez et al., 2001).

More recently, considerable effort has turned to pollen-climate reconstruction in Northwestern Patagonia which has led to the publication of several detailed qualitative reconstructions on well-dated high-resolution pollen sequences (e.g. Moreno, 2004; Pesce and Moreno, 2014). Thus, the potential for developing quantitative reconstructions from those sequences using modern pollen datasets is strong. Unfortunately, quantitative analyses on fossil pollen are currently hampered by the lack of comprehensive modern pollen datasets. As shown by many palynological records in this region including the one presented in Chapter Six, the impact of European settlement on the pollen spectra was significant, and therefore future developments in modern pollen studies should include sub-fossil, pre-deforestation data, perhaps following the approach made by Wilmshurst et al. (2007) in New Zealand. The development of a robust modern pollen dataset would represent a step–change for Patagonia research, not only for the fields of paleoecology and paleoclimatology, but also with relevance to current and future climate scenarios.

7.6.2 The role of climate and human activities in fire regimes

As discussed in Chapter Three, fire reconstructions based on charcoal accumulation in sediment sections represent a powerful and widely used tool to reconstruct past fire histories. However, the links between fire and atmospheric variations are subject of debate since other environmental variables such as volcanic eruptions and anthropogenic impact can drive significant changes in fire regimes. In Chapter Six, the impact of tephra fallout on charcoal accumulation at Lago Espejo was assessed, showing that these two variables were not significantly correlated. The anthropogenic impact on local fires was, however, impossible to assess directly from the pollen or charcoal data. As discussed previously in this chapter, I opted for interpreting the long-term changes in charcoal accumulation in the same way that pollen changes; i.e., as a proxy for changes in temperature and precipitation associated with past shifts of the SWW. This interpretation was based on the close link between climate variations and the occurrence of past and historical fires in Northwestern Patagonia, following the rationale of other charcoal reconstructions in this region (e.g. Abarzua and Moreno, 2006; Whitlock et al., 2007). In a wider perspective, the relative contribution of anthropogenic vs climate iniciated fires to the paleo-record is an ongoing debate (Westerling et al., 2012). At timescales of millennia and from regional to global scales, changes in fire activity tend to be controlled by large-scale climate trends. For instance, global fire regimes are higher during warm interglacials than during cold glaciations (Daniau et al., 2010), and global fire trends followed temperature changes during the Last Glacial Termination (Power et al., 2008). On the other hand, the impact of human colonization of uninhabited lands seems not to be highlighted in regional fire reconstructions (e.g. Mooney et al., 2011).

New Zealand might represent an exception this pattern because high-resolution charcoal analysis has reveals a significant increase in fire associated with the recent human arrival (e.g. McWethy et al., 2010). New Zealand also offers an exceptional opportunity for testing the role of human versus environmental variables on wildfires since the timing for human arrival is recent and well constrained. However, detailed fire reconstructions covering the period prior to human colonization are largely absent, which prevents an assessment regarding the importance of past environmental change in inducing fires.

New Zealand is well suited for the use of charcoal records as a proxy for past climate for two main reasons. First, this region is the last Southern Hemisphere continental landmass to be colonised by humans (750 cal yr BP; Wilmshurst et al., 2008), which means that wildfire activity had no anthropogenic influence for virtually all the Holocene and preceding epochs. Second, most of the territory has been densely forested since the end of the Last Glacial and therefore the effect of changing forest coverage on fire activity can, in most places, be dismissed. Thus, New Zealand offers the prospect of avoiding two key confounding factors for establishing the long-term relationship between wildfire and climate variability. Future charcoal reconstructions utilising the methodology demonstrated in Chapter Six of this thesis could be applied in New Zealand sedimentary sequences with the goal of elucidating the relationship between climate variability and fire.

7.6.3 Precipitation reconstructions for New Zealand

As indicated earlier, the Pollen Moisture Index presented in Chapter Five represents one of the few continuous pollen-based records of rainfall variability in New Zealand. This chapter also explored a potential precipitation proxy in the form of variable pollen degradation that may be applicable in raised bogs. The general lack of pollen-based precipitation proxies relative to temperature proxies in New Zealand can be explained by several different reasons. The oceanic context of New Zealand implies that most of the territory experiences abundant and consistent precipitation as well as relatively low seasonal variations in comparison to other terrestrial areas of the Southern Hemisphere mid-latitudes such as Patagonia, mainland Australia or Southern Africa. Additionally, the spatial array of precipitation anomalies is considerably more heterogeneous than temperature variations due to mainland New Zealand's rugged and diverse topography. The relative rainfall surplus of New Zealand is attested by a highly-forested landscape, the broad absence of deciduous elements within the native flora, and the lack of regional forest communities that distinguish low precipitation regimes at annual or seasonal scales.

On the other hand, New Zealand's boundary position between low- and high-latitude atmospheric systems, its small size, and the oceanic character exposes most of the territory to the interaction of sub-tropical and sub-Antarctic precipitation fronts. These factors determine that moisture-bearing air masses enter the territory from multiple directions (Brenstrum, 2007), limiting the potential of using precipitation proxies to reconstruct a single atmospheric system (e.g. the SWW). To overcome this limitation, future site-based precipitation reconstructions will need to investigate the relative contribution of the different circulation systems to the site's present-day precipitation regimes, considering time and spatial variability. This information will be critical for a better understanding of the rainfall trends that accompanied the prominent temperature changes experienced by New Zealand since the Last Glacial Maximum, as well as for the reconstruction of the underlying pattern of variation in the Southern Hemisphere atmospheric circulation. This thesis demonstrates how these advances may be achieved in future through judicious site selection in relation to atmospheric circulation patterns (see section 5.4) and by developing proxies that can be applied to reconstruct precipitation variability.

7.6.4 Comparing proxy-based data with modern climatology

Lorrey et al. (2007) introduced a new approach for analysing New Zealand paleo-climate records in which the spatial patterns in proxy data are compared against the modern climate regimes described by Kidson (2000). A further improvement of this technique involved the use of climate anomalies in instrumental time series as modern analogues for proxy-derived climate estimations (Lorrey et al., 2014). This latter methodology has the advantage of generating synoptic weather patterns, with their associated quantitative climate anomalies, that resemble the past climate anomalies detected in proxy data. The methodology seems to be highly applicable to pollen-based climate proxies because both the modern and paleo datasets are normalized by partitioning them into quantiles, which facilitates comparisons and does not limit the methodology to quantitative proxy data. In this regard, forthcoming studies should aim to use these methodologies on some of the pollen-based climate proxies presented in Chapter Four, Five and Six in order to test, in the light of modern climatology, the trends in large-scale atmospheric circulation inferred in this thesis.

8. References

- Abarzúa, A.M., Moreno, P.I., 2008. Changing fire regimes in the temperate rainforest region of southern Chile over the last 16,000 yr. Quaternary Research 69, 62-71.
- Abram, N.J., Mulvaney, R., Vimeux, F., Phipps, S.J., Turner, J., England, M.H., 2014. Evolution of the Southern Annular Mode during the past millennium. Nature Clim. Change 4, 564-569.
- Adams, J.B., Michael, E.M., Caspar, M.A., 2003. Proxy evidence for an El Niño-like response to volcanic forcing. Nature 426, 274-278.
- Agee, J.K., 1993. Fire ecology of Pacific Northwest forests. Island Press, Washington, DC.
- Alley, R.B., Brook, E.J., Anandakrishnan, S., 2002. A northern lead in the orbital band: north–south phasing of Ice-Age events. Quaternary Science Reviews 21, 431-441.
- Alley, R.B., Mayewski, P.A., Sowers, T., Stuiver, M., Taylor, K.C., Clark, P.U., 1997. Holocene climatic instability: a prominent, widespread event 8200 yr ago. Geology 25, 483-486.
- Alloway, B.V., Lowe, D.J., Barrell, D.J.A., Newnham, R.M., Almond, P.C., Augustinus, P.C., Bertler, N.A.N., Carter, L., Litchfield, N.J., McGlone, M.S., Shulmeister, J., Vandergoes, M.J., Williams, P.W., 2007. Towards a climate event stratigraphy for New Zealand over the past 30 000 years (NZ-INTIMATE project). Journal of Quaternary Science 22, 9-35.
- Alloway, B.V., Lowe, D.J., Larsen, G., Shane, P.A.R., Westgate, J.A., 2013. QUATERNARY STRATIGRAPHY | Tephrochronology A2 - Elias, Scott A, In: Mock, C.J. (Ed.), Encyclopedia of Quaternary Science (Second Edition). Elsevier, Amsterdam, pp. 277-304.

- Anderson, E., Libby, W., Weinhouse, S., Reid, A., Kirshenbaum, A., Grosse, A., 1947. Natural radiocarbon from cosmic radiation. Physical Review 72, 931.
- Anderson, R.F., Ali, S., Bradtmiller, L.I., Nielsen, S.H.H., Fleisher, M.Q., Anderson, B.E., Burckle, L.H., 2009. Wind-Driven Upwelling in the Southern Ocean and the Deglacial Rise in Atmospheric CO2. Science 323, 1443-1448.
- Aravena, J.C., Luckman, B.H., 2009. Spatio-temporal rainfall patterns in southern South America. International Journal of Climatology 29, 2106-2120.
- Ariztegui, D., Gilli, A., Anselmetti, F.S., Goñi, R.A., Belardi, J.B., Espinosa, S., 2010. Lake-level changes in central Patagonia (Argentina): crossing environmental thresholds for Lateglacial and Holocene human occupation. Journal of Quaternary Science 25, 1092-1099.
- Ashok, K., Behera, S.K., Rao, S.A., Weng, H., Yamagata, T., 2007. El Niño Modoki and its possible teleconnection. Journal of Geophysical Research: Oceans 112.
- Auer, V., 1934. The Finnish Expedition to Tierra Del Fuego in 1928-1929. Suomalaisen kirjallisuuden seuran kirjapainon.
- Augustinus, P., Cochran, U., Kattel, G., D’Costa, D., Shane, P., 2012. Late Quaternary paleolimnology of Onepoto maar, Auckland, New Zealand: Implications for the drivers of regional paleoclimate. Quaternary International 253, 18-31.
- Augustinus, P., D'Costa, D., Deng, Y., Hagg, J., Shane, P., 2011. A multi-proxy record of changing environments from ca. 30 000 to 9000 cal. a BP: Onepoto maar palaeolake, Auckland, New Zealand. Journal of Quaternary Science 26, 389-401.

- Ballantyne, A., Lavine, M., Crowley, T., Liu, J., Baker, P., 2005. Meta-analysis of tropical surface temperatures during the Last Glacial Maximum. Geophysical Research Letters 32, 1-5.
- Bard, E., Rostek, F., Turon, J.-L., Gendreau, S., 2000. Hydrological impact of Heinrich events in the subtropical northeast Atlantic. Science 289, 1321-1324.
- Barnola, J., Raynaud, D., Korotkevich, Y., Lorius, C., 1987. Vostok ice core provides 160,000-year record of atmospheric CO2. Nature 329, 408-414
- Barrell, D.J.A., Almond, P.C., Vandergoes, M.J., Lowe, D.J., Newnham, R.M., 2013. A composite pollen-based stratotype for inter-regional evaluation of climatic events in New Zealand over the past 30,000 years (NZ-INTIMATE project). Quaternary Science Reviews 74, 4-20.
- Barry, R.G., Chorley, R. J., 1992. Atmosphere, Weather and Climate. Routledge, New York.
- Bennett, K.D., 1996. Determination of the number of zones in a biostratigraphical sequence. New Phytologist 132, 155-170.
- Beuselinck, L., Govers, G., Poesen, J., Degraer, G., Froyen, L., 1998. Grain-size analysis by laser diffractometry: comparison with the sieve-pipette method. Catena 32, 193-208.
- Birks, H.J.B., 2013. POLLEN METHODS AND STUDIES | Numerical Analysis Methods A2 - Mock, Scott A. EliasCary J, Encyclopedia of Quaternary Science (Second Edition). Elsevier, Amsterdam, pp. 821-830.
- Birks, H.J.B., Gordon, A.D., 1985. Numerical methods in Quaternary pollen analysis. Academic Press, Orlando.

- Birks, H.J.B., Heiri, O., Seppä, H., Bjune, A.E., 2010. Strengths and Weaknesses of Quantitative Climate Reconstructions Based on Late-Quaternary. The Open Ecology Journal 3.
- Blaauw, M., 2010. Methods and code for 'classical'age-modelling of radiocarbon sequences. quaternary geochronology 5, 512-518.
- Blaauw, M., Christen, J., Mauquoy, D., van der Plicht, J., Bennett, K., 2007. Testing the timing of radiocarbon-dated events between proxy archives. The Holocene 17, 283-288.
- Blaauw, M., Christen, J.A., 2005. Radiocarbon Peat Chronologies and Environmental Change. Journal of the Royal Statistical Society. Series C (Applied Statistics) 54, 805-816.
- Blaauw, M., Christen, J.A., 2011. Flexible paleoclimate age-depth models using an autoregressive gamma process. 457-474.
- Boekestein, A., Stadhouders, A.M., Stols, A.L.H., Roomans, G.M., 1983. A comparison of ZAF-correction methods in quantitative X-ray microanalysis of light-element specimens. Ultramicroscopy 12, 65-68.
- Bond, G., Heinrich, H., Broecker, W., Labeyrie, L., McManus, J., Andrews, J., Huon, S., Jantschik, R., Clasen, S., Simet, C., 1992. Evidence for massive discharges of icebergs into the North Atlantic ocean during the last glacial period.
- Bradley, R.S., 1999. Paleoclimatology: reconstructing climates of the Quaternary. Academic Press.
- Brenstrum, E., 2007. The New Zealand Weather Book. Craig Potton Publ.
- Brewer, S., Guiot, J., Barboni, D., 2013. Pollen Methods and Studies | Use of Pollen as Climate Proxies A2 - Mock, Scott A. EliasCary J, Encyclopedia of Quaternary Science (Second Edition). Elsevier, Amsterdam, pp. 805-815.

- Briggs, D.J., Smithson, P., 1986. Fundamentals of physical geography. Rowman & Littlefield.
- Broecker, W., Denton G., 1990a. What drives glacial cycles? Scientific American 262, 43-50.
- Broecker, W.S., Denton, G.H., 1990b. The role of ocean-atmosphere reorganizations in glacial cycles. Quaternary Science Reviews 9, 305-341.
- Bunting, M., 2008. Pollen in wetlands: using simulations of pollen dispersal and deposition to better interpret the pollen signal. Biodiversity and conservation 17, 2079-2096.
- Bunting, M., Gaillard, M.-J., Sugita, S., Middleton, R., Broström, A., 2004. Vegetation structure and pollen source area. The Holocene 14, 651-660.
- Bussell, M.R., 1988. Modern pollen rain, central-western North Island, New Zealand. New Zealand Journal of Botany 26, 297-315.
- Caldenius, C.R.C., 1932. Las glaciaciones cuaternarias en la Patagonia y Tierra del Fuego: una investigación regional, estratigráfica y geocronológica, una comparación con la escala geocronológica sueca. Dirección General de Minas y Geología.
- Caniupán, M., Lamy, F., Lange, C., Kaiser, J., Arz, H., Kilian, R., Baeza Urrea, O., Aracena, C., Hebbeln, D., Kissel, C., 2011. Millennial-scale sea surface temperature and Patagonian Ice Sheet changes off southernmost Chile (53 S) over the past∼ 60 kyr. Paleoceanography 26.
- Carter, L., Manighetti, B., Ganssen, G., Northcote, L., 2008. Southwest Pacific modulation of abrupt climate change during the Antarctic Cold Reversal–Younger Dryas. Palaeogeography, Palaeoclimatology, Palaeoecology 260, 284-298.
- Clapperton, C.M., 1990. Quaternary glaciations in the Southern Hemisphere: an overview. Quaternary Science Reviews 9, 299-304.

- Clark, D.B., Palmer, M.W., Clark, D.A., 1999. Edaphic factors and the landscape-scale distributions of tropical rain forest trees. Ecology 80, 2662-2675.
- Clark, J.S., 1988. Stratigraphic charcoal analysis on petrographic thin sections: application to fire history in northwestern Minnesota. Quaternary Research 30, 81-91.
- Clark, J.S., 1990. Fire and climate change during the last 750 yr in northwestern Minnesota. Ecological Monographs 60, 135-159.
- Clark, J.S., Royall, P.D., Chumbley, C., 1996. The Role of Fire During Climate Change in an Eastern Deciduous Forest at Devil's Bathtub, New York. Ecology 77, 2148-2166.
- Clarkson, B.R., 1997. Vegetation recovery following fire in two Waikato peatlands at Whangamarino and Moanatuatua, New Zealand. New Zealand Journal of Botany 35, 167-179.
- Clayton-Greene, K.A., 1978. Aspects of the distribution of certain indigenous woody species in the Waikato District, New Zealand. Journal of the Royal Society of New Zealand 8, 283-291.
- Clymo, R., 1965. Experiments on breakdown of Sphagnum in two bogs. The Journal of Ecology, 747-758.
- Clymo, R., Mackay, D., 1987. Upwash And Downwash Of Pollen And Spores In The Unsaturated Surface Layer Of Sphangnum-Dominated Peat. New Phytologist 105, 175-183.
- Cockayne, L., 2011. The Vegetation of New Zealand. Cambridge University Press.
- Cockayne, L., Allan, H., 1934. An annotated list of groups of wild hybrids in the New Zealand flora. Annals of botany 48, 1-55.
- Conroy, J.L., Overpeck, J.T., Cole, J.E., Shanahan, T.M., Steinitz-Kannan, M., 2008. Holocene changes in eastern tropical Pacific climate

inferred from a Galápagos lake sediment record. Quaternary Science Reviews 27, 1166-1180.
- Coronato, A.M., Coronato, F., Mazzoni, E., Vázquez, M., Rabassa, J., 2008. The physical geography of Patagonia and Tierra del Fuego, The late cenozoic of Patagonia and Tierra del Fuego. Elsevier Amsterdam, pp. 13-56.
- Cotton, C.A., 1916. The structure and later geological history of New Zealand. Geological Maganzine 6, 314-320.
- Cruz, F.W., Burns, S.J., Karmann, I., Sharp, W.D., Vuille, M., Cardoso, A.O., Ferrari, J.A., Dias, P.L.S., Viana, O., 2005. Insolation-driven changes in atmospheric circulation over the past 116,000 years in subtropical Brazil. Nature 434, 63-66.
- Daniau, A.-L., Harrison, S., Bartlein, P., 2010. Fire regimes during the Last Glacial. Quaternary Science Reviews 29, 2918-2930.
- Davis, B.A., Brewer, S., Stevenson, A.C., Guiot, J., 2003. The temperature of Europe during the Holocene reconstructed from pollen data. Quaternary Science Reviews 22, 1701-1716.
- De Lisle, J.F., 1967. The climate of the Waikato Basin. New Zealand Meteorological Service.
- Dean Jr, W.E., 1974. Determination of carbonate and organic matter in calcareous sediments and sedimentary rocks by loss on ignition: comparison with other methods. Journal of Sedimentary Research 44.
- Denniston, R.F., Wyrwoll, K.-H., Asmerom, Y., Polyak, V.J., Humphreys, W.F., Cugley, J., Woods, D., LaPointe, Z., Peota, J., Greaves, E., 2013. North Atlantic forcing of millennial-scale Indo-Australian monsoon dynamics during the Last Glacial period. Quaternary Science Reviews 72, 159-168.

- Denton, G.H., Anderson, R.F., Toggweiler, J.R., Edwards, R.L., Schaefer, J.M., Putnam, A.E., 2010. The Last Glacial Termination. Science 328, 1652-1656.
- Denton, G.H., Bockheim, J.G., Wilson, S.C., Stuiver, M., 1989. Late Wisconsin and early Holocene glacial history, inner Ross embayment, Antarctica. Quaternary Research 31, 151-182.
- Denton, G.H., Heusser, C.J., Lowel, T.V., Moreno, P.I., Andersen, B.G., Heusser, L.E., Schlühter, C., Marchant, D.R., 1999. Interhemispheric Linkage of Paleoclimate During the Last Glaciation. Geografiska Annaler: Series A, Physical Geography 81, 107-153.
- Denton, G.H., Hughes, T.J., 1981. The Last great ice sheets. Wiley.
- Dillehay, T.D., Ramirez, C., Pino, M., Collins, M.B., Rossen, J., Pino-Navarro, J., 2008. Monte Verde: seaweed, food, medicine, and the peopling of South America. Science 320, 784-786.
- Donoso Zegers, C., 2006. Las especies arbóreas de los bosques templados del Chile y Argentina. Autoecología. Marisa Cuneo Ediciones, Valdivia.
- Ducker, S.C., Knox, R.B., 1985. Pollen and pollination: a historical review. Taxon, 401-419.
- Duncan, R.P., 1993. Flood disturbance and the coexistence of species in a lowland podocarp forest, south Westland, New Zealand. Journal of ecology, 403-416.
- Eaves, S.R., Mackintosh, A.N., Winckler, G., Schaefer, J.M., Alloway, B.V., Townsend, D.B., 2016. A cosmogenic 3 He chronology of late Quaternary glacier fluctuations in North Island, New Zealand (39° S). Quaternary Science Reviews 132, 40-56.
- Ellison, G.N., Gotelli, N., 2004. A primer of ecological statistics. Sinauer, Sunderland, Massachusetts, USA.

- EPICA_community_member, 2004. Eight glacial cycles from an Antarctic ice core. Nature 429, 623-628.
- Erdtman, G., 1969. Handbook of palynology: morphology, taxonomy, ecology.
- Faegri, K., Iversen, J., 1950. Text-book of modern pollen analysis. GFF 72, 363-364.
- Faegri, K., Iversen, J., 1989. Textbook of Pollen Analysis, four ed. Joh Wiley & Sons, New York.
- Faegri, K.a.I., J, 1975. Textbook of pollen analysis. Munksgaard, Copenhagen.
- Farrera, I., Harrison, S., Prentice, I., Ramstein, G., Guiot, J., Bartlein, P., Bonnefille, R., Bush, M., Cramer, W., Von Grafenstein, U., 1999. Tropical climates at the Last Glacial Maximum: a new synthesis of terrestrial palaeoclimate data. I. Vegetation, lake-levels and geochemistry. Clim Dyn 15, 823-856.
- Flenley, J., 1971. Measurements of the specific gravity of the pollen exine. Pollen et Spores 13, 179-186.
- Fletcher, M.-S., Moreno, P.I., 2011. Zonally symmetric changes in the strength and position of the Southern Westerlies drove atmospheric CO2 variations over the past 14 k.y. Geology 39, 419-422.
- Fletcher, M.-S., Moreno, P.I., 2012a. Have the Southern Westerlies changed in a zonally symmetric manner over the last 14,000 years? A hemisphere-wide take on a controversial problem. Quaternary International 253, 32-46.
- Fletcher, M.-S., Moreno, P.I., 2012b. Vegetation, climate and fire regime changes in the Andean region of southern Chile (38 S) covaried with centennial-scale climate anomalies in the tropical Pacific over the last 1500 years. Quaternary Science Reviews 46, 46-56.

- Fogt, R., Bromwich, D., Hines, K., 2011. Understanding the SAM influence on the South Pacific ENSO teleconnection. Clim Dyn 36, 1555-1576.
- Fontaine, M., Aerts, R., Özkan, K., Mert, A., Gülsoy, S., Süel, H., Waelkens, M., Muys, B., 2007. Elevation and exposition rather than soil types determine communities and site suitability in Mediterranean mountain forests of southern Anatolia, Turkey. Forest Ecology and Management 247, 18-25.
- Foster, C.R., 2013. Palaeolimnology of Adelaide Tarn, a~ 14,000-year-old low-alpine glacial lake, northwestern South Island, New Zealand, Earth Sciences. The University of Waikato, Hamilton, p. 218.
- Fowler, A.M., Boswijk, G., Lorrey, A.M., Gergis, J., Pirie, M., McCloskey, S.P.J., Palmer, J.G., Wunder, J., 2012. Multi-centennial tree-ring record of ENSO-related activity in New Zealand. Nature Clim. Change 2, 172-176.
- Franklin, D.A., 1968. Biological flora of New Zealand. New Zealand Journal of Botany 6, 493-513.
- Galle, O.K., Runnels, R.T., 1960. Determination of CO2 in carbonate rocks by controlled loss on ignition. Journal of Sedimentary Research 30.
- Garreaud, R., 2007. Precipitation and circulation covariability in the extratropics. Journal of Climate 20, 4789-4797.
- Garreaud, R., Battisti, D.S., 1999. Interannual (ENSO) and interdecadal (ENSO-like) variability in the Southern Hemisphere tropospheric circulation. Journal of Climate 12, 2113-2123.
- Garreaud, R., Lopez, P., Minvielle, M., Rojas, M., 2013. Large-scale control on the Patagonian climate. Journal of Climate 26, 215-230.

- Garreaud, R.D., Vuille, M., Compagnucci, R., Marengo, J., 2009. Present-day South American climate. Palaeogeography, Palaeoclimatology, Palaeoecology 281, 180-195.
- Gehrels, M.J., 2009. An enhanced ~1800 year record of recent volcanic ash-fall events for northern New Zealand from the analysis of cryptotephra, School of Geography, Faculty of Science. University of Plymouth, Pymouth, UK, p. 423.
- Gillett, N.P., Kell, T.D., Jones, P.D., 2006. Regional climate impacts of the Southern Annular Mode. Geophysical Research Letters 33, L23704.
- Glaser, B., Lehmann, J., Zech, W., 2002. Ameliorating physical and chemical properties of highly weathered soils in the tropics with charcoal–a review. Biology and fertility of soils 35, 219-230.
- Gomez, B., Carter, L., Orpin, A.R., Cobb, K.M., Page, M.J., Trustrum, N.A., Palmer, A.S., 2012. ENSO/SAM interactions during the middle and late Holocene. The Holocene 22, 23-30.
- Gomez, B., Carter, L., Trustrum, N.A., Page, M.J., Orpin, A.R., 2013. Coherent rainfall response to middle- and late-Holocene climate variability across the mid-latitude South Pacific. The Holocene 23, 1002-1007.
- González, M.E., Veblen, T.T., Donoso, C., Valeria, L., 2002. Tree regeneration responses in a lowland Nothofagus-dominated forest after bamboo dieback in South-Central Chile. Plant Ecology 161, 59-73.
- Grimm, E.C., 1987. CONISS: a FORTRAN 77 program for stratigraphically constrained cluster analysis by the method of incremental sum of squares. Computers & Geosciences 13, 13-35.
- Grootes, P. M., M. Stuiver., 1997. Oxygen 18/16 variability in Greenland snow and ice with 10− 3-to 105-year time resolution. Journal of Geophysical Research: Oceans 102, 26455-26470.

- Guiot, J., 1990. Methodology of the last climatic cycle reconstruction in France from pollen data. Palaeogeography, Palaeoclimatology, Palaeoecology 80, 49-69.
- Haberle, S., Bennett, K., 2001. Modern pollen rain and lake mud–water interface geochemistry along environmental gradients in southern Chile. Review of Palaeobotany and Palynology 117, 93-107.
- Haenfling, C., Newnham, R., Rees, A., Jara, I., Homes, A. and Clarkson, B., 2016. Holocene history of a raised bog, northern New Zealand, based on plant cuticles. The Holocene, 1-6.
- Hajdas, I., Bonani, G., Moreno, P.I., Ariztegui, D., 2003. Precise radiocarbon dating of Late-Glacial cooling in mid-latitude South America. Quaternary Research 59, 70-78.
- Hajdas, I., Lowe, D.J., Newnham, R.M., Bonani, G., 2006. Timing of the late-glacial climate reversal in the Southern Hemisphere using high-resolution radiocarbon chronology for Kaipo bog, New Zealand. Quaternary Research 65, 340-345.
- Hall, A., Visbeck, M., 2002. Synchronous variability in the Southern Hemisphere atmosphere, sea ice, and ocean resulting from the Annular Mode*. Journal of Climate 15, 3043-3057.
- Harsch, M.A., Hulme, P.E., McGlone, M.S., Duncan, R.P., 2009. Are treelines advancing? A global meta-analysis of treeline response to climate warming. Ecology letters 12, 1040-1049.
- Haug, G.H., Hughen, K.A., Sigman, D.M., Peterson, L.C., Röhl, U., 2001. Southward migration of the intertropical convergence zone through the Holocene. Science 293, 1304-1308.
- Hazell, Z.J., 2004. Holocene paleoclimate reconstruction from New Zealand peatlands, School of Geography, Faculty of Social Science and Buisness. Universty of Plymouth, Pymouth, England.

- Heenan, P.B., Smissen, R.D., 2013. Revised circumscription of Nothofagus and recognition of the segregate genera Fuscospora, Lophozonia, and Trisyngyne (Nothofagaceae). Phytotaxa 146, 1-31.
- Heiri, O., Lotter, A.F., Lemcke, G., 2001. Loss on ignition as a method for estimating organic and carbonate content in sediments: reproducibility and comparability of results. Journal of paleolimnology 25, 101-110.
- Hellstrom, J., McCulloch, M., Stone, J., 1998. A Detailed 31,000-Year Record of Climate and Vegetation Change, from the Isotope Geochemistry of Two New Zealand Speleothems. Quaternary Research 50, 167-178.
- Henríquez, W., Moreno, P., Alloway, B., Villarosa, G., 2015. Vegetation and climate change, fire-regime shifts and volcanic disturbance in Chiloé Continental (43° S) during the last 10,000 years. Quaternary Science Reviews 123, 158-167.
- Herve, F., Pankhurst, R.J., Fanning, C., Calderón, M., Yaxley, G., 2007. The South Patagonian batholith: 150 my of granite magmatism on a plate margin. Lithos 97, 373-394.
- Hesse, P.P., McTainsh, G.H., 1999. Last glacial maximum to early Holocene wind strength in the mid-latitudes of the Southern Hemisphere from aeolian dust in the Tasman Sea. Quaternary Research 52, 343-349.
- Heusser, C., 1995. Three late Quaternary pollen diagrams from Southern Patagonia and their palaeoecological implications. Palaeogeography, Palaeoclimatology, Palaeoecology 118, 1-24.
- Heusser, C.J., 1971. Pollen and spores of Chile: modern types of the Pteridophyta, Gymnospermae, Angiospermae. Tucson: Arizona UP xiv, 167p.. Map.
- Heusser, C.J., 1984. Late-glacial-Holocene climate of the Lake District of Chile. Quaternary Research 22, 77-90.

- Heusser, C.J., 1987. Fire history of Fuego-Patagonia. Quaternary of South America and Antarctic Peninsula 5, 93-109.
- Heusser, C.J., 2003. Ice Age Southern AndesA Chronicle of Paleoecological Events. Elsevier, Amsterdam.
- Heusser, C.J., Heusser, L.E., Lowell, T.V., 1999. Paleoecology of The Southern Chilean Lake District-Isla Grande de Chiloé During Middle–late Llanquihue Glaciation and Deglaciation. Geografiska Annaler: Series A, Physical Geography 81, 231-284.
- Higuera, P.E., Brubaker, L.B., Anderson, P.M., Hu, F.S., Brown, T.A., 2009. Vegetation mediated the impacts of postglacial climate change on fire regimes in the south-central Brooks Range, Alaska. Ecological Monographs 79, 201-219.
- Higuera, P.E., Gavin, D.G., Bartlein, P.J., Hallett, D.J., 2010. Peak detection in sediment–charcoal records: impacts of alternative data analysis methods on fire-history interpretations. International Journal of Wildland Fire 19, 996-1014.
- Hodder, A., De Lange, P., Lowe, D.J., 1991. Dissolution and depletion of ferromagnesian minerals from Holocene tephra layers in an acid bog, New Zealand, and implications for tephra correlation. Journal of Quaternary science 6, 195-208.
- Hogg, A.G., Hua, Q., Blackwell, P.G., Niu, M., Buck, C.E., Guilderson, T.P., Heaton, T.J., Palmer, J.G., Reimer, P.J., Reimer, R.W., Turney, C.S.M., Zimmerman, S.R.H., 2013. SHCal13 Southern Hemisphere Calibration, 0–50,000 Years cal BP. Radiocarbon 55, 1889-1903.
- Hogg, A.G., McCormac, F., Higham, T., Reimer, P.J., Baillie, M.G., Palmer, J., 2002. High-precision radiocarbon measurements of contemporaneous tree-ring dated wood from the British Isles and New Zealand: AD 1850-950. Radiocarbon 44, 633-640.

- Holz, A., Veblen, T.T., 2011. Variability in the Southern Annular Mode determines wildfire activity in Patagonia. Geophysical Research Letters 38, L14710.
- Huber, U.M., Markgraf, V., 2003. Holocene fire frequency and climate change at Rio Rubens Bog, southern Patagonia, Fire and climatic change in temperate ecosystems of the western Americas. Springer, pp. 357-380.
- Huber, U.M., Markgraf, V., Schäbitz, F., 2004. Geographical and temporal trends in Late Quaternary fire histories of Fuego-Patagonia, South America. Quaternary Science Reviews 23, 1079-1097.
- Hulton, N.R., Purves, R., McCulloch, R., Sugden, D.E., Bentley, M.J., 2002. The last glacial maximum and deglaciation in southern South America. Quaternary Science Reviews 21, 233-241.
- Huybers, P., Denton, G., 2008. Antarctic temperature at orbital timescales controlled by local summer duration. Nature Geosci 1, 787-792.
- Hyde, H., Williams, D., 1944. The right word. Pollen Analysis Circular 8.
- Iglesias, V., 2013. Holocene climate-vegetation-fire linkages along the Patagonian forest/steppe ecotone (41-43° S).
- Iglesias, V., Whitlock, C., 2014. Fire responses to postglacial climate change and human impact in northern Patagonia (41–43° S). Proceedings of the National Academy of Sciences 111, E5545-E5554.
- Iglesias, V., Whitlock, C., Markgraf, V., Bianchi, M.M., 2014. Postglacial history of the Patagonian forest/steppe ecotone (41–43 S). Quaternary Science Reviews 94, 120-135.
- Imbrie, J., Newell, N.D., 1964. Approaches to paleoecology. Wiley.

- Iversen, J., 1941. Landnam i Danmarks stenalder: En pollenanalytisk undersøgelse over det første landbrugs indvirkning paa vegetationsudviklingen. Reitzel.
- Iversen, J., 1944. Viscum, Hedera and Ilex as climate indicators: A contribution to the study of the post-glacial temperature climate. GFF 66, 463-483.
- Jacobson, G.L., Bradshaw, R.H., 1981. The selection of sites for paleovegetational studies. Quaternary research 16, 80-96.
- Jaffré, T., 1992. Floristic and ecological diversity of the vegetation on ultramafic rocks in New Caledonia. The vegetation of ultramafic (serpentine) soils, 101-107.
- Jansonius, J., McGregor, D.C., 1996. Palynology, principles and applications. American Association of Stratigraphic Palynologists Foundation.
- Jara, I.A., Moreno, P.I., 2012. Temperate rainforest response to climate change and disturbance agents in northwestern Patagonia (41°S) over the last 2600 years. Quaternary Research 77, 235-244.
- Jara, I.A., Moreno, P.I., 2014. Climatic and disturbance influences on the temperate rainforests of northwestern Patagonia (40 °S) since ∼14,500 cal yr BP. Quaternary Science Reviews 90, 217-228.
- Jemmett, G., Owen, J., 1990. Where has all the pollen gone? Review of Palaeobotany and Palynology 64, 205-211.
- Jiang, N., Griffiths, G., Lorrey, A., 2013. Influence of large-scale climate modes on daily synoptic weather types over New Zealand. International Journal of Climatology 33, 499-519.
- Jordan, T.E., Burns, W.M., Veiga, R., Pángaro, F., Copeland, P., Kelley, S., Mpodozis, C., 2001. Extension and basin formation in the southern Andes caused by increased convergence rate: A mid-Cenozoic trigger for the Andes. Tectonics 20, 308-324.

- Jouzel, J., Masson-Delmotte, V., Cattani, O., Dreyfus, G., Falourd, S., Hoffmann, G., Minster, B., Nouet, J., Barnola, J.M., Chappellaz, J. and Fischer, H., 2007. Orbital and millennial Antarctic climate variability over the past 800,000 years. *Science 317,* 793-796.
- Jowsey, P.C., 1966. An Improved Peat Sampler. New Phytologist 65, 245-248.
- Juggins, S., 2015. rioja: Analysis of Quaternary Science Data, In: 0.9-5, R.p.v. (Ed.).
- Kaplan, M., Fogwill, C., Sugden, D., Hulton, N., Kubik, P., Freeman, S., 2008. Southern Patagonian glacial chronology for the Last Glacial period and implications for Southern Ocean climate. Quaternary Science Reviews 27, 284-294.
- Kaplan, M.R., Schaefer, J.M., Denton, G.H., Doughty, A.M., Barrell, D.J.A., Chinn, T.J.H., Putnam, A.E., Andersen, B.G., Mackintosh, A., Finkel, R.C., Schwartz, R., Anderson, B., 2013. The anatomy of long-term warming since 15 ka in New Zealand based on net glacier snowline rise. Geology 41, 887-901.
- Kershaw, A., McGlone, M., 1995. The Quaternary history of the southern conifers. Ecology of Southern Conifers, edited by: Enright, NJ and Hill, RS, Melbourne University Press.
- Kershaw, A., Strickland, K., 1990. A 10 year pollen trapping record from rainforest in northeastern Queensland, Australia. Review of Palaeobotany and Palynology 64, 281-288.
- Khatep, M., Fitzharris, B., Bardsley, W., 1984. Water vapor transfer over the southwest Pacific: Mean patterns and variations during wet and dry periods. Monthly weather review 112, 1960-1976.
- Kidson, J.W., 2000. An analysis of New Zealand synoptic types and their use in defining weather regimes. International journal of climatology 20, 299-316.

- Kidson, J.W., Gordon, N.D., 1986. Interannual variations in New Zealand temperature and precipitation patterns. New Zealand Journal of Geology and Geophysics 29, 363-375.
- Kidson, J.W., Renwick, J.A., 2002. Patterns of convection in the tropical pacific and their influence on New Zealand weather. International Journal of Climatology 22, 151-174.
- Kidson, J.W., Revell, M.J., Bhaskaran, B., Mullan, A.B., Renwick, J.A., 2002. Convection Patterns in the Tropical Pacific and Their Influence on theAtmospheric Circulation at Higher Latitudes. Journal of Climate 15, 137-159.
- Kidston, J., Renwick, J.A., McGregor, J., 2009. Hemispheric-Scale Seasonality of the Southern Annular Mode and Impacts on the Climate of New Zealand. Journal of Climate 22, 4759-4770.
- Kilian, R., Lamy, F., 2012. A review of Glacial and Holocene paleoclimate records from southernmost Patagonia (49–55 S). Quaternary Science Reviews 53, 1-23.
- Kitzberger, T., Veblen, T.T., 1997. Influences of humans and ENSO on fire history of Austrocedrus chilensis woodlands in northern Patagonia, Argentina. Ecoscience 4, 508-520.
- Kitzberger, T., Veblen, T.T., 2003. Influences of climate on fire in northern Patagonia, Argentina, Fire and climatic change in temperate ecosystems of the western Americas. Springer, pp. 296-321.
- Kitzberger, T., Veblen, T.T., Villalba, R., 1997. Climatic influences on fire regimes along a rain forest-to-xeric woodland gradient in northern Patagonia, Argentina. Journal of Biogeography 24, 35-47.
- Kohfeld, K., Graham, R., De Boer, A., Sime, L., Wolff, E., Le Quéré, C., Bopp, L., 2013. Southern Hemisphere westerly wind changes during the Last Glacial Maximum: paleo-data synthesis. Quaternary Science Reviews 68, 76-95.

- Kula, J., Tulloch, A., Spell, T.L., Wells, M.L., 2007. Two-stage rifting of Zealandia-Australia-Antarctica: evidence from 40Ar/39Ar thermochronometry of the Sisters shear zone, Stewart Island, New Zealand. Geology 35, 411-414.
- Kutzbach, J.E., 1981. Monsoon climate of the early Holocene: climate experiment with the earth's orbital parameters for 9000 years ago. Science 214, 59-61.
- Lambeck, K., Yokoyama, Y., Purcell, T., 2002. Into and out of the Last Glacial Maximum: sea-level change during Oxygen Isotope Stages 3 and 2. Quaternary Science Reviews 21, 343-360.
- Lamy, F., Kilian, R., Arz, H.W., Francois, J.-P., Kaiser, J., Prange, M., Steinke, T., 2010. Holocene changes in the position and intensity of the southern westerly wind belt. Nature Geosci 3, 695-699.
- Lara, A., Villalba, R., Wolodarsky-Franke, A., Aravena, J.C., Luckman, B.H., Cuq, E., 2005. Spatial and temporal variation in Nothofagus pumilio growth at tree line along its latitudinal range (35 40′–55 S) in the Chilean Andes. Journal of Biogeography 32, 879-893.
- Le Maitre, R., 1984. A proposal by the IUGS Subcommission on the Systematics of Igneous Rocks for a chemical classification of volcanic rocks based on the total alkali silica (TAS) diagram: (on behalf of the IUGS Subcommission on the Systematics of Igneous Rocks). Australian Journal of Earth Sciences 31, 243-255.
- Libby, W.F., 1946. Atmospheric helium three and radiocarbon from cosmic radiation. Physical Review 69, 671.
- Linick, T., Damon, P., Donahue, D., Jull, A., 1989. Accelerator mass spectrometry: the new revolution in radiocarbon dating. Quaternary International 1, 1-6.
- Livingstone, D., 1955. A lightweight piston sampler for lake deposits. Ecology 36, 137-139.

- Lorrey, A., Fauchereau, N., Stanton, C., Chappell, P., Phipps, S., Mackintosh, A., Renwick, J., Goodwin, I., Fowler, A., 2014. The Little Ice Age climate of New Zealand reconstructed from Southern Alps cirque glaciers: a synoptic type approach. Clim Dyn 42, 3039-3060.
- Lorrey, A., Fowler, A.M., Salinger, J., 2007. Regional climate regime classification as a qualitative tool for interpreting multi-proxy palaeoclimate data spatial patterns: A New Zealand case study. Palaeogeography, Palaeoclimatology, Palaeoecology 253, 407-433.
- Lorrey, A.M., Vandergoes, M., Almond, P., Renwick, J., Stephens, T., Bostock, H., Mackintosh, A., Newnham, R., Williams, P.W., Ackerley, D., 2012. Palaeocirculation across New Zealand during the last glacial maximum at~ 21 ka. Quaternary Science Reviews 36, 189-213.
- Lowe, D.J., 1988. Stratigraphy, age, composition, and correlation of late Quaternary tephras interbedded with organic sediments in Waikato lakes, North Island, New Zealand. New Zealand Journal of Geology and Geophysics 31, 125-165.
- Lowe, D.J., Blaauw, M., Hogg, A.G., Newnham, R.M., 2013. Ages of 24 widespread tephras erupted since 30,000 years ago in New Zealand, with re-evaluation of the timing and palaeoclimatic implications of the Lateglacial cool episode recorded at Kaipo bog. Quaternary Science Reviews 74, 170-194.
- Lowe, D.J., Hogg, A.G., Green, J.D., Boubee, J.A.T., 1980. Stratigraphy and chronology of late Quaternary tephras in Lake Maratoto, Hamilton, New Zealand. New Zealand Journal of Geology and Geophysics 23, 481-485.
- Lowe, D.J.G., John D., 1987. Origins and Development of the Lakes.
- Lowe, J., 1982. Three Flandrian pollen profiles from the Teith Valley, Perthshire, Scotland. New Phytologist 90, 371-385.

- Lusk, C., 1999. Long-lived light-demanding emergents in southern temperate forests: the case of Weinmannia trichosperma (Cunoniaceae) in Chile. Plant Ecology 140, 111-115.
- Mackay, A., 2005. Global Change in the Holocene. Arnold.
- Mantua, N.J., Hare, S.R., 2002. The Pacific decadal oscillation. Journal of oceanography 58, 35-44.
- Markgraf, V., 1980. Pollen dispersal in a mountain area. Grana 19, 127-146.
- Markgraf, V., Dodson, J.R., Kershaw, A.P., McGlone, M.S., Nicholls, N., 1992. Evolution of late Pleistocene and Holocene climates in the circum-South Pacific land areas. Clim Dyn 6, 193-211.
- Markgraf, V., Webb, R.S., Anderson, K.H., Anderson, L., 2002. Modern pollen/climate calibration for southern South America. Palaeogeography, Palaeoclimatology, Palaeoecology 181, 375-397.
- Marshall, G.J., 2003. Trends in the Southern Annular Mode from observations and reanalyses. Journal of Climate 16, 4134-4143.
- Martin, T.J., Ogden, J., 2005. Experimental studies on the drought, waterlogging, and frost tolerance of Ascarina lucida Hook. f (Chloranthaceae) seedlings. New Zealand Journal of Ecology 29, 53-59.
- Martinić, M., 2004. De la Trapada al Aysén: una mirada reflexiva sobre el acontecer de la Región de Aysén desde la Prehistoria hasta nuestros días. Pehuén Editores, Santiago, Chile.
- Matheson, K.S., 1979. Moanatuatua: An Ecological Study of an Oligtrophic, Restiad Bog, Waikato, New Zealand. University of Waikato.
- McCarthy, A., Mackintosh, A., Rieser, U., Fink, D., 2008. Mountain Glacier Chronology from Boulder Lake, New Zealand, Indicates MIS 4 and MIS 2 Ice Advances of Similar Extent. Arctic, Antarctic, and Alpine Research 40, 695-708.

- McGlone, M., 1982. Modern pollen rain, Egmont National Park, New Zealand. New Zealand journal of botany 20, 253-262.
- McGlone, M., 1989. The Polynesian settlement of New Zealand in relation to environmental and biotic changes. New Zealand journal of ecology, 115-129.
- McGlone, M., 1995. Lateglacial landscape and vegetation change and the Younger Dryas climatic oscillation in New Zealand. Quaternary Science Reviews 14, 867-881.
- McGlone, M., Moar, N., 1998. Dryland Holocene vegetation history, Central Otago and the Mackenzie Basin, South Island, New Zealand. New Zealand Journal of Botany 36, 91-111.
- McGlone, M.S., 1983. Polynesian Deforestation of New Zealand: A Preliminary Synthesis. Archaeology in Oceania 18, 11-25.
- McGlone, M.S., 2009. Postglacial history of New Zealand wetlands and implications for their conservation. New Zealand Journal of Ecology 33, 1-23.
- McGlone, M.S., Basher, L., 2012. Holocene vegetation change at treeline Cropp Valley, Southern Alps, New Zealand. Terra Australis 34, 343-358.
- McGlone, M.S., Hall, G.M.J., Wilmshurst, J.M., 2011. Seasonality in the early Holocene: Extending fossil-based estimates with a forest ecosystem process model. The Holocene 21, 517-526.
- McGlone, M.S., Moar, N.T., 1977. The Ascarina decline and post-glacial climatic change in New Zealand. New Zealand Journal of Botany 15, 485-489.
- McGlone, M.S., Nelson, C.S., Todd, A.J., 1984. Vegetation history and environmental significance of pre-peat and surficial peat deposits at Ohinewai, Lower Waikato lowland. Journal of the Royal Society of New Zealand 14, 233-244.

- McGlone, M.S., Topping, W.W., 1977. Aranuian (post-glacial) pollen diagrams from the Tongariro region, North Island, New Zealand. New Zealand Journal of Botany 15, 749-760.
- McGlone, M.S., Turney, C.S.M., Wilmshurst, J.M., 2004. Late-glacial and Holocene vegetation and climatic history of the Cass Basin, central South Island, New Zealand. Quaternary Research 62, 267-279.
- McGlone, M.S., Turney, C.S.M., Wilmshurst, J.M., Renwick, J., Pahnke, K., 2010. Divergent trends in land and ocean temperature in the Southern Ocean over the past 18,000 years. Nature Geosci 3, 622-626.
- McGlone, M.S., Wilmshurst, J.M., 1999. Dating initial Maori environmental impact in New Zealand. Quaternary International 59, 5-16.
- McWethy, D.B., Whitlock, C., Wilmshurst, J.M., McGlone, M.S., Fromont, M., Li, X., Dieffenbacher-Krall, A., Hobbs, W.O., Fritz, S.C., Cook, E.R., 2010. Rapid landscape transformation in South Island, New Zealand, following initial Polynesian settlement. Proceedings of the National Academy of Sciences 107, 21343-21348.
- Mercer, J., 1976. Glacial history of southernmost South America. Quaternary Research 6, 125-166.
- Mermoz, M., Kitzberger, T., Veblen, T.T., 2005. Landscape influences on occurrence and spread of wildfires in Patagonian forests and shrublands. Ecology 86, 2705-2715.
- Mildenhall, D.C., 1980. New Zealand Late Cretaceous and Cenozoic plant biogeography: a contribution. Palaeogeography, palaeoclimatology, palaeoecology 31, 197-233.
- Millspaugh, S.H., Whitlock, C., Bartlein, P.J., 2000. Variations in fire frequency and climate over the past 17 000 yr in central Yellowstone National Park. Geology 28, 211-214.

- Moar, M.T., 1993. Pollen grains of New Zealand dicotyledonous plants. Manaaki Whenua Press, Lincoln, New Zealand.
- Moar, N., Suggate, R.P., Burrows, C., 2008. Environments during the Kaihinu Interglacial and Otira Glaciation, coastal north Westland, New Zealand. New Zealand Journal of Botany 46, 49-63.
- Moar, N.T., 1970. Recent pollen spectra from three localities in the South Island, New Zealand. New Zealand Journal of Botany 8, 210-221.
- Monnin, E., Steig, E.J., Siegenthaler, U., Kawamura, K., Schwander, J., Stauffer, B., Stocker, T.F., Morse, D.L., Barnola, J.-M., Bellier, B., Raynaud, D., Fischer, H., 2004. Evidence for substantial accumulation rate variability in Antarctica during the Holocene, through synchronization of CO2 in the Taylor Dome, Dome C and DML ice cores. Earth and Planetary Science Letters 224, 45-54.
- Moore, P.D., Webb, J.A., Collison, M.E., 1991. Pollen analysis. Blackwell scientific publications.
- Moreno, P.I., 2004. Millennial-scale climate variability in northwest Patagonia over the last 15 000 yr. Journal of Quaternary Science 19, 35-47.
- Moreno, P.I., Denton, G.H., Moreno, H., Lowell, T.V., Putnam, A.E., Kaplan, M.R., 2015. Radiocarbon chronology of the last glacial maximum and its termination in northwestern Patagonia. Quaternary Science Reviews 122, 233-249.
- Moreno, P.I., Francois, J.P., Moy, C.M., Villa-Martínez, R., 2010. Covariability of the Southern Westerlies and atmospheric CO2 during the Holocene. Geology 38, 727-730.
- Moreno, P.I., Jacobson, G.L., Lowell, T.V., Denton, G.H., 2001. Interhemispheric climate links revealed by a late-glacial cooling episode in southern Chile. Nature 409, 804-808.

- Moreno, P.I., León, A.L., 2003. Abrupt vegetation changes during the last glacial to Holocene transition in mid-latitude South America. Journal of Quaternary Science 18, 787-800.
- Moreno, P.I., Lowell, T.V., Jacobson Jr, G.L., Denton, G.H., 1999. Abrupt Vegetation and Climate Changes During the Last Glacial Maximumand Last Termination in The Chilean Lake District: A Case Study from Canal De La Puntilla (41° S). Geografiska Annaler: Series A, Physical Geography 81, 285-311.
- Moreno, P.I., Vilanova, I., Villa-Martínez, R., Garreaud, R.D., Rojas, M., De Pol-Holz, R., 2014. Southern Annular Mode-like changes in southwestern Patagonia at centennial timescales over the last three millennia. Nat Commun 5.
- Moy, C.M., Seltzer, G.O., Rodbell, D.T., Anderson, D.M., 2002. Variability of El Nino/Southern Oscillation activity at millennial timescales during the Holocene epoch. Nature 420, 162-165.
- Muller, J., Kylander, M., Wüst, R.A., Weiss, D., Martinez-Cortizas, A., LeGrande, A.N., Jennerjahn, T., Behling, H., Anderson, W.T., Jacobson, G., 2008. Possible evidence for wet Heinrich phases in tropical NE Australia: the Lynch's Crater deposit. Quaternary Science Reviews 27, 468-475.
- Müller, R.A., 1977. Radioisotope dating with a cyclotron. Science 196, 489-494.
- Mustaphi, C.J.C., Pisaric, M.F., 2014. A classification for macroscopic charcoal morphologies found in Holocene lacustrine sediments. Progress in Physical Geography 38, 734-754.
- Newnham, R., McGlone, M., Moar, N., Wilmshurst, J., Vandergoes, M., 2013. The vegetation cover of New Zealand at the Last Glacial Maximum. Quaternary Science Reviews 74, 202-214.

- Newnham, R.M., 1990. Late Quaternary palynological investigations into the history of vegetation and climate in northern New Zealand. ResearchSpace@ Auckland.
- Newnham, R.M., de Lange, P.J., Lowe, D.J., 1995. Holocene vegetation, climate and history of a raised bog complex, northern New Zealand based on palynology, plant macrofossils and tephrochronology. The Holocene 5, 267-282.
- Newnham, R.M., Lowe, D.J., 2000. Fine-resolution pollen record of late-glacial climate reversal from New Zealand. Geology 28, 759-762.
- Newnham, R.M., Lowe, D.J., Green, J.D., 1989. Palynology, vegetation and climate of the Waikato lowlands, North Island, New Zealand, since c. 18,000 years ago. Journal of the Royal Society of New Zealand 19, 127-150.
- Newnham, R.M., Lowe, D.J., Williams, P.W., 1999. Quaternary environmental change in New Zealand: a review. Progress in Physical Geography 23, 567-610.
- Newnham, R.M., Vandergoes, M.J., Hendy, C.H., Lowe, D.J., Preusser, F., 2007. A terrestrial palynological record for the last two glacial cycles from southwestern New Zealand. Quaternary Science Reviews 26, 517-535.
- Newnham, R.M., Vandergoes, M.J., Sikes, E., Carter, L., Wilmshurst, J.M., Lowe, D.J., McGlone, M.S., Sandiford, A., 2012. Does the bipolar seesaw extend to the terrestrial southern mid-latitudes? Quaternary Science Reviews 36, 214-222.
- Nichols, G.J., Cripps, J.A., Collinson, M.E., Scott, A.C., 2000. Experiments in waterlogging and sedimentology of charcoal: results and implications. Palaeogeography, Palaeoclimatology, Palaeoecology 164, 43-56.

- Norton, D., McGlone, M., Wigley, T., 1986. Quantitative analyses of modern pollen-climate relationships in New Zealand indigenous forests. New Zealand journal of botany 24, 331-342.
- Norton, D.A., Palmer, J.G., Ogden, J., 1987. Dendroecological studies in New Zealand 1. An evaluation of tree age estimates based on increment cores. New Zealand Journal of Botany 25, 373-383.
- Oberdorfer, E., 1960. Pflanzensoziologische Studien in Chile. Cramer, Verlag von J., Weinheim.
- Ogden, J., Wilson, A., Hendy, C., Newnham, R.M., Hogg, A.G., 1992. The Late Quaternary History of Kauri (Agathis australis) in New Zealand and Its Climatic Significance. Journal of Biogeography 19, 611-622.
- Osborn, T.J., Briffa, K.R., 2006. The spatial extent of 20th-century warmth in the context of the past 1200 years. Science 311, 841-844.
- Ovington, J.D., 1983. Temperate broad-leaved evergreen forest. Elsevier Science Publisher B.V., Amsterdam.
- Paez, M.M., Schäbitz, F., Stutz, S., 2001. Modern pollen–vegetation and isopoll maps in southern Argentina. Journal of Biogeography 28, 997-1021.
- Pahnke, K., Sachs, J.P., 2006. Sea surface temperatures of southern midlatitudes 0–160 kyr B.P. Paleoceanography 21, PA2003.
- Paruelo, J.M., Beltran, A., Jobbagy, E., Sala, O.E., Golluscio, R.A., 1998. The climate of Patagonia: general patterns and controls on biotic. Ecol Austral 8, 85-101.
- Pask, J.A., Warner, M.F., 1953. Differential thermal analysis methods and techniques. DTIC Document.
- Patterson, W., 1978. The effects of past and current land disturbances on Squaw Lake, Minnesota, and its watershed. University of Minnesota, College of Forestry, St. Paul, MN. Ph. D. thesis.

- Patterson, W.A., Edwards, K.J., Maguire, D.J., 1987. Microscopic charcoal as a fossil indicator of fire. Quaternary Science Reviews 6, 3-23.
- Pedro, J.B., Bostock, H.C., Bitz, C.M., He, F., Vandergoes, M.J., Steig, E.J., Chase, B.M., Krause, C.E., Rasmussen, S.O., Markle, B.R., Cortese, G., 2016. The spatial extent and dynamics of the Antarctic Cold Reversal. Nature Geosci 9, 51-55.
- Peltier, W., Fairbanks, R.G., 2006. Global glacial ice volume and Last Glacial Maximum duration from an extended Barbados sea level record. Quaternary Science Reviews 25, 3322-3337.
- Perry, G.L., Wilmshurst, J.M., McGlone, M.S., 2014. Ecology and long-term history of fire in New Zealand. New Zealand Journal of Ecology, 157-176.
- Pesce, O.H., Moreno, P.I., 2014. Vegetation, fire and climate change in central-east Isla Grande de Chiloé (43°S) since the Last Glacial Maximum, northwestern Patagonia. Quaternary Science Reviews 90, 143-157.
- Power, M.J., Marlon, J., Ortiz, N., Bartlein, P.J., Harrison, S.P., Mayle, F.E., Ballouche, A., Bradshaw, R.H.W., Carcaillet, C., Cordova, C., Mooney, S., Moreno, P.I., Prentice, I.C., Thonicke, K., Tinner, W., Whitlock, C., Zhang, Y., Zhao, Y., Ali, A.A., Anderson, R.S., Beer, R., Behling, H., Briles, C., Brown, K.J., Brunelle, A., Bush, M., Camill, P., Chu, G.Q., Clark, J., Colombaroli, D., Connor, S., Daniau, A.L., Daniels, M., Dodson, J., Doughty, E., Edwards, M.E., Finsinger, W., Foster, D., Frechette, J., Gaillard, M.J., Gavin, D.G., Gobet, E., Haberle, S., Hallett, D.J., Higuera, P., Hope, G., Horn, S., Inoue, J., Kaltenrieder, P., Kennedy, L., Kong, Z.C., Larsen, C., Long, C.J., Lynch, J., Lynch, E.A., McGlone, M., Meeks, S., Mensing, S., Meyer, G., Minckley, T., Mohr, J., Nelson, D.M., New, J., Newnham, R., Noti, R., Oswald, W.,

Pierce, J., Richard, P.J.H., Rowe, C., Sanchez Goñi, M.F., Shuman, B.N., Takahara, H., Toney, J., Turney, C., Urrego-Sanchez, D.H., Umbanhowar, C., Vandergoes, M., Vanniere, B., Vescovi, E., Walsh, M., Wang, X., Williams, N., Wilmshurst, J., Zhang, J.H., 2008. Changes in fire regimes since the Last Glacial Maximum: an assessment based on a global synthesis and analysis of charcoal data. Clim Dyn 30, 887-907.

- Prager, M.H., Hoenig, J.M., 1992. Can We Determine the Significance of Key-Event Effects on a Recruitment Time Series?—A Power Study of Superposed Epoch Analysis. Transactions of the American Fisheries Society 121, 123-131.
- Prentice, I.C., 1985. Pollen representation, source area, and basin size: toward a unified theory of pollen analysis. Quaternary Research 23, 76-86.
- Putnam, A.E., Denton, G.H., Schaefer, J.M., Barrell, D.J.A., Andersen, B.G., Finkel, R.C., Schwartz, R., Doughty, A.M., Kaplan, M.R., Schluchter, C., 2010. Glacier advance in southern middle-latitudes during the Antarctic Cold Reversal. Nature Geosci 3, 700-704.
- Putnam, A.E., Schaefer, J.M., Denton, G.H., Barrell, D.J.A., Andersen, B.G., Koffman, T.N.B., Rowan, A.V., Finkel, R.C., Rood, D.H., Schwartz, R., Vandergoes, M.J., Plummer, M.A., Brocklehurst, S.H., Kelley, S.E., Ladig, K.L., 2013. Warming and glacier recession in the Rakaia valley, Southern Alps of New Zealand, during Heinrich Stadial 1. Earth and Planetary Science Letters 382, 98-110.
- Quinn, W.H., Neal, V.T., Antunez de Mayolo, S.E., 1987. El Niño occurrences over the past four and a half centuries. Journal of Geophysical Research: Oceans 92, 14449-14461.
- Rabassa, J., Coronato, A.M., Salemme, M., 2005. Chronology of the Late Cenozoic Patagonian glaciations and their correlation with

biostratigraphic units of the Pampean region (Argentina). Journal of South American Earth Sciences 20, 81-103.

- Ramírez-Marcial, N., González-Espinosa, M., Williams-Linera, G., 2001. Anthropogenic disturbance and tree diversity in montane rain forests in Chiapas, Mexico. Forest Ecology and Management 154, 311-326.
- Ramos, V.A., Ghiglione, M.C., 2008. Tectonic evolution of the Patagonian Andes. The late cenozoic of Patagonia and Tierra del Fuego 11, 73-95.
- Ramsey, C.B., 2009. Bayesian analysis of radiocarbon dates. Radiocarbon 51, 337-360.
- Raymo, M., 1997. The timing of major climate terminations. Paleoceanography 12, 577-585.
- Rees, A.B.H., Cwynar, L.C., Fletcher, M.-S., 2015. Southern Westerly Winds submit to the ENSO regime: A multiproxy paleohydrology record from Lake Dobson, Tasmania. Quaternary Science Reviews 126, 254-263.
- Reimer, P.J., Baillie, M.G., Bard, E., Bayliss, A., Beck, J.W., Blackwell, P.G., Bronk, R.C., Buck, C.E., Burr, G.S., Edwards, R.L., 2009. IntCal09 and Marine09 radiocarbon age calibration curves, 0-50,000 years cal BP.
- Reimer, P.J., Bard, E., Bayliss, A., Beck, J.W., Blackwell, P.G., Ramsey, C.B., Buck, C.E., Cheng, H., Edwards, R.L., Friedrich, M., 2013. IntCal13 and Marine13 radiocarbon age calibration curves 0–50,000 years cal BP. Radiocarbon 55, 1869-1887.
- Renwick, J., Thompson, D., 2006. The Southern Annular Mode and New Zealand Climate. Water & Atmosphere 14, 24-25.

- Rogers, G., McGlone, M., 1989. A postglacial vegetation history of the southern-central uplands of North Island, New Zealand. Journal of the Royal Society of New Zealand 19, 229-248.
- Salinger, M.J., Basher, R., Fitzharris, B., Hay, J., Jones, P., MacVeigh, J., Schmidely-Leleu, I., 1995. Climate trends in the South-west Pacific. International Journal of Climatology 15, 285-302.
- Salinger, M.J., Mullan, A.B., 1999. New Zealand climate: temperature and precipitation variations and their links with atmospheric circulation 1930–1994. International Journal of Climatology 19, 1049-1071.
- Sandiford, A., Newnham, R., Alloway, B., Ogden, J., 2003. A 28 000–7600 cal yr BP pollen record of vegetation and climate change from Pukaki Crater, northern New Zealand. Palaeogeography, Palaeoclimatology, Palaeoecology 201, 235-247.
- Schaefer, J.M., Denton, G.H., Barrell, D.J.A., Ivy-Ochs, S., Kubik, P.W., Andersen, B.G., Phillips, F.M., Lowell, T.V., Schlüchter, C., 2006. Near-Synchronous Interhemispheric Termination of the Last Glacial Maximum in Mid-Latitudes. Science 312, 1510-1513.
- Schmithüsen, J., 1956b. Die räumliche Ordnung der chilenischen Vegetation Bonner Geographische Abhandlungen 17, 1-86.
- Schmithüsen, J., 1966. Problems of vegetation history in Chile and New Zealand. Plant Ecology 13, 189-206.
- Schneider, R.F., 1969. A coring device for unconsolidated lake sediments. Water Resources Research 5, 524-526.
- Selby, J.M., Lowe J David, 1992. The Middle Waikato Basin and hills. Longman Paul, Auckland, New Zealand.
- Seluchi, M., Serafini, Y., Le Treut, H., 1998. The impact of the Andes on transient atmospheric systems: A comparison between observations and GCM results. Monthly weather review 126, 895-912.

- Shackleton, N.J., Opdyke, N.D., 1973. Oxygen isotope and palaeomagnetic stratigraphy of Equatorial Pacific core V28-238: Oxygen isotope temperatures and ice volumes on a 10 5 year and 10 6 year scale. Quaternary research 3, 39-55.
- Shakun, J.D., Clark, P.U., He, F., Marcott, S.A., Mix, A.C., Liu, Z., Otto-Bliesner, B., Schmittner, A., Bard, E., 2012. Global warming preceded by increasing carbon dioxide concentrations during the last deglaciation. Nature 484, 49-54.
- Shevenell, A.E., Ingalls, A.E., Domack, E.W., Kelly, C., 2011. Holocene Southern Ocean surface temperature variability west of the Antarctic Peninsula. Nature 470, 250-254.
- Shulmeister, J., Fink, D., Augustinus, P.C., 2005. A cosmogenic nuclide chronology of the last glacial transition in North-West Nelson, New Zealand—new insights in Southern Hemisphere climate forcing during the last deglaciation. Earth and Planetary Science Letters 233, 455-466.
- Shulmeister, J., Fink, D., Hyatt, O.M., Thackray, G.D., Rother, H., 2010. Cosmogenic 10Be and 26Al exposure ages of moraines in the Rakaia Valley, New Zealand and the nature of the last termination in New Zealand glacial systems. Earth and Planetary Science Letters 297, 558-566.
- Shulmeister, J., McLea, W.L., Singer, C., McKay, R.M., Hosie, C., 2003. Late Quaternary pollen records from the Lower Cobb Valley and adjacent areas, North-West Nelson, New Zealand. New Zealand Journal of Botany 41, 503-533.
- Sikes, E.L., Medeiros, P.M., Augustinus, P., Wilmshurst, J.M., Freeman, K.R., 2013. Seasonal variations in aridity and temperature characterize changing climate during the last deglaciation in New Zealand. Quaternary Science Reviews 74, 245-256.

- Smale, M.C., Burns, B.R., Smale, P.N., Whaley, P.T., 1997. Dynamics of upland podocarp/broadleaved forest on Mamaku Plateau, central North Island, New Zealand. Journal of the Royal Society of New Zealand 27, 513-532.
- Steubing, L., Alberdi, M., Wenzel, H., 1983. Seasonal changes of cold resistance of Proteaceae of the South Chilean laurel forest. Plant Ecol 52, 35-44.
- Stott, L., Cannariato, K., Thunell, R., Haug, G.H., Koutavas, A., Lund, S., 2004. Decline of surface temperature and salinity in the western tropical Pacific Ocean in the Holocene epoch. Nature 431, 56-59.
- Stuiver, R., 1993. Extended 14C data base and revised CALIB 3.0 14C age calibration program. Radiocarbon 35, 215-230.
- Suggate, R.P., Stevens, G.R., Te Punga, M. T., 1978. The Geology of New Zealand, Wellington, New Zealand.
- Tauber, H., 1965. Differential pollen dispersion and the interpretation of pollen diagrams, with a contribution to the interpretation of the elm fall.
- Taylor, R.E., 1997. Radiocarbon dating. Springer.
- Team, R.C., 2014. R: A language and environment for statistical computing. R Foundation for Statistical Computing, Vienna, Austria. 2013. ISBN 3-900051-07-0.
- ter Braak, C.J., Juggins, S., 1993. Weighted averaging partial least squares regression (WA-PLS): an improved method for reconstructing environmental variables from species assemblages. Hydrobiologia 269, 485-502.
- Thompson, D.W., Solomon, S., 2002. Interpretation of recent Southern Hemisphere climate change. Science 296, 895-899.
- Thompson, D.W.J., Solomon, S., Kushner, P.J., England, M.H., Grise, K.M., Karoly, D.J., 2011. Signatures of the Antarctic ozone hole in

Southern Hemisphere surface climate change. Nature Geosci 4, 741-749.

- Timmins, S.M., 1992. Wetland vegetation recovery after fire: Eweburn Bog, Te Anau, New Zealand. New Zealand Journal of Botany 30, 383-399.
- Toggweiler, J.R., Russell, J., 2008. Ocean circulation in a warming climate. Nature 451, 286-288.
- Toggweiler, J.R., Russell, J.L., Carson, S.R., 2006. Midlatitude westerlies, atmospheric CO2, and climate change during the ice ages. Paleoceanography 21, PA2005.
- Trenberth, K.E., 1991. Storm tracks in the Southern Hemisphere. Journal of the Atmospheric Sciences 48, 2159-2178.
- Turner, J., Colwell, S.R., Marshall, G.J., Lachlan-Cope, T.A., Carleton, A.M., Jones, P.D., Lagun, V., Reid, P.A., Iagovkina, S., 2005. Antarctic climate change during the last 50 years. International Journal of Climatology 25, 279-294.
- Ummenhofer, C.C., England, M.H., 2007. Interannual Extremes in New Zealand Precipitation Linked to Modes of Southern Hemisphere Climate Variability. Journal of Climate 20, 5418-5440.
- Vandergoes, M.J., Dieffenbacher-Krall, A.C., Newnham, R.M., Denton, G.H., Blaauw, M., 2008. Cooling and changing seasonality in the Southern Alps, New Zealand during the Antarctic Cold Reversal. Quaternary Science Reviews 27, 589-601.
- Vandergoes, M.J., Fitzsimons, S.J., 2003. The last glacial–interglacial transition (LGIT) in south westland, New Zealand: paleoecological insight into mid-latitude southern hemisphere climate change. Quaternary Science Reviews 22, 1461-1476.
- Vandergoes, M.J., Newnham, R.M., Preusser, F., Hendy, C.H., Lowell, T.V., Fitzsimons, S.J., Hogg, A.G., Kasper, H.U., Schluchter, C., 2005.

Regional insolation forcing of late Quaternary climate change in the Southern Hemisphere. Nature 436, 242-245.
- Veblen, T., Ashton, D., 1978. Catastrophic influences on the vegetation of the Valdivian Andes, Chile. Plant Ecol 36, 149-167.
- Veblen, T., Schlegel, F., Oltremari, J., 1983. Temperate broad-leaved evergreen forests of South America. Ecosystems of the World.
- Veblen, T.T., Hill, R.S., Read, J., 1996. The Ecology and Biogeography of Nothofagus Forests. Yale University Press.
- Veblen, T.T., Kitzberger, T., Lara, A., 1992. Disturbance and forest dynamics along a transect from Andean rain forest to Patagonian shrubland. Journal of Vegetation Science 3, 507-520.
- Veblen, T.T., Markgraf, V., 1988. Steppe expansion in Patagonia? Quaternary research 30, 331-338.
- Veblen, T.T., Stewart, G.H., 1982. On the Conifer Regeneration Gap in New Zealand: The Dynamics of Libocedrus Bidwillii Stands on South Island. Journal of Ecology 70, 413-436.
- Villagran, C., 1990. Glacial climates and their effects on the history of the vegetation of Chile: a synthesis based on palynological evidence from Isla de Chiloé. Review of Palaeobotany and Palynology 65, 17-24.
- Villagrán, C., 1980. Vegetationsgeschichtliche und pflanzensoziologische Untersuchungen im Vicente Perez Rosales Nationalpark Chile. Dissertationes Botanicae 54, 1-165.
- Villagrán, C., 1993. Excursion guide. International Workshop: The Quaternary of Chile. Universidad de Chile, Santiago.
- Villalba, R., Lara, A., Masiokas, M.H., Urrutia, R., Luckman, B.H., Marshall, G.J., Mundo, I.A., Christie, D.A., Cook, E.R., Neukom, R., Allen, K., Fenwick, P., Boninsegna, J.A., Srur, A.M., Morales, M.S., Araneo, D., Palmer, J.G., Cuq, E., Aravena, J.C., Holz, A., LeQuesne,

C., 2012. Unusual Southern Hemisphere tree growth patterns induced by changes in the Southern Annular Mode. Nature Geosci 5, 793-798.

- Von Post, L., 1929. Die Zeichenschrift der Pollenstatistik. GFF 51, 543-565.
- Walker, M., Walker, M.J.C., 2005. Quaternary dating methods. John Wiley and Sons.
- Walker, M.J., Berkelhammer, M., Björck, S., Cwynar, L.C., Fisher, D.A., Long, A.J., Lowe, J.J., Newnham, R.M., Rasmussen, S.O., Weiss, H., 2012. Formal subdivision of the Holocene Series/Epoch: a Discussion Paper by a Working Group of INTIMATE (Integration of ice-core, marine and terrestrial records) and the Subcommission on Quaternary Stratigraphy (International Commission on Stratigraphy). Journal of Quaternary Science 27, 649-659.
- Wang, G., Cai, W., 2013. Climate-change impact on the 20th-century relationship between the Southern Annular Mode and global mean temperature. Scientific reports 3.
- Ward Jr, J.H., 1963. Hierarchical grouping to optimize an objective function. Journal of the American statistical association 58, 236-244.
- Wardle, P., 1980. Primary succession in Westland national park and its vicinity, New Zealand. New Zealand journal of botany 18, 221-232.
- Wardle, P., 1985. Environmental influences on the vegetation of New Zealand. New Zealand Journal of Botany 23, 773-788.
- Wardle, P., 1988. Effects of glacial climates on floristic distribution in New Zealand 1. A review of the evidence. New Zealand journal of botany 26, 541-555.
- Wardle, P., 1991. Vegetation of New Zealand. Cambridge University Press, Cambridge
- Wardle, P., Bulfin, M., Dugdale, J., 1983. Temperate broad-leaved evergreen forests of New Zealand. Ecosystems of the World.

- Wardle, P., Ezcurra, C., Ramírez, C., Wagstaff, S., 2001. Comparison of the flora and vegetation of the southern Andes and New Zealand. New Zealand Journal of Botany 39, 69-108.
- Watt, S.F., Pyle, D.M., Mather, T.A., 2013. Evidence of mid-to late-Holocene explosive rhyolitic eruptions from Chaitén Volcano, Chile. Andean Geology 40, 216-226.
- Watt, S.F., Pyle, D.M., Naranjo, J.A., Rosqvist, G., Mella, M., Mather, T.A., Moreno, H., 2011. Holocene tephrochronology of the Hualaihue region (Andean southern volcanic zone,∼ 42 S), southern Chile. Quaternary International 246, 324-343.
- Waugh, W.N., Hill Jr, W.E., 1960. Determination of carbon dioxide and other volatiles in pyritic limestones by loss on ignition. Journal of Sedimentary Research 30.
- Webb, T., Bryson, R.A., 1972. Late-and postglacial climatic change in the northern Midwest, USA: quantitative estimates derived from fossil pollen spectra by multivariate statistical analysis. Quaternary Research 2, 70-115.
- Westgate, J.A., Gorton, M.P., 1981. Correlation techniques in tephra studies, Tephra studies. Springer, pp. 73-94.
- Whitlock, C., Larsen, C., 2001. Charcoal as a fire proxy. Smol JP, Birks HJB, Last WM (eds) Tracking environmental change using lake sediments, 3—terrestrial, algal, and siliceous indicators. Kluwer Academic Publishers, Dordrecht, The Netherlands.
- Whitlock, C., Millspaugh, S.H., 1996. Testing the assumptions of fire-history studies: an examination of modern charcoal accumulation in Yellowstone National Park, USA. The Holocene 6, 7-15.
- Whitlock, C., Moreno, P.I., Bartlein, P., 2007. Climatic controls of Holocene fire patterns in southern South America. Quaternary Research 68, 28-36.

- Williams, J., Shuman, B., 2008. Obtaining accurate and precise environmental reconstructions from the modern analog technique and North American surface pollen dataset. Quaternary Science Reviews 27, 669-687.
- Williams, P.A., 1993. The subalpine and alpine vegetation on the Central Sedimentary Belt of Paleozoic rocks in north-west Nelson, New Zealand. New Zealand Journal of Botany 31, 65-90.
- Williams, P.W., King, D.N.T., Zhao, J.X., Collerson, K.D., 2005. Late Pleistocene to Holocene composite speleothem 18O and 13C chronologies from South Island, New Zealand—did a global Younger Dryas really exist? Earth and Planetary Science Letters 230, 301-317.
- Williams, P.W., Neil., H.L, Zhao Jian-Xin, 2010. Age frequency distribution and revised stable isotope curves for New Zealand speleothems: palaeoclimatic implications. International Journal of Speleology 39, 99-112.
- Wilmshurst, J.M., Anderson, A.J., Higham, T.F.G., Worthy, T.H., 2008. Dating the late prehistoric dispersal of Polynesians to New Zealand using the commensal Pacific rat. Proceedings of the National Academy of Sciences 105, 7676-7680.
- Wilmshurst, J.M., McGlone, M.S., 1996. Forest disturbance in the central North Island, New Zealand, following the 1850 BP Taupo eruption. The Holocene 6, 399-411.
- Wilmshurst, J.M., McGlone, M.S., Leathwick, J.R., Newnham, R.M., 2007. A pre-deforestation pollen-climate calibration model for New Zealand and quantitative temperature reconstructions for the past 18 000 years BP. Journal of Quaternary Science 22, 535-547.
- Wilmshurst, J.M., McGlone, M.S., Partridge, T.R., 1997. A late Holocene history of natural disturbance in lowland podocarp/hardwood

forest, Hawke's Bay, New Zealand. New Zealand Journal of Botany 35, 79-96.

- Wodehouse, R.P., 1935. Pollen Grains: Their Structure, Identification and Significance in Science and Significance in Science and Medicine. Hafner.
- Wold, S., Ruhe, A., Wold, H., Dunn, I.W., 1984. The Collinearity Problem in Linear Regression. The Partial Least Squares (PLS) Approach to Generalized Inverses. SIAM Journal on Scientific and Statistical Computing 5, 735-743.
- Woodward, F.I., 1987. Climate and plant distribution. Cambridge University Press.
- Wright, H., 1974. Landscape development, forest fires, and wilderness management. Science 186, 487-495.
- Wright, H.E., 1967. A square-rod piston sampler for lake sediments. Journal of Sedimentary Research 37, 975-976.
- Zhao, Y., Sayer, C.D., Birks, H.H., Hughes, M., Peglar, S.M., 2006. Spatial representation of aquatic vegetation by macrofossils and pollen in a small and shallow lake. Journal of Paleolimnology 35, 335-350.
- Zolitschka, B., Anselmetti, F., Ariztegui, D., Corbella, H., Francus, P., Lücke, A., Maidana, N., Ohlendorf, C., Schäbitz, F., Wastegård, S., 2013. Environment and climate of the last 51,000 years–new insights from the Potrok Aike maar lake Sediment Archive Drilling prOject (PASADO). Quaternary Science Reviews 71, 1-12.

Appendix 1

Supplementary information of Chapter Four

A1.1 Deglaciation of Adelaide Tarn

The presence of sand and gravel units at the base of the cores of Adelaide Tarn indicates that the sediment sequence extends back to an early stage of lake formation. The age of the most basal level dated (100 cm above the base of the core sediments) was 14,000-13,800 cal yr BP. The estimated age of 16,100 cal yr BP for the beginning of sediment accumulation is based on direct extrapolation of our age model derived from the accumulation rate of the overlying sediment. However, this age is possibly overestimated because the undated basal 100 cm comprise coarser, more inorganic sediment indicative of a higher energy depositional environment which could have accumulated at a faster rate. Since the Tasman Mountains in Northwest Nelson feature widespread evidence of glacier cover as low as 600 m asl during the last glacial period (Shulmeister et al., 2005), the glacial cirque now occupied by Adelaide Tarn would have been covered by ice during the Last Glacial Maximum (LGM). The chronology suggests that permanent ice had retreated from the Adelaide Tarn cirque prior to 14,000 cal yr BP and possibly, assuming the extrapolated age model is appropriate, as early as 16,100 cal yr BP.

The timing for ice retreat and lake formation inferred at Adelaide Tarn is in good agreement with comparable local and regional evidence. Based on basal radiocarbon ages from sediments impounded by recessional moraines in the Cobb Valley (22 km southeast from Adelaide Tarn; Figure 4.1), glacial retreat commenced as early as ~21,000 cal yr BP, but may not have reached the elevation of Adelaide Tarn at 1300 masl until 15,500-16,100 cal yr BP (Shulmeister et al., 2003). A subsequently determined cosmogenic glacial chronology from the same valley indicated that widespread ice retreat could have started by 18,000 cal yr BP, yet the average of the whole set of ages is younger, being centred at 16,500 cal yr BP (Shulmeister et al., 2005). Based on a newest and widely accepted ^{10}Be production rate published by Putnam et al (2010), the cosmogenic dataset is now centred at 19,200 cal yr BP, which means that it is now more closely aligned to the radiocarbon age for the onset of the deglaciation in Northwest Nelson.

A uranium-series dated speleothem record from Mt. Arthur Range in northwest Nelson (35 km southeast from Adelaide Tarn; Figure 4.1) reported the onset of a warming pulse that terminated glacial conditions at 18,000 cal yr BP (Hellstrom et al., 1998). In the central South Island, detailed cosmogenic chronologies from the Lake Pukaki area (44°S; 550-770 m range of elevation) and the Rakaia Valley (43°S; 540-830 m range of elevation) (270-370 km south from Adelaide Tarn) date the beginning of the final Last Glacial Maximum ice retreat to 17,800-17,400 cal yr BP (Schaefer et al., 2006; Shulmeister et al., 2010; Putnam et al., 2013). The differences between this age range and the chronologies obtained in Northwest Nelson including the extrapolated age in Adelaide Tarn might be associated with the distance between these two regions or with dating uncertainties. However, the most likely explanation may be related to the wide range of elevation of the published sites. The age obtained in Adelaide Tarn suggests that permanent ice abandonment of the high elevations of Northwest Nelson at the last glacial termination – leading to the formation of Adelaide Tarn – had occurred by ~16,100 cal yr BP. No evidence was observed for re-occupation of the Adelaide Tarn cirque by ice after 16,100 cal yr BP.

A1.2 *Isoetes* variation in the pollen stratigraphy

I note the appearance and progressive increase of *Isoetes* over the last 9000 years of the record (Figure 4.5). The genus *Isoetes* comprises macrophyte species that usually occupy littoral regions in the margins of freshwater bodies. Variations in aquatic taxa in lacustrine sediments have been recently used to infer changes in water level in some Southern Hemisphere pollen profiles, which in turn may be linked to climate (Fletcher and Moreno, 2011). Since the steady increase in *Isoetes* at Adelaide Tarn is not accompanied by any major change in sediment composition or grain size distribution (Figure 4.3), and because the total depth of sediments (550 cm) equates to more than 70% of the water depth of the lake today, such an increase seems more consistent with the expansion of the zone of littoral environments as a result of a sediment-driven increase in water level, rather than resulting from a climate signal.

A1.3 Quantitative reconstruction and the validation of the PTP index

Despite showing similar long-term trends (Figure A1.1), there are some differences between the modern analogue technique and the partial least squares reconstructions relating to the abruptness of the changes showed in these two quantitative reconstructions. For instance, the cooling between 14,000-12,000 cal yr BP is more conspicuous in the modern analogue reconstruction and less pronounced in the partial least squares reconstruction (Figure A1.1). From 12,000-6000 cal yr BP, both reconstructions show increasing temperature, although, again, this is clearer in the modern analogue reconstruction and more variable in the partial least squares curve. Peak temperatures in both records are achieved between 6000-3000 cal yr BP, after which there is a minor temperature decline until the uppermost assemblage is attained (Figure A1.1).

Despite their quantitative nature, these two reconstructions are fundamentally at odds with the observation from our pollen and plant macrofossil records. For example, both temperature curves show relatively cool conditions during the period 11,000-9000 cal yr BP when the pollen and plant macrofossil record suggests a significant phase of regional forest expansion, including the notable establishment of beech forest around Adelaide Tarn by 9000 cal yr BP (Figure A1.1). Also, as discussed in Chapter Four, there is ample evidence across New Zealand for a thermal optimum ~11,000-9000 cal yr BP (McGlone and Moar, 1977; Wilmshurst et al., 2007; McGlone et al., 2011). On the other hand, both quantitative curves show a generally progressive warming trend through the Holocene culminating at an implied thermal maximum of ~ 3000-2500 cal yr BP (Figure A1.1). This is precisely the time when arboreal macrofossils disappear from the Adelaide Tarn record, after having been previously abundant, implying suppression of treeline and hence colder conditions.

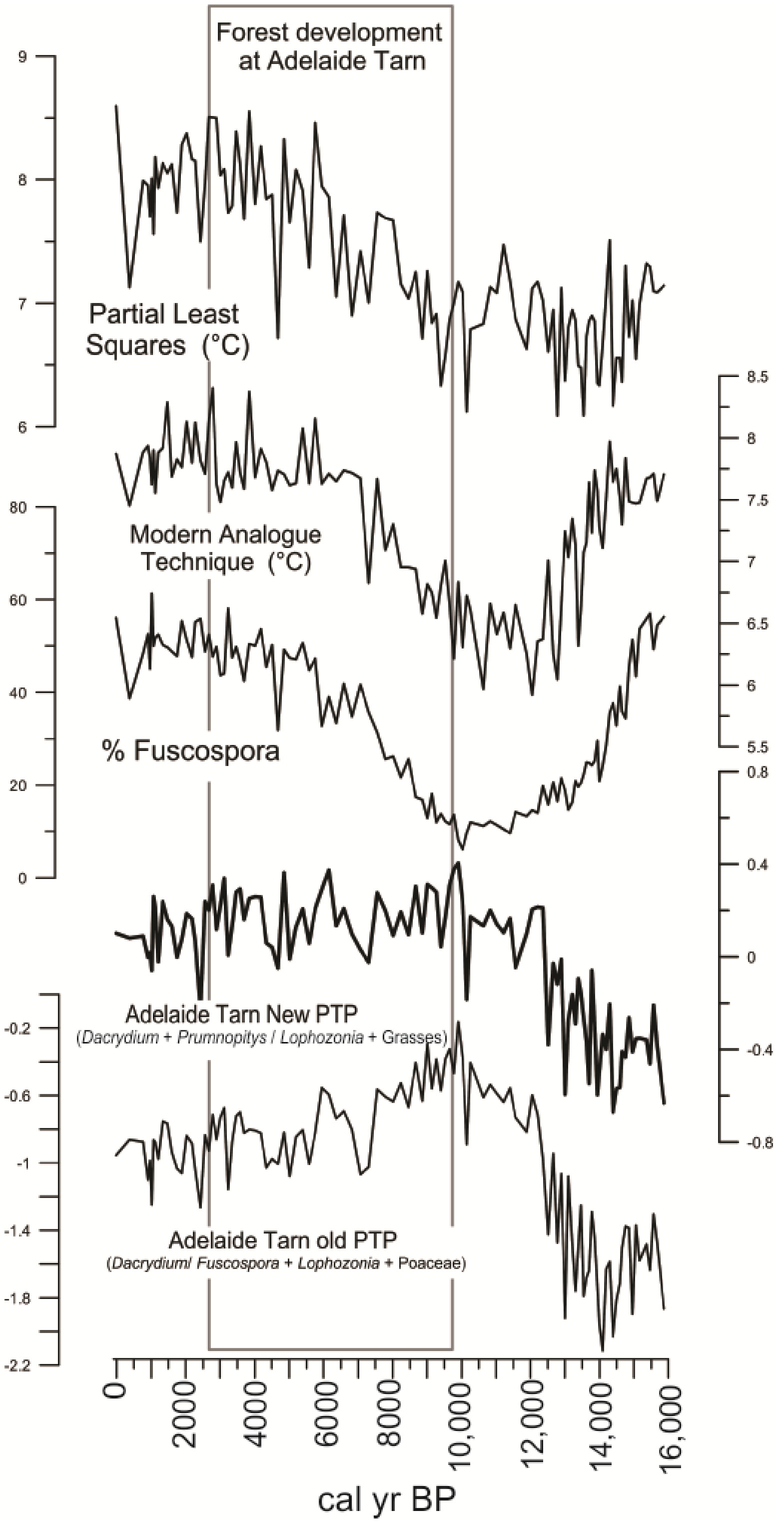

Figure A1.1 Adelaide Tarn temperature proxies. The two lower curves are the Pollen Temperature Proxy (PTP) calculated from a pollen ratio with two alternative taxa selections excluding the taxon *Fuscospora*. The figure also plots the percentage of *Fuscospora* as a reference. The upper curves correspond to the two quantitative temperature reconstructions generated by the transfer function approach. The modern analogue technique and the partial least squares reconstruction were obtained using a pre-deforestation dataset based on Wilmshurst et al. (2007).

It has been suggested that the pollen-climate transfer function approach in New Zealand may currently be less reliable in cold climate situations because of (i) lack of good modern analogues from cool, high-elevation sites, and (ii) cold-climate limitations in the pre-deforestation database (Wilmshurst et al., 2007; Newnham et al., 2013). Given these considerations, I question the applicability of the temperature reconstructions based on the partial least squares method and the modern analogue technique from the Adelaide Tarn pollen dataset. Furthermore, I point out that both these quantitative reconstructions – and in particular the modern analogue technique – are strongly influenced by *Fuscospora*, the predominant pollen taxon at this site.

This is evident in Figure A1.1. In New Zealand pollen records, *Fuscospora* is strongly over-represented, widely dispersed and has been described as 'masking' or distorting signals from other taxa in pollen assemblages formed in open landscapes, such as the Adelaide Tarn setting (Bussell, 1988). I contend therefore that the quantitative reconstructions from Adelaide Tarn are strongly distorted by the masking effect of *Fuscospora*, especially during the late glacial when beech trees were dominant in the lowland and montane areas. As a result of the clear masking effect by *Fuscospora* at this site, and independently-reported inadequacies with the transfer function approach at cold, high altitude sites, I conclude that these quantitative reconstructions from the Adelaide Tarn pollen spectra are mostly unreliable.

On the other hand, our qualitative pollen temperature proxy (PTP) reconstructions based on the ratio of individual taxa explicitly excludes *Fuscospora* and therefore it lacks the problems associated with the presence of this taxon. Indeed, the general trends observed in PTP reconstruction are coherent with the temperature changes inferred from our pollen and plant macrofossil diagrams. For example, the temperature maximum at 10,000 cal yr BP recorded in the PTP index is coherent with peak in lowland taxa abundance and the appearance of plant macrofossil at Adelaide Tarn. Additionally, peak temperatures during the early Holocene are consistent with the evidence of many other records from New Zealand (as discussed in Chapter Four). Likewise, the PTP reconstruction shows a cooling trend over the last 3000 years which is consistent with the disappearance of arboreal elements from the plant macrofossil record (Figure 4.7). Based on the good agreement between the PTP reconstruction, our pollen and macrofossil data, and some general and widely accepted temperature trends across New Zealand, I contend that the PTP reconstruction can be used as a reliable, albeit qualitative, temperature proxy at this site.

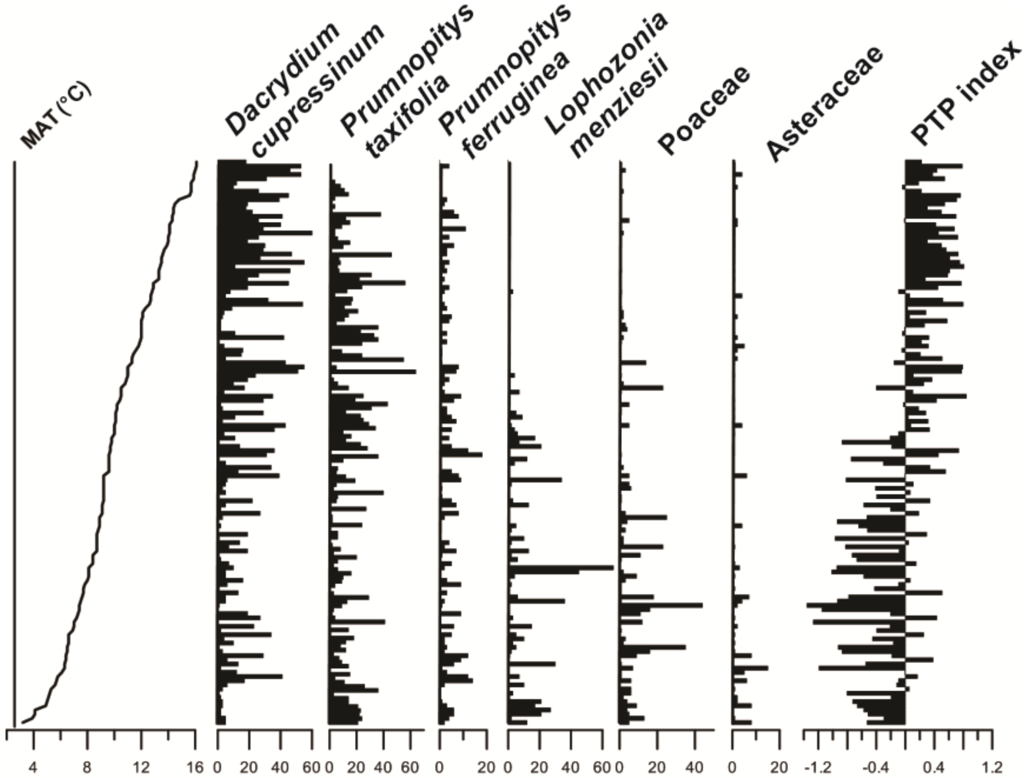

Figure A1.2 Pollen diagram showing the relationship between the Mean Annual Temperature (MAT) of 135 pollen sites (percentage) across New Zealand and their corresponding abundances of selected taxa in the pre-deforestation pollen dataset (see Wimshurst et al 2007). The MAT of the sites are arranged from the coldest (bottom) to the warmest (top) on the left panel. The pollen taxa selected for this diagram are the ones that make up the Adelaide Tarn Pollen Temperature Proxy (PTP). Additionally, the diagram shows the values of the PTP thought the MATs gradient. The PTP index shows a strong positive correlation with MAT (correlation coefficient =0.58; P<0.001).

Appendix 2

Supplementary information of Chapter Five

A.2.1 Previous investigation at Moanatuatua

Moanatuatua peatbog has been the focus of several ecology, paleoecology and paleoclimate studies. Hogg et al. (1987) presented ^{14}C ages, including a basal age for peat accumulation of 13,300±110 ^{14}C years (16,800-15,500 cal yr BP). The present-day vegetation dynamics of the bog have been discussed by Matheson (1979) and Clarkson (1997). Hazell (2004) reported a radiocarbon chronology, peat humification record, organic carbon, charcoal accumulation rate and plant macrofossil analyses for the interval between 7000-2000 cal yr BP, bracketed by two prominent tephra layers. More recently, plant cuticle and macrofossil analyses document a more complete Holocene history of the bog (Haenfling et al., 2016). Gehrels (2009) carried out a comprehensive tephrostratigraphy and geochemistry study of the bog's sediments supplemented by a detailed radiocarbon chronology of the last 1600 cal yr BP. This work showed that cryptotephra – tephra layers not visible to the naked eye – are a regular feature in the peat deposits. Natural fire has been a common occurrence to many New Zealand wetlands throughout the Holocene, particularly domed restiad bogs (Perry et al., 2014). Fires within large raised bogs have reportedly been occurring during periods of sustained water shortages (McGlone 2009), and both Haenfling et al. (2016) and Gehrels (2009) have reported the presence of charcoal layers in the stratigraphic column indicating the occurrence of pre-human fire during much of the bog's history.

A2.2 Geochemical characterisation of tephra

Glass shard major element determinations were conducted on an orange-brown fine-textured vitric ash prominently exposed near the base of the c. 7.5 m-long Moanatuatua core between 684-675 cm depth (Figure 5.3). Glass shard major element data were acquired using a JEOL Superprobe (JXA-8230) housed at Victoria University of Wellington, using the ZAF correction method. Analyses were performed with 15 kV accelerating voltage, 8 nA beam current, and an electron beam defocused to between 20-10 μm. Standardization was achieved by means of mineral and glass standards. A rhyolitic glass standard (ATHO-G) was routinely used to monitor calibration during the analytical run. All analyses are normalized to 100 wt %. Percentage of anhydrous, with H_2O by difference being given, and total Fe is reported as FeO. Glass shard major element analyses are presented in Table A2.1. Electronic Micro Probe results acquired in this study are compared against reference Waiohau Tephra data from both proximal Okataina Volcanic Centre (OVC) (B.V. Alloway - unpublished data; E. Bilderback, unpublished PhD data) and distal Central North Island occurrences (Eaves et al. 2016; B.V. Alloway - unpublished data). Glass shard compositional data for Waiohau tephra correlatives from Moanatuatua is also compared against similar major element data from proximal occurrences of Rotorua and Rerewhakaaitu tephras acquired on the same EMP instrument using the same standards and under the same analytical conditions (see Figure A2.1).

Figure A2.1 shows weight percent FeO vesus CaO and K_2O composition of glass shards from the orange-brown fine-textured vitric ash exposed at base of the Moanatuatua section (A, B). The distribution of elemental data points is directly compared against analyses of Waiohau Tephra from proximal Okataina Volcanic Centre (OVC) (C, D) and distal Central North Island occurrences (E, F). Grey-scale background clusters of Waiohau tephra correlatives highlight the tight correspondence of elemental glass data and affirms correlation. Elemental glass data points of Waiohau Tephra correlative from Moanatuatua (G, H) are also compared against Rotorua and Rerewhakaaitu tephra (I, J) erupted from the OVC. Waiohau (14.0 cal. ka), Rotorua (15.6 ca. ka) and Rerewhakaaitu (17.5 cal. ka) tephras can all be clearly distinguished from each other on the basis of their major element glass chemistry.

A.2.3 Crypto-tephra

Previous studies of the Moanatuatua stratigraphy indicate that the number of tephra and charcoal layers determined by microscopic analysis is much higher than can be determined by the naked eye (Gehrels, 2009). This is probably because the primary charcoal and tephra deposits become concealed within the peat due to dissolution and discoloration of the glass material (Hodder et al., 1991). Despite the presence of various discrete peaks in the magnetic susceptibility record attributable to ferromagnesian-rich volcanic deposits, and the observation volcanic glass shards in several pollen samples; it was not considered necessary to document and identified these putative volcanic layers since the aim of the study was not to detect the presence of microscopic tephra layers and also because the great majority of the sediment section is well constrained by the radiocarbon chronology presented in this study. Similarly, a detailed description of the macroscopic charcoal layers was not necessary since I developed a detailed CHAR record together with the palynological analysis.

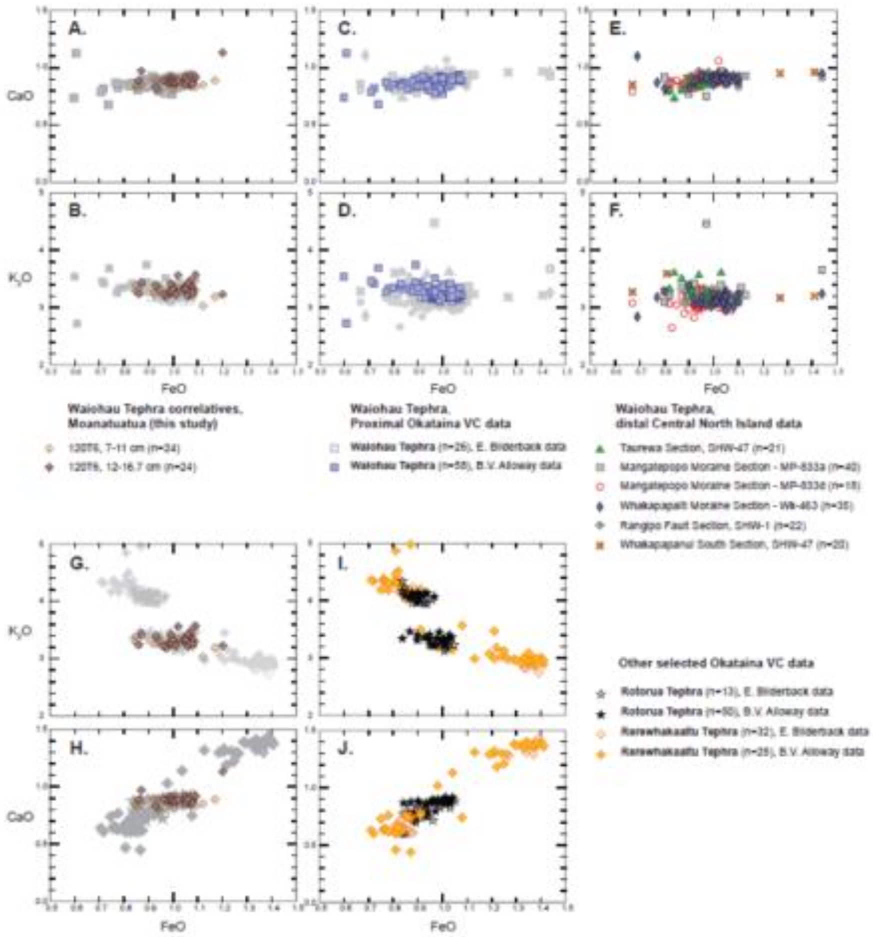

Figure A2.1 shows weight percent FeO vesus CaO and K_2O composition of glass shards from the orange-brown fine-textured vitric ash exposed at base of the Moanatuatua section (A, B). The distribution of elemental data points is directly compared against analyses of Waiohau Tephra from proximal Okataina Volcanic Centre (OVC) (C, D) and distal Central North Island occurrences (E, F). Grey-scale background clusters of Waiohau tephra correlatives highlight the tight correspondence of elemental glass data and affirms correlation. Elemental glass data points of Waiohau Tephra correlative from Moanatuatua (G, H) are also compared against Rotorua and Rerewhakaaitu tephra (I, J) erupted from the OVC. Waiohau (14.0 cal. ka), Rotorua (15.6 ca. ka) and Rerewhakaaitu (17.5 cal. ka) tephras can all be clearly distinguished from each other on the basis of their major element glass chemistry.

Section	Tephra (Probe Mount)	SiO_2	Al_2O_3	TiO_2	FeO	MgO	MnO	CaO	Na_2O	K_2O	Cl	Total	*n*
Moanatuatua (THIS STUDY)													
	120T6, 7-11 cm *(16-04-02)*	78.53 (0.19)	12.49 (0.08)	0.12 (0.06)	1.01 (0.08)	0.12 (0.02)	0.06 (0.05)	0.87 (0.04)	3.81 (0.18)	3.29 (0.08)	0.11 (0.01)	98.01 (1.51)	*24*
	120T6, 12-16.7 cm *(16-04-03)*	78.51 (0.28)	12.51 (0.10)	0.12 (0.05)	1.02 (0.07)	0.12 (0.02)	0.05 (0.03)	0.90 (0.06)	3.73 (0.27)	3.34 (0.11)	0.12 (0.05)	97.27 (1.79)	*24*
Waiohau Tephra distal Central North Island occurrences													
Taurewa, SHW-47	Waiohau (Wh) *(13-16-27)*	78.23 (0.25)	12.31 (0.12)	0.14 (0.02)	0.96 (0.07)	0.11 (0.02)	0.05 (0.03)	0.87 (0.05)	3.96 (0.23)	3.27 (0.16)	0.09 (0.01)	98.48 (1.66)	*21*
Mangatepopo moraine	Waiohau (Wh) *(13-16-28)*	78.13 (0.28)	12.39 (0.12)	0.15 (0.03)	0.98 (0.08)	0.13 (0.01)	0.05 (0.03)	0.89 (0.04)	3.96 (0.14)	3.23 (0.10)	0.09 (0.01)	98.21 (1.28)	*20*
	Waiohau (Wh) *(MP-833a; 13-16-26)*	78.21 (0.29)	12.38 (0.10)	0.14 (0.03)	1.00 (0.14)	0.12 (0.03)	0.05 (0.03)	0.88 (0.04)	3.84 (0.14)	3.28 (0.31)	0.09 (0.02)	98.20 (1.58)	*20*
	Geliflucted Waiohau correlative *(MP-833d)*	78.86 (0.24)	12.39 (0.10)	0.14 (0.02)	0.91 (0.09)	0.13 (0.03)	0.05 (0.03)	0.88 (0.06)	3.50 (0.14)	2.99 (0.12)	0.15 (0.02)	99.30 (1.00)	*18*
Whakapapanui moraine	Waiohau (Wh) *(463; 12-09-7)*	78.32 (0.26)	12.44 (0.15)	0.13 (0.02)	0.98 (0.13)	0.11 (0.04)	0.05 (0.02)	0.90 (0.06)	3.94 (0.26)	3.13 (0.12)	*nd*	97.80 (1.66)	*17*
	Waiohau *(463 low; 12-09-8)*	78.21 (0.22)	12.40 (0.10)	0.13 (0.02)	1.03 (0.11)	0.14 (0.05)	0.07 (0.02)	0.90 (0.03)	3.98 (0.15)	3.14 (0.09)	*nd*	98.83 (2.05)	*18*
Rangipo, SHW-1	Waiohau (Wh) *(13-17-34)*	78.25 (0.16)	12.38 (0.09)	0.14 (0.03)	0.99 (0.07)	0.12 (0.03)	0.04 (0.03)	0.89 (0.04)	3.92 (0.12)	3.18 (0.09)	0.09 (0.03)	98.26 (1.83)	*22*
Whakapapaiti south, SHW-47	Waiohau (Wh) *(13-16-25)*	78.19 (0.24)	12.38 (0.10)	0.14 (0.03)	1.00 (0.16)	0.12 (0.06)	0.05 (0.03)	0.90 (0.04)	3.91 (0.12)	3.22 (0.11)	0.09 (0.02)	98.96 (1.39)	*20*
Proximal Okataina VC tephra (Honeycomb Trench)													
	Waiohau (Wh) *(11-08-12, 11-09-13 to -15)*	78.27 (0.30)	12.37 (0.14)	0.14 (0.02)	0.90 (0.16)	0.23 (0.10)	0.05 (0.02)	0.86 (0.07)	3.70 (0.18)	3.33 (0.14)	0.14 (0.02)	98.26 (1.62)	*58*
	Rotorua (Ro) *(11-08-08 to -11)*	77.32 (0.66)	12.68 (0.30)	0.17 (0.09)	1.06 (0.25)	0.32 (0.24)	0.06 (0.02)	1.00 (0.35)	3.63 (0.19)	3.63 (0.68)	0.14 (0.02)	99.21 (1.30)	*50*
	Rerewhakaaitu (Rk) *(11-07-06, 11-08-07)*	77.90 (0.22)	12.48 (0.09)	0.12 (0.04)	0.93 (0.06)	0.19 (0.09)	0.05 (0.01)	0.83 (0.06)	3.64 (0.15)	3.70 (0.37)	0.14 (0.02)	99.67 (0.96)	*28*
ATHO-G Standard	April 14th, 2016 **THIS STUDY**	75.60 (0.47)	12.20 (0.09)	0.23 (0.04)	3.27 (0.13)	0.10 (0.01)	0.10 (0.05)	1.70 (0.03)	3.75 (0.34)	2.64 (0.12)	0.03 (0.01)	99.65 (0.59)	*35*
	September 14th, 2012	75.60 (0.55)	12.20 (0.12)	0.23 (0.02)	3.27 (0.09)	0.10 (0.01)	0.10 (0.02)	1.72 (0.03)	3.75 (0.10)	2.61 (0.03)	*nd*	99.57 (0.65)	*31*
	October 1st, 2013	75.57 (0.60)	12.20 (0.09)	0.26 (0.03)	3.27 (0.10)	0.09 (0.01)	0.10 (0.03)	1.70 (0.03)	3.73 (0.13)	2.64 (0.05)	0.02 (0.01)	99.58 (0.75)	*48*
	December, 2013	75.62 (0.36)	12.20 (0.07)	0.24 (0.02)	3.27 (0.09)	0.09 (0.01)	0.11 (0.04)	1.70 (0.02)	3.73 (0.11)	2.64 (0.06)	0.08 (0.06)	99.68 (0.41)	*20*

Table A2.1: Summary of glass shard major element compositions of the basal rhyolitic tephra bed preserved at the base of the Moanatuatua core. Proximal and/or distal Waiohau (Wh), Rotorua (Ro) and Rerewhakaaitu (Rk) tephra glass data is included for comparative purposes.

A2.4 Pollen corrosion analysis

Rationale

A general inspection of the pollen samples revealed a significant amount of corroded pollen which varied considerably throughout the sediment section. As a consequence, the identification of certain taxa was sometimes problematic and required the use of generic or multi-generic categories such as *Prumnopitys* undifferentiated or *Podocarpus*/*Prumnopitys*. These and other taxa such as the fern *Gleichenia* and CHAR exhibit prominent regular oscillatory cycles, raising the question that they may be linked to environmental variability or simply an artefact of varying degrees of pollen preservation. Significant correlation between the oscillations of *Prumnopitys taxifolia* and levels of corrosion would indicate that the variation of these elements can mostly be explained as a response to the varying degrees of pollen preservation of the sample, rather than as a response to a genuine environmental signal. Conversely, to rule out the possibility that changes in the percentage of corrosion between samples were an artefact of the different pollen composition (there are certain pollen types with higher predisposition to be corroded than others), I also calculated the percentage of corrosion for a single taxa (Restiads: *Empodisma* and *Sporadanthus*) throughout the analysed interval. If the percentage of corroded grains in the total pollen spectra correlates with the percentage of the single taxa, then variations in preservation are taxa-independent.

Methodology

I calculated the percentage of corroded pollen from 59 samples covering the period of oscillatory cycles and then carried out a correlation analysis (Pearson correlation coefficient) between this percentage and the taxa mentioned above (Table 5.3). Significant correlation with levels of corrosion would indicate that the variation of these taxa can mostly be explained as a response to the varying degrees of pollen preservation of the sample, rather than as a direct response to an environmental signal.

Results

The average percentage of total corroded pollen is presented for the period 5000-1000 cal yr BP is 45.2% (Standard deviation= 7.3%) and the average percentage of corroded restiads is 44.9 (10.8%) which indicates that the corrosion changes are taxa-independent. A strong positive correlation ($r=0.71$; $P<0.001$) between the percentages of corroded restiads and the total corroded pollen which rules out the possibility that the changes in pollen composition between samples drove the observed changes in total corroded pollen (Table 5.3). Interestingly, the percentage of corroded pollen shows a significant negative correlation (r= -0.42; P=0.019) with the abundance of *P. taxifolia*, suggesting that pollen preservation is driving the changes of this taxon. This interpretation of the cycles of *P. taxifolia* is also supported by the observed compensating changes of the other variables that include this taxon (e.g *Podocarpus/Prumnopitys*) in the percentage diagram and in the Principal Component Analysis (Figures 5.3 and 5.4). Thus, when pollen preservation conditions preclude confident identification to species level, generic groups such as *Prumnopitys* undifferentiated and *Podocarpus*/*Prumnopitys* increases (Figure 5.4). These observations strongly suggest that many of the grains identified as *Prumnopitys undifferentiated* and *Podocarpus/Prumnopitys* in the samples with high percentage of corroded pollen correspond to corroded *P. taxifolia* grains, highlighting the indirect effect of corrosion on the quasi-regular oscillations of *P. taxifolia*. The percentage of corroded pollen showed a positive, albeit weak correlation, with *Gleichenia* (0.11) and CHAR (0.2); while no correlation was observed between corroded pollen and the Pollen Moisture Index.

Fires and pollen corrosion

Fluctuation in the water table and fire activity are interrelated to in two ways. First, water table level not only regulates pollen preservation, but also governs fire susceptibility in raised bogs, through drying or moistening of the bog surface and drying/accumulation of fuel. Second, the aftermath of fire at the bog surface is likely to influence pollen preservation conditions in various ways that could promote pollen corrosion. Both of these factors could apply to varying extents but, either way, a link between corroded palynomorphs, low water tables and fire events can be inferred.

A2.5 Top portion of the sediment sequence

The Moanatuatua sedimentary sequence comprises homogenous dark brown organic peat with several macrofossil and charcoal layers, and two visible tephra layers towards the base (Fig. 5.3). The chronology of the sediments suggest overall continuous organic peat accumulation for most of the section, the exception being the top 155 cm of the record that where three radiocarbon ages are in clear stratigraphic unconformity. I rejected the radiocarbon date for level 155 cm (1304 ±23 ^{14}C years) because its calibrated age (median probability of 1277 cal yr BP) is clearly offset from the 95% confidence ranges delivered by the age model. The 2-sigma calendar ranges from the other two radiocarbon dates overlap with these confidence ranges and therefore are included in the age model (Figure 5.4). Similarly, I consider the result of a "modern" age for the first centimetre of the section as an underestimation since the first 30 cm of the top-most core were disturbed by the root system of the surface vegetation. The pollen record shows, however, evidence for human disturbance for the first 5 cm of the section. The mean accumulation rate of 0.05 cm/yr is relatively compared to other peat sections but of similar magnitude than other ombrogenous bogs in the Waikato region (Newnham et al., 1995). Despite the observation of several volcanic glass shards in the pollen samples, the number of macroscopic tephra layers identified by the visual inspection were the two deposits described in Chapter Four.

A2.6 *Ascarina* and *Prumnopitys taxifola* between 12,000-11,000 cal yr BP

Between 11,500-11,000 cal yr BP, *P. taxifolia* increases rapidly at the expense of *Dacrydium* (Figure 5.3). The higher drought tolerance of the former suggests a trend towards drier conditions. The fact that the abundances of the drought-intolerant *Ascarina* were not affected during this inferred dry interval might be reconciled by considering that (1) it is a sub-canopy species and not a direct competitor of the other two emergent trees, and (2) it is an early successional species that proliferates in recently disturbed forest of in canopy openings (Martin and Ogden, 2005). Thus, our interpretation is that conditions were dry enough to drive an increment of *P. taxifolia* relative to *Dacrydium* abundances, although still quite warm to allow *Ascarina* to proliferate in the sub-canopy under relative independence of the changes in canopy composition mentioned above.

A2.7 Temperature reconstructions

As mentioned in Chapter Five, the modern analogue technique produced overall warmer temperatures than the partial least squares method and reproduced more accurately the present-day regional temperature. These differences between the two methods are consistent with other applications of the pollen transfer function approach in New Zealand (Wilmshurst et al., 2007). As the vegetation communities depicted in these Holocene pollen assemblages are consistent with their modern day analogues, these observations give further confidence that the modern analogue technique may be the more accurate of the two. However, I note that it is impossible for the modern analogue technique to reproduce warmer or cooler temperatures than the ones constrained by the set of available modern analogues. The partial least squares reconstruction does not have this limitation and often delivers temperatures that are significantly warmer or colder that modern ones (Wilmshurst et al., 2007), and therefore it might be useful to pinpoint periods where temperatures exceeded the present-day range of variation. Thus, in Chapter Five I rely on both temperature reconstructions in this discussion.

Appendix 3

Supplementary information of Chapter Six

A3.1. Glass shard major element determinations

Glass shard major element determinations were conducted on selected tephra inter-beds from core sections 1502SC and 1502AT1 to 9 (Figure A3.1). Glass shard major element data werea cquired using a JEOL Superprobe (JXA-8230) housed at Victoria University of Wellington, using the ZAF correction method. Analyses were performed with 15 kV accelerating voltage, 8 nA beam current, and an electron beam defocused to between 20-10 μm. Standardization was achieved by means of mineral and glass standards. A rhyolitic glass standard (ATHO-G) was routinely used to monitor calibration during the analytical run. All analyses are normalized to 100 wt. % anhydrous, with H_2O by difference being given, and total Fe is reported as FeO. Glass shard major element analyses are presented in Table S1. EMP results acquired in this study were compared against an equivalent-aged tephra sequences from Chile (Pumalin-4) and Argentina (Alérce-6 and La Zeta, Esquel) (B.V. Alloway - *unpublished data*) using the same standards and under the same analytical conditions (see Figures S1 and S2).

The compositionally diverse sequence of tephras retrieved from Lago Espejo exhibit strong correspondence with those tephra described from La Zeta indicating strong potential for tephra to be correlated between these two sites. In particular, five tephra inter-beds (F4, F15, F18, F19 and F23) from Lago Espejo can be confidently correlated with tephra from other distal sections in both Chile and Argentina. Tephras are correlated between sections based on a combination of bedding characteristics, correspondence of glass shard major element compositions and chronostratigraphic association (see Figure A.3.2). F4 with a Chaitén-geochemical signature is correlated with LAZ-D TII (la Zeta), A6-1 (Alerce-6), and 4-3 (Pumalin-4). These tephra are collectively correlated with Cha-2 tephra with an age of c. 4.95 cal. ka (Watt et al. 2013). F15 also with a Chaitén-geochemical signature is correlated with T13 (la Zeta), A6-3 (Alerce-6), and 4-8 (Pumalin-4). These tephra are correlated with the widespread Cha-1 tephra with an age of c. 9.75 cal. ka (Watt et al. 2011). F19 is correlated with T7 (La Zeta) and 4-9 (Pumalin-4). These tephra are correlated with Lepue Tephra with a weighted mean (n=8) modeled age of c. 11 cal. ka (B.V. Alloway, *unpublished data*) and is likely sourced from Michinmahuida Volcano. F18 and F23 can be correlated with two similarly geochemically distinctive rhyo-dacite eruptives (T10 and T1) of unknown origin at La Zeta, Esquel. So far, correlatives of these tephras have yet to be identified at other proximal (Chile) and distal (Argentine) sites. The lower of these two tephra correlatives at La Zeta (T1) has an associated radiocarbon age of 12,935 ± 50 years B.P. (15,400 cal yr BP). This radiocarbon age can directly applied to date F23 within the Lago Espejo record - an interval, where coincidentally, there is a paucity of radiocarbon chronology.

A3.2 Cupressaceae pollen analysis

Methodology

The Lago Espejo pollen diagram features two distinctive and widely separated phases of Cupressaceae expansion between 700-900 and 1-100 cm (Figure A3.3).

Pollen description and size analysis of the Cupressaceae pollen was conducted in order to explore the possibility that these expansions are represented by different species.

According to Heusser (1971), grain size is the only criteria to distinguish between the three Patagonian species of the Cupressaceae family, i.e. *Fitzroya cupressoides* (34-43 μm), *Pilgerodendron uviferum* (36-38 μm) and *Austrocedrus chilensis* (22-26 μm).

Based on this information, we measured the size (longest axis) of (1) 50 Cupressaceae grains from samples of the 700-800 cm phase and (2) 50 grains from the 1-100 cm phase (selected images in Figure A.3.4 and A3.5). Pollen grains from below 800 cm were not measured due to their scarcity. We tested for significant size differences between the mean sizes of these two ranges by using a t-Test assuming equal variances. The results are shown in Table A3.2.

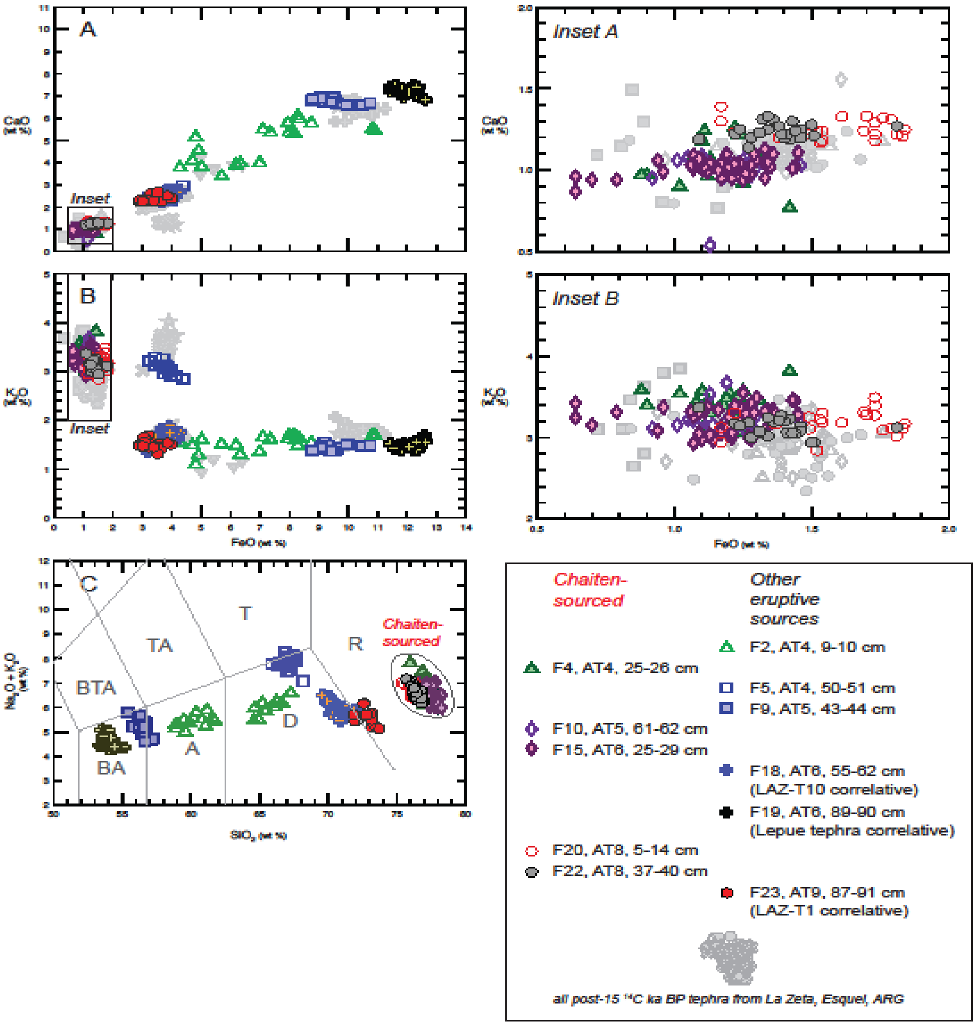

Figure A31 Selected major element compositions (weight percent FeO vs. CaO and K_2O (**A, B**) and SiO_2 vs. Na_2O + K_2O (**C**)) of glass shards from tephra inter-beds within core sections 1502SC and 1502AT1-9. Tephra represented at Lago Espejo are compositionally diverse and include multiple, discrete events of basaltic andesite (BA) to basaltic trachyandesite (BTA), andesite (A), trachyte (T), dacite (D) and rhyolite (R) compositions (Le Maitre, 1984). All post-15 ^{14}C ka B.P. distal tephra recorded from La Zeta, Argentina, are plotted for comparison and are indicated by background grayscale symbols. **Insets A' and B'** indicate the compositional field occupied by distal Chaiten-sourced tephra.

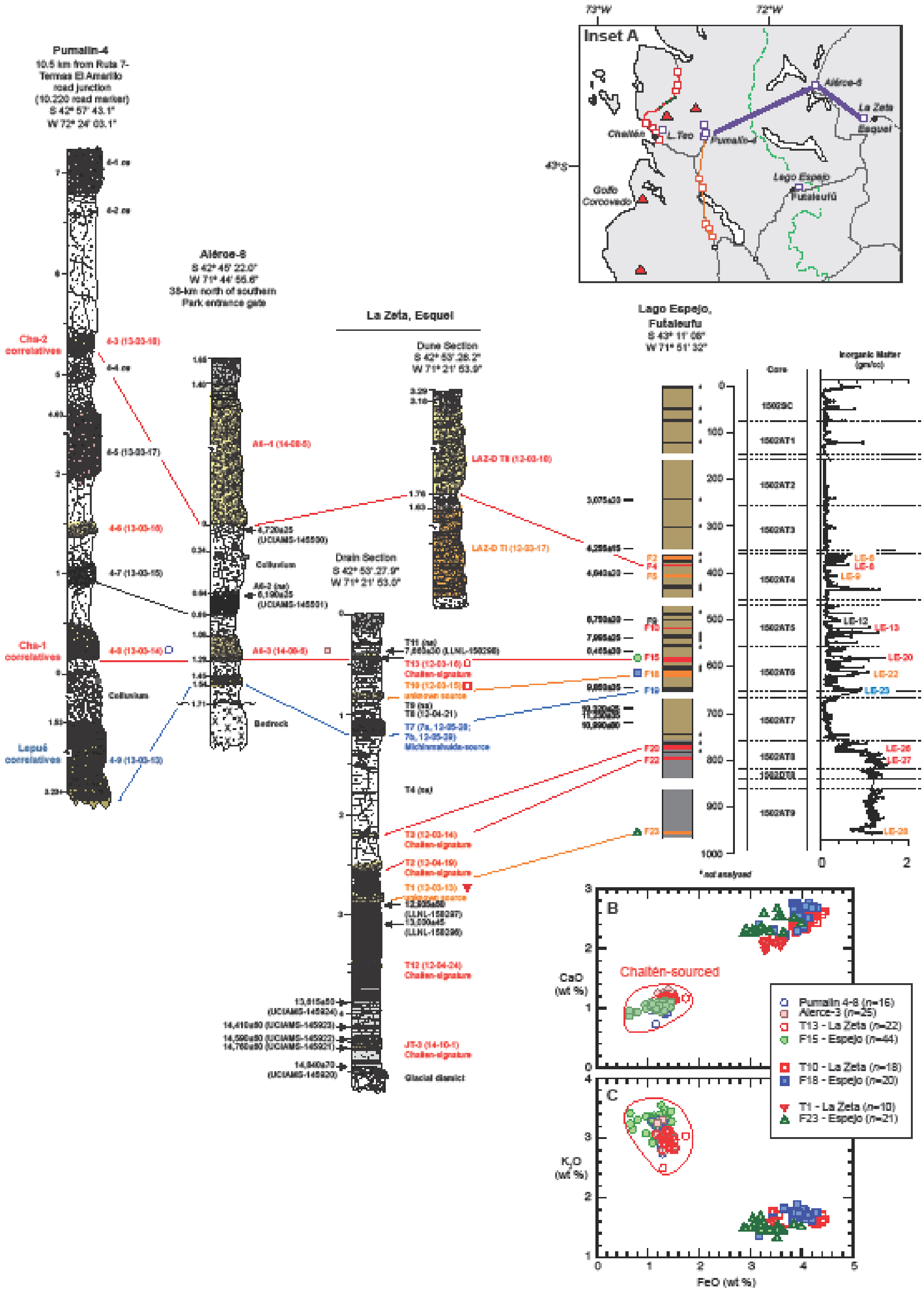

Figure A3.2 Stratigraphic correlation of tephra from distal sections in both Chile (Pumalin-4) and Argentina (Alérce-6 and La Zeta) to Lago Espejo (B.V. Alloway, *unpublished data*). Locations of these sites are indicated in inset A. Correlation is based on a combination of bedding characteristics, correspondence of glass shard major element compositions and chronostratigraphic association. Selected major element compositions (weight percent FeO vs. CaO and K_2O) of glass shards from F15, F18 and F23 (insets B and C) plotted against other distal correlatives to affirm correlation.

Section	Tephra	Sample	*Probe Run*	SiO_2	Al_2O_3	TiO_2	FeO	MgO	MnO	CaO	Na_2O	K_2O	Cl	Total	*n*
Lago Espejo, Futuleufu	**1502AT 4,** 9-10-cm	(16-07-F2)	*May 6, 2016*	62.73 (2.90)	15.34 (0.63)	1.47 (0.33)	7.14 (1.91)	2.46 (0.75)	0.14 (0.06)	4.88 (0.86)	4.15 (0.47)	1.53 (0.16)	0.16 (0.03)	98.96 (1.19)	20
	1502AT 4, 25-26-cm (LE-8)	(16-07-F4)		76.87 (0.38)	13.57 (0.22)	0.08 (0.04)	1.14 (0.13)	0.23 (0.12)	0.05 (0.05)	1.06 (0.13)	3.55 (0.34)	3.36 (0.21)	0.09 (0.08)	96.54 (2.55)	22
	1502AT 4, 50-51-cm	(16-07-F5)		67.09 (0.48)	16.09 (0.15)	1.19 (0.07)	3.77 (0.25)	1.34 (0.14)	0.15 (0.05)	2.43 (0.18)	4.72 (0.22)	3.08 (0.11)	0.13 (0.04)	98.17 (1.53)	22
	1502AT 5, 43-44-cm	(16-05-F9)		56.48 (0.40)	15.41 (0.40)	2.36 (0.15)	9.45 (0.46)	4.08 (0.16)	0.20 (0.08)	6.78 (0.10)	3.71 (0.33)	1.44 (0.05)	0.09 (0.01)	97.85 (0.83)	22
	1502AT 5, 61-62-cm	(16-07-F10)		77.46 (0.56)	13.48 (0.32)	0.06 (0.03)	1.17 (0.11)	0.22 (0.07)	0.08 (0.05)	1.01 (0.11)	3.25 (0.23)	3.21 (0.15)	0.07 (0.01)	96.92 (1.73)	22
	1502AT 6, 25-29-cm (LE-20)	(16-07-F15)		77.39 (0.41)	13.52 (0.15)	0.08 (0.05)	1.16 (0.19)	0.20 (0.10)	0.06 (0.05)	1.02 (0.05)	3.26 (0.25)	3.23 (0.16)	0.09 (0.02)	93.95 (1.02)	44
	1502AT 6, 55-62-cm (LE-22)	(16-07-F18)		70.64 (0.66)	15.81 (0.14)	0.27 (0.07)	3.91 (0.26)	0.49 (0.11)	0.14 (0.05)	2.57 (0.17)	4.31 (0.27)	1.71 (0.10)	0.16 (0.02)	98.15 (1.04)	20
	1502AT 6, 89-90-cm (LE-23)	(16-08-F19)		54.04 (0.47)	14.83 (0.31)	2.34 (0.09)	12.04 (0.35)	4.70 (0.19)	0.18 (0.06)	7.19 (0.18)	3.11 (0.25)	1.49 (0.07)	0.08 (0.01)	101.60 (0.78)	22
	1502AT 8, 5-14-cm	(16-08-F20)		76.14 (0.31)	13.95 (0.16)	0.06 (0.04)	1.57 (0.21)	0.18 (0.08)	0.08 (0.05)	1.25 (0.06)	3.51 (0.24)	3.18 (0.14)	0.07 (0.01)	97.93 (1.24)	22
	1502AT 8, 37-40-cm	(16-08-F22)		76.46 (0.32)	13.91 (0.16)	0.06 (0.03)	1.38 (0.14)	0.20 (0.07)	0.06 (0.05)	1.24 (0.05)	3.49 (0.26)	3.12 (0.11)	0.07 (0.01)	97.89 (1.46)	22
	1502AT 9, 87-91-cm (LE-28)	(16-08-F23)		72.72 (0.53)	15.19 (0.14)	0.17 (0.05)	3.31 (0.30)	0.36 (0.10)	0.15 (0.06)	2.37 (0.13)	4.08 (0.24)	1.52 (0.08)	0.13 (0.01)	96.74 (1.21)	21
Glass standards	***ATHO-G***		*May 6, 2016*	*75.64 (0.60)*	*12.20 (0.15)*	*0.26 (0.06)*	*3.27 (0.39)*	*0.10 (0.06)*	*0.10 (0.05)*	*1.70 (0.05)*	*3.75 (0.52)*	*2.64 (0.08)*	*0.03 (0.01)*	*99.69 (0.85)*	*34*

All major element determinations were made on a JEOL Superprobe (JXA-8230) housed at Victoria University of Wellington, using the ZAF correction method. Analyses were performed using an accelerating voltage of 15 kV under a static electron beam operating at 8 nA. The electron beam was defocused between 10 and 20 µm. Oxide values are recalculated to 100% on a volatile-free basis. Total Fe expressed as FeOt. Mean and ± 1 standard deviation (in parentheses), based on n analyses. All samples normalised against glass standard ATHO-G. Analyst: B.V. Alloway.

Table A3.1. Summary of glass shard major element compositions of tephra beds retrieved from Lago Espejo

Grains from the 700-800 cm section have a larger average size (27.4 µm) than grains from the 1-100 cm section (25.1 µm). The average of both groups are considerable smaller than the size proposed by Heusser (1971), although this difference might be explained by swelling of the grains mounted in the glycerine gelatine medium used by Heusser (1971). Despite the small difference in the mean size between the two groups the t-Test indicated that the differences are significant ($P<0.05$), suggesting that the pollen grains from the two sections represents different taxonomical groups (Table A3.2). We also note that the tectum of the grains from the 700-800 cm section is mostly scrabrate; whereas the grains from the 1-100 cm section show a psilate sculpture (Figure A3.4 and A3.5). Heusser (1971) mentions that all the sculptural elements of the three Cupressaceae species are prone to be removed by attrition during laboratory procedures. However, the same laboratory procedure was applied to all samples throughout the stratigraphy. I therefore conclude that the sculptural traits presented here are genuine taxonomic features. On the basis of these results and interpretations, and with the assumption that Heusser's grains were proportionately inflated in size, the Cupressaceae pollen from the 700-800 cm phase is likley to represent *Fitzroya* and/or *Pilgerodendron* and the Cupressaceae pollen from the 1-100 cm section is likley to represent *Austrocedrus chilensis*.

These results indicate the possibility of distinguishing between ecologically distinctive components of the Chilean Cupressaceae on the basis of pollen morphology. However, the distinctions currently able to be drawn are tenuous due to the preliminary nature of this analysis and the possibility that the reference material used to determine the size distinctions may not have been suited to this purpose and the overlapping size ranges in our analysis. We have references of extensive populations of *F. cupressoides* in the Futaleufú area (Duncan Christie, person. Comm.). For these reasons, we have not separated the taxon Cupressaceae in this study. Nevertheless, we suggest the limitations in our analysis may be overcome by future work based on fresh modern reference material and with a larger sample size than was achieved here.

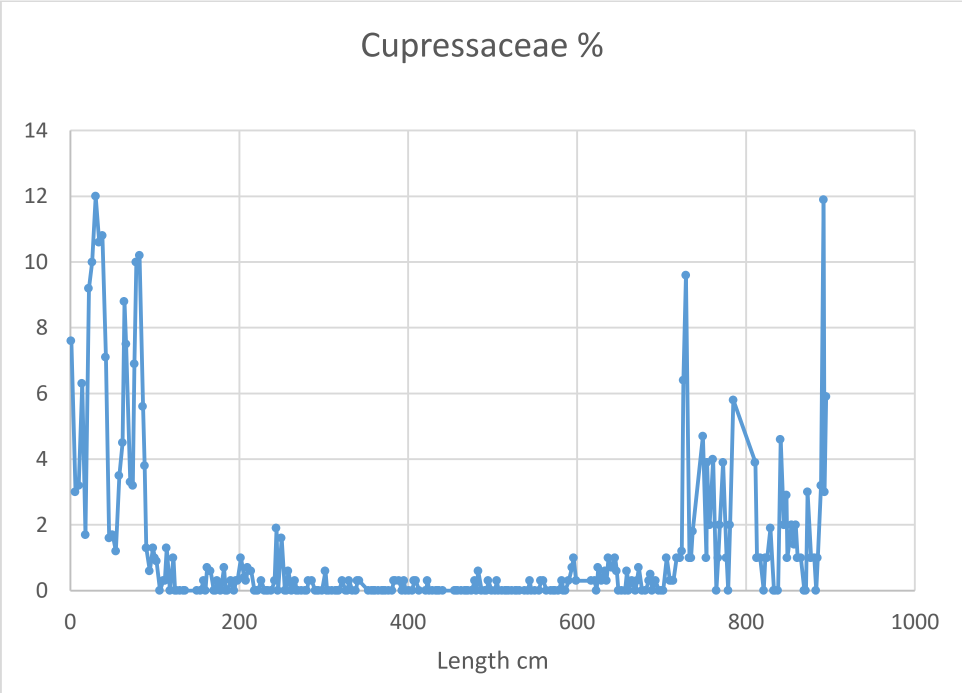

Figure A3.3. Lago Espejo Cupressaceae percentage record. The variation of this taxon along with all major taxa of Lago Espejo can be seen in Figure 6.4.

	712-722 cm	**6-70 cm**
Grain description	Monad, isopolar, inaperturate, tectum scabrate (tectum uneven)	Monad, isopolar, inaperturate, tectum psilate (tectum uneven)
	exine less than 1 um	exine less than 1 um
n	50	50
average size (um)	27.3	25.0
Standard deviation	3.2	3.3
p-value	<0.05	

Table A3.2 Summary of the size analysis of Cupressaceae pollen grains.

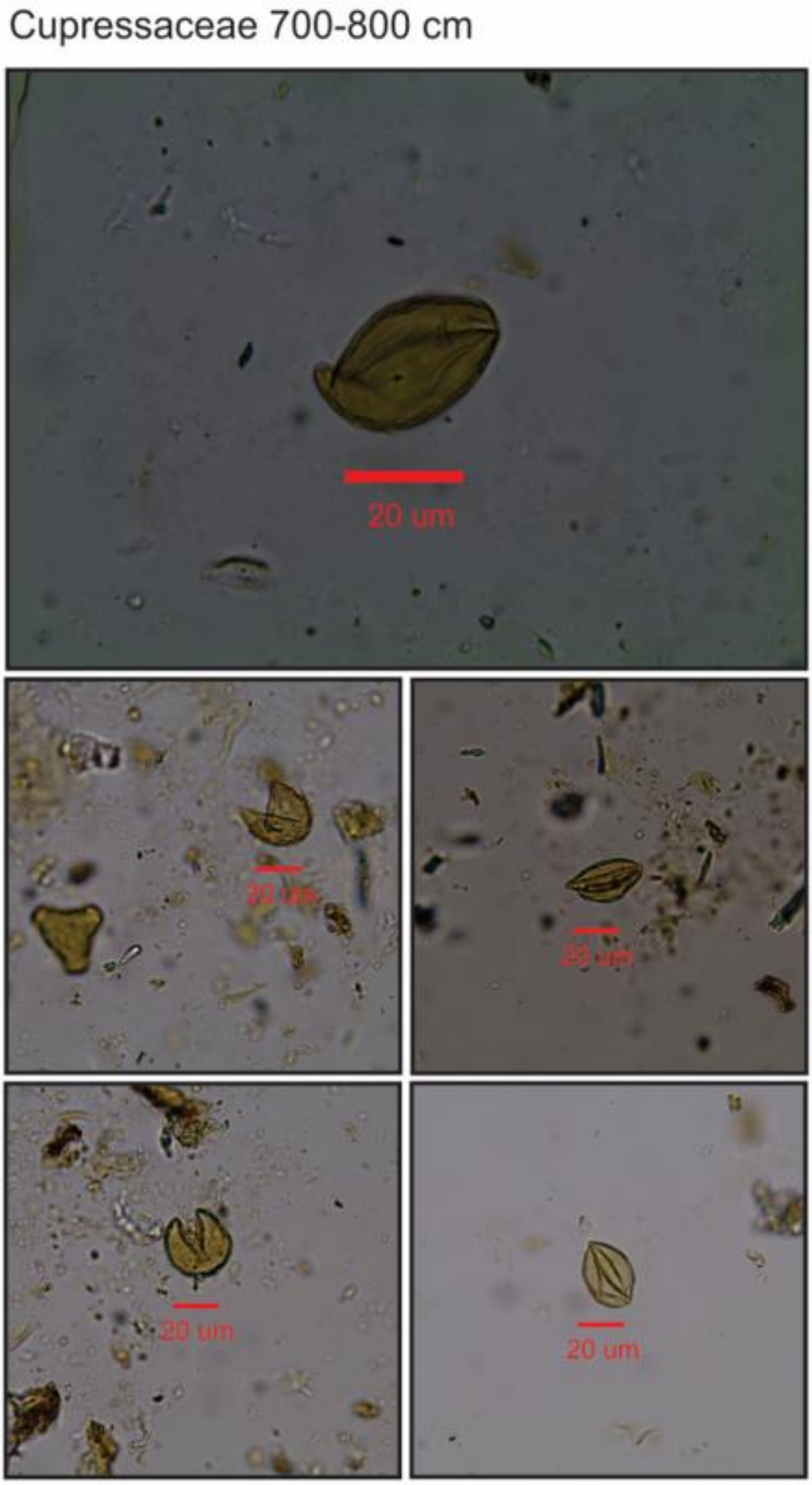

Figure A3.4. Selected images from Cupressaceae pollen grains of the 700-800 cm section

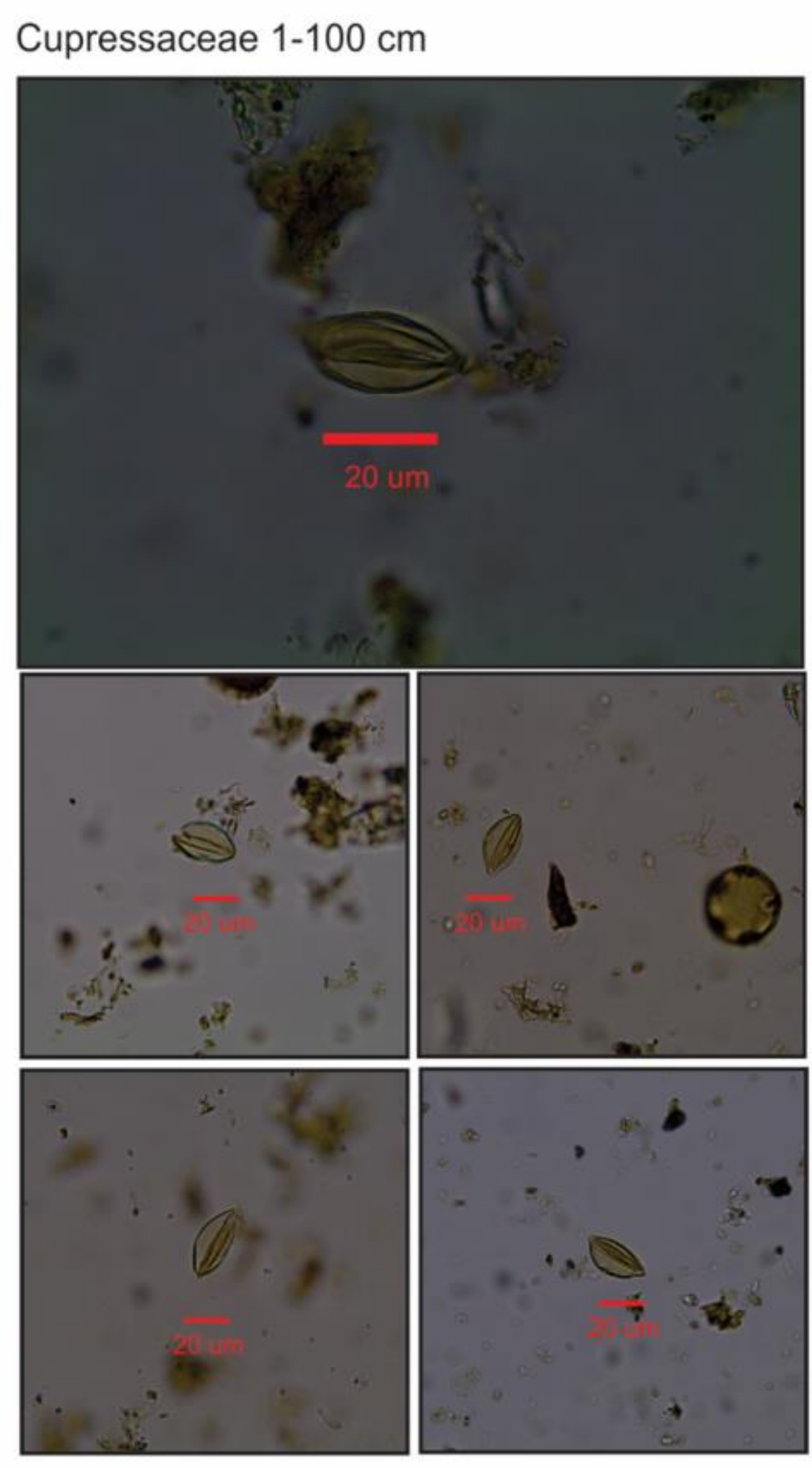

Figure A3.5 Selected images of the Cupressaceae pollen grains of the 1-100 cm section.

Appendix Four

Raw data from Chapter Four, Five and Six

A4.1 Adelaide Tarn pollen percentage

taxon	code
Fuscospora	FUSC
L. menziesii	LMEN
Dacrydium cupressinum	DACU
Prumnopitys ferruginea	PFER
Prumnopitys taxifolia	PTAX
Podocarpoid	PODO
Metrosideros	METRO
Halocarpus	HALO
Phyllocladus	PHY
Coprosma	COP
Dracophyllum	DRA
Hebe	HEB
Myrsine	MYR
Apiaceae	API
Asteraceae	ASTR
Astelia	ASTL
Poaceae	POA
other terrestrial	OTTE
Cyperaceae	CYP
Isoetes	ISO
Cyathea	CYA
total trees	TTRE
total shrubs	TSHR
total herbs	THER
total aquatics	TAQU
total tree ferns	TTFR
Undifferentiated and unknown	UAU
total terrestrial pollen concentration (grains *cm-3)	TCON

Depth (cm)	Age (cal yr BP)	FUSC	LMEN	DACU	PFER	PTAX	PODO	METR	HALO	PHY	COP	DRA	HEB	MYR	API	ASTR	ASTL	POA	OTTE	CYP	ISO	CYA	TTRE	TSHR	THER	TAQU	TTFR	UAU	TCON
1	-15	56	7	7	0	1	3	1	0	2	2	0	0	1	3	1	3	6	7	0	20	1	83	3	14	20	1	7	305
5	374	39	5	8	1	1	9	0	1	11	0	0	1	1	1	1	2	16	3	0	2	2	78	2	19	3	2	12	323
10	764	48	11	9	1	1	3	1	0	1	1	0	1	1	2	1	1	12	6	0	45	0	80	3	17	45	0	12	227
15	904	53	11	6	1	1	4	1	0	2	1	0	0	0	0	1	2	11	7	1	16	0	84	2	14	17	0	5	331
20	962	45	17	7	1	2	7	0	0	2	1	0	1	0	1	1	2	8	4	0	13	1	85	2	13	13	1	7	397
25	1014	61	3	4	0	0	4	1	1	2	0	0	0	1	1	2	0	13	5	0	17	2	81	2	16	17	2	9	337
30	1064	50	10	9	1	3	5	0	1	4	0	1	0	1	1	2	0	7	5	1	17	0	87	4	10	17	0	6	404
35	1112	52	9	9	1	2	3	0	2	2	1	0	2	1	2	1	2	6	7	1	21	1	84	4	11	22	1	7	348
40	1200	52	11	7	0	0	5	0	1	2	0	0	1	0	1	1	3	9	6	0	33	1	83	2	15	33	1	9	280
45	1334	50	8	12	0	1	2	1	0	4	0	1	1	1	1	1	1	11	4	0	17	0	82	4	14	17	0	7	365
50	1475	50	10	12	0	0	2	0	0	4	0	0	0	0	1	1	3	11	6	0	16	1	84	1	15	16	1	7	318
55	1601	49	13	8	1	2	5	1	1	1	0	0	1	1	2	2	1	7	6	0	18	0	85	3	12	18	0	8	334
60	1752	48	8	6	1	1	6	2	1	2	0	1	0	1	1	1	3	13	6	1	18	1	80	1	18	19	1	7	341
65	1890	55	7	6	0	1	4	2	1	1	1	0	0	1	1	1	1	9	9	0	19	1	84	3	13	19	1	9	435
70	2028	51	12	10	1	2	3	1	0	2	1	0	0	1	2	1	2	5	7	1	21	2	86	3	11	22	2	7	410
75	2182	48	10	8	1	2	7	2	0	4	1	0	0	0	0	2	2	8	6	1	19	1	85	3	12	20	1	8	573
78	2275	55	9	6	1	1	4	2	0	2	0	0	1	1	1	1	3	9	4	0	23	1	82	3	15	23	1	7	520
83	2426	56	12	4	0	0	0	1	1	3	0	0	0	0	0	1	1	12	9	0	16	0	85	1	15	16	0	5	494
88	2557	49	10	9	1	2	7	1	1	2	1	0	1	0	1	1	2	6	5	1	11	2	87	2	11	12	2	6	448
93	2667	53	6	8	1	1	7	1	0	1	0	0	0	1	0	1	2	11	6	1	11	1	84	3	14	12	1	9	732
98	2780	48	9	12	1	2	5	1	0	2	1	0	0	1	1	1	1	7	8	1	14	0	86	2	11	15	0	8	481
103	2898	50	9	9	0	1	1	1	1	2	2	0	1	1	1	1	4	7	10	1	11	0	81	4	14	12	0	8	386
108	3012	44	10	12	0	1	1	0	1	3	0	0	0	0	1	1	0	9	15	0	11	2	85	1	14	11	2	11	368
113	3122	44	8	13	1	3	0	1	2	2	1	0	0	0	1	1	1	9	13	1	15	0	83	3	14	16	0	6	294
118	3235	58	8	5	1	1	0	0	2	2	0	0	0	1	1	1	2	9	9	1	14	1	84	2	13	15	1	5	305
123	3349	47	10	9	1	1	4	0	2	2	2	1	0	0	1	3	1	9	8	0	12	1	83	3	14	12	1	10	474
128	3465	50	10	12	0	0	10	1	2	2	0	1	0	0	0	1	2	4	5	1	12	1	90	2	8	12	1	5	364
133	3577	47	10	13	1	1	4	1	3	2	1	0	0	0	1	1	1	7	8	0	16	2	86	2	11	16	2	10	375

Depth (cm)	Age (cal yr BP)	FUSC	LMEN	DACU	PFER	PTAX	PODO	METR	HALO	PHY	COP	DRA	HEB	MYR	API	ASTR	ASTL	POA	OTTE	CYP	ISO	CYA	TTRE	TSHR	THER	TAQU	TTFR	UAU	TCON
138	3691	43	13	9	1	3	3	2	2	4	0	0	0	1	1	1	3	8	7	1	5	2	83	3	14	6	2	8	445
143	3841	50	9	10	2	1	8	1	0	2	1	0	1	0	1	0	3	6	4	0	17	1	86	3	12	17	1	7	502
148	4009	50	9	11	1	2	5	1	2	2	0	0	0	1	1	1	1	9	3	0	16	2	86	1	13	16	2	6	448
153	4175	54	8	11	1	1	4	0	1	2	1	1	1	0	0	0	1	10	6	0	11	3	85	3	12	11	3	6	484
158	4344	46	14	6	1	2	8	2	2	3	0	0	0	1	1	0	3	6	6	0	23	1	88	2	11	23	1	10	818
163	4511	50	9	7	1	1	4	0	1	2	0	0	0	1	2	2	4	9	7	0	6	2	81	2	17	6	2	7	589
168	4678	32	12	5	1	1	10	0	2	15	0	2	1	0	0	0	4	7	7	1	5	0	84	4	12	6	0	12	297
173	4853	49	9	10	1	5	4	2	3	2	1	0	0	0	1	1	2	5	6	1	21	1	88	2	10	21	1	7	593
178	5016	47	11	5	1	1	7	1	3	4	0	0	2	0	1	2	2	6	9	1	17	1	84	4	12	18	1	11	490
183	5197	47	9	9	1	1	7	2	1	1	1	0	0	1	0	3	2	11	4	0	19	1	81	3	16	19	1	5	521
188	5390	51	10	11	1	1	2	0	0	2	1	1	0	0	0	1	1	10	7	0	10	1	85	2	13	10	2	6	566
193	5576	45	16	6	2	1	7	0	1	6	0	0	0	0	1	1	2	5	7	0	8	2	89	2	10	8	2	8	597
198	5758	47	9	9	1	3	7	1	1	2	0	1	0	0	2	0	4	7	6	0	17	1	83	2	14	17	1	6	352
203	5952	33	13	15	3	1	7	2	1	5	0	1	0	0	1	0	4	8	8	0	12	2	84	3	14	12	2	11	720
208	6155	39	9	14	3	2	8	1	3	2	1	1	0	0	1	1	3	9	4	1	13	1	84	2	14	13	1	8	1088
213	6366	33	12	9	1	1	7	0	3	11	1	0	0	0	1	1	4	6	8	0	10	1	84	3	13	10	1	10	1070
218	6584	42	12	12	1	2	6	0	1	5	1	0	0	0	1	1	4	8	5	0	7	0	84	1	14	7	0	7	408
223	6819	35	12	8	2	0	4	1	1	16	1	1	0	0	0	1	4	7	7	0	5	2	84	4	13	5	2	9	408
228	7062	42	14	5	1	3	8	0	3	3	1	1	0	1	0	0	3	9	5	0	14	3	83	4	13	14	3	7	467
233	7311	36	12	5	1	2	7	1	4	10	1	0	1	0	1	1	3	11	5	0	8	2	79	4	17	8	2	8	637
238	7557	31	14	15	2	4	6	0	2	3	1	1	0	0	1	2	4	8	8	0	7	1	81	3	16	7	1	6	863
243	7792	26	15	11	2	3	6	1	3	5	2	1	0	1	2	0	6	6	11	0	8	4	78	6	16	8	4	6	1101
248	8015	26	11	11	0	2	11	1	4	5	1	2	0	0	2	2	7	8	9	0	8	3	75	5	20	8	3	8	577
253	8236	22	10	13	1	1	9	1	1	14	1	1	3	1	1	2	4	12	6	0	2	1	75	7	18	2	1	11	555
258	8456	26	16	12	1	2	3	0	2	3	1	2	0	2	0	2	3	14	11	0	2	2	75	5	20	2	2	4	556
263	8677	17	13	15	1	2	6	1	7	8	2	1	1	1	1	1	3	7	13	0	3	3	81	6	13	3	3	7	521
268	8867	17	15	9	1	2	11	1	7	10	1	1	0	1	1	1	4	9	11	0	2	1	80	4	16	3	1	8	564
273	9012	13	14	19	1	2	6	1	3	10	1	3	0	0	2	1	3	10	10	1	1	2	76	7	17	1	3	5	508
278	9142	18	8	11	0	7	8	0	6	12	2	2	0	1	1	0	3	13	10	0	0	4	76	6	18	0	4	8	566

Depth (cm)	Age (cal yr BP)	FUSC	LMEN	DACU	PFER	PTAX	PODO	METR	HALO	PHY	COP	DRA	HEB	MYR	API	ASTR	ASTL	POA	OTTE	CYP	ISO	CYA	TTRE	TSHR	THER	TAQU	TTFR	UAU	TCON
283	9271	12	14	14	1	4	8	1	6	11	3	1	0	0	1	1	3	8	10	1	0	2	81	5	15	1	2	6	675
288	9401	14	13	11	1	1	11	0	8	9	2	3	0	0	1	2	3	16	6	0	0	2	72	6	22	0	2	8	425
293	9527	12	18	17	1	0	0	1	6	11	2	3	0	1	1	1	4	11	10	0	0	3	73	9	18	0	3	5	894
298	9650	12	15	15	2	4	8	1	7	10	1	1	0	2	2	3	4	6	9	0	0	2	81	4	15	0	2	6	1105
303	9773	14	14	18	5	3	8	1	3	8	1	0	1	0	2	2	3	10	8	0	0	2	80	3	17	0	2	6	0
308	9899	8	16	21	1	3	7	1	3	12	3	2	2	2	1	1	3	5	10	0	0	0	79	11	10	0	1	7	481
313	10,029	6	13	12	1	8	0	2	3	12	4	1	0	1	4	2	4	10	16	0	0	2	68	10	22	0	2	6	766
318	10,156	10	13	5	0	3	8	0	3	14	3	1	1	1	0	3	6	18	11	0	1	2	66	6	27	1	2	8	494
322	10,264	12	16	16	2	1	8	1	1	13	1	2	1	0	1	3	4	11	8	1	0	4	75	4	21	1	4	7	624
332	10,635	11	16	10	5	4	2	0	0	11	2	0	1	0	0	2	6	13	16	0	0	2	72	5	23	0	2	8	839
337	10,832	12	11	11	2	5	9	2	1	9	1	1	0	0	2	3	2	16	15	1	0	3	74	4	23	1	3	8	417
342	11,020	11	14	10	4	5	2	1	0	6	2	1	2	2	1	4	5	15	14	1	0	4	66	7	26	1	4	9	1129
347	11,215	11	11	8	2	6	2	5	1	6	2	1	2	0	3	2	5	13	20	1	0	4	66	8	26	1	4	8	496
352	11,402	10	16	12	3	6	5	2	1	4	3	1	1	1	2	3	2	16	15	0	0	3	70	6	24	0	4	6	1053
357	11,568	14	10	7	3	2	4	1	0	9	2	0	3	1	3	6	4	16	16	0	0	1	62	8	30	0	1	13	420
367	11,890	13	16	6	3	7	2	1	1	12	2	0	1	1	2	1	6	14	11	0	0	2	70	6	24	0	2	9	386
372	12,050	15	9	9	4	6	6	1	0	9	2	0	0	1	3	3	7	12	13	0	0	2	70	5	26	0	2	7	859
377	12,206	14	14	8	1	11	3	1	0	11	3	0	1	1	3	3	3	12	12	1	0	3	72	7	21	1	3	5	347
382	12,358	20	8	4	2	12	0	1	1	12	2	0	1	1	3	2	6	12	14	0	0	3	68	8	24	0	3	8	439
387	12,510	16	7	1	1	3	7	1	1	9	1	1	0	0	4	5	10	20	13	0	1	2	56	4	40	1	2	9	132
392	12,656	21	7	5	2	5	5	1	1	12	2	0	1	0	7	2	5	17	7	1	0	1	63	5	32	1	1	8	558
397	12,773	17	15	1	5	3	0	0	1	12	2	0	1	1	2	3	6	15	16	0	0	2	69	6	26	0	2	4	339
402	12,890	21	12	4	2	7	1	1	0	8	3	0	1	1	2	1	3	18	14	1	0	2	67	6	27	1	2	6	837
407	13,007	19	9	0	0	2	4	2	0	12	2	0	0	0	2	7	7	20	12	0	0	1	59	3	38	0	1	8	378
411	13,102	15	10	3	1	3	3	1	0	12	2	1	0	1	2	5	5	21	14	0	0	2	57	7	36	0	2	11	196
416	13,217	16	10	1	0	7	1	3	0	13	3	1	1	0	6	4	4	17	13	0	0	1	60	8	32	1	2	7	631
421	13,308	21	7	1	0	5	8	2	0	14	2	0	0	0	2	6	5	17	9	1	0	2	64	4	32	1	2	8	471
426	13,388	20	9	0	2	7	3	2	0	15	3	1	1	1	2	4	3	18	9	1	0	1	65	7	28	1	1	8	0
431	13,465	20	7	2	4	2	0	1	1	12	2	1	1	0	5	3	5	16	17	1	0	1	64	5	31	1	1	6	186

Depth (cm)	Age (cal yr BP)	FUSC	LMEN	DACU	PFER	PTAX	PODO	METR	HALO	PHY	COP	DRA	HEB	MYR	API	ASTR	ASTL	POA	OTTE	CYP	ISO	CYA	TTRE	TSHR	THER	TAQU	TTFR	UAU	TCON
436	13,543	22	9	1	6	0	2	1	0	15	6	0	0	0	2	7	3	18	8	1	0	1	62	8	30	1	1	7	586
441	13,623	25	6	1	1	3	3	3	0	12	3	0	0	1	4	4	5	18	11	1	0	1	63	5	32	1	1	7	254
446	13,698	25	6	1	0	1	3	2	0	17	3	0	1	2	5	5	3	18	10	1	0	2	59	10	31	1	2	10	702
451	13,778	24	4	2	0	6	1	3	1	21	4	0	1	1	5	4	2	12	9	0	0	1	66	8	26	0	1	9	260
456	13,858	25	6	2	0	4	1	1	0	14	6	0	1	0	2	4	5	22	7	0	0	1	57	9	35	0	1	8	297
461	13,937	29	8	1	0	1	4	1	1	17	3	0	1	2	1	4	3	19	6	0	0	2	66	6	28	0	2	6	555
464	13,993	21	8	0	2	1	0	1	0	15	1	0	0	1	2	5	7	21	16	0	0	3	62	2	36	0	3	6	450
469	14,088	24	9	0	0	5	1	0	0	15	2	0	0	1	2	4	8	15	11	0	0	3	63	6	32	0	3	12	1447
474	14,190	29	5	1	0	2	4	4	0	11	4	0	1	3	2	4	2	16	13	1	0	1	63	11	27	1	1	11	528
479	14,292	36	3	1	1	3	2	2	0	15	6	0	2	0	3	4	2	12	9	0	0	2	65	12	22	0	2	12	141
484	14,394	38	4	0	0	1	6	0	1	16	3	0	1	1	2	6	2	18	3	0	0	1	67	5	28	0	1	14	175
489	14,496	33	7	1	0	1	3	2	0	16	4	0	1	2	1	3	2	19	4	0	0	1	66	8	27	0	1	8	347
494	14,597	41	3	1	0	0	0	2	0	20	2	0	0	1	1	6	1	17	6	0	0	0	72	3	26	0	0	13	180
497	14,658	36	7	1	1	1	5	1	1	14	4	0	1	1	1	5	2	17	2	0	0	1	68	6	26	0	1	12	155
502	14,759	34	6	1	0	1	1	2	0	12	9	0	1	0	0	5	0	14	12	0	0	1	68	10	22	0	1	13	88
507	14,859	45	8	2	0	1	3	0	2	13	3	0	1	3	1	4	0	8	6	0	0	0	79	6	15	0	0	11	147
512	14,958	51	2	0	1	0	8	2	1	12	2	0	0	1	0	4	0	13	4	0	0	0	80	3	18	0	0	12	116
517	15,058	44	7	2	1	0	0	2	2	14	3	0	0	0	1	8	0	11	6	1	0	1	75	4	21	1	1	9	126
522	15,160	54	3	1	0	0	3	1	3	10	3	0	0	3	1	5	0	10	4	0	0	2	76	6	18	0	2	9	115
532	15,361	56	6	1	0	0	7	2	1	11	1	0	0	2	0	4	0	8	2	0	0	1	84	3	13	0	1	12	94
537	15,461	57	1	0	0	0	3	1	2	9	6	0	0	1	0	3	0	13	4	0	0	0	74	7	18	0	0	13	71
542	15,564	49	3	1	0	0	7	1	2	14	5	0	1	0	0	1	0	9	5	0	0	0	83	7	11	0	0	14	49
547	15,667	55	2	1	0	0	3	1	2	11	1	0	1	1	0	7	0	10	4	0	0	0	77	3	20	0	0	14	94
557	15,872	56	8	0	0	0	3	1	2	3	4	0	1	1	0	5	0	11	3	0	0	0	75	7	18	0	0	11	135

A4.2 Adelaide Tarn Pollen accumulation rate (particle*cm^{-2}*yr^{-1})

taxon	code
Fuscospora	FUSC
L. menziesii	LMEN
Dacrydium cupressinum	DACU
Prumnopitys ferruginea	PFER
Prumnopitys taxifolia	PTAX
Podocarpoid	PODO
Metrosideros	METR
Halocarpus	HALO
Phyllocladus	PHY
Coprosma	COP
Dracophyllum	DRA
Hebe	HEB
Myrsine	MYR
Apiaceae	API
Asteraceae	ASTR
Astelia	ASTL
Poaceae	POA
Cyperaceae	CYP
Isoetes	ISO
Cyathea	CYA
total trees	TTRE
total shrubs	TSHR
total herbs	THER
total aquatics	TAQU
total terrestrial Pollen	TTAC

(cm)	(cal yr BP)	FUSC	LMEN	DACU	PFER	PTAX	PODO	METR	HALO	PHY	COP	DRA	HEB	MYR	API	ASTR	ASTL	POA	CYP	ISO	CYA	TTRE	TSHR	THER	TAQU	TTAC
1	-15	171127	19979	22585		2606	9555	1737	869	6949	6081		869	1737	8687	3475	9555	18242	869	75574	1737	252782	9555	42565	76443	304902
5	374	125088	17721	26060	2085	3127	30230	1042	3127	35442		1042	3127	2085	3127	2085	6254	51078	1042	7297	5212	253303	7297	62544	8339	323144
10	764	109620	24211	20848	1345	2690	6725	2018	673	3363	1345	673	2018	1345	4035	3363	2690	26901	1345	186960	0	181579	7398	37661	188305	226638
15	904	173733	37725	18863	3971	2978	12906	1986	993	5957	2978	0	0	993	993	1986	5957	35739	3971	62544	0	277973	6949	45667	66515	330590
20	962	179048	68676	28206	2453	9811	26980	0	1226	8585	3679	0	2453	1226	3679	3679	9811	31885	1226	60091	2453	337247	8585	51507	61318	397338
25	1014	206495	9928	13899	993	993	13899	2978	4964	6949	993	993	0	1986	2978	5957	993	43682	993	68501	6949	274002	7942	54602	69493	336546
30	1064	201965	41696	36484	2606	11727	20848	0	5212	16939		2606	1303	3909	2606	6515	1303	27363	2606	82089	1303	350507	14333	39090	84695	403930
35	1112	180051	30324	30324	1895	6634	9476	948	6634	7581	3791	0	6634	1895	6634	2843	7581	21796	3791	94764	4738	292820	15162	39801	98554	347783
40	1200	146805	32141	20848	0	869	13030	0	1737	5212	869	869	3475	0	3475	2606	7818	24323	1737	138118	1737	231934	6081	41696	139855	279711
45	1334	182999	27797	44012	1158	2316	8108	3475	1158	16215	1158	2316	4633	2316	3475	2316	3475	41696	1158	72968	1158	297663	15057	52120	74126	364840
50	1475	157849	31768	37725	0	993	6949	993	0	13899		993	0	0	1986	3971	7942	33754	993	58573	1986	268046	1986	47653	59566	317684
55	1601	162614	43781	26060	4170	7297	15636	2085	4170	3127	1042	0	2085	3127	5212	6254	3127	22933	1042	72968	1042	283533	10424	39611	74010	333568
60	1752	162813	26805	20848	1986	4964	20848	5957	3971	7942		2978	0	1986	2978	3971	9928	43682	2978	77435	2978	273010	4964	62544	81407	340517
65	1890	241055	29969	26060	1303	5212	16939	9121	3909	5212	3909	1303	1303	2606	2606	5212	3909	37787	1303	101634	3909	366143	11727	57332	102937	435202
70	2028	211086	49514	40393	2606	6515	10424	3909	1303	6515	2606	1303	0	2606	9121	2606	9121	22151	3909	110755	7818	351810	13030	45605	114664	410445
75	2182	272761	57332	48645	3475	8687	38221	12161	1737	20848	6949	0	0	1737	0	8687	8687	46908	10424	133775	5212	486453	19111	67756	144199	573320

(cm)	(cal yr BP)	FUSC	LMEN	DACU	PFER	PTAX	PODO	METR	HALO	PHY	COP	DRA	HEB	MYR	API	ASTR	ASTL	POA	CYP	ISO	CYA	TTRE	TSHR	THER	TAQU	TTAC
78	2275	287061	44903	33678	4811	6415	19244	8019	1604	11226	1604	0	4811	4811	4811	3207	17641	46507	0	158766	3207	428186	16037	75374	158766	519596
83	2426	276236	61241	20848	0	0	0	2606	5212	13030	1303	0	0	1303	1303	2606	5212	59938	1303	95119	1303	419566	2606	71665	96422	493837
88	2557	218209	44476	41696	5560	9729	31967	2780	2780	9729	2780	1390	2780	1390	5560	5560	11119	26408	4170	55595	6949	387773	8339	51425	59764	447537
93	2667	384530	46329	60228	9266	9266	50962	4633	2316	6949	2316	2316	0	4633	2316	4633	11582	83392	6949	92658	9266	611541	18532	101924	99607	731996
98	2780	229328	44674	59566	2978	7446	22337	4467	0	11913	4467	0	1489	2978	4467	4467	5957	35739	2978	78925	0	415471	11913	53609	81903	480993
103	2898	192265	35905	34747	0	4633	4633	3475	4633	5791	5791	0	2316	2316	4633	3475	13899	27797	2316	48645	1158	313878	16215	55595	50962	385688
108	3012	160993	35905	42854	1158	4633	4633	1158	3475	12740	1158	0	0	1158	3475	4633	1158	34747	0	46329	5791	313878	4633	49804	46329	368315
113	3122	129431	24323	38221	3475	7818	0	1737	5212	5212	2606	0	869	869	2606	2606	3475	27797	1737	52120	869	244964	8687	39959	53857	293609
118	3235	177208	24639	15162	2843	1895	0	948	7581	4738	948	948	0	1895	2843	1895	7581	26534	3791	51172	1895	257757	7581	39801	54963	305139
123	3349	224861	49142	41696	2978	5957	17870	1489	7446	10424	7446	2978	1489	1489	2978	11913	2978	43185	0	64033	2978	394623	14891	64033	64033	473547
128	3465	181500	36791	44149	0	0	35564	2453	6132	7358	1226	3679	1226	0	1226	2453	7358	15943	2453	49054	2453	326210	7358	30659	51507	364227
133	3577	175369	38017	47828	3679	3679	14716	4905	9811	6132	2453	1226	1226	0	2453	4905	3679	26980	0	69902	6132	323757	8585	42922	69902	375264
138	3691	189022	58374	41696	5560	11119	11119	6949	9729	16678	1390	1390	0	4170	4170	5560	12509	33357	2780	25018	6949	371094	12509	61154	27797	444757
143	3841	253383	46507	51318	9622	3207	41696	6415	0	9622	6415	0	3207	1604	3207	1604	12830	28867	1604	102636	6415	431393	12830	57733	104240	501956
148	4009	223769	41696	47256	5560	9729	20848	2780	11119	9729	1390	0	1390	2780	5560	2780	5560	41696	1390	84782	6949	383603	5560	58374	86172	447537
153	4175	259905	38916	51425	2780	5560	20848	1390	4170	8339	2780	2780	2780	0	0	1390	2780	47256	0	59764	12509	412790	13899	56985	59764	483674
158	4344	372658	112058	49514	10424	13030	62544	18242	18242	20848		0	2606	5212	7818	2606	20848	52120	2606	242358	10424	716650	13030	88604	244964	818284

(cm)	(cal yr BP)	FUSC	LMEN	DACU	PFER	PTAX	PODO	METR	HALO	PHY	COP	DRA	HEB	MYR	API	ASTR	ASTL	POA	CYP	ISO	CYA	TTRE	TSHR	THER	TAQU	TTAC
163	4511	295663	51172	41696	3791	7581	22743	1895	5686	9476	1895	1895	0	3791	11372	13267	20848	53068	1895	37906	11372	479504	9476	100450	39801	589430
168	4678	94764	35063	14215	2843	1895	29377	948	6634	44539	948	5686	2843	0	948	948	12319	21796	2843	17058	948	248281	12319	36010	19900	296610
173	4853	291872	54963	56858	5686	30324	20848	11372	15162	9476	5686	0	0	0	3791	5686	11372	32220	3791	157308	5686	523095	11372	58754	161098	593220
178	5016	232306	52120	25315	4467	2978	32761	5957	13402	19359	1489	1489	7446	1489	2978	7446	8935	28294	4467	104240	4467	413982	17870	58077	108707	489928
183	5197	245709	47653	49142	5957	2978	38718	8935	5957	5957	2978	0	1489	4467	1489	13402	10424	55098	0	119131	5957	422917	16381	81903	119131	521200
188	5390	287061	57733	62544	6415	3207	12830	1604	1604	9622	3207	6415	0	0	0	8019	8019	57733	0	64148	6415	482711	9622	73770	64148	566103
193	5576	267234	92868	37906	11372	5686	43591	0	3791	37906	1895	0	1895	1895	3791	3791	11372	32220	1895	51172	9476	530676	9476	56858	54963	597011
198	5758	166784	32314	33357	2085	9382	22933	4170	2085	7297	1042	3127	0	1042	6254	1042	13551	26060	0	69841	3127	293957	8339	50035	69841	352331
203	5952	236277	90341	106556	18532	4633	53278	16215	4633	34747	2316	4633	0	0	9266	2316	25481	55595	0	99607	11582	602276	18532	99607	99607	720414
208	6155	423909	97291	156360	31272	24323	86867	6949	27797	20848	6949	10424	0	0	10424	6949	34747	93816	6949	159835	10424	910363	24323	152885	166784	1087571
213	6366	357891	125088	100765	13899	6949	72968	3475	27797	121613	13899	0	3475	3475	10424	6949	41696	69493	0	118139	10424	896464	31272	142461	118139	1070197
218	6584	170693	49514	50817	2606	6515	23454	1303	3909	22151	3909	0	0	0	3909	2606	14333	31272	0	29969	1303	343992	5212	58635	29969	407839
223	6819	142027	46908	33878	6515	0	14333	3909	5212	65150	2606	5212	0	1303	0	2606	18242	29969	0	22151	6515	341386	14333	52120	23454	407839
228	7062	194581	66714	25018	4170	13899	38916	1390	15289	13899	4170	2780	1390	4170	1390		15289	40306	1390	73663	16678	387773	19458	59764	75053	466995
233	7311	227433	73916	34115	3791	15162	45487	5686	22743	62544	5686	1895	3791	0	5686	9476	20848	68230	0	54963	11372	506038	24639	106135	54963	636812
238	7557	271024	122482	125088	13030	36484	54726	0	13030	23454	10424	5212	0	0	7818	13030	33878	65150	2606	62544	10424	695802	26060	140724	65150	862586
243	7792	281448	159835	125088	20848	34747	69493	10424	31272	52120	20848	10424	3475	6949	17373	3475	62544	66019	0	100765	48645	861717	66019	173733	100765	1101469
248	8015	151148	64281	60807	1737	12161	62544	3475	22585	26060	3475	8687	1737	1737	10424	8687	38221	48645	0	50383	1737	430859	29535	116401	50383	576795

(cm)	(cal yr BP)	FUSC	LMEN	DACU	PFER	PTAX	PODO	METR	HALO	PHY	COP	DRA	HEB	MYR	API	ASTR	ASTL	POA	CYP	ISO	CYA	TTRE	TSHR	THER	TAQU	TTAC
253	8236	120277	52922	70563	4811	8019	51318	3207	4811	75374	6415	3207	14433	4811	3207	9622	22452	64148	0	12830	6415	415356	36885	102636	12830	554878
258	8456	142461	90341	66019	6949	10424	13899	1737	10424	17373	6949	12161	0	8687	0	12161	19111	76443	0	13899	10424	418697	27797	109452	13899	555947
263	8677	90838	65522	75946	7446	10424	32761	7446	37229	40207	10424	7446	2978	4467	5957	2978	17870	35739	0	17870	17870	421427	32761	67011	17870	521200
268	8867	94618	84996	52922	8019	12830	60940	3207	38489	57733	3207	3207	0	3207	3207	6415	24055	48111	0	12830	8019	453845	20848	89807	19244	564500
273	9012	65751	72166	97825	6415	9622	32074	3207	14433	52922	4811	14433	1604	1604	8019	4811	16037	52922	3207	3207	11226	388094	35281	84996	6415	508371
278	9142	102503	43433	60807	1737	38221	43433	0	36484	66019	8687	8687	1737	3475	3475	1737	15636	74705	0	1737	20848	429121	36484	100765	1737	566371
283	9271	81307	93816	95901	8339	25018	56290	8339	41696	75053	20848	4170	0	2085	6254	8339	22933	56290	4170	0	12509	544133	31272	100070	6254	675475
288	9401	58635	53423	48211	2606	3909	48211	1303	32575	37787	6515	13030	1303	1303	2606	9121	13030	67756	1303	0	9121	304902	24757	95119	1303	424778
293	9527	109452	158966	151148	7818	2606	0	5212	57332	96422	15636	31272	0	7818	13030	13030	33878	96422	0	0	23454	654106	80786	158966	0	893858
298	9650	128563	163309	170259	20848	48645	83392	10424	76443	111189	10424	6949	0	17373	17373	34747	41696	66019	3475	0	27797	892989	41696	170259	3475	1104944
303	9773	46	46	62	17	11	27	3	11	27	2	0	4	0	6	6	11	34	0	1	7	271	9	59	1	339
308	9899	38916	77833	98681	5560	12509	33357	4170	16678	55595	12509	11119	8339	8339	2780	6949	12509	25018	0	0	1390	378044	52815	50035	0	480894
313	10,029	46908	101634	93816	10424	59938	0	15636	26060	91210	28666	10424	2606	5212	31272	13030	33878	72968	0	0	13030	523806	72968	169390	0	766164
318	10,156	48111	65751	25659	0	14433	41696	0	16037	67355	12830	4811	6415	3207	0	12830	28867	89807	0	4811	9622	327153	32074	134710	4811	493937
322	10,264	74705	100765	97291	12161	8687	48645	3475	5212	78180	5212	12161	5212	1737	3475	19111	27797	71231	5212	0	26060	467343	27797	128563	5212	623703
332	10,635	93816	138118	83392	39090	31272	18242	2606	2606	96422	13030	2606	7818	2606	2606	15636	49514	109452	2606	0	20848	607198	41696	190238	2606	839132

(cm)	(cal yr BP)	FUSC	LMEN	DACU	PFER	PTAX	PODO	METR	HALO	PHY	COP	DRA	HEB	MYR	API	ASTR	ASTL	POA	CYP	ISO	CYA	TTRE	TSHR	THER	TAQU	TTAC
337	10,832	50817	44302	46908	7818	20848	36484	7818	5212	36484	5212	3909	0	0	6515	10424	6515	66453	5212	0	11727	307508	15636	93816	5212	416960
342	11,020	128563	159835	118139	41696	59069	17373	13899	3475	69493	24323	6949	20848	20848	13899	48645	55595	170259	6949	0	41696	747053	83392	298821	6949	1129267
347	11,215	52120	52120	38718	8935	29783	8935	23826	2978	29783	11913	5957	10424	0	14891	11913	26805	65522	2978	0	19359	329101	38718	128066	2978	495885
352	11,402	100765	166784	121613	27797	62544	55595	24323	6949	45171	27797	6949	6949	6949	17373	31272	20848	170259	3475	0	34747	736629	66019	250176	3475	1052824
357	11,568	59764	41696	30577	11119	6949	18068	2780	1390	37526	6949	0	12509	4170	11119	26408	18068	65324	0	0	4170	259905	34747	125088	1390	419740
367	11,890	51507	60091	24527	12264	28206	8585	3679	2453	47828	8585	1226	2453	4905	7358	2453	24527	52733	0	0	9811	272250	22074	91977	0	386301
372	12,050	125088	76443	76443	32430	55595	50962	11582	2316	74126	16215	2316	2316	11582	25481	25481	60228	101924	0	2316	16215	597643	41696	220062	2316	859401
377	12,206	48645	49638	26805	3971	39711	8935	2978	0	36732	8935	0	1986	4964	10920	9928	8935	41696	2978	0	9928	251169	22834	73464	2978	347467
382	12,358	86796	37016	17870	8935	52333	0	5106	2553	51056	10211	1276	2553	5106	12764	10211	24252	51056	0	0	12764	299956	35739	103389	0	439084
387	12,510	20848	9786	1276	1702	4255	9360	851	1276	11488	1702	851	426	0	4680	7233	13190	26805	426	851	2127	74457	4680	53184	1276	132321
392	12,656	114664	38221	27797	10424	27797	26060	6949	3475	69493	13899	1737	5212	1737	36484	12161	27797	97291	3475	0	5212	350941	27797	178945	3475	557684
397	12,773	55960	50474	4389	17556	10973	0	1097	3292	41696	5486	1097	3292	4389	5486	10973	18654	50474	0	0	6584	232620	19751	86684	0	339054

(cm)	(cal yr BP)	FUSC	LMEN	DACU	PFER	PTAX	PODO	METR	HALO	PHY	COP	DRA	HEB	MYR	API	ASTR	ASTL	POA	CYP	ISO	CYA	TTRE	TSHR	THER	TAQU	TTAC
402	12,890	179814	104240	36484	15636	54726	5212	10424	0	70362	23454	2606	5212	7818	20848	5212	26060	148542	5212	2606	18242	557684	49514	229328	7818	836526
407	13,007	71129	34338	1226	1226	7358	13490	6132	1226	46601	8585	0	0	0	8585	26980	26980	77260	1226	0	4905	223196	12264	142257	1226	377717
411	13102	28819	19622	6745	1840	6132	6745	2453	0	23301	3066	1226	613	2453	3679	9198	10424	41696	0	0	3066	110985	13490	71129	0	195603
416	13,217	102895	64562	8070	2018	46404	6053	20176	0	82720	20176	4035	4035	2018	36316	22193	24211	104913	2018	2018	6053	379299	52456	199737	4035	631493
421	13,308	98681	34747	2780	0	23628	36137	9729	1390	65324	8339	0	1390	1390	11119	29187	22238	80612	2780	0	9729	301601	20848	148716	2780	471165
426	13,388	60	28	1	6	22	8	5	1	46	9	2	4	2	7	13	10	55	4	0	3	199	20	87	4	306
431	13,465	38017	12264	3679	7971	3066	0	1840	2453	22688	4292	1226	1226	613	9811	5519	9811	30046	1226	0	1226	118343	9811	57639	1226	185793
436	13,543	130774	53068	3791	32220	0	13267	7581	1895	87183	32220	0	0	1895	11372	39801	17058	108031	3791	0	3791	363892	45487	176260	3791	585639
441	13,623	63378	15845	1668	2502	6671	8339	6671	834	30855	8339	834	0	1668	9173	10007	12509	45866	2502	834	2502	159279	13343	81724	3336	254346
446	13,698	173733	44012	6949		6949	18532	16215	2316	115822	23164	0	4633	13899	32430	32430	18532	125088	4633	0	11582	414644	71810	215429	4633	701883
451	13,778	63307	11441	4576	0	16017	1526	8390	1526	54917	9153	0	2288	3051	12204	11441	4576	31272	0	0	3051	171615	20594	67883	0	260092
456	13,858	74863	18005	4738	948	11372	3791	1895	0	41696	17058	948	1895	948	4738	11372	16110	64439	948	0	2843	167732	26534	102345	948	296610

(cm)	(cal yr BP)	FUSC	LMEN	DACU	PFER	PTAX	PODO	METR	HALO	PHY	COP	DRA	HEB	MYR	API	ASTR	ASTL	POA	CYP	ISO	CYA	TTRE	TSHR	THER	TAQU	TTAC
461	13,937	163577	43300	4811	0	3207	20848	3207	3207	96222	14433	0	3207	9622	8019	24055	16037	105844	1604	0	11226	364038	33678	157162	1604	554878
464	13,993	93816	34250	1489	10424	2978	0	2978	0	67011	2978	0	0	2978	7446	23826	32761	93816	1489	0	14891	276981	10424	162317	1489	449721
469	14,088	348459	134023	4467	4467	67011	17870	4467	0	214437	31272	0	4467	17870	35739	62544	116153	223371	4467	0	49142	906888	80414	460145	4467	1447447
474	14,190	151148	26060	5212	1737	8687	19111	19111	1737	55595	19111	1737	5212	13899	12161	22585	10424	85129	3475	0	6949	330093	55595	142461	3475	528149
479	14,292	50307	3626	906	906	4079	2719	3173	0	21301	8611	0	3173	453	4079	5892	2719	16769	453	0	2266	92456	17222	31725	453	141404
484	14,394	65925	6762		0	1127	11269	0	1127	28173	4508	0	1127	1127	2817	10142	3944	31554	564	0	1127	117763	8452	48458	564	174672
489	14,496	114115	25237	2195	0	3292	12070	6584	1097	53766	15362	1097	2195	6584	4389	12070	7681	65836	0	0	2195	227134	27432	92170	0	346735
494	14,597	74457	4765	1191	596	0	0	3574	596	35739	2978	0	0	1191	1787	10126	1191	30974	0	0	0	129258	4765	46461	0	180484
497	14,658	55595	10424	1986	1489	993	8439	1489	1489	21344	6453	0	1986	993	1489	7942	2978	26308	0	0	1489	105233	9431	40207	0	154871
502	14,759	30403	5212	1158	0	579	1158	1448	0	11003	7818	0	869	0	0	4633	290	12740	0	0	1158	60228	8687	19400	0	88314
507	14,859	66808	11372	2843	474	948	4738	474	2369	18479	4738	0	948	3791	1422	5686	0	12319	0	0	474	116086	9476	21322	0	146884
512	14,958	59566	1861		1117	0	9307	1861	745	13775	2234	0	0	745	0	4840	372	14519	0	0	0	92327	2978	20476	0	115781

(cm)	(cal yr BP)	FUSC	LMEN	DACU	PFER	PTAX	PODO	METR	HALO	PHY	COP	DRA	HEB	MYR	API	ASTR	ASTL	POA	CYP	ISO	CYA	TTRE	TSHR	THER	TAQU	TTAC
517	15,058	54777	8993	2453	818	409	0	2453	2044	17169	3270	409	409	0	818	10220	0	14308	818	0	818	94838	4905	26162	818	125906
522	15,160	61813	2926	1097	366	366	4023	732	2926	10973	3292	0	366	2926	732	5852	0	12070	0	0	1829	87781	6949	20482	0	115213
532	15,361	52436	5370	1264	0	0	6318	1579	632	10108	632	0	0	1895	316	3791	0	7897	0	0	948	78654	2843	12319	0	93816
537	15,461	40321	458	229	229	0	2291	458	1146	6186	4353	0	0	687	229	2291	0	9393	0	0	229	52693	5269	12830	0	70792
542	15,564	24031	1592	637	159	0	3501	477	1114	6684	2228	159	477	0	0	637	159	4456	0	0	159	40264	3183	5252	0	48698
547	15,667	51063	2115	1209	302	0	3021	906	1813	10575	604	0	1209	604	0	6949	302	9064	0	0	0	72213	3021	18431	0	93665
557	15,872	76159	10211	426	0	0	4255	1702	2978	4680	5531	426	1276	1702	0	6382	0	15317	0	0	0	102113	9360	23826	0	135299

A4.3 Adelaide Tarn quantitative and qualitative temperature reconstructions

age (cal yr BP)	PTP index	modern analogue technique (°C)	partial least squares (°C)
-15	0,10	7,9	8,6
374	0,08	7,5	7,1
764	0,09	7,9	8
904	0,00	7,9	8
962	0,02	7,8	7,7
1014	-0,06	7,6	8
1064	0,26	7,9	7,6
1112	0,21	7,6	8,2
1200	-0,02	7,9	7,9
1334	0,24	7,9	8,1
1475	0,16	8,3	8,1
1601	0,13	7,7	8,1
1752	0,00	7,8	7,7
1890	0,07	7,8	8,3
2028	0,19	8,1	8,4
2182	0,16	7,8	8,2
2275	0,07	8,1	8,2
2426	-0,23	7,8	7,5
2557	0,24	7,7	8
2667	0,20	8,1	8,5
2780	0,31	8,4	8,5
2898	0,12	7,6	8,5
3012	0,22	7,5	8
3122	0,34	7,7	8,1
3235	0,01	7,7	7,7
3349	0,13	7,6	7,8
3465	0,28	8	8,4
3577	0,29	7,7	8,1
3691	0,16	7,6	7,7
3841	0,25	8,4	8,6
4009	0,26	7,7	7,8
4175	0,26	7,9	8,3
4344	0,06	7,8	7,8
4511	0,04	7,6	7,9
4678	-0,05	7,7	6,7
4853	0,36	7,7	8,3
5016	-0,01	7,6	7,7
5197	0,13	7,6	8,1
5390	0,21	8,1	7,9
5576	0,06	7,6	7,3
5758	0,21	8,2	8,5
5952	0,29	7,6	7,9
6155	0,37	7,7	7,9
6366	0,13	7,6	7,1

age (cal yr BP)	PTP index	modern analogue technique (°C)	partial least squares (°C)
6584	0,21	7,7	7,7
6819	0,10	7,7	6,9
7062	0,03	7,7	7,4
7311	-0,02	6,8	7
7557	0,28	7,7	7,7
7792	0,20	7,1	7,7
8015	0,09	7,3	7,7
8236	0,19	7	7,2
8456	0,09	7	7
8677	0,30	6,9	7,3
8867	0,10	6,6	6,7
9012	0,31	6,8	7,3
9142	0,30	6,7	6,8
9271	0,28	6,5	6,9
9401	0,04	6,8	6,3
9527	0,17	7	6,6
9650	0,31	6,7	6,9
9773	0,38	6,2	7
9899	0,40	6,8	7,2
10,029	0,24	6,3	7,1
10,156	-0,18	6,7	6,1
10,264	0,17	6,6	6,8
10,635	0,13	6	6,8
10,832	0,20	6,7	7,1
11,020	0,14	6,4	7,1
11,215	0,10	6,6	7,5
11,402	0,17	6,3	7,2
11,568	-0,05	6,6	6,9
11,890	0,10	6,3	6,6
12,050	0,20	5,9	7,1
12,206	0,21	6,4	7,2
12,358	0,21	6,4	7
12,510	-0,38	7	6,6
12,656	-0,03	6,2	6,9
12,773	-0,12	6	6,1
12,890	-0,01	6,6	7,1
13,007	-0,59	7,2	6,4
13,102	-0,27	7	6,8
13,217	-0,16	7,3	6,9
13,308	-0,29	7,1	6,9
13,388	-0,10	6,3	6,5
13,465	-0,16	6,6	6,5
13,543	-0,27	7,1	6,1
13,623	-0,37	7,2	6,7
13,698	-0,55	7,6	6,9
13,778	-0,06	7,2	6,9
13,858	-0,30	7,7	6,9

age (cal yr BP)	PTP index	modern analogue technique (°C)	partial least squares (°C)
13,937	-0,60	7,6	6,4
13,993	-0,49	7,3	6,3
14,088	-0,34	7,1	6,7
14,190	-0,40	7,5	7,1
14,292	-0,20	8	7,5
14,394	-0,67	7,6	6,2
14,496	-0,57	7,7	6,6
14,597	-0,56	7,5	6,6
14,658	-0,41	7,3	6,4
14,759	-0,43	7,8	7,3
14,859	-0,26	7,5	6,7
14,958	-0,41	7,5	7
15,058	-0,35	7,5	6,6
15,160	-0,35	7,5	7
15,361	-0,36	7,7	7,3
15,461	-0,46	7,7	7,3
15,564	-0,21	7,7	7,1
15,667	-0,38	7,5	7,1

A4.4 Moanatuatua pollen percentage

taxon	code
Fuscospora	FUSC
Dacrydium cupressinum	DACU
Prumnopitys ferruginea	PFER
Prumnopitys taxifolia	PTAX
Podocarpus spp.	POSP
Prumnopitys spp.	PRSP
Podocarpus/Prumnopitys	PDPR
Podocarpoid	PODO
Metrosideros	METR
Nestegis	NEST
Phyllocladus	PHY
Agathis	AGA
Ascarina	ASCA
Coprosma	COP
Griselinia	GRIS
Myrsine	MYR
Apiaceae	API
Poaceae	POA
Pinus	PIN
other terrestrial	OTTE
Pteridium	PTER
Epacris	EPAC
Leptospermum	LEPT
Empodisma	EMPO
Sporadanthus	ESPO
Gleichenia	GLEI
Dicksonia	DICK
Cyathea	CYA
Undifferentiated and unknown	UAU
total trees	TTRE
total shrubs	TSHR
total herbs	THER
total wetland	TWET
Microscopic CHAR (particles*cm^{-2}*yr^{-1})	MICH
Principal Component 1	PC1
Principal Component 2	PC2
Principal Component 3	PC3

cm	cal yr BP	FUSC	DACU	PFER	PTAX	POSP	PRSP	PDPR	PODO	METR	NEST	PHY	AGA	ASCA	COP	GRIS	MYR	API	POA	PIN	OTTE	PTER	EPAC	LEPT	EMPO	ESPO	GLEI	DICK	CYA	UAU	TTRE	TSHR	THER	TWET	MICH	PC1	PC2	PC3
1	-92	6	41	4	8	0	2	3	1	2	2	2	0	0	5	0	0	2	12	4	6	32	0	0	11	42	1	1	16	14	78	5	17	53	1457	-1.0	1.1	-3.3
6	54	3	55	3	11	3	3	5	1	3	1	6	0	1	0	0	1	0	0	0	5	0	0	1	18	6	0	0	8	8	96	2	2	24	2557	-1.2	0.1	-2.4
11	212	1	48	3	17	2	1	5	1	2	1	6	0	0	2	0	2	1	2	0	6	0	0	0	22	14	0	0	3	4	91	5	4	36	8194	-0.9	0.1	-3.6
16	391	3	58	1	16	1	3	8	0	2	2	4	0	0	0	0	2	0	0	0	1	0	1	2	12	15	0	0	5	7	98	2	0	29	2296	0.1	0.3	-2.9
21	558	5	38	5	25	2	1	3	0	1	3	10	1	1	0	0	1	2	0	0	1	0	2	3	15	21	2	1	5	0	96	3	2	41	1261	0.5	1.6	-1.5
26	720	2	53	3	30	0	1	1	0	2	2	5	0	1	0	0	1	0	0	0	0	0	1	1	19	18	0	0	6	1	99	1	0	39	1531	2.4	1.2	-2.1
31	892	1	53	2	32	0	2	2	0	0	1	5	1	0	0	0	0	0	0	0	1	0	0	2	21	22	2	0	10	3	99	1	0	45	14	2.7	0.2	-1.4
36	1066	2	62	2	19	0	1	4	0	1	2	5	0	0	1	0	0	0	0	0	1	0	0	3	25	23	1	0	8	3	99	1	0	51	427	1.1	0.6	-2.2
41	1245	2	59	2	20	0	1	3	0	1	1	6	0	0	0	0	3	0	0	0	2	0	0	5	7	15	0	0	6	3	97	3	0	27	1039	2.1	0.2	-3.2
46	1409	0	56	2	24	0	0	1	0	1	0	8	0	0	1	0	2	0	0	0	4	0	0	4	18	27	1	0	5	2	97	3	0	48	1151	2.3	1.1	-3.2
51	1593	5	52	1	4	4	7	8	6	2	1	2	0	0	0	1	1	0	1	0	6	0	1	0	7	16	0	8	10	22	94	3	4	24	3368	-4.9	-1.7	-0.8
56	1713	2	57	3	13	3	3	8	0	3	1	4	0	0	0	0	0	0	0	0	1	0	0	3	15	5	0	1	5	7	99	1	0	24	3058	-2	-0	-2

cm	cal yr BP	FUSC	DACU	PFER	PTAX	POSP	PRSP	PDPR	PODO	METR	NEST	PHY	AGA	ASCA	COP	GRIS	MYR	API	POA	PIN	OTTE	PTER	EPAC	LEPT	EMPO	ESPO	GLEI	DICK	CYA	UAU	TTRE	TSHR	THER	TWET	MICH	PC1	PC2	PC3
																																			6	.6	.7	.6
61	1792	2	52	3	26	1	1	3	1	2	2	3	0	1	0	0	0	0	0	0	3	0	0	1	9	6	0	1	8	4	98	2	0	16	1866	0.6	-0.6	-1.7
67	1879	2	50	2	29	0	1	1	0	2	1	5	0	2	0	0	1	0	0	0	3	0	1	1	21	9	1	0	8	2	97	3	0	31	3947	1.5	1.4	-2.2
71	1928	2	59	5	19	1	1	4	0	0	2	4	0	1	0	0	2	0	0	0	0	0	1	2	10	24	5	0	6	5	97	3	0	37	5267	1.5	1.0	-1.5
76	1985	1	58	2	23	0	2	2	0	1	3	6	0	0	0	0	1	0	0	0	1	0	1	0	6	36	9	0	8	5	99	1	0	43	1679	2.1	1.5	-1.4
81	2040	2	57	4	23	1	3	3	0	2	1	2	0	0	0	0	0	0	0	0	1	0	0	0	8	13	1	0	9	3	99	0	0	21	12631	0.0	-0.9	-1.4
86	2098	2	59	2	23	0	2	1	0	2	2	4	1	0	0	0	0	0	0	0	1	0	1	0	24	13	3	0	10	0	99	1	0	38	5573	1.2	0.7	-1.1
91	2153	3	58	1	26	0	1	2	0	1	1	3	0	0	0	0	1	1	0	0	2	0	0	2	13	20	1	0	7	2	97	2	1	35	6615	1.3	1.1	-2.0
96	2210	2	54	1	12	4	5	5	3	2	0	4	0	1	0	1	1	0	1	0	3	0	2	0	15	12	0	1	11	18	94	4	2	28	14619	-3.4	0.0	-1.3
100	2252	2	57	4	16	2	4	7	2	1	0	2	0	0	0	0	1	0	0	0	2	0	0	1	26	10	0	1	4	7	99	1	0	37	4642	-1.6	-1.6	-2.3
105	2318	2	54	2	22	0	3	5	5	2	0	4	0	0	0	0	0	0	0	0	2	0	1	3	10	10	0	0	5	2	99	1	0	24	13911	-0.7	-0.9	-2.6
110	2391	2	50	5	24	1	2	3	1	2	1	5	0	0	0	0	1	0	0	0	2	0	0	1	17	12	0	1	13	1	98	2	0	31	10364	0.0	0.0	-2.5
115	2466	1	62	3	17	2	2	4	0	0	1	5	0	0	0	0	1	0	0	0	2	0	0	1	12	16	2	0	10	4	98	1	1	29	2120	0.	-0	-1

cm	cal yr BP	FUSC	DACU	PFER	PTAX	POSP	PRSP	PDPR	PODO	METR	NEST	PHY	AGA	ASCA	COP	GRIS	MYR	API	POA	PIN	OTTE	PTER	EPAC	LEPT	EMPO	ESPO	GLEI	DICK	CYA	UAU	TTRE	TSHR	THER	TWET	MICH	PC1	PC2	PC3
																																				5	.6	.2
120	2542	2	63	2	19	1	0	1	2	0	1	5	0	1	0	0	1	0	0	0	0	0	1	3	7	24	4	1	7	3	97	3	0	35	4735	0.9	1.0	-0.3
125	2618	1	58	5	24	0	2	2	0	1	1	2	0	0	0	0	2	0	0	0	1	0	0	1	12	21	6	1	7	6	97	3	0	35	4247	1.5	0.5	-1.1
130	2693	1	53	2	25	1	1	3	2	1	2	3	0	2	0	0	2	0	0	0	2	0	0	1	10	26	4	1	7	4	95	5	0	37	5698	0.5	1.3	-0.7
135	2769	3	50	1	30	1	1	2	0	1	2	5	0	1	0	0	2	0	0	0	0	0	0	1	13	15	1	0	8	2	96	3	0	29	3761	1.3	1.2	-1.6
140	2844	1	48	2	33	0	1	2	0	1	3	5	0	0	0	0	1	1	0	0	2	0	0	2	14	17	2	0	9	2	98	1	1	33	8592	1.6	1.7	-1.9
145	2919	3	55	1	8	9	1	7	1	2	1	6	0	2	1	1	1	0	0	0	2	0	0	2	25	4	0	1	7	8	95	5	0	31	33178	-4.0	-0.1	-2.0
150	2996	1	63	2	11	3	2	6	0	1	1	4	0	1	0	0	2	0	0	0	2	0	0	4	18	6	0	2	7	5	96	4	0	29	32887	-1.6	-0.2	-1.6
155	3071	2	53	6	18	1	5	6	1	1	0	2	0	0	0	0	1	0	0	0	3	0	0	2	11	3	0	0	7	5	98	2	0	16	6441	-0.9	-1.5	-2.6
160	3158	1	52	2	22	1	3	4	3	1	3	4	0	1	1	0	1	0	0	0	1	0	0	2	11	14	0	0	7	5	97	3	0	28	1440	0.2	-0.3	-1.9
165	3252	2	56	2	23	1	1	4	0	1	1	5	0	1	0	0	1	0	0	0	2	0	1	1	16	21	9	1	8	2	98	2	0	38	799	0.2	0.9	-0.7
170	3344	2	64	2	23	1	0	2	0	2	0	2	0	0	0	0	1	1	0	0	0	0	1	13	11	12	7	2	11	2	98	1	1	37	5924	1.0	1.5	0.3
175	3439	3	56	2	21	0	1	6	0	0	1	5	0	1	0	0	4	0	0	0	1	0	0	2	14	28	7	2	8	6	95	5	0	45	11598	1.7	1.2	-1.

cm	cal yr BP	FUSC	DACU	PFER	PTAX	POSP	PRSP	PDPR	PODO	METR	NEST	PHY	AGA	ASCA	COP	GRIS	MYR	API	POA	PIN	OTTE	PTER	EPAC	LEPT	EMPO	ESPO	GLEI	DICK	CYA	UAU	TTRE	TSHR	THER	TWET	MICH	PC1	PC2	PC3
																																						2
180	3532	1	63	3	21	0	1	1	0	1	2	2	0	1	0	1	1	0	0	0	1	0	0	2	15	25	2	2	9	3	97	3	0	42	1798	1.6	0.8	-0.3
185	3626	1	60	3	23	0	3	0	0	1	0	4	0	0	0	0	2	0	0	0	2	0	0	2	15	17	3	0	6	1	97	2	0	34	2581	2.1	0.7	-1.4
190	3726	2	59	3	4	13	2	5	1	2	1	3	0	0	0	0	2	2	0	0	3	0	0	1	22	11	0	0	6	8	95	3	2	34	6417	-3.6	-0.7	-2.0
195	3827	2	65	3	15	3	2	3	0	1	1	2	0	0	0	0	1	0	0	0	1	0	1	1	22	6	0	1	11	4	98	2	0	30	5488	-0.9	-0.9	-0.7
198	3888	2	58	2	20	1	2	6	0	1	1	1	0	0	0	0	1	0	0	0	4	0	0	2	16	14	4	1	2	10	98	2	0	32	5249	0.3	-0.1	-2.2
203	3987	1	60	5	16	1	4	6	0	0	2	3	0	0	0	0	1	0	0	0	1	0	0	4	15	15	0	0	8	4	97	3	0	34	272	0.3	-0.6	-2.0
208	4088	1	62	3	15	2	4	3	0	3	1	2	0	1	0	0	2	0	0	0	2	0	2	4	16	19	2	2	6	7	96	4	0	40	2017	-1.0	0.9	-1.3
213	4191	1	54	0	27	1	1	5	1	2	2	3	0	0	0	0	1	0	0	0	2	0	0	2	12	14	1	0	6	4	98	2	0	27	6050	0.4	0.8	-1.5
218	4291	3	71	2	16	0	2	3	0	1	0	0	0	1	0	0	1	0	0	0	0	0	2	1	15	28	2	0	8	2	98	2	0	46	502	0.7	0.5	-0.3
223	4393	2	65	1	25	0	0	0	1	0	0	2	0	0	0	0	0	1	0	0	1	0	1	6	9	32	0	1	10	2	99	1	1	48	143	1.8	1.0	-0.5
228	4495	1	62	1	21	0	0	4	1	1	2	2	0	1	1	0	0	0	0	0	3	0	0	3	17	11	0	1	10	3	96	3	0	31	3251	0.1	-0.3	0.0
233	4595	2	57	2	19	1	1	4	1	1	2	4	0	1	0	0	2	0	0	0	2	0	0	3	24	5	0	0	6	2	96	4	0	32	3057	0.	0.	-2

cm	cal yr BP	FUSC	DACU	PFER	PTAX	POSP	PRSP	PDPR	PODO	METR	NEST	PHY	AGA	ASCA	COP	GRIS	MYR	API	POA	PIN	OTTE	PTER	EPAC	LEPT	EMPO	ESPO	GLEI	DICK	CYA	UAU	TTRE	TSHR	THER	TWET	MICH	PC1	PC2	PC3
																																				1	1	.3
238	4698	4	57	2	6	7	2	7	2	2	1	4	0	0	0	1	1	1	0	0	5	0	0	0	21	4	0	0	10	4	97	3	1	25	3228	-3.8	-1.0	-2.0
243	4801	4	57	4	14	2	1	2	1	0	2	4	0	1	1	0	0	0	0	0	5	0	1	3	21	9	0	2	9	5	95	4	1	34	8817	-1.2	-0.1	-1.3
248	4906	3	60	3	15	1	2	4	1	2	2	3	0	1	0	0	0	1	0	0	3	0	0	1	14	25	4	3	13	4	97	2	1	41	4062	-1.1	0.8	0.0
253	5006	2	61	1	18	1	3	5	1	2	1	1	0	1	0	1	1	0	0	0	4	0	0	0	30	17	5	1	8	6	98	2	0	47	1562	-1.1	0.1	-0.2
258	5104	3	52	1	28	1	1	2	0	2	0	4	0	1	0	0	1	0	0	0	2	0	0	1	24	23	9	1	8	1	97	3	0	47	3742	0.7	1.7	-1.2
263	5203	2	46	2	30	0	1	4	1	2	1	4	0	2	1	0	1	0	0	0	2	0	1	1	15	17	7	0	8	5	96	3	0	34	788	1.0	2.0	-1.8
268	5307	3	61	2	20	1	1	2	0	2	0	3	0	1	0	0	1	1	0	0	3	0	1	1	15	19	3	0	13	5	96	3	1	36	5527	-0.2	1.4	-0.7
273	5411	6	59	1	21	1	1	0	0	2	1	0	0	1	1	0	1	0	0	0	3	0	0	1	10	28	3	0	7	1	96	4	0	40	4180	1.4	1.3	-1.3
278	5519	3	58	1	19	1	1	5	0	3	0	2	0	1	0	1	1	0	0	0	3	0	0	2	20	8	1	1	8	4	97	3	0	31	1642	-1.2	0.2	-1.3
283	5624	3	55	0	8	12	2	5	1	3	0	4	0	0	0	1	1	1	0	0	4	0	0	1	36	8	0	2	9	8	96	2	2	45	4791	-4.6	0.5	-1.5
288	5727	1	52	1	11	4	6	6	3	2	1	3	0	2	0	0	1	2	0	0	4	0	2	0	14	21	6	3	9	9	94	3	2	36	40247	-5.0	0.8	0.2
293	5830	1	55	6	14	4	4	6	1	2	1	2	0	0	1	0	0	1	0	0	2	0	0	0	24	22	6	6	7	7	98	1	1	47	3166	-3	-1	0.

cm	cal yr BP	FUSC	DACU	PFER	PTAX	POSP	PRSP	PDPR	PODO	METR	NEST	PHY	AGA	ASCA	COP	GRIS	MYR	API	POA	PIN	OTTE	PTER	EPAC	LEPT	EMPO	ESPO	GLEI	DICK	CYA	UAU	TTRE	TSHR	THER	TWET	MICH	PC1	PC2	PC3
																																				.0	.3	0
297	5915	3	59	3	17	2	3	4	0	3	0	2	0	1	0	0	0	1	0	0	1	0	0	1	23	21	9	0	5	5	98	2	1	45	492	-0.7	1.2	-1.6
302	6022	2	63	2	17	2	3	4	2	0	1	2	0	1	0	0	1	0	0	0	1	0	0	0	19	19	2	1	9	7	98	2	0	38	1212	-0.5	-1.1	0.0
307	6125	1	60	1	23	0	1	2	1	3	2	2	0	1	0	0	0	1	0	0	1	0	0	2	17	17	9	2	8	3	98	1	1	37	3050	0.3	1.2	0.8
312	6226	2	61	2	18	1	1	2	1	2	1	2	0	1	0	1	1	3	0	0	3	0	0	0	15	20	3	0	5	1	93	3	3	36	3508	0.0	1.4	-1.3
317	6329	2	62	1	23	0	2	1	1	1	1	0	0	2	0	0	1	1	0	0	3	0	0	1	17	24	1	0	9	1	96	3	1	42	965	0.9	1.4	0.0
322	6433	2	64	1	19	0	1	3	0	1	1	2	0	2	0	0	2	0	0	0	1	0	0	1	29	26	6	1	12	2	95	5	0	57	3855	0.5	2.3	0.3
327	6536	0	60	4	6	7	3	8	2	3	1	1	0	1	1	0	0	1	0	0	2	0	1	0	39	7	0	3	13	8	96	3	1	48	6893	-5.0	-1.3	0.4
332	6638	2	61	3	10	9	2	7	0	1	1	0	0	1	0	0	1	0	0	0	1	0	1	1	35	13	0	4	15	8	97	2	0	50	1032	-3.0	-1.1	0.4
337	6742	2	66	3	10	2	2	5	2	1	1	0	0	0	0	1	2	0	0	0	2	0	0	0	25	24	6	1	9	7	96	3	1	50	2113	-1.4	0.2	-0.3
342	6844	2	65	1	21	0	1	2	0	1	0	0	0	0	0	0	2	0	0	0	3	0	1	2	15	17	2	1	10	5	97	3	0	34	3175	0.8	0.7	-0.3
346	6927	2	64	2	20	0	1	1	0	2	0	2	0	2	0	0	1	0	0	0	3	0	1	1	12	21	2	1	7	5	96	3	0	34	13325	0.0	0.5	-0.2
351	7028	3	58	0	24	0	0	4	3	0	1	2	0	1	0	0	1	0	0	0	2	0	0	1	22	20	2	1	6	3	97	3	0	43	4401	0.4	1.1	0.0
356	7129	3	61	1	20	0	1	2	3	0	1	0	0	1	0	0	2	2	0	0	3	0	0	0	50	11	0	0	9	7	95	3	2	62	130	0.	0.	-0

cm	cal yr BP	FUSC	DACU	PFER	PTAX	POSP	PRSP	PDPR	PODO	METR	NEST	PHY	AGA	ASCA	COP	GRIS	MYR	API	POA	PIN	OTTE	PTER	EPAC	LEPT	EMPO	ESPO	GLEI	DICK	CYA	UAU	TTRE	TSHR	THER	TWET	MICH	PC1	PC2	PC3
																																				0	7	.4
361	7230	3	68	1	17	0	1	0	1	1	1	0	0	2	0	1	2	0	0	0	2	0	0	1	22	38	6	1	9	4	95	5	0	61	8388	0.5	2.6	1.1
366	7330	2	64	1	18	0	0	3	0	1	2	0	0	4	0	0	1	1	0	0	3	0	0	2	23	46	9	1	12	5	94	6	1	70	1857	0.6	2.8	1.8
371	7432	2	64	2	17	0	0	4	0	2	1	1	0	3	0	1	1	0	0	0	3	0	0	3	17	35	15	3	10	5	94	5	0	55	5090	0.9	2.6	1.2
376	7531	2	57	1	22	2	1	4	1	1	2	0	0	4	0	0	1	0	0	0	2	0	0	1	26	36	9	8	13	5	94	6	0	63	6558	-1.0	1.7	2.8
381	7632	2	55	1	18	1	3	6	0	1	2	1	0	3	0	0	3	1	0	0	2	0	0	2	39	14	0	2	13	4	92	6	2	55	8576	-2.0	1.6	-0.5
386	7733	3	58	2	15	4	1	7	0	1	1	0	0	1	0	1	3	1	0	0	3	0	1	0	27	25	4	0	10	5	94	5	1	53	6187	-2.0	1.6	0.1
391	7835	1	70	1	11	1	1	4	2	1	1	0	0	4	0	1	1	0	0	0	0	0	2	2	23	22	3	2	12	8	93	7	0	49	11087	-1.7	1.0	2.0
395	7921	3	60	5	18	0	2	4	1	1	1	1	0	1	0	0	1	0	0	0	2	0	1	2	15	29	2	0	12	6	97	2	0	47	15885	-0.6	1.8	-1.0
400	8023	2	63	3	21	0	1	1	0	0	2	0	0	2	0	0	2	1	0	0	2	0	1	1	18	19	4	0	9	5	95	4	1	38	3503	1.5	0.8	0.5
405	8123	2	65	1	14	0	1	3	0	2	1	0	0	4	0	0	3	1	0	0	1	0	1	0	13	31	1	0	9	9	91	7	1	46	4219	-0.2	2.2	0.1
410	8222	3	60	2	20	0	2	1	0	1	1	1	0	1	0	0	1	3	0	0	2	0	0	2	17	22	8	0	10	4	94	3	4	41	4004	1.2	1.7	-0.7
415	8324	2	69	0	14	2	0	2	1	1	1	1	0	3	0	0	2	0	0	0	3	0	1	1	22	21	7	0	11	4	93	6	2	44	2370	-0.3	2.5	1.1
420	8427	1	67	1	3	6	6	6	1	0	0	0	0	3	0	1	1	1	0	0	2	0	2	1	33	14	0	3	16	6	94	5	1	49	1027	-5	-0	1.

cm	cal yr BP	FUSC	DACU	PFER	PTAX	POSP	PRSP	PDPR	PODO	METR	NEST	PHY	AGA	ASCA	COP	GRIS	MYR	API	POA	PIN	OTTE	PTER	EPAC	LEPT	EMPO	ESPO	GLEI	DICK	CYA	UAU	TTRE	TSHR	THER	TWET	MICH	PC1	PC2	PC3
																																			6	.1	.7	6
425	8528	1	66	4	10	3	3	5	0	1	1	1	0	3	0	0	0	1	0	0	2	0	1	1	29	17	0	2	14	7	95	4	1	48	7586	-2.6	-0.4	0.9
430	8631	2	62	3	10	5	2	5	1	2	0	0	0	2	0	0	2	2	0	0	1	0	0	1	27	18	5	1	12	9	93	5	2	47	11021	-2.8	0.4	1.0
435	8730	2	69	3	16	0	1	2	0	0	1	1	0	1	0	0	1	0	0	0	2	0	1	1	10	30	7	3	12	8	98	2	0	41	3032	0.7	0.4	1.4
440	8831	2	72	1	6	4	2	2	3	1	1	0	0	3	0	0	1	1	0	0	2	0	0	0	24	29	12	2	12	9	95	4	1	53	489	-1.6	0.3	2.7
445	8939	2	67	1	17	0	0	2	0	1	2	0	0	4	0	0	1	0	0	0	3	0	0	2	28	21	10	1	13	3	94	7	0	51	2420	1.4	2.3	1.7
450	9045	0	70	2	14	1	2	4	0	0	2	0	0	2	0	0	0	0	0	0	2	0	1	2	15	21	8	0	18	9	97	3	0	39	5478	0.0	0.5	2.0
455	9148	1	65	2	20	0	1	0	2	0	3	0	0	4	0	0	1	0	0	0	0	0	1	3	9	25	9	1	19	3	95	5	0	38	5063	1.8	1.9	2.3
460	9250	2	71	1	15	0	1	3	1	0	1	0	0	3	0	0	0	0	0	0	1	0	1	1	16	16	9	2	17	3	96	3	0	34	2266	-0.3	0.7	2.9
465	9352	2	66	1	10	4	2	1	3	0	1	1	0	4	0	0	1	1	0	0	3	0	1	3	17	17	5	1	18	7	93	6	1	38	13361	-2.0	1.2	1.7
470	9457	1	67	1	14	0	1	2	0	1	1	1	0	7	0	2	0	0	0	0	2	0	0	3	14	18	11	3	16	2	91	9	0	35	5245	0.4	1.2	2.9
475	9560	2	65	0	12	1	0	5	2	1	2	0	0	5	0	0	3	0	0	0	3	0	1	2	19	9	8	1	18	11	92	8	0	30	15216	-1.3	1.6	2.7
480	9661	1	61	2	18	1	3	5	1	1	1	1	0	3	0	1	1	0	0	0	2	0	0	1	15	20	4	1	19	5	95	5	0	36	2471	-0.5	0.4	1.6
485	9762	2	60	1	14	2	0	4	0	0	2	0	0	10	0	0	2	1	0	0	1	0	1	3	18	12	7	1	18	8	86	13	1	33	2478	-0.	2.2	2.5

cm	cal yr BP	FUSC	DACU	PFER	PTAX	POSP	PRSP	PDPR	PODO	METR	NEST	PHY	AGA	ASCA	COP	GRIS	MYR	API	POA	PIN	OTTE	PTER	EPAC	LEPT	EMPO	ESPO	GLEI	DICK	CYA	UAU	TTRE	TSHR	THER	TWET	MICH	PC1	PC2	PC3
																																				1		
490	9862	3	51	0	24	1	1	1	2	1	2	1	0	10	0	0	1	1	0	0	2	0	1	2	11	14	7	1	17	5	88	11	1	29	4133	0.0	2.9	1.8
495	9961	2	66	0	19	0	2	2	1	1	2	0	0	4	0	0	0	0	0	0	0	0	1	0	18	10	7	1	22	6	96	4	0	30	4325	-0.6	1.0	3.2
500	10,067	1	56	1	25	0	1	1	1	2	3	1	0	6	0	0	1	0	0	0	3	0	0	3	11	12	5	2	17	4	93	7	0	27	1768	0.8	1.7	1.6
505	10,169	1	58	1	21	0	0	3	1	2	2	2	0	7	0	0	1	0	0	0	1	0	0	2	27	25	10	2	18	6	92	8	0	54	9988	0.6	3.0	2.0
510	10,277	1	52	2	24	0	1	2	1	2	2	0	0	11	0	0	1	0	0	0	0	0	1	6	18	8	6	1	20	2	88	12	0	32	14028	-0.1	2.7	1.8
515	10,38	3	54	0	6	12	5	5	1	1	1	0	0	8	0	1	0	1	0	0	2	0	0	1	21	12	0	2	20	5	89	9	2	33	10639	-5.3	0.1	2.6
520	10,481	0	49	0	31	3	0	6	0	1	0	0	0	7	0	0	0	1	0	0	1	0	1	2	19	12	9	2	18	3	93	7	1	34	2723	0.1	1.6	3.3
525	10,606	1	52	1	22	6	1	8	1	0	1	0	0	4	0	0	1	0	0	0	3	0	0	0	18	7	8	3	16	5	93	6	1	26	1045	-1.1	-0.7	2.6
530	10,733	0	59	1	21	1	1	5	1	0	1	1	0	9	0	0	0	0	0	0	0	0	1	1	7	18	7	2	17	8	91	9	0	27	13910	0.1	0.4	3.1
535	10,858	1	49	1	25	0	4	5	0	2	1	0	0	8	0	0	1	1	0	0	1	0	0	4	5	21	10	1	18	6	89	10	1	30	4867	0.4	2.1	1.8
540	10,981	1	41	1	36	0	1	3	0	3	0	0	0	12	0	0	1	0	0	0	1	0	0	1	5	17	10	3	15	4	87	13	0	23	4419	1.3	1.8	2.0
545	11,105	3	55	1	26	0	2	4	0	1	0	0	0	5	0	0	1	0	0	0	2	0	0	1	13	21	8	1	20	8	94	6	0	35	10204	-0.2	1.4	2.1
550	11,232	1	45	1	37	0	1	3	1	1	1	0	0	8	0	0	1	0	0	0	1	0	1	1	23	24	13	2	11	2	90	10	0	48	2895	1.1	2.5	2.0
555	11,36	3	42	2	35	0	2	4	0	1	4	0	0	6	0	0	1	0	0	0	1	0	0	2	9	25	14	2	14	3	93	7	0	37	2486	1.	2.	1.

cm	cal yr BP	FUSC	DACU	PFER	PTAX	POSP	PRSP	PDPR	PODO	METR	NEST	PHY	AGA	ASCA	COP	GRIS	MYR	API	POA	PIN	OTTE	PTER	EPAC	LEPT	EMPO	ESPO	GLEI	DICK	CYA	UAU	TTRE	TSHR	THER	TWET	MICH	PC1	PC2	PC3
	3																																			9	6	4
560	11,488	2	57	2	6	9	3	7	1	1	1	0	0	3	0	0	1	0	0	0	8	0	0	1	21	12	0	2	21	7	90	5	6	33	4193	-3.4	-0.9	0.8
565	11,614	1	51	2	18	6	3	6	1	2	1	0	0	5	0	0	1	0	0	0	3	0	0	1	22	11	0	2	17	7	93	6	1	34	6903	-2.6	0.2	0.8
570	11,756	0	53	2	17	6	2	9	2	1	1	0	0	4	0	0	0	0	0	0	3	0	0	1	20	11	9	2	12	7	95	5	0	32	1415	-1.5	-1.0	2.3
575	11,906	2	60	1	23	2	1	4	2	0	0	0	0	3	0	1	1	0	0	0	1	0	1	1	8	20	8	1	7	4	95	5	0	29	943	1.1	-0.6	1.6
580	12,061	1	64	1	26	0	1	3	0	0	2	0	0	2	0	0	0	0	0	0	0	0	0	1	5	15	6	2	8	3	98	2	0	21	19724	2.5	-0.7	1.8
585	12,211	3	63	1	22	0	1	2	1	0	2	0	0	3	0	0	1	0	0	0	1	0	0	2	6	16	5	1	9	4	96	4	1	24	4670	1.9	0.3	1.3
590	12,362	1	63	2	23	0	1	2	1	1	2	0	0	2	0	0	1	0	0	0	1	0	0	1	11	5	7	0	8	3	97	3	0	17	1733	2.2	-0.2	0.2
595	12,515	2	65	1	23	0	1	2	0	0	0	0	0	0	4	0	0	1	0	0	1	0	0	0	4	2	0	2	7	4	96	4	1	6	3982	1.6	-3.7	0.7
600	12,668	1	63	2	22	0	1	1	0	0	1	0	0	0	4	1	0	1	0	0	4	0	0	2	3	5	1	6	13	3	92	7	1	9	2928	2.4	-3.2	2.0
605	12,766	1	61	2	9	5	2	7	1	0	0	0	0	0	9	0	0	0	0	0	3	0	0	1	14	4	0	3	12	7	89	11	0	19	2472	-1.8	-5.5	1.3
610	12,849	1	55	3	21	1	4	4	0	0	1	0	0	0	3	0	0	1	0	0	5	0	0	2	18	4	0	3	12	5	95	4	1	24	4644	-0.5	-2.7	0.1
615	12,936	1	56	4	24	1	3	3	2	0	1	1	0	0	2	0	0	0	0	0	2	0	0	0	11	8	12	1	9	6	98	2	0	20	429	0.9	-2.	0.7

cm	cal yr BP	FUSC	DACU	PFER	PTAX	POSP	PRSP	PDPR	PODO	METR	NEST	PHY	AGA	ASCA	COP	GRIS	MYR	API	POA	PIN	OTTE	PTER	EPAC	LEPT	EMPO	ESPO	GLEI	DICK	CYA	UAU	TTRE	TSHR	THER	TWET	MICH	PC1	PC2	PC3
																																					6	
620	13,02	0	62	4	24	0	2	3	1	0	1	0	0	0	1	0	0	0	0	0	1	0	0	0	7	11	10	2	11	5	98	2	0	18	1065	2.0	-3.1	1.7
625	13,103	1	68	4	18	0	4	2	1	0	1	0	0	0	0	0	0	0	0	0	1	0	0	0	1	10	6	1	12	4	99	1	0	10	4871	1.4	-3.3	1.1
630	13,187	1	60	2	31	0	0	1	1	0	1	0	0	0	0	0	0	1	0	0	1	0	0	0	4	5	7	1	6	4	98	2	1	10	3043	3.1	-1.8	1.4
635	13,271	2	66	2	21	0	1	3	0	1	2	1	0	0	0	0	1	0	0	0	1	0	0	0	11	6	8	1	12	9	98	2	0	16	894	1.4	-1.3	0.8
640	13,355	1	65	1	25	0	1	1	0	0	2	0	0	0	0	0	1	0	0	0	2	0	0	2	3	5	8	2	8	3	98	1	0	11	4361	3.1	-1.2	1.0
645	13,441	0	66	1	29	0	1	1	0	0	1	0	0	0	0	0	0	0	0	0	1	0	0	0	4	11	8	2	7	3	100	0	0	15	1150	2.9	-2.1	1.9
650	13,527	1	51	0	14	9	6	7	3	1	0	1	0	0	2	0	1	0	1	0	4	0	0	1	8	13	0	2	17	13	93	3	4	22	967	-3.5	-3.1	0.6
655	13,611	1	55	3	32	0	1	1	0	0	1	1	0	0	3	0	0	0	0	0	2	0	0	1	20	8	11	1	11	2	97	3	0	29	2661	2.7	-1.6	0.7
660	13,697	2	55	2	17	2	1	6	2	1	1	0	0	0	8	0	0	0	0	0	4	0	0	1	18	8	7	1	11	9	90	9	0	27	871	-0.9	-2.5	0.7
665	13,784	1	58	5	17	1	2	4	1	2	0	0	0	0	8	0	0	0	0	0	1	0	0	1	1	1	2	3	10	7	92	8	0	3	9955	-0.4	-5.2	0.7
670	13,872	1	50	3	19	1	2	4	0	0	1	0	0	0	15	0	1	0	0	0	3	0	0	4	6	2	1	4	10	8	82	18	0	11	21992	1.2	-4.7	0.7
685	13,95	1	53	5	22	1	0	4	3	0	3	0	0	0	5	0	0	1	0	0	3	0	0	0	0	1	0	3	10	8	92	6	3	2	947	1.	-4	0.

cm	cal yr BP	FUSC	DACU	PFER	PTAX	POSP	PRSP	PDPR	PODO	METR	NEST	PHY	AGA	ASCA	COP	GRIS	MYR	API	POA	PIN	OTTE	PTER	EPAC	LEPT	EMPO	ESPO	GLEI	DICK	CYA	UAU	TTRE	TSHR	THER	TWET	MICH	PC1	PC2	PC3
	6																																			4	.1	3
690	14,041	1	60	5	22	0	1	3	0	0	1	0	0	0	3	0	1	0	0	0	3	0	0	0	1	2	1	3	13	4	95	4	1	4	5168	1.8	-3.8	1.0
695	14,126	0	78	1	5	3	6	4	1	0	0	0	1	0	1	0	0	0	0	0	1	0	0	0	0	0	0	4	9	4	98	2	0	1	319	-1.4	-6.0	1.7
700	14,204	1	66	1	23	0	0	2	0	0	1	0	0	0	6	0	1	0	0	0	1	0	0	0	1	3	0	3	7	3	92	7	1	4	1386	3.1	-3.9	1.2
705	14,279	1	67	3	13	1	3	5	2	0	1	0	0	0	3	0	0	0	0	0	3	0	0	1	2	1	0	1	10	5	96	3	1	3	321	0.4	-4.6	0.3
710	14,354	2	64	2	21	0	0	2	0	0	0	0	0	0	4	0	1	0	0	0	4	0	1	0	1	3	0	0	7	5	91	8	1	6	94	3.2	-3.0	-0.2
715	14,429	1	63	2	25	0	0	1	0	0	0	0	0	0	7	0	1	0	0	0	0	0	0	0	3	2	0	0	5	3	92	8	0	5	1201	4.1	-4.5	-0.1
719	14,488	2	63	2	26	0	0	1	0	0	1	0	0	2	0	0	0	0	0	0	2	0	0	1	5	12	5	0	6	4	96	3	0	18	10873	3.2	-0.4	0.4
724	14,563	4	59	3	16	0	4	6	0	0	0	0	0	0	4	0	2	1	0	0	1	0	1	0	9	13	0	1	5	5	93	5	2	23	126	-0.4	-2.5	-1.5
729	14,638	3	49	4	28	0	3	1	0	0	1	0	0	0	4	0	3	0	0	0	3	0	1	1	1	7	0	1	5	9	90	8	1	9	38	3.3	-2.5	-2.1

A4.5 Moanatuatua temperature and moisture reconstruction

Age (cal yr BP)	Depth (cm)	modern analogue technique (°C)	partial least squares (°C)	Pollen Moisture Index (PMI) index
-92	1	11,1	11,2	-0,07
54	6	14,2	13,1	0,06
212	11	14,3	12,6	-0,08
391	16	13,8	12,7	-0,01
558	21	14,1	12,8	-0,12
720	26	13,9	12,7	-0,12
892	31	13,9	12,8	-0,16
1066	36	13,9	12,8	0,04
1245	41	13,9	12,7	0,03
1409	46	14,3	12,8	-0,02
1593	51	14	12,3	0
1713	56	13,9	12,7	-0,05
1792	61	14	12,9	-0,12
1879	67	14	13	-0,14
1928	71	13,8	12,4	-0,02
1985	76	13,9	12,9	-0,01
2040	81	14	12,7	-0,08
2098	86	14,2	13,2	0
2153	91	13,9	12,7	-0,03
2210	96	14,4	12,8	-0,04
2252	100	13,8	12,3	-0,08
2318	105	13,6	12,5	-0,09
2391	110	13,8	12,9	-0,16
2466	115	13,9	12,6	0,03
2542	120	14,1	12,8	0,09
2618	125	13,8	12,4	-0,07
2693	130	14,1	12,8	-0,1
2769	135	13,9	12,9	-0,16
2844	140	13,8	12,8	-0,2
2919	145	14,4	13,2	0
2996	150	13,9	12,7	0,1
3071	155	13,7	12,4	-0,14
3158	160	14,1	12,8	-0,1
3252	165	13,9	12,9	-0,06
3344	170	13,8	12,6	0,03
3439	175	13,9	12,5	-0,04
3532	180	14	12,9	0,05
3626	185	14,1	12,7	0
3726	190	13,8	12,6	0,02
3827	195	14	12,6	0,07
3888	198	14	12,3	-0,05
3987	203	14	12,5	-0,03

Age (cal yr BP)	Depth (cm)	modern analogue technique (°C)	partial least squares (°C)	Pollen Moisture Index (PMI) index
4088	208	14	12,7	0,03
4191	213	14,1	13	-0,11
4291	218	12,7	12,3	0,14
4393	223	13,4	12,6	0,06
4495	228	14,2	13,1	0,05
4595	233	14	12,8	-0,01
4698	238	14	13,1	0,06
4801	243	14	12,5	0,05
4906	248	13,9	13	0,05
5006	253	13,9	12,8	0,03
5104	258	14,1	13	-0,12
5203	263	14	13	-0,2
5307	268	13,9	13	0,06
5411	273	13,8	12,7	0,05
5519	278	14,3	13	0
5624	283	14,1	13,3	-0,01
5727	288	14,4	13,1	-0,05
5830	293	14,3	12,5	-0,11
5915	297	13,8	12,6	-0,02
6022	302	13,9	12,6	0,04
6125	307	14,1	13,1	0,02
6226	312	14	12,5	0,09
6329	317	13,6	12,8	0,04
6433	322	14,2	13,1	0,1
6536	327	14,1	12,8	0
6638	332	13,8	12,6	-0,02
6742	337	13,6	12,3	0,13
6844	342	13,3	12,6	0,07
6927	346	13,8	12,8	0,08
7028	351	13,8	12,8	-0,01
7129	356	12,3	12,4	0,06
7230	361	13,6	12,7	0,2
7330	366	13,7	12,8	0,12
7432	371	14	13	0,11
7531	376	13,2	12,7	-0,04
7632	381	14,1	13,1	-0,05
7733	386	13,7	12,6	-0,01
7835	391	14,3	12,9	0,22
7921	395	13,7	12,6	0
8023	400	13,7	12,4	0,07
8123	405	14	12,9	0,17
8222	410	14,1	12,7	0,05
8324	415	13,6	12,9	0,22
8427	420	13,8	12,8	0,14
8528	425	14,1	12,8	0,1
8631	430	13,7	12,5	0,07
8730	435	13,9	12,6	0,13

Age (cal yr BP)	Depth (cm)	modern analogue technique (°C)	partial least squares (°C)	Pollen Moisture Index (PMI) index
8831	440	13,3	12,6	0,31
8939	445	13,9	13	0,17
9045	450	14,1	13	0,15
9148	455	13,9	13	0,11
9250	460	13,9	13	0,21
9352	465	14	13	0,2
9457	470	14,2	13,4	0,2
9560	475	13,8	13,2	0,19
9661	480	13,8	12,9	0
9762	485	13,6	12,9	0,1
9862	490	14,1	13,4	-0,05
9961	495	13,7	13,2	0,11
10,067	500	14,1	13,4	-0,01
10,169	505	14	13,4	0,03
10,277	510	14,1	13,3	-0,07
10,381	515	13,9	13,2	-0,04
10,481	520	13,2	13,2	-0,22
10,606	525	13	12,7	-0,16
10,733	530	14	13,2	0
10,858	535	12,9	12,9	-0,17
10,981	540	14,2	13,2	-0,29
11,105	545	13,6	13	-0,09
11,232	550	13,1	12,7	-0,26
11,363	555	12,4	12,5	-0,31
11,488	560	14	13,1	0
11,614	565	12,6	12,5	-0,14
11,756	570	12,7	12,2	-0,14
11,906	575	11,5	11,9	-0,03
12,06	580	13	12,4	0
12,21	585	12,3	12,3	0,05
12,362	590	13,9	12,6	0,02
12,515	595	12,2	12,2	0,06
12,668	600	12,1	12,3	0,06
12,766	605	12,6	12,2	0,07
12,849	610	11,6	12	-0,1
12,936	615	13,6	12,4	-0,11
13,02	620	11,4	11,9	-0,03
13,103	625	13,1	12,3	0,06
13,187	630	12	11,9	-0,07
13,271	635	13,5	12,7	0,07
13,355	640	11,7	12,1	0,03
13,441	645	12,6	12,3	0
13,527	650	13,2	12,4	-0,15
13,611	655	12,5	12,1	-0,14
13,697	660	11,1	11,9	-0,03
13,784	665	12,8	12,2	-0,03
13,872	670	10,3	11,6	-0,08

Age (cal yr BP)	Depth (cm)	modern analogue technique (°C)	partial least squares (°C)	Pollen Moisture Index (PMI) index
13,956	685	12,1	12	-0,09
14,041	690	10,6	11,8	-0,02
14,126	695	14	12,8	0,28
14,204	700	12,1	12,1	0,09
14,279	705	11	11,9	0,11
14,354	710	11,1	11,4	0,09
14,429	715	11,8	11,8	0,03
14,488	719	12,7	12,3	0,01
14,563	724	11	11,5	-0,02
14,638	729	10,6	11,4	-0,17

A4.6 Lago Espejo pollen percentage

taxon	**code**
Cupressaceae	CUPP
Podocarpus nubigena	PODN
Saxegothaea conspicua	SAXE
Nothofagus	NOTH
Misodendrum	MISO
Weinmannia trichosperma	WEIN
Myrtaceae	MYR
Eucryphia/*Caldcluvia*	EUC
Poaceae	POA
Asteraceae/*Asteroidae*	ASAS
Ericaceae	ERI
Gunnera	GUN
Lomatia/*Gevuina*	LOMT
Asteraceae/*Cichorioideae*	ASCI
other terrestrial (native)	OTHT
Plantago	PLAN
Rumex	RUM
Blechnum type	BLEC
total trees	TTRE
total shrubs and herbs	TSHH
total introduced	TINT

depth no tephra (cm)	age (cal yr BP)	CUPP	PODN	SAXE	NOTH	MISO	WEIN	MYR	EUC	POA	ASAS	ERI	GUN	LOMT	ASCI	OTHT	PLAN	RUM	BLEC	TTRE	TSHH	TINT
1	-60	8	1	1	56	1	0	2	0	29	0	0	0	0	1	2	11	6	0	69	31	18
6	-2	3	0	4	66	1	0	0	0	19	0	0	0	0	5	2	12	13	2	76	24	26
10	45	3	1	0	72	1	0	1	0	16	0	0	0	0	3	3	10	9	0	80	20	19
14	103	6	0	2	74	0	1	0	0	15	0	0	0	0	0	2	6	4	1	85	15	10
18	161	2	0	1	90	0	0	0	0	6	0	0	0	0	0	0	2	4	0	94	6	6
22	216	9	1	2	86	0	0	0	0	2	0	0	0	1	0	1	1	0	0	98	2	1
26	265	10	0	4	81	2	1	1	0	2	0	0	0	0	0	0	0	0	0	98	2	1
30	315	12	1	1	82	2	0	1	0	1	0	0	0	1	0	0	1	0	0	99	1	1
34	366	11	1	2	82	2	0	0	0	1	0	0	0	0	0	2	0	0	0	99	1	0
38	418	11	0	2	84	1	0	0	0	1	0	0	0	1	0	0	0	0	0	99	1	0
42	469	7	0	2	86	1	0	0	0	1	0	0	0	1	0	0	1	0	0	98	2	1
46	520	2	0	4	90	2	0	0	0	2	0	0	0	0	0	1	0	0	0	98	2	0
50	572	2	0	2	90	0	1	0	0	1	0	0	0	1	0	1	0	0	1	98	2	0
54	616	1	1	3	85	2	0	1	0	4	0	0	0	0	0	3	0	0	2	96	5	0
58	660	4	1	2	88	1	1	1	0	1	0	0	0	0	0	0	0	0	0	99	1	0
62	707	5	1	1	88	2	0	0	0	3	0	0	0	0	0	1	0	0	0	97	3	0

depth no tephra (cm)	age (cal yr BP)	CUPP	PODN	SAXE	NOTH	MISO	WEIN	MYR	EUC	POA	ASAS	ERI	GUN	LOMT	ASCI	OTHT	PLAN	RUM	BLEC	TTRE	TSHH	TINT
64	735	9	1	0	86	2	0	1	0	1	0	0	0	0	0	0	0	0	0	99	1	0
66	762	8	0	0	89	2	0	0	0	1	0	0	0	0	0	0	0	0	0	99	1	0
71	816	3	1	1	90	3	0	1	0	1	0	0	0	0	0	0	0	0	0	99	1	0
74	872	3	2	4	85	2	0	1	0	3	0	0	0	0	0	0	0	0	0	97	3	0
76	900	7	0	0	89	3	0	0	0	1	0	0	0	0	0	0	0	0	0	99	1	0
78	929	10	1	1	85	3	0	0	0	0	0	0	0	0	0	1	0	0	0	100	0	0
82	981	10	1	1	85	2	0	0	0	1	0	0	0	0	0	1	0	0	0	99	1	0
86	1029	6	0	1	90	2	0	0	0	0	0	0	0	0	0	0	0	0	0	99	1	0
88	1052	4	0	4	86	2	0	1	0	1	0	0	0	0	0	2	0	0	0	98	2	0
90	1076	1	1	2	92	2	0	0	0	1	0	0	0	0	0	1	0	0	0	98	2	0
94	1127	1	1	1	92	1	0	1	0	0	0	0	0	0	0	1	0	0	0	99	1	0
98	1181	1	1	3	88	1	0	2	0	2	0	0	0	0	0	2	0	0	0	97	3	0
100	1207	1	0	1	93	2	0	0	0	1	0	0	0	0	0	0	0	0	1	97	3	0
102	1237	1	1	2	90	3	0	0	0	3	0	0	0	0	0	1	0	0	1	97	3	0
106	1299	0	0	2	89	4	0	0	0	1	1	0	0	2	0	2	0	0	1	98	2	0
110	1360	0	1	2	90	1	0	1	0	3	0	0	0	1	0	2	0	0	0	97	4	0
112	1390	0	1	2	89	1	0	3	0	1	0	0	1	0	0	1	0	0	0	98	2	0

depth no tephra (cm)	age (cal yr BP)	CUPP	PODN	SAXE	NOTH	MISO	WEIN	MYR	EUC	POA	ASAS	ERI	GUN	LOMT	ASCI	OTHT	PLAN	RUM	BLEC	TTRE	TSHH	TINT
114	1419	1	1	0	87	0	0	1	0	7	0	0	0	0	0	2	0	0	0	93	8	0
118	1476	0	2	2	89	1	0	0	0	6	0	0	0	0	0	1	0	0	1	95	6	0
122	1533	1	2	2	87	2	0	0	0	6	0	1	0	0	0	0	0	0	0	94	6	0
124	1562	0	3	1	86	2	0	1	0	7	0	0	0	0	0	1	0	0	0	94	7	0
126	1591	0	1	3	89	2	0	0	0	3	0	0	0	0	0	2	0	0	0	96	5	0
130	1649	0	3	0	87	1	1	1	0	5	0	0	0	1	0	1	0	0	1	95	5	0
134	1716	0	1	1	89	0	0	2	0	5	0	0	0	0	0	0	0	0	0	95	6	0
136	1750	0	2	1	91	1	0	1	0	4	1	0	0	0	0	1	0	0	1	96	5	0
150	1973	0	2	1	87	1	0	0	0	6	0	0	0	1	0	2	0	0	0	93	7	0
154	2035	0	3	3	86	2	0	1	0	5	0	0	0	0	0	1	0	0	1	95	6	0
158	2097	0	3	1	87	1	0	0	0	6	0	0	0	1	0	0	0	0	0	94	6	0
160	2127	0	1	1	86	1	0	1	0	8	0	0	0	0	0	1	0	0	1	92	8	0
162	2158	1	2	2	86	1	0	1	0	6	0	0	1	0	0	1	0	0	1	93	7	0
166	2217	1	1	2	87	3	0	1	0	2	0	1	0	0	0	1	0	0	2	96	4	0
170	2275	0	2	0	90	0	0	1	0	4	1	0	0	1	0	1	0	0	0	95	5	0
172	2305	0	1	0	88	1	0	1	0	6	0	0	1	0	0	1	0	0	1	93	7	0
174	2334	0	2	2	86	1	0	1	0	4	1	1	0	0	0	2	0	0	1	94	6	0

depth no tephra (cm)	age (cal yr BP)	CUPP	PODN	SAXE	NOTH	MISO	WEIN	MYR	EUC	POA	ASAS	ERI	GUN	LOMT	ASCI	OTHT	PLAN	RUM	BLEC	TTRE	TSHH	TINT
178	2393	0	2	1	87	2	0	1	0	6	0	0	0	1	0	1	0	0	0	94	6	0
182	2452	1	3	1	86	1	0	2	0	4	0	1	0	0	0	1	0	0	1	95	6	0
184	2481	0	3	1	85	1	0	0	0	9	0	0	0	0	0	0	0	0	0	91	9	0
186	2510	0	1	1	87	2	0	1	0	5	0	0	0	0	0	2	0	0	1	95	6	0
190	2568	0	3	2	80	3	1	2	0	7	1	0	0	0	0	1	0	0	1	92	8	0
194	2627	0	3	0	85	2	0	2	0	8	0	0	0	0	0	0	0	0	1	92	8	0
196	2656	0	2	2	84	2	0	1	0	7	1	0	1	0	0	0	0	0	0	91	9	0
198	2685	0	1	1	83	2	1	2	0	9	1	1	0	0	0	1	0	0	1	90	10	0
202	2745	1	2	2	83	2	0	0	0	8	1	0	0	0	0	0	0	0	1	90	10	0
206	2808	0	1	1	84	3	0	3	0	5	0	0	0	0	0	2	0	0	1	94	6	0
208	2839	0	2	1	86	1	0	0	0	7	0	1	0	0	0	1	0	0	0	92	8	0
210	2872	1	2	1	86	2	0	0	0	7	1	0	0	0	0	1	0	0	1	93	8	0
214	2933	1	1	1	83	2	1	2	0	9	0	0	0	0	0	1	0	0	1	91	9	0
218	2996	0	2	1	82	2	0	1	0	7	0	0	1	1	0	3	0	0	1	92	8	0
220	3027	0	1	1	83	2	0	2	0	9	0	0	0	0	0	2	0	0	1	90	10	0
222	3057	0	3	0	82	1	0	3	0	5	0	1	0	2	0	3	0	0	1	93	7	0
226	3118	0	1	1	76	2	0	2	0	10	0	1	1	0	0	5	0	0	1	87	13	0

depth no tephra (cm)	age (cal yr BP)	CUPP	PODN	SAXE	NOTH	MISO	WEIN	MYR	EUC	POA	ASAS	ERI	GUN	LOMT	ASCI	OTHT	PLAN	RUM	BLEC	TTRE	TSHH	TINT
230	3179	0	4	0	75	2	1	1	0	11	1	0	1	1	0	4	0	0	1	87	13	0
232	3206	0	2	1	83	3	0	1	0	8	1	0	1	0	0	2	0	0	1	90	11	0
234	3233	0	1	2	71	2	0	3	0	17	0	0	1	1	0	3	0	0	0	81	19	0
238	3286	0	4	0	83	1	0	1	0	6	0	0	0	1	0	3	0	0	1	93	7	0
242	3340	0	2	2	84	2	1	1	0	7	0	0	0	0	0	2	0	0	1	93	7	0
244	3368	2	2	1	85	1	0	1	0	5	1	1	0	0	0	2	0	0	0	94	6	0
246	3396	0	4	4	81	1	1	0	0	7	0	0	0	1	0	1	0	0	1	92	8	0
250	3451	2	2	0	84	1	0	0	0	8	1	0	0	0	0	2	0	0	0	91	9	0
254	3511	0	3	3	86	2	0	0	0	5	0	0	0	0	0	1	0	0	0	94	6	0
256	3542	0	4	4	83	0	0	0	0	6	1	0	0	1	0	1	0	0	1	93	7	0
258	3572	1	3	5	82	2	0	1	0	5	1	0	0	1	0	0	0	0	0	94	6	0
262	3630	0	2	3	83	2	0	1	0	5	1	0	0	1	0	2	0	0	1	94	6	0
266	3688	0	1	6	82	2	0	1	0	4	0	1	1	0	0	2	0	0	0	94	6	0
268	3717	0	1	3	89	1	0	1	0	4	0	0	0	0	0	1	0	0	0	96	4	0
270	3746	0	2	3	91	1	0	0	2	1	0	0	0	0	0	1	0	0	0	99	1	0
274	3806	0	1	7	86	2	0	1	0	1	0	0	0	1	0	2	0	0	0	99	1	0
278	3867	0	1	5	88	1	0	1	0	4	0	0	0	0	0	1	0	0	0	97	4	0

depth no tephra (cm)	age (cal yr BP)	CUPP	PODN	SAXE	NOTH	MISO	WEIN	MYR	EUC	POA	ASAS	ERI	GUN	LOMT	ASCI	OTHT	PLAN	RUM	BLEC	TTRE	TSHH	TINT
280	3897	0	1	5	89	2	0	1	0	1	0	0	0	0	0	1	0	0	0	98	2	0
282	3927	0	0	3	91	2	0	0	0	3	0	0	0	0	0	1	0	0	0	97	3	0
286	3987	0	2	3	91	0	0	1	0	1	0	0	0	0	0	1	0	0	0	99	1	0
290	4047	0	1	3	89	1	0	0	0	4	0	0	0	0	0	2	0	0	0	96	4	0
292	4077	0	1	2	88	1	1	1	1	2	0	0	0	2	0	2	0	0	0	97	3	0
294	4106	0	1	4	85	1	0	0	0	4	0	0	0	2	0	2	0	0	0	95	5	0
298	4166	0	4	3	83	1	0	0	0	7	0	1	0	0	0	1	0	0	0	93	8	0
302	4223	1	2	4	81	2	1	1	0	7	0	0	0	0	0	1	0	0	0	92	8	0
304	4250	0	0	1	96	1	0	0	0	1	0	0	0	0	0	0	0	0	0	99	1	0
306	4276	0	1	1	94	1	0	0	0	1	0	0	0	0	0	1	0	0	0	98	2	0
310	4331	0	2	0	92	3	0	0	0	2	0	0	0	0	0	0	0	0	0	98	2	0
314	4393	0	2	0	92	1	0	1	0	3	0	0	0	0	0	1	0	0	0	97	3	0
316	4424	0	0	3	94	1	0	0	0	1	0	0	0	0	0	1	0	0	0	99	1	0
318	4456	0	2	2	90	1	0	1	0	4	0	0	0	0	0	0	0	0	0	96	4	0
322	4517	0	2	1	85	2	1	2	0	6	0	0	0	0	0	2	0	0	1	95	6	0
326	4574	0	1	1	89	2	0	1	0	4	0	0	0	0	0	1	0	0	0	96	4	0
328	4602	0	3	2	91	2	0	1	0	1	0	0	0	0	0	1	0	0	0	99	1	0

depth no tephra (cm)	age (cal yr BP)	CUPP	PODN	SAXE	NOTH	MISO	WEIN	MYR	EUC	POA	ASAS	ERI	GUN	LOMT	ASCI	OTHT	PLAN	RUM	BLEC	TTRE	TSHH	TINT
330	4631	0	2	1	93	2	0	1	0	1	0	0	0	0	0	1	0	0	0	98	2	0
334	4688	0	1	0	94	1	0	1	0	1	0	0	0	0	0	1	0	0	0	98	2	0
338	4745	0	1	1	91	3	0	0	0	3	0	0	0	0	0	0	0	0	1	96	4	0
340	4774	0	1	0	92	1	1	1	0	2	0	1	0	0	0	0	0	0	0	97	3	0
342	4802	0	1	1	91	1	0	0	0	4	0	0	0	0	0	1	0	0	0	96	4	0
353	4968	0	1	1	87	7	0	2	0	1	0	0	0	0	0	1	0	0	0	98	2	0
357	5041	0	2	1	92	3	0	1	0	1	0	0	0	0	0	1	0	0	0	99	1	0
359	5077	0	2	0	84	4	0	2	0	6	0	0	0	0	0	2	0	0	0	94	6	0
361	5111	0	0	1	89	6	0	1	0	1	0	0	0	0	0	2	0	0	0	99	1	0
365	5177	0	1	0	90	3	0	0	0	3	0	0	1	0	0	0	0	0	0	96	4	0
369	5243	0	0	1	90	3	0	1	0	4	0	0	0	0	0	2	0	0	0	96	5	0
371	5275	0	3	0	91	2	0	0	0	2	0	0	0	0	0	2	0	0	0	98	2	0
373	5307	0	5	1	82	2	0	2	0	5	0	0	0	0	0	2	0	0	1	94	6	0
377	5372	0	3	0	82	2	0	2	1	10	0	0	0	0	0	1	0	0	0	90	10	0
381	5438	0	1	2	88	1	0	1	0	5	0	0	0	1	0	2	0	0	1	95	5	0
383	5472	0	2	1	84	1	0	2	0	5	0	1	0	3	0	2	0	0	0	94	6	0
385	5506	0	1	1	85	1	0	1	0	10	0	0	0	2	0	1	0	0	0	90	10	0

depth no tephra (cm)	age (cal yr BP)	CUPP	PODN	SAXE	NOTH	MISO	WEIN	MYR	EUC	POA	ASAS	ERI	GUN	LOMT	ASCI	OTHT	PLAN	RUM	BLEC	TTRE	TSHH	TINT
389	5575	0	2	0	85	1	0	1	0	9	0	0	0	2	0	1	0	0	1	91	9	0
393	5647	0	1	0	92	2	1	1	0	2	0	0	0	0	0	1	0	0	0	98	2	0
395	5685	0	1	0	93	1	0	3	0	2	0	0	0	0	0	0	0	0	0	98	2	0
397	5721	0	2	0	93	2	0	0	0	3	0	0	0	0	0	0	0	0	0	97	3	0
401	5798	0	1	0	94	0	0	1	0	4	0	0	0	0	0	0	0	0	0	96	4	0
405	5887	0	1	0	92	2	0	2	0	3	0	0	0	0	0	1	0	0	0	97	3	0
407	5931	0	0	1	92	1	1	3	0	2	0	0	0	0	0	0	0	0	0	97	3	0
409	5974	0	2	0	93	0	0	1	1	1	0	0	0	0	0	2	0	0	0	99	1	0
413	6057	0	1	0	94	0	0	1	0	2	0	0	0	0	0	1	0	0	0	98	2	0
421	6218	0	2	0	90	1	0	1	0	5	0	0	0	0	0	1	0	0	0	95	5	0
423	6263	0	1	0	90	1	0	1	0	1	1	1	0	2	0	2	0	0	0	97	3	0
425	6308	0	1	0	92	1	0	1	0	3	0	0	0	1	0	1	0	0	0	97	3	0
429	6398	0	1	1	92	2	0	0	0	3	0	0	0	0	0	2	0	0	0	97	4	0
433	6491	0	1	0	97	0	0	1	0	2	0	0	0	0	0	0	0	0	0	98	2	0
435	6538	0	2	0	95	1	0	1	0	1	0	0	0	0	0	0	0	0	0	99	1	0
437	6586	0	2	0	92	3	0	2	0	1	0	0	0	0	0	0	0	0	0	98	2	0
441	6679	0	0	0	95	1	0	2	0	1	0	0	0	0	0	1	0	0	0	99	1	0

depth no tephra (cm)	age (cal yr BP)	CUPP	PODN	SAXE	NOTH	MISO	WEIN	MYR	EUC	POA	ASAS	ERI	GUN	LOMT	ASCI	OTHT	PLAN	RUM	BLEC	TTRE	TSHH	TINT
455	6977	0	1	0	91	2	0	2	0	2	0	0	0	0	0	2	0	0	0	97	3	0
457	7024	0	1	0	90	4	0	2	0	1	0	0	0	0	0	1	0	0	0	98	2	0
459	7071	0	1	0	88	3	0	3	0	3	0	0	0	0	0	1	0	0	0	97	3	0
463	7156	0	1	0	90	0	0	1	0	7	0	0	0	0	0	1	0	0	0	94	7	0
467	7235	0	3	0	86	0	0	3	0	6	0	0	0	1	0	2	0	0	1	94	6	0
469	7274	0	3	0	86	1	0	3	0	4	0	0	0	1	0	2	0	0	0	96	4	0
471	7314	0	1	0	93	4	1	1	0	0	0	0	0	0	0	0	0	0	0	100	0	0
475	7400	0	2	0	95	0	0	1	0	1	0	0	0	0	0	1	0	0	0	98	2	0
479	7486	0	1	0	89	0	0	1	0	4	1	0	1	1	0	2	0	0	0	93	7	0
481	7529	0	3	0	88	1	0	2	0	3	1	1	0	1	0	1	0	0	1	95	5	0
483	7574	1	2	0	88	1	0	3	0	3	0	0	0	0	0	2	0	0	0	97	3	0
487	7664	0	2	0	82	1	0	2	0	9	0	0	0	2	0	2	0	0	0	91	9	0
491	7764	0	4	0	87	1	0	0	0	5	0	0	0	1	0	2	0	0	2	95	5	0
493	7841	0	2	0	93	1	0	1	0	2	0	0	0	0	0	1	0	0	2	98	2	0
495	7918	0	7	0	86	1	0	1	0	3	0	0	0	0	0	2	0	0	5	96	4	0
499	8070	0	2	0	90	4	0	1	0	0	0	0	0	0	0	2	0	0	0	100	0	0
503	8241	0	2	0	91	1	0	2	0	2	0	0	0	0	0	1	0	0	0	98	2	0

depth no tephra (cm)	age (cal yr BP)	CUPP	PODN	SAXE	NOTH	MISO	WEIN	MYR	EUC	POA	ASAS	ERI	GUN	LOMT	ASCI	OTHT	PLAN	RUM	BLEC	TTRE	TSHH	TINT
505	8332	0	7	0	85	1	0	0	0	4	0	0	1	0	0	1	0	0	0	95	5	0
507	8424	0	5	0	88	2	0	1	0	4	0	0	0	0	0	1	0	0	0	96	4	0
511	8602	0	4	0	88	2	0	1	0	5	0	0	0	0	0	0	0	0	0	95	5	0
515	8761	0	4	0	89	3	0	1	0	2	0	0	0	0	0	1	0	0	0	98	2	0
517	8841	0	3	0	94	2	0	1	0	1	0	0	0	0	0	0	0	0	0	99	1	0
519	8923	0	3	0	90	1	0	2	0	3	0	0	0	0	0	0	0	0	0	97	3	0
523	9041	0	3	0	92	3	0	0	0	1	0	0	0	0	0	1	0	0	0	99	1	0
527	9134	0	3	0	92	2	0	2	0	1	0	0	0	0	0	1	0	0	0	99	1	0
529	9180	0	3	0	92	3	0	1	0	0	0	0	0	0	0	2	0	0	0	99	1	0
532	9248	0	3	0	88	5	0	0	0	1	0	0	0	0	0	3	0	0	1	98	2	0
538	9382	0	2	0	92	1	1	0	0	1	0	0	0	2	0	2	0	0	0	99	1	0
542	9478	0	5	0	85	2	1	0	0	3	1	0	0	1	0	3	0	0	5	96	4	0
544	9531	0	2	1	94	2	0	1	0	0	0	0	0	0	0	1	0	0	1	100	0	0
546	9585	0	7	0	84	3	0	0	0	2	1	0	1	1	0	2	0	0	3	96	4	0
550	9692	0	1	0	90	3	1	0	0	1	0	0	0	2	0	2	0	0	1	98	2	0
555	9837	0	4	0	91	0	0	0	0	2	0	0	1	0	0	1	0	0	4	97	3	0
557	9895	0	4	0	90	0	1	1	0	1	0	0	0	0	0	4	0	0	3	99	1	0

depth no tephra (cm)	age (cal yr BP)	CUPP	PODN	SAXE	NOTH	MISO	WEIN	MYR	EUC	POA	ASAS	ERI	GUN	LOMT	ASCI	OTHT	PLAN	RUM	BLEC	TTRE	TSHH	TINT
560	9981	0	4	0	85	2	0	1	0	4	1	0	1	0	0	2	0	0	4	94	6	0
564	10,098	0	1	0	94	2	0	0	0	1	0	0	0	0	0	1	0	0	2	99	1	0
569	10,271	0	3	0	91	2	0	1	0	0	0	0	0	0	0	2	0	0	0	100	0	0
572	10,331	0	1	0	85	4	3	1	0	2	0	0	0	0	0	4	0	0	3	97	3	0
574	10,391	0	4	1	78	6	0	1	0	3	1	1	1	0	0	3	0	0	4	94	6	0
578	10,512	0	3	0	84	2	1	0	0	4	1	1	0	0	0	4	0	0	6	94	6	0
582	10,629	0	4	0	86	3	1	0	0	1	0	0	3	0	0	2	0	0	3	96	4	0
584	10,684	0	3	0	86	1	1	1	0	3	0	0	1	0	0	3	0	0	4	95	5	0
586	10,739	0	5	1	82	2	2	1	0	3	1	0	1	0	0	3	0	0	6	95	6	0
590	10,848	0	4	0	83	2	3	0	0	2	1	1	2	0	0	2	0	0	7	95	6	0
594	10,976	1	4	1	84	2	1	0	0	2	1	1	0	1	0	2	0	0	3	96	4	0
596	11,042	1	4	0	76	2	5	0	0	3	3	1	2	0	0	3	0	0	4	91	9	0
599	11,141	0	3	0	77	1	3	1	0	2	1	1	5	1	0	6	0	0	4	91	9	0
617	11,565	0	10	0	83	1	1	0	0	1	0	2	0	0	0	1	0	0	9	97	3	0
621	11,637	0	8	0	80	1	1	0	0	2	3	2	0	2	0	1	0	0	7	94	7	0
623	11,676	0	5	0	83	3	1	0	0	1	2	2	0	1	0	2	0	0	7	95	5	0
625	11,715	1	8	0	69	3	3	1	0	5	4	1	1	2	0	2	0	0	10	90	10	0

depth no tephra (cm)	age (cal yr BP)	CUPP	PODN	SAXE	NOTH	MISO	WEIN	MYR	EUC	POA	ASAS	ERI	GUN	LOMT	ASCI	OTHT	PLAN	RUM	BLEC	TTRE	TSHH	TINT
629	11,793	0	4	0	83	2	1	0	0	3	2	1	0	2	0	2	0	0	9	93	7	0
633	11,87	1	8	0	81	1	1	1	0	1	1	1	1	3	0	1	0	0	5	96	4	0
635	11,909	0	12	0	69	3	1	0	0	4	4	2	0	2	0	2	0	0	8	89	11	0
637	11,948	1	13	0	68	4	2	1	0	4	4	1	0	3	0	1	0	0	10	92	8	0
641	12,028	1	7	0	77	2	0	0	0	4	2	3	0	2	0	3	0	0	10	91	9	0
645	12,121	1	11	0	74	3	0	0	0	5	2	1	0	1	0	2	0	0	8	92	8	0
647	12,168	1	11	0	75	2	0	0	0	7	1	2	0	1	0	1	0	0	4	91	9	0
649	12,215	0	5	0	77	4	0	0	0	7	0	1	0	1	0	4	0	0	7	91	9	0
653	12,326	0	5	0	79	11	0	0	0	4	0	0	0	0	0	1	0	0	5	96	4	0
657	12,447	0	15	0	68	3	0	0	0	10	0	1	1	0	0	1	0	0	4	88	12	0
659	12,507	1	4	0	84	2	0	0	0	6	1	3	1	0	0	0	0	0	1	91	9	0
661	12,565	0	6	0	80	3	0	1	0	7	1	1	0	0	0	2	0	0	1	91	9	0
665	12,678	0	4	0	86	2	0	1	0	3	1	1	1	0	0	1	0	0	2	93	7	0
669	12,791	0	9	0	85	0	0	0	0	3	0	1	1	0	0	1	0	0	2	96	4	0
671	12,846	0	3	1	83	0	0	0	0	8	1	2	1	1	0	1	0	0	2	90	11	0
673	12,898	1	2	0	93	3	0	0	0	1	0	0	0	0	0	0	0	0	1	99	1	0
677	13,001	0	1	0	89	5	0	0	0	2	0	1	0	0	0	2	0	0	1	96	4	0

depth no tephra (cm)	age (cal yr BP)	CUPP	PODN	SAXE	NOTH	MISO	WEIN	MYR	EUC	POA	ASAS	ERI	GUN	LOMT	ASCI	OTHT	PLAN	RUM	BLEC	TTRE	TSHH	TINT
681	13,096	0	3	0	92	3	0	0	0	2	0	0	0	0	0	0	0	0	0	98	2	0
685	13,145	0	3	0	93	2	0	0	0	1	0	1	0	0	0	0	0	0	1	98	2	0
687	13,171	1	1	0	96	2	0	0	0	1	0	0	0	0	0	0	0	0	1	100	1	0
689	13,194	0	3	0	93	2	0	0	0	1	0	0	0	0	0	1	0	0	1	98	2	0
693	13,242	0	1	1	91	4	0	0	0	2	0	0	0	0	0	0	0	0	0	97	3	0
697	13,292	0	1	0	87	10	0	0	0	1	0	1	0	0	0	1	0	0	1	99	1	0
700	13,328	0	2	0	92	5	0	0	0	1	0	1	0	0	0	0	0	0	0	98	2	0
702	13,352	0	4	0	86	8	0	0	0	1	0	0	0	0	0	1	0	0	1	98	2	0
706	13,399	1	4	0	81	4	0	0	0	3	0	3	0	0	0	4	0	0	3	91	9	0
710	13,446	0	2	0	80	15	0	0	0	3	0	0	0	0	0	0	0	0	4	97	3	0
712	13,471	0	4	0	74	18	0	0	0	2	0	0	0	0	0	1	0	0	4	97	3	0
714	13,495	0	1	0	87	7	0	0	0	2	0	1	1	0	0	1	0	0	2	97	3	0
718	13,543	1	5	0	70	16	0	0	0	6	0	1	0	1	0	1	0	0	5	92	8	0
722	13,592	1	3	0	78	11	0	0	0	4	0	1	0	0	0	2	0	0	6	95	6	0
724	13,616	1	2	0	77	11	0	0	0	5	0	2	0	0	0	1	0	0	5	93	7	0
726	13,641	6	9	0	47	15	0	0	0	13	1	4	1	1	0	3	0	0	18	81	19	0
729	13,676	10	10	0	35	7	0	2	0	28	1	3	0	3	0	2	0	0	23	68	32	0

depth no tephra (cm)	age (cal yr BP)	CUPP	PODN	SAXE	NOTH	MISO	WEIN	MYR	EUC	POA	ASAS	ERI	GUN	LOMT	ASCI	OTHT	PLAN	RUM	BLEC	TTRE	TSHH	TINT
733	13,724	1	2	0	40	2	1	3	0	30	5	5	1	1	0	9	0	0	19	53	47	0
735	13,749	1	4	0	27	0	0	1	0	37	9	20	0	0	0	2	0	0	9	32	68	0
737	13,773	2	0	0	50	0	0	0	0	36	4	7	0	2	0	0	0	0	26	54	46	0
749	13,921	5	5	0	47	7	0	7	0	21	2	0	0	2	0	5	0	0	17	74	26	0
753	13,969	1	2	0	28	0	0	3	0	49	6	2	0	0	0	9	0	0	5	36	64	0
754	13,982	4	0	0	34	0	0	1	0	41	10	3	1	0	0	7	0	0	10	43	57	0
755	13,994	3	0	0	45	0	0	0	0	39	8	1	0	0	0	5	0	0	6	50	51	0
757	14,019	2	3	2	57	0	0	4	0	25	4	3	0	0	0	0	0	0	12	68	32	0
761	14,069	4	0	0	44	0	0	2	0	40	4	1	0	1	0	3	0	0	7	54	47	0
765	14,116	0	0	0	61	0	0	6	0	21	2	2	1	0	0	6	0	0	3	69	31	0
767	14,139	1	0	0	35	0	0	2	0	49	5	4	1	0	0	4	0	0	2	39	61	0
769	14,163	2	1	2	58	0	0	0	0	11	10	7	1	1	0	8	0	0	9	70	30	0
773	14,212	4	1	0	56	0	0	2	0	27	6	0	2	1	0	2	0	0	8	65	35	0
777	14,263	1	0	0	52	0	0	4	0	20	7	6	0	2	0	8	0	0	10	62	38	0
779	14,288	0	0	0	54	0	0	8	0	22	4	7	0	0	0	5	0	0	8	63	37	0
781	14,313	2	1	0	48	0	0	5	0	29	4	4	0	0	0	7	0	0	8	57	43	0
785	14,361	6	0	3	61	0	0	4	0	7	5	7	0	1	0	7	0	0	3	76	24	0

depth no tephra (cm)	age (cal yr BP)	CUPP	PODN	SAXE	NOTH	MISO	WEIN	MYR	EUC	POA	ASAS	ERI	GUN	LOMT	ASCI	OTHT	PLAN	RUM	BLEC	TTRE	TSHH	TINT
811	14,675	4	1	0	43	0	0	5	0	30	6	6	0	0	0	6	0	0	9	54	46	0
813	14,701	1	0	0	45	0	0	6	0	32	6	4	1	1	0	4	0	0	9	54	46	0
817	14,752	1	3	0	60	0	0	6	0	24	0	4	0	0	0	3	0	0	10	71	29	0
821	14,802	0	0	0	58	0	0	7	0	21	3	7	1	0	0	3	0	0	3	66	34	0
823	14,826	1	2	0	60	0	0	4	0	23	3	3	1	0	0	3	0	0	7	70	30	0
825	14,851	1	0	0	43	0	0	4	0	34	12	1	0	0	0	5	0	0	5	51	49	0
829	14,901	2	1	0	53	0	0	5	0	28	6	0	2	0	2	2	0	0	4	62	39	0
833	14,948	0	1	0	43	0	0	8	0	33	3	6	2	0	0	4	0	0	3	54	46	0
835	14,973	0	0	0	45	0	2	8	0	31	6	3	1	1	0	4	0	0	5	56	44	0
838	14,997	0	0	0	50	0	0	3	0	30	8	6	2	1	0	0	0	0	3	54	46	0
841	15,046	5	0	0	48	0	0	5	0	25	6	4	3	1	0	5	0	0	12	59	41	0
845	15,096	2	1	0	47	0	0	7	0	29	5	6	2	1	0	1	0	0	11	57	43	0
848	15,133	3	3	0	74	1	0	6	0	6	2	1	2	0	0	3	0	0	0	87	13	0
849	15,145	1	2	0	65	0	0	9	0	15	2	4	0	0	0	2	0	0	7	78	22	0
854	15,195	2	0	0	57	0	0	14	0	19	3	0	1	0	0	4	0	0	4	77	23	0
857	15,244	1	0	0	69	0	0	5	0	19	1	0	1	0	0	3	0	0	5	77	23	0
859	15,271	2	0	0	44	0	0	12	0	28	3	7	0	0	0	4	0	0	3	62	38	0

depth no tephra (cm)	age (cal yr BP)	CUPP	PODN	SAXE	NOTH	MISO	WEIN	MYR	EUC	POA	ASAS	ERI	GUN	LOMT	ASCI	OTHT	PLAN	RUM	BLEC	TTRE	TSHH	TINT
861	15,294	1	1	0	67	0	0	17	0	9	1	2	0	0	0	3	0	0	6	87	13	0
865	15,342	1	0	0	56	0	2	15	0	12	1	5	5	0	0	3	0	0	5	76	24	0
869	15,391	0	0	0	55	0	0	16	0	20	4	5	0	0	0	1	0	0	4	71	29	0
871	15,415	0	1	0	56	0	0	13	0	19	3	0	3	1	0	4	0	0	7	73	27	0
873	15,438	3	3	0	68	0	0	3	0	17	1	3	0	0	0	2	0	0	4	78	22	0
877	15,487	1	1	0	59	1	0	9	0	15	5	5	2	0	0	2	0	0	5	73	27	0
881	15,535	1	1	0	64	0	0	5	1	17	1	5	0	0	0	5	0	0	7	76	24	0
883	15,559	0	0	1	52	0	0	8	0	29	2	6	0	0	0	2	0	0	9	63	37	0
885	15,583	1	0	0	63	0	0	7	0	23	1	3	2	0	0	1	0	0	2	72	28	0
889	15,631	3	0	0	51	1	1	3	0	33	0	1	3	0	0	4	0	0	5	61	39	0
892	15,668	12	0	0	45	0	0	5	0	24	6	2	3	0	0	4	0	0	8	61	39	0
893	15,679	3	1	0	55	0	1	6	0	21	2	4	3	0	0	4	0	0	2	68	32	0
895	15,716	6	1	0	43	0	0	5	0	37	1	2	3	0	0	3	0	0	4	56	44	0

A4.7 Lago Espejo pollen accumulation rate (particle*cm^{-2}*yr^{-1})

taxon	code
Cupressaceae	CUPP
Podocarpus nubigena	PODN
Saxegothaea conspicua	SAXE
Nothofagus	NOTH
Misodendrum	MISO
Weinmannia trichosperma	WEIN
Myrtaceae	MYR
Poaceae	POA
Asteraceae/Asteroidae	ASAS
Asteraceae/Cichorioideae	ASCI
Ericacea	ERI
Gunnera	GUN
Plantago	PLAN
Rumex	RUM
Blechum type	BLEC
total trees	TTRE
total shrubs and herbs	TSHH
total ferns	TFRN
total introduced	TINT
total terrestrial	TTER
total pollen	TPOL

Depth no tephra (cm)	age (cal yr BP)	CUPP	PODN	SAXE	NOTH	MISO	WEIN	MYR	POA	ASAS	ASCI	ERI	GUN	PLAN	RUM	BLEC	TTRE	TSHH	TFRN	TINT	TTER	TPOL
1	-60	300	32	32	2224	32	0	63	1152	16	32	0	0	536	300	16	2745	1215	32	883	3960	5332
6	-2	172	0	221	3675	74	25	0	1053	0	270	0	0	906	1004	123	4238	1323	221	1935	5561	8182
10	45	127	48	0	2821	32	0	48	618	16	111	0	0	475	412	16	3138	777	32	887	3914	5055
14	103	250	0	74	2960	15	29	0	589	0	15	0	0	265	191	29	3416	604	59	457	4020	4653
18	161	122	0	98	6389	0	0	25	392	0	0	0	25	171	294	0	6658	416	0	465	7074	7662
22	216	941	65	162	8728	0	0	0	162	0	0	0	0	65	0	32	10026	162	32	65	10188	10578
26	265	662	0	235	5319	107	43	64	107	21	0	0	0	21	21	0	6472	128	0	43	6600	6793
30	315	1234	67	133	8406	167	0	100	100	0	0	0	0	67	0	0	10174	133	0	67	10307	10574
34	366	1175	147	184	9072	184	0	37	74	0	0	0	0	37	0	0	10982	110	0	37	11093	11203
38	418	955	0	140	7414	56	0	0	112	0	0	0	0	0	0	0	8678	112	0	0	8790	8819
42	469	821	37	187	9890	112	0	0	149	37	0	37	37	75	0	0	11197	261	0	75	11458	11682
46	520	147	0	353	8271	147	0	29	206	0	0	0	0	0	0	0	9037	206	0	0	9243	9360
50	572	143	29	200	7786	29	86	29	86	29	0	0	29	0	0	115	8530	143	115	0	8673	9017
54	616	97	97	242	6388	121	0	73	290	24	0	0	0	0	0	121	7210	339	121	0	7549	7815
58	660	569	103	310	14163	207	155	207	155	0	0	52	0	0	0	52	15817	207	52	0	16024	16541
62	707	655	94	140	12869	281	0	0	374	0	0	0	0	0	0	0	14179	374	0	0	14554	14694
64	735	706	78	26	6872	183	0	52	52	0	0	0	0	0	0	0	7970	52	0	0	8022	8048
66	762	107	47	0	1288	233	0	47	187	0	0	0	0	0	0	0	1428	187	0	0	144	145

Depth no tephra (cm)	age (cal yr BP)	CUPP	PODN	SAXE	NOTH	MISO	WEIN	MYR	POA	ASAS	ASCI	ERI	GUN	PLAN	RUM	BLEC	TTRE	TSHH	TFRN	TINT	TTER	TPOL
		4			2												2				69	16
70	816	400	80	160	10917	400	0	80	120	0	0	0	40	0	0	0	12037	160	0	0	12197	12397
74	872	334	167	400	8838	234	0	133	300	0	0	0	0	0	0	33	10139	300	33	0	10439	10572
76	900	932	44	0	11977	355	0	44	89	0	0	0	0	0	0	44	13396	89	44	0	13485	13618
78	929	1658	104	104	14094	466	0	0	52	0	0	0	0	0	0	0	16582	52	52	0	16634	16685
82	981	1207	75	75	9992	264	0	0	113	0	0	0	0	0	0	0	11688	113	0	0	11802	11877
86	1029	999	56	167	16094	333	0	56	56	0	0	0	56	0	0	0	17759	111	0	0	17870	18092
88	1052	351	29	322	7994	205	0	88	88	29	0	0	0	0	0	0	9107	146	0	0	9254	9342
90	1076	116	58	203	8281	174	0	0	87	29	0	0	0	0	0	0	8891	145	0	0	9037	9356
94	1127	36	72	72	5135	36	18	72	18	18	0	18	0	0	0	0	5513	54	0	0	5567	5693
98	1181	82	41	164	5623	82	20	102	123	20	0	0	0	0	0	0	6216	164	0	0	6379	6563
100	1207	75	0	100	7056	150	0	25	100	25	0	25	25	0	0	50	7405	200	100	0	7605	7754
102	1237	68	45	158	6374	180	0	23	203	0	0	0	0	0	0	45	6892	225	45	0	7118	7253
106	1299	0	30	209	8116	328	0	0	119	60	0	0	0	0	0	60	8981	179	60	0	9160	9339
110	1360	24	73	121	6891	49	24	73	218	0	0	24	0	0	0	24	7400	267	24	0	7667	7740
112	1390	20	59	137	5309	39	0	176	59	20	0	20	39	0	0	0	5836	137	0	0	5972	6304
114	1419	78	78	0	5192	0	20	59	429	20	0	0	0	0	0	0	5543	449	0	0	5992	6187
118	1476	0	78	94	4311	47	0	16	266	0	0	0	0	0	16	31	4576	266	31	16	4842	5076
122	1533	48	97	80	4326	97	16	16	273	16	0	32	0	0	0	0	4679	322	0	0	500	514

Depth no tephra (cm)	age (cal yr BP)	CUPP	PODN	SAXE	NOTH	MISO	WEIN	MYR	POA	ASAS	ASCI	ERI	GUN	PLAN	RUM	BLEC	TTRE	TSHH	TFRN	TINT	TTER	TPOL
																					1	6
124	1562	0	226	75	6621	151	0	50	502	0	0	0	0	0	0	25	7197	502	50	0	7699	8075
126	1591	0	64	170	5919	128	0	0	213	0	0	0	21	0	0	21	6345	298	21	0	6643	6749
130	1649	0	141	0	4857	53	35	53	265	18	0	0	0	0	0	35	5281	283	35	0	5564	5793
134	1716	0	74	56	5065	19	19	111	278	19	0	0	19	0	0	0	5380	315	0	0	5696	5826
136	1750	0	87	35	4867	35	0	35	191	35	0	0	0	0	0	52	5110	243	52	0	5353	5579
150	1973	0	71	57	3910	28	0	14	256	0	0	0	14	0	0	14	4180	299	14	0	4478	4478
154	2035	0	148	148	4920	111	0	37	278	0	0	19	19	0	0	74	5420	314	74	0	5734	5938
158	2097	16	145	32	4326	48	16	0	274	16	0	16	0	0	0	16	4648	307	16	0	4955	5133
160	2127	0	65	65	4268	65	0	65	376	16	0	16	0	0	0	65	4546	409	65	0	4955	5151
162	2158	36	90	126	4705	54	0	36	343	0	0	0	36	0	0	72	5102	379	72	0	5481	5643
166	2217	30	59	74	3989	148	0	44	103	15	0	30	15	0	0	74	4402	177	74	0	4580	4846
170	2275	0	134	19	5325	19	0	38	229	57	0	0	0	0	0	19	5649	286	19	0	5936	6146
172	2305	0	71	18	4760	71	0	71	335	0	0	18	35	0	0	53	5024	388	53	0	5412	5624
174	2334	22	154	110	5736	88	0	44	264	66	0	66	0	0	0	44	6263	418	44	0	6681	6813
178	2393	0	77	47	4275	77	16	31	279	16	0	0	0	0	0	16	4616	294	16	0	4910	5111
182	2452	76	340	151	9971	76	38	189	491	38	0	113	0	0	0	113	10953	642	113	0	11595	12161
184	2481	0	211	63	5508	63	21	21	549	0	0	21	0	0	0	0	5909	570	0	0	6479	6605
186	2510	0	79	79	5287	118	20	59	295	20	0	0	0	0	0	39	5758	334	39	0	609	625

Depth no tephra (cm)	age (cal yr BP)	CUPP	PODN	SAXE	NOTH	MISO	WEIN	MYR	POA	ASAS	ASCI	ERI	GUN	PLAN	RUM	BLEC	TTRE	TSHH	TFRN	TINT	TTER	TPOL
																					3	0
190	2568	19	149	112	4762	168	56	112	392	37	0	19	19	0	0	37	5471	467	37	0	5938	6087
194	2627	0	194	22	5590	108	0	108	516	0	0	22	0	0	0	43	6021	538	43	0	6558	6859
196	2656	17	104	87	4482	87	0	35	382	35	0	17	35	0	0	0	4847	469	0	0	5316	5490
198	2685	16	66	33	4292	82	49	82	444	33	0	33	16	0	0	66	4654	543	66	0	5196	5361
202	2745	36	72	60	3087	60	0	12	298	36	0	12	12	0	0	36	3350	358	36	0	3707	3838
206	2808	17	52	35	4070	121	17	121	259	17	0	0	17	0	0	52	4552	293	52	0	4846	5173
208	2839	21	150	86	5611	64	0	21	450	21	0	43	0	0	0	0	6018	514	0	0	6532	6789
210	2872	55	164	55	7195	136	27	27	545	82	0	0	0	0	0	82	7740	627	82	0	8367	8775
214	2933	37	73	55	4738	110	37	110	494	18	0	0	0	0	0	55	5232	512	73	0	5744	6001
218	2996	0	172	49	6148	123	0	98	541	25	0	0	49	0	0	98	6910	615	98	0	7525	7869
220	3027	0	75	50	6417	150	25	150	699	0	0	0	25	0	0	50	6991	749	50	0	7740	8065
222	3057	0	194	24	6309	97	0	243	413	24	0	49	24	0	0	49	7158	534	49	0	7692	8201
226	3118	17	67	67	3821	100	17	83	501	17	0	67	33	0	0	67	4405	634	67	0	5039	5356
230	3179	0	152	14	3185	69	28	55	469	41	0	0	41	0	0	41	3695	552	69	0	4247	4385
232	3206	0	110	44	5694	197	0	66	526	44	0	0	66	0	0	66	6176	723	66	0	6899	7337
234	3233	0	65	98	3545	98	16	130	846	0	0	0	33	0	0	0	4066	927	0	0	4993	5416
238	3286	0	241	20	5300	80	20	60	361	20	0	20	20	0	0	40	5983	442	40	0	6425	6947
242	3340	18	91	12	4890	91	36	55	382	0	0	18	0	0	0	73	5436	400	73	0	583	607

Depth no tephra (cm)	age (cal yr BP)	CUPP	PODN	SAXE	NOTH	MISO	WEIN	MYR	POA	ASAS	ASCI	ERI	GUN	PLAN	RUM	BLEC	TTRE	TSHH	TFRN	TINT	TTER	TPOL
				7																	6	2
244	3368	117	117	59	5296	78	0	39	293	39	0	39	20	0	0	20	5823	391	20	0	6214	6566
246	3396	0	184	169	3861	46	31	0	337	15	0	15	0	0	0	31	4381	368	31	0	4749	4856
250	3451	71	85	0	3681	56	0	14	338	42	0	0	14	0	0	14	3977	409	14	0	4386	4611
254	3511	0	174	174	5951	109	0	0	348	22	0	22	22	0	0	0	6494	413	0	0	6906	7058
256	3542	0	191	209	4378	17	17	17	313	35	0	17	0	0	0	52	4917	365	52	0	5282	5560
258	3572	41	164	288	5282	144	0	62	308	62	0	0	21	0	0	21	6043	391	41	0	6433	6742
262	3630	0	85	169	4428	118	0	51	287	34	0	0	0	0	0	34	4969	338	34	0	5307	5712
266	3688	19	37	374	4818	112	19	37	243	19	0	37	37	0	0	19	5490	355	37	0	5845	5938
268	3717	0	61	162	5487	81	20	41	243	0	0	0	0	0	0	0	5913	243	0	0	6156	6277
270	3746	0	195	312	10749	156	0	0	117	0	0	0	0	0	0	0	11683	156	0	0	11839	11839
274	3806	0	44	487	6062	133	22	66	44	0	0	0	0	0	0	0	6947	66	0	0	7014	7257
278	3867	0	141	528	9614	106	0	70	387	0	0	0	0	0	0	0	10530	387	0	0	10917	11058
280	3897	0	60	453	8210	211	0	60	121	0	0	0	30	0	0	0	9116	151	0	0	9267	9508
282	3927	39	39	354	11045	197	0	39	393	0	0	0	0	0	0	0	11792	393	0	0	12185	12303
286	3987	34	204	307	9675	34	0	102	102	0	0	0	0	0	0	0	10492	102	0	0	10594	11139
290	4047	0	92	306	8448	92	0	31	337	0	0	31	0	0	0	0	9183	367	0	0	9550	9734
292	4077	0	48	97	4440	48	48	32	113	0	0	0	0	0	0	0	4908	129	0	0	5037	5279
294	4106	0	71	33	6420	71	24	0	284	0	0	24	0	0	0	0	7178	355	0	0	753	796

Depth no tephra (cm)	age (cal yr BP)	CUPP	PODN	SAXE	NOTH	MISO	WEIN	MYR	POA	ASAS	ASCI	ERI	GUN	PLAN	RUM	BLEC	TTRE	TSHH	TFRN	TINT	TTER	TPOL
				2																	4	0
298	4166	0	219	164	4656	55	18	18	365	18	0	37	0	0	0	18	5168	420	18	0	5588	5935
302	4223	48	144	337	6135	144	48	96	553	0	0	0	0	0	0	0	7025	577	0	0	7603	7747
304	4250	0	33	100	9816	100	33	33	100	0	0	0	0	0	0	0	10183	100	0	0	10283	10550
306	4276	0	146	98	14338	195	0	49	195	0	0	49	0	0	0	0	15020	244	0	0	15264	15459
310	4331	0	282	0	13476	470	0	47	235	0	0	0	0	0	0	0	14321	282	0	0	14603	15167
314	4393	0	191	0	10621	153	0	153	382	0	0	0	0	0	0	0	11194	382	0	0	11576	11652
316	4424	0	0	116	3803	26	0	0	39	0	0	13	0	0	0	0	3984	52	0	0	4036	4088
318	4456	0	183	183	8313	61	30	61	365	0	0	0	0	0	0	0	8861	365	0	0	9226	9470
322	4517	62	370	123	16078	308	185	308	1047	0	0	0	0	0	0	123	17864	1047	123	0	18912	19589
326	4574	0	100	150	13729	350	50	150	649	0	0	0	0	0	0	0	14727	649	0	0	15376	15726
328	4602	0	380	333	13454	238	0	95	143	0	0	0	0	0	0	0	14642	143	48	0	14785	14833
330	4631	61	306	122	17557	428	0	122	184	0	0	61	0	0	0	0	18658	306	0	0	18964	19025
334	4688	0	176	44	12649	176	0	132	132	0	0	0	44	0	0	0	13263	220	0	0	13483	13615
338	4745	0	91	91	8446	272	0	0	241	30	0	30	30	0	0	91	8928	332	91	0	9260	9502
340	4774	35	104	35	9919	104	104	104	243	0	0	104	0	0	0	35	10404	347	35	0	10751	10890
342	4802	58	234	234	16517	117	58	58	759	0	0	0	0	0	0	0	17393	759	0	0	18152	18327
353	4968	0	67	101	9047	704	0	201	134	0	0	34	0	0	0	34	10220	168	34	0	10387	10488
357	5041	0	104	35	5207	174	0	52	52	0	0	0	0	0	0	0	5641	52	0	0	569	574

Depth no tephra (cm)	age (cal yr BP)	CUPP	PODN	SAXE	NOTH	MISO	WEIN	MYR	POA	ASAS	ASCI	ERI	GUN	PLAN	RUM	BLEC	TTRE	TSHH	TFRN	TINT	TTER3	TPOL5
359	5077	0	212	42	11126	592	0	254	846	0	0	0	0	0	0	0	12480	846	0	0	13326	13538
361	5111	0	38	115	10708	691	0	154	115	0	0	0	0	0	0	38	12013	115	38	0	12128	12358
365	5177	0	138	35	9540	346	0	35	311	0	0	35	69	0	0	0	10162	415	0	0	10577	10681
369	5243	0	23	69	6473	185	0	69	277	0	23	0	0	0	0	0	6912	324	0	0	7236	7352
371	5275	0	152	0	4746	118	17	17	85	0	0	0	0	0	0	0	5135	85	0	0	5219	5253
373	5307	0	408	96	6163	144	0	120	408	0	0	0	0	0	0	48	7050	456	48	0	7506	7554
377	5372	0	187	23	5967	140	0	117	749	0	0	0	0	0	0	23	6575	749	47	0	7324	7488
381	5438	0	87	131	5835	65	22	44	305	0	0	0	0	0	0	87	6335	305	87	0	6640	6749
383	5472	19	97	77	4932	39	0	97	290	0	0	39	0	0	0	0	5571	329	0	0	5899	6093
385	5506	22	45	45	5858	45	0	45	673	22	0	0	22	0	0	22	6195	718	22	0	6913	7048
389	5575	20	99	0	5254	59	20	40	533	0	0	0	20	0	0	59	5609	573	59	0	6182	6340
393	5647	0	60	0	8451	208	89	119	149	0	0	0	0	0	0	0	9017	179	0	0	9195	9344
395	5685	12	36	12	3477	36	0	95	59	0	0	0	12	0	0	0	3679	71	0	0	3750	3774
397	5721	0	314	0	12912	224	0	0	448	0	0	0	0	0	0	0	13495	448	0	0	13944	14078
401	5798	0	70	0	10693	35	0	140	491	0	0	0	0	0	0	0	10938	491	0	0	11429	11534
405	5887	0	55	0	5169	92	0	110	147	0	0	0	0	0	0	0	5499	147	0	0	5646	5701
407	5931	24	24	73	6927	48	48	194	170	0	0	0	0	0	0	0	7339	194	0	0	7533	7581
409	5974	38	188	0	1071	38	0	15	75	0	0	0	0	0	0	0	1138	75	0	0	114	116

Depth no tephra (cm)	age (cal yr BP)	CUPP	PODN	SAXE	NOTH	MISO	WEIN	MYR	POA	ASAS	ASCI	ERI	GUN	PLAN	RUM	BLEC	TTRE	TSHH	TFRN	TINT	TTER	TPOL
					0			0									6				61	11
413	6057	0	91	0	6894	23	0	91	137	0	0	0	23	0	0	0	7168	160	0	0	7327	7396
421	6218	0	135	0	6372	45	0	45	359	0	0	0	0	0	0	0	6686	359	22	0	7045	7090
423	6263	17	68	0	4758	51	17	51	51	34	0	34	17	0	0	0	5150	136	0	0	5287	5389
425	6308	0	64	0	6172	43	21	86	171	21	0	0	0	0	0	0	6515	214	0	0	6729	6837
429	6398	0	35	52	5101	87	0	0	157	0	0	0	0	0	0	0	5328	192	0	0	5520	5590
433	6491	0	84	0	8387	28	0	56	140	0	0	0	0	0	0	0	8555	140	0	0	8694	8862
435	6538	0	106	0	4505	30	0	61	61	0	0	0	0	0	0	0	4702	61	0	0	4762	4778
437	6586	0	148	0	6017	170	0	127	85	0	0	0	0	0	0	0	6462	106	0	0	6568	6716
441	6679	0	0	0	16655	115	0	402	115	0	0	0	0	0	0	57	17345	115	115	0	17460	17460
455	6977	0	48	0	6677	166	0	119	166	0	0	0	0	0	0	0	7129	214	48	0	7343	7462
457	7024	0	62	0	5859	269	21	145	83	0	0	0	0	0	0	0	6377	104	0	0	6481	6667
459	7071	0	40	13	3636	133	13	107	133	0	0	0	0	0	0	0	3995	133	0	0	4128	4195
463	7156	0	130	0	12639	43	43	174	912	0	0	0	0	0	0	0	13117	912	0	0	14029	14159
467	7235	0	191	19	5178	0	0	153	363	0	0	0	0	0	0	38	5675	363	38	0	6038	6229
469	7274	0	174	0	5861	65	0	195	239	0	0	22	0	0	0	22	6512	282	22	0	6795	7012
471	7314	0	87	29	8460	320	87	87	0	0	0	0	0	0	0	0	9071	0	0	0	9071	9158
475	7400	0	282	0	11663	0	0	80	161	0	0	0	0	0	0	0	12145	201	0	0	12346	12668
479	7486	19	78	0	5350	19	0	78	252	39	0	0	39	0	0	0	5641	407	0	0	604	624

Depth no tephra (cm)	age (cal yr BP)	CUPP	PODN	SAXE	NOTH	MISO	WEIN	MYR	POA	ASAS	ASCI	ERI	GUN	PLAN	RUM	BLEC	TTRE	TSHH	TFRN	TINT	TTER	TPOL
																					8	2
481	7529	0	112	0	3886	42	14	84	140	28	0	28	14	0	0	28	4207	224	28	0	4431	4543
483	7574	29	73	15	4079	29	15	132	117	15	0	0	15	0	0	15	4475	147	15	0	4622	4725
487	7664	0	284	0	10634	162	0	244	1136	0	0	0	0	0	0	41	11770	1177	41	0	12947	13272
491	7764	0	128	11	2957	32	0	11	160	11	0	0	0	0	0	75	3224	182	85	0	3405	3491
493	7841	0	58	0	2770	29	10	29	58	0	0	10	0	0	0	49	2926	68	58	0	2994	3130
495	7918	6	117	0	1542	23	0	12	58	0	0	0	0	0	0	88	1735	64	117	0	1799	1910
499	8070	0	42	6	1692	78	0	12	0	0	0	0	0	0	0	0	1872	0	6	0	1872	1931
503	8241	0	165	28	7770	83	28	138	165	0	0	0	0	0	0	0	8321	193	0	0	8514	8624
505	8332	12	255	0	3217	36	0	12	158	0	0	0	24	0	0	0	3593	182	0	0	3775	3848
507	8424	0	136	0	2471	55	0	36	109	0	0	0	0	0	0	0	2716	109	0	0	2825	2852
511	8602	0	414	0	8340	148	0	59	444	0	0	0	0	0	0	0	8991	444	0	0	9435	9612
515	8761	0	292	0	6661	219	0	97	122	0	0	0	0	0	0	0	7342	146	0	0	7487	7658
517	8841	0	135	0	4708	105	0	30	45	0	0	0	0	0	0	0	4978	60	0	0	5038	5053
519	8923	0	279	0	7799	84	0	195	279	0	0	0	0	0	0	0	8383	279	0	0	8662	8746
523	9041	0	542	0	16847	481	0	60	241	0	0	0	0	0	0	0	18171	241	0	0	18411	18471
527	9134	0	490	0	15337	272	0	326	163	0	0	0	0	0	0	0	16533	163	0	0	16697	16969
529	9180	0	415	0	15190	415	0	104	52	52	0	0	0	0	0	0	16331	207	0	0	16538	16694
532	9248	0	701	0	1907	105	0	0	281	70	0	0	0	0	0	14	2145	351	14	0	218	228

Depth no tephra (cm)	age (cal yr BP)	CUPP	PODN	SAXE	NOTH	MISO	WEIN	MYR	POA	ASAS	ASCI	ERI	GUN	PLAN	RUM	BLEC	TTRE	TSHH	TFRN	TINT	TTER	TPOL
					2	2										0	6		0		06	58
538	9382	0	262	0	12640	88	131	44	88	0	0	0	0	0	0	44	13602	88	44	0	13690	13996
542	9478	0	180	0	2954	67	23	0	90	23	0	0	11	0	0	180	3336	135	191	0	3471	3673
544	9531	24	121	48	7096	121	0	48	0	0	0	0	0	0	0	48	7532	0	48	0	7532	7678
546	9585	0	414	0	5282	186	21	21	104	62	0	0	62	0	0	166	6049	249	166	0	6298	6567
550	9692	0	45	0	3172	102	23	11	45	11	0	0	0	0	0	23	3489	56	34	0	3545	3601
555	9837	0	113	0	2917	10	10	10	62	10	0	0	21	0	0	134	3092	103	134	0	3195	3360
557	9895	27	299	27	7465	27	54	54	54	0	0	0	27	0	0	244	8252	81	244	0	8334	8551
560	9981	14	171	0	3960	100	0	29	185	43	0	0	43	0	0	185	4387	271	199	0	4658	4786
564	10,098	0	71	0	5159	107	0	18	36	0	0	0	0	0	0	125	5444	36	143	0	5480	5676
569	10,271	0	324	0	9230	227	32	97	32	0	0	0	0	0	0	32	10072	32	32	0	10105	10234
572	10,331	0	81	0	10781	483	362	81	241	40	0	40	0	0	0	362	12269	402	362	0	12671	13355
574	10,391	0	224	35	4125	328	0	69	173	52	17	35	35	0	0	224	4954	311	242	0	5265	5748
578	10,512	0	68	0	1950	53	30	0	99	23	0	15	0	0	0	159	2186	144	159	0	2330	2565
582	10,629	15	165	15	3971	135	45	15	30	0	0	0	135	0	0	150	4451	180	150	0	4631	4856
584	10,684	0	157	0	4093	47	63	32	157	16	0	16	32	0	0	173	4518	252	173	0	4770	5258
586	10,739	0	164	22	2760	66	55	22	109	44	0	0	33	0	0	207	3186	186	218	0	3371	3644
590	10,848	8	87	0	2036	40	79	8	48	16	0	24	48	0	0	182	2314	135	190	0	2448	2623
594	10,97	28	169	28	3622	84	42	14	84	28	0	42	14	0	0	14	4113	183	14	0	429	456

Depth no tephra (cm)	age (cal yr BP)	CUPP	PODN	SAXE	NOTH	MISO	WEIN	MYR	POA	ASAS	ASCI	ERI	GUN	PLAN	RUM	BLEC	TTRE	TSHH	TFRN	TINT	TTER	TPOL
	6															0			0		6	3
596	11,042	27	107	9	2122	54	125	9	81	81	0	18	63	0	0	116	2542	242	116	0	2784	3089
599	11,141	8	65	0	1890	24	73	32	49	24	0	16	130	0	0	97	2238	227	97	0	2465	2733
617	11,565	14	423	0	3506	55	27	0	41	14	0	68	0	0	0	437	4079	123	437	0	4202	4339
621	11,637	16	411	0	3918	63	47	0	79	126	0	111	0	0	0	379	4582	316	379	0	4898	5135
623	11,676	0	220	0	3863	132	59	0	59	88	0	88	0	0	0	367	4421	235	382	0	4656	4876
625	11,715	34	410	0	3618	171	171	68	239	205	0	34	34	0	0	580	4693	529	580	0	5222	5546
629	11,793	18	201	0	4811	109	73	0	164	128	0	73	0	0	0	565	5394	383	583	0	5777	6178
633	11,87	36	450	0	4515	54	36	54	72	54	0	36	36	0	0	270	5342	216	306	0	5558	5900
635	11,909	16	569	16	3445	126	63	16	205	190	0	111	16	0	0	411	4409	553	411	0	4962	5278
637	11,948	50	681	0	3523	183	116	67	199	183	0	33	0	0	0	598	4803	416	615	0	5218	5401
641	12,028	26	263	0	3100	79	13	0	145	79	0	105	13	0	0	434	3678	355	486	0	4033	4401
645	12,121	31	365	0	2399	83	0	10	156	52	0	42	0	0	0	271	2972	250	282	0	3222	3431
647	12,168	28	475	0	3239	84	14	14	293	28	0	70	0	0	0	182	3910	391	182	0	4301	4622
649	12,215	0	238	0	3811	191	0	0	349	16	0	48	16	0	0	365	4494	429	429	0	4923	5335
653	12,326	0	248	17	4046	562	0	17	182	0	0	17	0	0	0	264	4938	198	264	0	5136	5383
657	12,447	0	759	0	3399	158	0	16	490	16	0	32	63	0	0	221	4395	601	269	0	4996	5328
659	12,507	29	202	14	3926	72	0	0	260	29	0	116	29	0	0	29	4258	433	58	0	4691	4879
661	12,56	0	251	0	3552	118	0	30	310	44	0	44	0	0	0	44	4039	413	74	0	445	476

Depth no tephra (cm)	age (cal yr BP)	CUPP	PODN	SAXE	NOTH	MISO	WEIN	MYR	POA	ASAS	ASCI	ERI	GUN	PLAN	RUM	BLEC	TTRE	TSHH	TFRN	TINT	TTER	TPOL
	5																				2	1
665	12,678	22	239	0	5871	152	0	65	217	44	22	65	44	0	0	152	6393	457	152	0	6849	7154
669	12,791	0	371	0	3471	0	0	0	106	0	0	40	27	0	0	80	3895	172	172	0	4067	4332
671	12,846	14	113	56	3566	14	0	0	324	28	0	71	28	0	0	85	3848	451	85	0	4299	4567
673	12,898	51	180	0	7285	231	0	26	77	0	0	0	0	0	0	77	7772	77	77	0	7849	8054
677	13,001	0	143	0	9806	573	0	36	251	0	0	72	0	0	0	143	10665	394	143	0	11059	11381
681	13,096	0	489	0	17418	489	0	61	306	0	0	61	61	0	0	0	18518	428	0	0	18945	19251
685	13,145	59	530	0	17130	294	0	0	177	0	0	118	0	0	0	236	18013	353	294	0	18366	19072
687	13,171	129	259	0	25597	453	0	0	129	0	0	0	0	0	0	194	26566	129	194	0	26696	27083
689	13,194	0	622	0	17715	435	0	0	124	0	0	62	62	0	0	249	18834	311	373	0	19145	19518
693	13,242	54	216	108	15146	595	54	0	325	54	0	54	0	0	0	0	16174	433	0	0	16607	16986
697	13,292	0	247	0	18653	2038	0	0	185	0	0	124	0	0	0	124	21186	309	309	0	21495	21865
700	13,328	0	465	0	26122	1302	0	0	372	0	0	186	0	0	0	0	27981	558	0	0	28539	29097
702	13,352	0	1014	0	25069	2304	0	0	369	0	0	0	92	0	0	369	28479	553	461	0	29032	29770
706	13,399	125	501	0	10684	584	42	0	334	42	0	334	0	0	0	376	12020	1127	376	0	13147	13606
710	13,446	24	141	0	5936	1107	0	0	189	0	0	0	0	0	0	306	7232	212	306	0	7444	7915
712	13,471	13	138	0	2964	716	0	13	88	13	0	13	0	0	0	151	3881	113	264	0	3994	4245
714	13,495	8	32	0	2142	175	0	0	40	0	0	24	16	0	0	40	2372	79	48	0	2451	2554
718	13,54	71	354	0	5169	118	0	0	472	0	0	47	24	0	0	37	6821	614	37	0	743	797

Depth no tephra (cm)	age (cal yr BP)	CUPP	PODN	SAXE	NOTH	MISO	WEIN	MYR	POA	ASAS	ASCI	ERI	GUN	PLAN	RUM	BLEC	TTRE	TSHH	TFRN	TINT	TTER	TPOL
	3					0										8			8		5	8
722	13,592	58	154	0	4597	654	0	19	212	19	0	58	0	0	0	385	5577	327	385	0	5904	6154
724	13,616	126	221	32	7856	1073	32	0	505	32	0	189	0	0	0	568	9433	757	631	0	10191	10727
726	13,641	116	163	0	843	273	0	6	227	17	0	76	12	0	0	384	1453	337	407	0	1790	2098
729	13,676	269	269	0	976	195	9	65	790	28	0	74	9	9	0	873	1905	911	985	9	2815	3549
733	13,724	1	1	0	22	1	1	2	17	3	0	3	1	0	0	13	30	26	14	0	56	69
735	13,749	11	44	0	295	0	0	11	416	98	0	219	0	0	0	109	361	755	153	0	1115	1301
737	13,773	2	0	0	42	0	0	0	30	3	0	6	0	0	0	32	45	39	38	0	84	96
749	13,921	1	1	0	12	2	0	2	5	1	0	0	0	0	0	5	18	6	5	0	25	33
753	13,969	1	2	0	21	0	0	2	37	5	0	2	0	0	0	4	27	49	5	0	76	96
754	13,982	7	0	0	63	0	0	2	76	18	0	5	2	0	0	22	79	106	25	0	186	220
755	13,994	5	0	0	81	0	0	0	70	14	0	2	0	0	0	13	90	92	18	0	181	203
757	14,019	1	1	1	27	0	0	2	12	2	0	1	0	0	0	7	32	15	7	0	47	56
761	14,069	6	0	0	62	0	0	3	56	6	0	1	0	0	0	10	75	65	13	0	140	155
765	14,116	0	0	0	59	0	0	6	21	2	0	2	1	0	0	3	67	29	3	0	96	111
767	14,139	2	0	0	77	0	0	4	108	11	0	9	2	0	0	4	86	136	9	0	222	259
769	14,163	6	3	6	171	0	0	0	32	29	0	20	3	0	0	29	206	90	38	0	296	389
773	14,212	9	2	0	124	0	0	4	59	13	0	0	4	0	0	20	143	78	24	0	221	256
777	14,26	2	0	0	82	0	0	6	32	11	0	9	0	0	0	17	97	59	20	0	157	172

Depth no tephra (cm)	age (cal yr BP)	CUPP	PODN	SAXE	NOTH	MISO	WEIN	MYR	POA	ASAS	ASCI	ERI	GUN	PLAN	RUM	BLEC	TTRE	TSHH	TFRN	TINT	TTER	TPOL
	3																					
779	14,288	0	0	0	8	0	0	1	3	1	0	1	0	0	0	1	9	5	2	0	15	16
780	14,313																					
781	14,361	2	1	0	39	0	0	4	24	3	0	3	0	0	0	7	47	35	7	0	82	93
785	14,675	10	0	5	104	0	0	7	12	8	0	12	0	0	0	5	129	41	5	0	170	206
811	14,701	3	1	0	33	0	0	4	23	5	0	5	0	0	0	8	42	35	8	0	78	88
813	14,752	1	0	0	52	0	0	7	38	7	0	5	1	0	0	11	63	53	15	0	116	126
817	14,802	2	6	0	115	0	0	11	45	0	0	8	0	0	0	23	135	56	26	0	192	226
821	14,826	0	0	0	77	0	0	9	28	4	0	9	1	0	0	4	88	45	5	0	133	149
823	14,851	1	3	0	86	0	0	6	33	4	0	4	1	0	0	10	101	43	12	0	144	163
825	14,901	1	0	0	41	0	0	4	33	12	0	1	0	0	0	5	49	47	7	0	96	105
829	14,948	3	1	0	77	0	0	7	41	8	3	0	3	0	0	6	89	56	10	0	145	165
833	14,973	0	2	0	66	0	0	13	50	5	0	9	3	0	0	5	83	70	5	0	153	170
835	14,997	0	0	0	114	0	5	22	79	14	0	7	2	0	0	14	143	112	17	0	255	269
837	15,046	0	0	0	57	0	0	3	34	9	0	7	2	0	0	3	62	52	6	0	114	125
841	15,096	9	0	0	95	0	0	9	49	11	0	7	6	0	0	27	117	80	27	0	197	215
845	15,133	2	1	0	45	0	0	7	28	5	0	6	2	0	0	12	55	41	13	0	96	108
848	15,145	4	4	0	103	1	0	8	8	3	0	1	3	0	0	0	123	18	0	0	140	150
849	15,19	1	1	0	40	0	0	6	9	1	0	3	0	0	0	5	48	14	6	0	62	66

Depth no tephra (cm)	age (cal yr BP)	CUPP	PODN	SAXE	NOTH	MISO	WEIN	MYR	POA	ASAS	ASCI	ERI	GUN	PLAN	RUM	BLEC	TTRE	TSHH	TFRN	TINT	TTER	TPOL
	5																					
853	15,244	2	0	0	56	0	0	14	19	3	0	0	1	0	0	4	76	23	6	0	99	106
857	15,271	1	0	0	49	0	0	4	14	1	0	0	1	0	0	4	55	16	4	0	72	83
859	15,294	1	0	0	30	0	0	8	19	2	0	5	0	0	0	2	44	26	2	0	70	80
861	15,342	4	4	0	253	0	0	63	34	4	0	7	0	0	0	26	332	48	26	0	380	421
865	15,391	1	0	0	44	0	2	12	10	1	0	4	4	0	0	5	60	19	5	0	78	84
869	15,415	0	0	0	26	0	0	8	10	2	0	2	0	0	0	2	34	14	2	0	48	53
871	15,438	0	1	0	54	0	0	12	18	3	0	0	3	0	0	8	70	26	10	0	96	100
873	15,487	1	1	0	31	0	0	1	8	0	0	1	0	0	0	2	35	10	2	0	45	49
877	15,535	2	2	0	102	2	0	16	26	9	0	9	4	0	0	9	126	47	10	0	173	186
881	15,559	2	2	0	96	0	0	8	25	2	0	8	0	0	0	11	114	36	11	0	149	160
883	15,583	0	0	1	37	0	0	6	21	1	0	4	0	0	0	7	45	26	8	0	71	77
885	15,631	1	0	0	81	0	0	9	29	1	0	4	3	0	0	3	93	37	5	0	130	144
889	15,668	4	0	0	62	1	1	4	40	0	0	1	4	0	0	7	75	48	9	0	123	139
892	15,679	4	0	0	13	0	0	1	7	2	0	0	1	0	0	3	18	11	3	0	29	32
893	15,716	3	1	0	63	0	1	7	24	2	0	5	3	0	0	2	78	37	2	0	114	120
896	15,716	3	1	0	24	0	0	3	21	1	0	1	2	0	0	2	32	25	2	0	57	60

A4.8 Lago Espejo charcoal accumulation data

depth no tephra (cm)	Age (cal yr BP)	Microscopic CHAR (particle*cm^{-2}*year^{-1})	macroscopic CHAR (particle*cm^{-2}*year^{-1})
1	-60	78900	2.2
2	-48		3.3
3	-36		7.8
4	- 25		10.1
5	-13		11.9
6	- 2	89800	12.2
7	10		13.2
8	22		13.5
9	33		16.2
10	45	84500	12.6
11	58		12.1
12	73		17
13	88		8.8
14	103	34400	7.3
15	117		11
16	132		13.7
17	147		11
18	161	195800	6.1
19	176		1.4
20	190		0.9
21	203		0.5
22	216		0.7
23	228		2.3
24	241		1.9
25	253		0.8
26	265	21400	0.9
27	278		1
28	290		0.9
29	302		0.7
30	315	11100	1.1
31	327		1.2
32	340		1.4

depth no tephra (cm)	Age (cal yr BP)	Microscopic CHAR (particle*cm^{-2}*year^{-1})	macroscopic CHAR (particle*cm^{-2}*year^{-1})
33	353		2.5
34	366	12200	0.3
35	379		1.7
36	392		0.9
37	405		0.8
38	418	18700	0.6
39	431		4.3
40	444		2.4
41	457		2.7
42	469	12400	0.8
43	482		1.3
44	495		2.1
45	508		1.3
46	520		1.6
47	533		1.4
48	546		2.3
49	559		3.8
50	572	66800	5.5
51	583		5.8
52	594		7.3
53	605		8.3
54	616	121000	10.8
55	627		11.3
56	638		12
57	649		14.4
58	660	448000	21.7
59	671		13.8
60	681		11.1
61	694		2.5
62	707		2.1
63	721		0.7
64			1.5

depth no tephra (cm)	Age (cal yr BP)	Microscopic CHAR (particle*cm^{-2}*year^{-1})	macroscopic CHAR (particle*cm^{-2}*year^{-1})
	735		
65	748		1.6
66	762		0.3
67	775		0.4
68	789		1.3
69	803		1.7
70	816	13300	1.2
71	830		0.9
72	844		2.9
73	858		5.1
74	872	122300	4.5
75	886		9.2
76	900	103500	19.7
77	914		9.8
78	929		4.6
79	943		1.1
80	957		1.2
81	969		1.3
82	981		0.4
83	993		0
84	1,005		0.6
85	1,017		0.2
86	1,029		0.5
87	1,040		0.2
88	1,052		0.3
89	1,064		0.9
90	1,076	96900	1.5
91	1,088		2.8
92	1,101		1.3
93	1,114		2.7
94	1,127	42000	6.2
95	1,140		3.6

depth no tephra (cm)	Age (cal yr BP)	Microscopic CHAR (particle*cm^{-2}*year^{-1})	macroscopic CHAR (particle*cm^{-2}*year^{-1})
96	1,154		3.2
97	1,167		3.6
98	1,181	34100	5.5
99	1,194		2.6
100	1,207	33200	1.7
101	1,222		9.2
102	1,237	22500	2.5
103	1,253		2.6
104	1,268		3.2
105	1,284		6.9
106	1,299	39800	2.3
107	1,315		0.7
108	1,330		0.8
109	1,345		0.2
110	1,360	80900	4
111	1,375		1.4
112	1,390		0.1
113	1,404		0.2
114	1,419	104100	2.3
115	1,434		2.8
116	1,448		4
117	1,462		5.7
118	1,476	15600	2.3
119	1,490		5.3
120	1,505		2.7
121	1,519		3.3
122	1,533	53600	5.5
123	1,547		5.1
124	1,562	183900	3.3
125	1,577		2.4
126	1,591	42600	1.9
127			3.8

depth no tephra (cm)	Age (cal yr BP)	Microscopic CHAR (particle*cm^{-2}*year^{-1})	macroscopic CHAR (particle*cm^{-2}*year^{-1})
	1,606		
128	1,620		2.9
129	1,634		3.8
130	1,649	17700	3.5
131	1,665		2.2
132	1,682		2.5
133	1,699		5.1
134	1,716	80400	5.5
135	1,733		2.4
136	1,750	11600	1.5
137	1,767		0
138	1,784		0
139	1,801		0
140	1,818		0
141	1,834		0
142	1,849		0
143	1,865		0
144	1,881		0
145	1,896		0
146	1,911		0
147	1,927		0
148	1,942		0
149	1,958		2.5
150	1,973	109000	6.2
151	1,989		5.8
152	2,004		5.2
153	2,019		3.3
154	2,035	308300	3.3
155	2,050		5
156	2,065		5.5
157	2,081		7.1
158	2,097	26900	6.5

depth no tephra (cm)	Age (cal yr BP)	Microscopic CHAR (particle*cm^{-2}*year^{-1})	macroscopic CHAR (particle*cm^{-2}*year^{-1})
159	2,112		3.8
160	2,127	16400	4.7
161	2,143		3.2
162	2,158	42100	4.4
163	2,172		3.7
164	2,187		4.5
165	2,202		6.8
166	2,217	133000	7.5
167	2,231		3.9
168	2,246		3
169	2,261		6.6
170	2,275	12700	9.1
171	2,290		3.9
172	2,305	76400	4.7
173	2,319		2.8
174	2,334	124500	4.6
175	2,349		2.3
176	2,364		4.1
177	2,378		6.4
178	2,393	62000	7.6
179	2,408		2.7
180	2,422		4.4
181	2,437		4
182	2,452	62900	3.8
183	2,466		3.6
184	2,481	84400	7.2
185	2,495		3.7
186	2,510	6600	3.5
187	2,525		2.1
188	2,539		2.8
189	2,554		5.6
190		130700	7

depth no tephra (cm)	Age (cal yr BP)	Microscopic CHAR (particle*cm^{-2}*year^{-1})	macroscopic CHAR (particle*cm^{-2}*year^{-1})
	2,568		
191	2,583		5.2
192	2,598		5.2
193	2,612		4.2
194	2,627		4.2
195	2,641		2.3
196	2,656	17400	8.5
197	2,670		3.2
198	2,685		6.1
199	2,699		1.4
200	2,714		1.5
201	2,729		4.5
202	2,745	111300	9.9
203	2,761		1.4
204	2,776		4.8
205	2,792		3.4
206	2,808	11500	8.6
207	2,823		7.7
208	2,839	71400	6.8
209	2,856		8.6
210	2,872	45400	5.1
211	2,887		3.1
212	2,902		5
213	2,918		3.9
214	2,933	85400	9.9
215	2,949		12.6
216	2,964		13.6
217	2,980		14.1
218	2,996		7.4
219	3,011		3.8
220	3,027		5.7
221	3,042		7.6

depth no tephra (cm)	Age (cal yr BP)	Microscopic CHAR (particle*cm^{-2}*year^{-1})	macroscopic CHAR (particle*cm^{-2}*year^{-1})
222	3,057	24300	6.8
223	3,072		9.2
224	3,087		8.7
225	3,102		7.3
226	3,118	55600	8
227	3,133		8.6
228	3,149		6.7
229	3,164		2.2
230	3,179	183800	15.5
231	3,193		3.6
232	3,206	94900	3.6
233	3,219		3.3
234	3,233	81300	5.6
235	3,246		7.1
236	3,259		7.6
237	3,272		4.1
238	3,286	60200	4.5
239	3,299		4.7
240	3,312		3.4
241	3,326		1
242	3,340	42400	5.2
243	3,354		2
244	3,368	39100	3.2
245	3,382		4.5
246	3,396	25500	3.9
247	3,410		3.9
248	3,423		3.5
249	3,438		7
250	3,451	103400	9.7
251	3,466		13.3
252	3,481		8.1
253			10.5

depth no tephra (cm)	Age (cal yr BP)	Microscopic CHAR (particle*cm^{-2}*$year^{-1}$)	macroscopic CHAR (particle*cm^{-2}*$year^{-1}$)
	3,496		
254	3,511	115800	7
255	3,527		4.9
256	3,542	191100	6.3
257	3,557		2.8
258	3,572	68500	3.2
259	3,587		2.5
260	3,602		3
261	3,616		2
262	3,630	22500	1
263	3,645		3.6
264	3,659		5.7
265	3,673		6.6
266	3,688	155600	5.8
267	3,703		3.1
268	3,717	74200	3.9
269	3,731		6.2
270	3,746		3.2
271	3,760		0.3
272	3,776		0.3
273	3,791		1.4
274	3,806	51600	1.7
275	3,821		2.7
276	3,836		2.5
277	3,852		5.2
278	3,867	270000	7.6
279	3,882		0.1
280	3,897	40200	0.5
281	3,912		0.3
282	3,927	13100	0.2
283	3,943		0.3
284	3,958		0.3

depth no tephra (cm)	Age (cal yr BP)	Microscopic CHAR (particle*cm-2*year-1)	macroscopic CHAR (particle*cm-2*year-1)
285	3,972		0.4
286	3,987		0.3
287	4,003		0.1
288	4,017		0.1
289	4,033		0
290	4,047		0.3
291	4,062		0.1
292	4,077	16100	0.1
293	4,091		0.3
294	4,106	7900	0.8
295	4,121		1.1
296	4,136		2
297	4,151		2.8
298	4,166		5.9
299	4,180		13
300	4,195		14.3
301	4,209		5.7
302	4,223	104300	10.6
303	4,236		6.4
304	4,250	89000	3.1
305	4,263		6.1
306	4,276	48800	16
307	4,290		4.1
308	4,303		0.1
309	4,317		0.1
310	4,331		0.2
311	4,345		0.4
312	4,361		0.4
313	4,377		1.3
314	4,393		1
315	4,408		1.5
316		25900	2.5

depth no tephra (cm)	Age (cal yr BP)	Microscopic CHAR (particle*cm^{-2}*year^{-1})	macroscopic CHAR (particle*cm^{-2}*year^{-1})
	4,424		
317	4,439		0.9
318	4,456		0.7
319	4,472		3.5
320	4,487		4.3
321	4,502		7
322	4,517		1.5
323	4,531		1.1
324	4,545		2
325	4,559		1.8
326	4,574	99800	7.2
327	4,588		1.3
328	4,602		0.3
329	4,617		0.1
330	4,631	20400	0.1
331	4,645		0.1
332	4,659		0.5
333	4,674		0.7
334	4,688	43900	0.1
335	4,702		1
336	4,716		0.9
337	4,731		1.5
338	4,745	20100	1.3
339	4,760		2.6
340	4,774	69400	2.7
341	4,788		10.8
342	4,802	19500	2.6
343	4,816		0.1
344	4,831		0
345	4,844		0
346	4,859		0
347	4,873		0

depth no tephra (cm)	Age (cal yr BP)	Microscopic CHAR (particle*cm^{-2}*year^{-1})	macroscopic CHAR (particle*cm^{-2}*year^{-1})
348	4,887		0
349	4,901		0
350	4,915		0
351	4,931		0.7
352	4,949		0.4
353	4,968	11200	0.5
354	4,986		0.2
355	5,004		0.2
356	5,022		0.3
357	5,041	11600	0.1
358	5,059		0.1
359	5,077	14100	0.4
360	5,094		0.1
361	5,111		0.2
362	5,128		0.6
363	5,144		0
364	5,161		0.2
365	5,177		0.1
366	5,194		0.1
367	5,210		0.1
368	5,226		0.1
369	5,243		0.1
370	5,259		0.6
371	5,275		1.5
372	5,291		2.8
373	5,307	71900	5.9
374	5,324		5
375	5,340		5.1
376	5,356		1.4
377	5,372	7800	1.2
378	5,389		2
379			3.9

depth no tephra (cm)	Age (cal yr BP)	Microscopic CHAR (particle*cm^{-2}*year^{-1})	macroscopic CHAR (particle*cm^{-2}*year^{-1})
	5,405		
380	5,421		4.7
381	5,438	7300	0.2
382	5,455		0.4
383	5,472	58000	1.5
384	5,489		1.8
385	5,506	15000	5.2
386	5,523		12.3
387	5,541		6.3
388	5,558		1.3
389	5,575	79000	0.6
390	5,592		1.6
391	5,610		7.6
392	5,628		20.6
393	5,647	9900	0.1
394	5,666		0.3
395	5,685	4000	0.1
396	5,703		0.1
397	5,721		0.2
398	5,740		0.3
399	5,759		0.1
400	5,777		0
401	5,798	11700	0.5
402	5,820		0.1
403	5,842		0.2
404	5,864		0.1
405	5,887	6100	0
406	5,909		0.3
407	5,931	24200	1.4
408	5,953		0
409	5,974		0.1
410	5,996		0

depth no tephra (cm)	Age (cal yr BP)	Microscopic CHAR (particle*cm^{-2}*year^{-1})	macroscopic CHAR (particle*cm^{-2}*year^{-1})
411	6,017		0.2
412	6,037		0
413	6,057	15200	1.6
414	6,077		1.4
415	6,097		0.3
416	6,117		0.2
417	6,137		0.7
418	6,157		0
419	6,176		0
420	6,197		0
421	6,218		0.7
422	6,240		0.2
423	6,263		0.2
424	6,286		1.4
425	6,308	7100	1.7
426	6,331		3.7
427	6,353		3.2
428	6,376		4
429	6,398	198000	4.6
430	6,420		3.1
431	6,443		0.3
432	6,467		0.3
433	6,491		0.3
434	6,515		0.6
435	6,538		0.1
436	6,562		0.1
437	6,586	14100	0.4
438	6,610		0.3
439	6,634		0.2
440	6,658		1.8
441	6,679		0.2
442			0

depth no tephra (cm)	Age (cal yr BP)	Microscopic CHAR (particle*cm^{-2}*year^{-1})	macroscopic CHAR (particle*cm^{-2}*year^{-1})
	6,699		
443	6,719		0
444	6,740		0
445	6,760		0
446	6,780		0
447	6,800		0
448	6,821		0
449	6,841		0
450	6,862		0
451	6,883		0
452	6,907		0
453	6,930		0
454	6,954		0
455	6,977		0.1
456	7,001		0.1
457	7,024	6900	0.1
458	7,048		0.1
459	7,071		0.3
460	7,095		0.1
461	7,117		0.2
462	7,136		0.1
463	7,156		0.2
464	7,176		8.4
465	7,195		0.6
466	7,215		0.6
467	7,235	70100	0.6
468	7,254		0.6
469	7,274	50700	1.4
470	7,294		1.8
471	7,314		0.2
472	7,335		0.3
473	7,357		0.1

depth no tephra (cm)	Age (cal yr BP)	Microscopic CHAR (particle*cm^{-2}*year^{-1})	macroscopic CHAR (particle*cm^{-2}*year^{-1})
474	7,378		0.5
475	7,400		0.3
476	7,422		0.6
477	7,443		0.7
478	7,465		2.3
479	7,486	51700	0.5
480	7,508		0.6
481	7,529	23300	1.3
482	7,552		3.4
483	7,574	88000	4.3
484	7,597		1.6
485	7,619		0.1
486	7,641		0.1
487	7,664		0.2
488	7,687		0.3
489	7,710		0.8
490	7,733		1
491	7,764	39100	1.1
492	7,802		1.8
493	7,841	42100	3.3
494	7,880		2.8
495	7,918	66200	4.6
496	7,956		3.6
497	7,994		0.9
498	8,032		0.4
499	8,070		0.1
500	8,108		0.1
501	8,150		0
502	8,196		0
503	8,241		0.1
504	8,287		0
505		12100	0.3

depth no tephra (cm)	Age (cal yr BP)	Microscopic CHAR (particle*cm-2*year-1)	macroscopic CHAR (particle*cm-2*year-1)
	8,332		
506	8,378		0.6
507	8,424		0
508	8,469		0
509	8,515		0.1
510	8,559		0.1
511	8,602	9900	0.2
512	8,641		8.2
513	8,681		0.1
514	8,721		0
515	8,761		0
516	8,801		0.3
517	8,841		0.2
518	8,882		0.3
519	8,923	65000	2.6
520	8,963		0.3
521	8,994		0.6
522	9,017		0.2
523	9,041	20100	0
524	9,064		0.1
525	9,087		0.3
526	9,110		0.3
527	9,134		0.1
528	9,157		0
529	9,180		0.1
530	9,203		0.4
531	9,226		0
532	9,248		0.3
533	9,270		0.1
534	9,292		0.1
535	9,315		0
536	9,338		0

depth no tephra (cm)	Age (cal yr BP)	Microscopic CHAR (particle*cm^{-2}*year^{-1})	macroscopic CHAR (particle*cm^{-2}*year^{-1})
537	9,360		0.2
538	9,382	29200	0.2
539	9,404		0.6
540	9,426		0.9
541	9,451		1.6
542	9,478	30000	2.3
543	9,505		0.4
544	9,531		0.3
545	9,558		0.2
546	9,585	41400	0.4
547	9,613		0
548	9,639		0.1
549	9,666		0.2
550	9,692	3800	0.3
551	9,720		0
552	9,750		0.3
553	9,779		0.9
554	9,808		3.1
555	9,837	34400	1
556	9,866		1.5
557	9,895	18100	1
558	9,924		0.6
559	9,952		1.8
560	9,981	76000	3.4
561	10,010		2
562	10,039		2.1
563	10,068		0.6
564	10,098	59500	0.3
565	10,127		0.8
566	10,156		0.5
567	10,186		1.8
568			1.7

depth no tephra (cm)	Age (cal yr BP)	Microscopic CHAR (particle*cm^{-2}*year^{-1})	macroscopic CHAR (particle*cm^{-2}*year^{-1})
	10,215		
569	10,243		0.9
570	10,271	10500	0.5
571	10,301		0.8
572	10,331	187700	1.4
573	10,361		1.8
574	10,391	189900	1.5
575	10,421		3.6
576	10,452		2.8
577	10,482		3.8
578	10,512	25300	3.9
579	10,543		3
580	10,573		1.4
581	10,602		4.4
582	10,629	59900	2.6
583	10,657		2.7
584	10,684	57700	3.5
585	10,711		4.3
586	10,739	207300	5.2
587	10,766		1.8
588	10,794		3.3
589	10,821		4.4
590	10,848	7900	2.8
591	10,878		3.8
592	10,910		3.3
593	10,943		2.8
594	10,976	65500	2.4
595	11,009		1.4
596	11,042	35800	1.5
597	11,075		0.7
598	11,108		1.1
599	11,141	83800	1.4

depth no tephra (cm)	Age (cal yr BP)	Microscopic CHAR (particle*cm^{-2}*year^{-1})	macroscopic CHAR (particle*cm^{-2}*year^{-1})
600	11,174		0.5
601	11,203		0
602	11,229		0
603	11,255		0
604	11,280		0
605	11,306		0
606	11,331		0
607	11,356		0
608	11,382		0
609	11,407		0
610	11,433		0
611	11,455		0
612	11,473		0
613	11,492		0
614	11,510		0
615	11,529		0
616	11,547		0
617	11,565	9100	5.1
618	11,583		3.4
619	11,600		3.8
620	11,618		2.3
621	11,637	73700	2.7
622	11,656		1.7
623	11,676	49000	8.8
624	11,696		3.1
625	11,715	39800	2.1
626	11,735		3.7
627	11,754		4.6
628	11,774		3.4
629	11,793	164000	3.2
630	11,813		2.7
631			3.9

depth no tephra (cm)	Age (cal yr BP)	Microscopic CHAR (particle*cm^{-2}*year^{-1})	macroscopic CHAR (particle*cm^{-2}*year^{-1})
	11,832		
632	11,851		3.8
633	11,870		5.2
634	11,889		4.9
635	11,909	36900	5.8
636	11,928		4.6
637	11,948	22200	2.1
638	11,967		5.8
639	11,987		4.1
640	12,006		4.8
641	12,028	170800	6.6
642	12,051		3.6
643	12,074		5.5
644	12,097		5.2
645	12,121	10400	5.2
646	12,145		8.9
647	12,168	51200	4.4
648	12,192		7.1
649	12,215	90000	7.2
650	12,238		8.6
651	12,265		5.7
652	12,295		5.3
653	12,326	5500	4.3
654	12,356		3.3
655	12,386		2.5
656	12,416		3.7
657	12,447	252900	7.2
658	12,477		5.8
659	12,507	322400	5
660	12,537		5.8
661	12,565	363600	2.6
662	12,594		6.3

depth no tephra (cm)	Age (cal yr BP)	Microscopic CHAR (particle*cm^{-2}*year^{-1})	macroscopic CHAR (particle*cm^{-2}*year^{-1})
663	12,621		9.6
664	12,649		6.7
665	12,678	326200	6.6
666	12,706		8.7
667	12,734		5.2
668	12,763		8.1
669	12,791	172200	11.2
670	12,819		8.1
671	12,846	178500	4.9
672	12,872		8
673	12,898	42700	1.3
674	12,923		0.7
675	12,949		0
676	12,974		0
677	13,000		0
678	13,026		0
679	13,051		0
680	13,077		0
681	13,096	20400	0.2
682	13,108		0
683	13,120		0
684	13,133		0
685	13,145		0
686	13,158		0
687	13,170	21500	0
688	13,182		0.1
689	13,194	20700	0
690	13,205		0
691	13,218		0
692	13,230		0
693	13,242		0
694			0

depth no tephra (cm)	Age (cal yr BP)	Microscopic CHAR (particle*cm^{-2}*year^{-1})	macroscopic CHAR (particle*cm^{-2}*year^{-1})
	13,255		
695	13,267		0
696	13,279		0
697	13,292	20600	0
698	13,304		0
699	13,316		0
700	13,328		0
701	13,340		0.2
702	13,352		0
703	13,363		0
704	13,375		0.2
705	13,387		1.5
706	13,399		0
707	13,411		0
708	13,422		0
709	13,434		0
710	13,446	7900	0
711	13,458		0
712	13,471	8400	0
713	13,482		0
714	13,495		0
715	13,507		0.1
716	13,519		0
717	13,531		0
718	13,543		0
719	13,555		0
720	13,567		0
721	13,579		0
722	13,592	12800	0.1
723	13,604		0
724	13,616	10500	0
725	13,627		0

depth no tephra (cm)	Age (cal yr BP)	Microscopic CHAR (particle*cm^{-2}*year^{-1})	macroscopic CHAR (particle*cm^{-2}*year^{-1})
726	13,640	1900	0
727	13,652		0.1
728	13,664		0
729	13,676	161000	1.9
730	13,688		0.7
731	13,700		0
732	13,712		0
733	13,724		0
734	13,737		0
735	13,749		0
736	13,761		0
737	13,773		0
738	13,785		0
739	13,797		0
740	13,809		0
741	13,822		0
742	13,834		0
743	13,846		0
744	13,859		0
745	13,871		0
746	13,883		0
747	13,895		0
748	13,908		0
749	13,920		0
750	13,932		0
751	13,944		0
752	13,956		0
753	13,969	500	0
754	13,982		0
755	13,994		0
756	14,007		0
757			0

depth no tephra (cm)	Age (cal yr BP)	Microscopic CHAR (particle*cm^{-2}*year^{-1})	macroscopic CHAR (particle*cm^{-2}*year^{-1})
	14,019		
758	14,031		0
759	14,044		0
760	14,057		0
761	14,069		0
762	14,080		0
763	14,092		0
764	14,104		0
765	14,116		0
766	14,128		0
767	14,139		0
768	14,151		0
769	14,163		0
770	14,175		0
771	14,187		0
772	14,200		0
773	14,212		0
774	14,225		0
775	14,238		0
776	14,250		0
777	14,263		0
778	14,276		0
779	14,288		0
780	14,301		0
781	14,313		0
782	14,324		0
783	14,337		0
784	14,349		0
785	14,360		0
786	14,372		0
787	14,384		0
788	14,396		0

depth no tephra (cm)	Age (cal yr BP)	Microscopic CHAR (particle*cm^{-2}*year^{-1})	macroscopic CHAR (particle*cm^{-2}*year^{-1})
789	14,408		0
790	14,419		0
791	14,431		0
792	14,443		0
793	14,455		0
794	14,467		0
795	14,479		0
796	14,490		0
797	14,503		0
798	14,514		0
799	14,527		0
800	14,539		0
801	14,551		0
802	14,563		0
803	14,576		0
804	14,588		0
805	14,600		0
806	14,613		0
807	14,626		0
808	14,638		0
809	14,650		0
810	14,663		0
811	14,675		0
812	14,688		0
813	14,701		0
814	14,713		0
815	14,726		0
816	14,739		0
817	14,752		0
818	14,764		0
819	14,777		0
820			0

depth no tephra (cm)	Age (cal yr BP)	Microscopic CHAR (particle*cm^{-2}*year^{-1})	macroscopic CHAR (particle*cm^{-2}*year^{-1})
	14,789		
821	14,802		0
822	14,814		0
823	14,826		0
824	14,838		0
825	14,851		0
826	14,863		0
827	14,875		0
828	14,887		0
829	14,900		0
830	14,911		0
831	14,924		0
832	14,936		0
833	14,948		0
834	14,960		0
835	14,973		0
836	14,985		0
837	14,997		0
838	15,009		0
839	15,021		0
840	15,033		0
841	15,046		0
842	15,058		0
843	15,071		0
844	15,083		0
845	15,096		0
846	15,109		0
847	15,121		0
848	15,133		0
849	15,145	200	0
850	15,158		0
851	15,170		0

depth no tephra (cm)	Age (cal yr BP)	Microscopic CHAR (particle*cm^{-2}*year^{-1})	macroscopic CHAR (particle*cm^{-2}*year^{-1})
852	15,183		0
853	15,195		0
854	15,207		0
855	15,220		0
856	15,232		0
857	15,244		0
858	15,257		0
859	15,270		0
860	15,282		0
861	15,294		0
862	15,306		0
863	15,318		0
864	15,330		0
865	15,342		0
866	15,354		0
867	15,366		0
868	15,378		0
869	15,390		0
870	15,403		0
871	15,415		0
872	15,427		0
873	15,438		0
874	15,451		0
875	15,463		0
876	15,475		0
877	15,487		0
878	15,499		0
879	15,511		0
880	15,523		0
881	15,535		0
882	15,547		0
883			0

depth no tephra (cm)	Age (cal yr BP)	Microscopic CHAR (particle*cm^{-2}*year^{-1})	macroscopic CHAR (particle*cm^{-2}*year^{-1})
	15,559		
884	15,571		0
885	15,583		0
886	15,595		0
887	15,608		0
888	15,619		0
889	15,631		0
890	15,644		0
891	15,656		0
892	15,668		0
893	15,679		0
894	15,692		0
895	15,704		0
896	15,716		0
897	15,728		0